Helmut Josef PELZMANN, Dipl.-Ing., BSc.

Characterization of the N-acetylaspartate pathway in adipocyte metabolism *in vitro* and *in vivo*

Doctoral Thesis

to obtain the university degree of

Doktor der technischen Wissenschaften

submitted to

Graz University of Technology

Supervisor

Assoc. Prof. Mag.rer.nat. Dr.rer.nat. Juliane G. Bogner-Strauss

Institute of Biochemistry

Graz, April 2016

Helmut Josef PELZMANN, Dipl.-Ing., BSc.

Characterization of the N-acetylaspartate pathway in adipocyte metabolism *in vitro* and *in vivo*

Dissertation

zur Erlangung des akademischen Grades

Doktor der technischen Wissenschaften

eingereicht an der

Technischen Universität Graz

Betreuerin

Assoc. Prof. Mag.rer.nat. Dr.rer.nat. Juliane G. Bogner-Strauss

Institut für Biochemie

Graz, April 2016

EIDESSTATTLICHE ERKLÄRUNG

AFFIDAVIT

Ich erkläre an Eides statt, dass ich die vorliegende Arbeit selbstständig verfasst, andere als die angegebenen Quellen/Hilfsmittel nicht benutzt, und die den benutzten Quellen wörtlich und inhaltlich entnommenen Stellen als solche kenntlich gemacht habe. Das in TUGRAZonline hochgeladene Textdokument ist mit der vorliegenden Dissertation identisch.

I declare that I have authored this thesis independently, that I have not used other than the declared sources/resources, and that I have explicitly indicated all material which has been quoted either literally or by content from the sources used. The text document uploaded to TUGRAZonline is identical to the present doctoral thesis.

Datum (*Date*)	Unterschrift (*Signature*)

Danksagung / Acknowledgement

„Wir können den Wind nicht ändern, aber wir können die Segel richtig setzen."

Aristoteles

In diesem Sinne möchte ich mich am Beginn dieser Arbeit bei allen bedanken, die mich gelehrt haben den Wind zu lesen und mir beim Setzen der Segel geholfen haben.

Am Anfang soll meine Familie stehen, allen voran meine wunderbare Frau Elisabeth, meine Eltern, Großeltern, und Geschwister. Familie prägt, hört zu, hilft, spornt an, fordert, unterstürzt, liebt, ist sinnstiftend. Ich bin glücklich eine solche Familie um mich zu wissen.

Als nächstes möchte ich mich bei meiner Betreuerin Juliane Bogner-Strauss bedanken. Liebe Julia, du hast mir diese Arbeit ermöglicht und mich in meiner Zeit als Doktoratsstudent geleitet und unterstützt. Deine Leidenschaft für die Wissenschaft hat mich stets motiviert. Danke für alles, was du mich in den letzten vier Jahren gelehrt hast, du bist mir als gute Freundin ans Herz gewachsen!

Nicht weniger herzlich möchte ich mich bei allen Kollegen im Labor bedanken. Danke für die viele Hilfe und die zeitintensiven Diskussionen. Vor allem Ariane Pessentheiner, Evelyn Walenta und Florian Stöger haben mich von Beginn an begleitet. Herzlichen Dank!

Ich danke meinem Mentor Andreas Prokesch und meinem Prüfungskomitee, Günter Hämmerle und Peter Macheroux, die mir immer wieder neue Ideen und Wege aufgezeigt haben, meine Forschung voranzutreiben.

I would also like to thank Atsumi Nitta and Andrew Pospisilik, who provided me the opportunity to work in their labs, gain experience, and improve my scientific skills during my stays at the University of Toyama (Japan) and the Max-Planck-Institute of Immunobiology and Epigenetics (Germany).

The number of people directly or indirectly contributing to the accomplishment of this thesis is much bigger than mentioned above. A simple "thank you" shall express my highest appreciation to all my friends and companions.

Abstract

Obesity constitutes a major health issue as it is a prerequisite for the progression of medical conditions such as hypertension, insulin resistance, and dyslipidemia, finally leading to comorbidities such as cardiovascular disease and type 2 diabetes mellitus. Adipose tissue significantly contributes to the development of these diseases by regulating whole body lipid and glucose homeostasis. Two major types of adipose tissue can be distinguished. White adipose tissue is the main organ to store nutrients in the body whereas brown adipose tissue (BAT) uses glucose and fatty acids (FAs) to produce heat via the uncoupling protein 1 (UCP1). Understanding the molecular regulatory mechanisms controlling adipose tissue function and metabolism is important to develop novel therapeutic approaches to counteract obesity-related diseases.

N-acetylaspartate (NAA) is an important metabolite in brain physiology. We were the first to show that NAA is synthesized by mitochondrial N-acetyltransferase 8-like (NAT8L) and catabolized by cytoplasmic aspartoacylase (ASPA) in adipocytes. These two enzymes build the so called NAA pathway. We showed that manipulation of the NAA pathway impacts lipid turnover (lipogenesis and lipolysis), marker gene expression, and cellular respiration in brown adipocytes. The first part of this thesis shows that *Nat8l* overexpression regulates lipid and energy metabolism by activating the main triglyceride hydrolase ATGL and the transcription factor PPARα. The increased metabolic flux through the NAA pathway is a prerequisite to increase the expression of UCP1 in brown adipocytes. Further, the NAA pathway in BAT provides a novel route to transport acetyl-CoA from mitochondria to the cytoplasm. Cytoplasmic acetyl-CoA controls histone / protein acetylation, thereby regulating cellular metabolism. ATP citrate lyase (ACLY) has been described as the main enzyme to provide cytoplasmic acetyl-CoA. Analysis of *Nat8l*-silenced brown adipocytes and BAT from total body *Nat8l*-knock-out (*Nat8l*-ko) mice revealed a compensatory upregulation of ACLY. Further, we show a connection of the NAA pathway to the regulation of the histone / protein deacetylase sirtuin 1. This compensatory upregulation of ACLY and the connection to sirtuin signaling argues for considering NAA metabolism as an important regulator of intracellular acetyl-CoA availability and distribution, thereby impacting energy homeostasis.

In the second part of this thesis, we show that the NAA pathway is highly regulated by metabolic triggers such as high / low nutrient availability, circulating FAs, insulin secretion, and β-adrenergic stimulation. Analysis of NAA concentrations in *Nat8l*-ko mice revealed that NAT8L is the main enzyme to produce NAA. On chow diet, *Nat8l*-ko mice show reduced body weight and decreased blood glucose levels (mild hypoglycemia), whereas glucose tolerance and insulin sensitivity are not different when compared to wt mice. Weight loss upon overnight fasting and total energy expenditure (EE) is increased in *Nat8l*-ko mice. On high-fat diet (HFD), *Nat8l*-ko mice show reduced weight gain and mild hypoglycemia accompanied by improved glucose

tolerance while insulin sensitivity was unchanged. Further, weight loss upon overnight fasting and total EE is also increased in *Nat8l*-ko mice on HFD when compared controls. Finally, cold exposure revealed that *Nat8l*-ko mice on chow diet loose more weight than *Nat8l*-ko mice on HFD. This suggests that the carbohydrate to lipid ratio in the diet impacts substrate utilization and energy homeostasis in *Nat8l*-ko mice. Thus, although the function of the NAA pathway in adipose tissue is not clear yet, this thesis provides fundamental evidence for an important role of NAA metabolism in adipocyte energy homeostasis. Taken together, we show that the NAA pathway is important to regulate whole body physiology.

Kurzfassung

Fettleibigkeit stellt ein ernsthaftes Gesundheitsproblem dar und ist die Voraussetzung für die Entwicklung von Symptomen wie Bluthochdruck, Insulinresitenz und Dyslipidämie und führt letztendlich zu Begleiterkrankungen des Herz-Kreislaufsystems und Diabetes Mellitus. Fettgewebe trägt als wichtiger Regulator des Lipid- und Zuckerhaushalts maßgeblich zur Entwicklung dieser Krankheiten bei. Es gibt zwei Hauptarten von Fettgewebe; weißes Fettgewebe stellt den Hauptenergiespeicher des Körpers dar und braunes Fettgewebe (BAT) besitzt die Fähigkeit, Glukose und Fettsäuren (FAs) mit Hilfe des Proteins Uncoupling Protein 1 (UCP1) zu verbrennen. Es ist daher notwendig die molekularen Mechanismen, welche die Funktion und den Stoffwechsel in den Fettgeweben kontrollieren, zu verstehen, um neue Therapieansätze gegen die oben genannten Krankheiten zu entwickeln.

N-Acetylaspartat (NAA) ist ein wichtiger Metabolit in der Physiologie des Gehirns. Wir haben gezeigt, dass NAA in Fettzellen durch das mitochondriale Enzym N-acteyltransferase 8-like (NAT8L) gebildet und vom zytosolischen Enzym Aspartoacylase (ASPA) wieder abgebaut wird. Wir konnten ebenfalls zeigen, dass eine Veränderung des NAA Stoffwechsels in braunen Fettzellen Auswirkungen auf den Lipidstoffwechsel (Lipogenese und Lipolyse), die Genexpression und die zelluläre Atmung dieser Zellen hat. Im ersten Teil dieser Arbeit wird gezeigt, dass die Überexpression von *Nat8l* in braunen Adipozyten den Lipid- und Energiestoffwechsel über die Aktivierung der Triglyzerid-Hydrolase ATGL und des Transkriptionsfaktors PPARα reguliert. Der erhöhte metabolische Fluss durch den NAA Stoffwechselweg ist notwendig, um die Expression von UCP1 in diesen Zellen zu erhöhen. Außerdem konnte gezeigt werden, dass NAA eine Transportform für Acetyl-CoA vom Mitochondrium in das Zytosol darstellt. Zytosolisches acetyl-CoA beeinflusst den zellulären Stoffwechsel durch die Regulierung von Histon- und Proteinacetylierungen, wobei bisher das Enzym ATP-Citrat Lyase (ACLY) als Hauptlieferant für zytosolisches acetyl-CoA galt. Die Analyse von braunen Adipozyten, in denen *Nat8l* gesilenced wurde bzw. BAT von *Nat8l*-knock-out (*Nat8l*-ko) Mäusen zeigt, dass ACLY kompensatorisch hochreguliert ist. Außerdem konnte eine Verbindung des NAA Stoffwechsels mit der Regulierung der Histon / Proteindeacetylase Sirtuin 1 gezeigt werden. Daher ist es wahrscheinlich, dass der NAA Stoffwechsel die intrazelluläre Verteilung und Verfügbarkeit von Acetyl-CoA reguliert und dadurch den Energiestoffwechsel beeinflusst.

Im zweiten Teil dieser Arbeit wird gezeigt, dass der NAA Stoffwechsel durch verschiedene Faktoren wie Nährstoffverfügbarkeit, freie FAs, Insulinsekretion und β-adrenerge Stimulation beeinflusst wird. Die Analyse von NAA in *Nat8l*-ko Mäusen zeigt, dass NAT8L das Hauptenzym für die NAA Synthese ist. *Nat8l*-ko Mäuse auf Chow-Diät (CD) sind im Vergleich zu Wildtypen leichter und haben verringerte Blutglukosewerte (milde Hypoglykämie), die Glukosetoleranz bzw. die Insulinsensitivität ist unverändert. Der Gewichtsverlust über Nacht (ohne Futter), sowie

der Totalenergieverbrauch (EE) sind allerdings erhöht in *Nat8l*-ko Mäusen. *Nat8l*-ko Mäuse auf High-Fat Diät (HFD) nehmen im Vergleich mit den Kontrollmäusen weniger Gewicht zu und zeigen ebenfalls milde Hypoglykämie in Verbindung unveränderter Insulinsensitivität, aber erhöhte Glukosetoleranz. Der Gewichtsverlust über Nacht und EE sind erhöht in *Nat8l*-ko Mäusen im Vergleich zu Wildtypen. Interessanterweise verlieren *Nat8l*-ko Mäuse auf CD mehr Gewicht während Kälteexposition als *Nat8l*-ko Mäuse auf HFD, was darauf hindeutet, dass das Kohlenhydrat zu Lipid-Verhältnis in der Nahrung maßgeblich auf den Energiehaushalt dieser Mäuse wirkt.

Zusammenfassend wird in dieser Arbeit gezeigt, dass NAA ein wichtiger Metabolit und Regulator des gesamten Energiehaushalts ist und den Stoffwechsel von Fettzellen maßgeblich beeinflusst.

Table of contents

1. Introduction....2
   1.1. Socio-economic significance: obesity, type II diabetes mellitus, and the metabolic syndrome....2
   1.2. Different types and functions of adipose tissue – storage, thermogenesis, and beyond....3
      1.2.1. White adipose tissue – a physiological snapshot....3
      1.2.2. Brown and beige adipose tissue....4
      1.2.2.1. Molecular regulation of brown adipocyte development and function....6
      1.2.2.2. Therapeutic potential of brown adipose tissue....7
   1.3. The N-acetylaspartate (NAA) pathway from brain to brown fat....8
      1.3.1. NAA metabolism in brain....8
      1.3.2. NAA metabolism outside the central nervous system....11
      1.3.3. NAA and mitochondrial energy metabolism in neurons and adipocytes. 12
      1.3.4. NAA synthesis and breakdown and its connection to lipid metabolism in neurons and adipocytes....13
      1.3.5. NAA catabolism and histone / protein acetylation....15
   1.4. Thesis aim and model system....15
   1.5. Hypothesis....16
2. Materials and Methods....18
   2.1. Animal care....18
   2.2. Genotyping....18
   2.3. Cold Exposure....19
   2.4. Chronic adrenergic stimulation with CL 316,243....19
   2.5. Animal phenotyping....20
   2.6. Histological analyses and immunohistochemistry....20
   2.7. Measurement of lipolysis from organ explants....20
   2.8. Cell culture....21
   2.9. Respiration....22
      2.9.1. Set-Up for respiration measurement using the Strathkelvin Instruments 782 System....22
      2.9.2. Data analysis using the Strathkelvin Instruments 782 System....25
   2.10. Lipid staining and quantification....25
   2.11. RNA isolation, reverse transcription, and gene expression analysis....26
   2.12. Western blot analysis....27
   2.13. HPLC / HRMS....27
   2.14. ^{14}C-glucose incorporation and lipid extraction (DNL – de novo lipogenesis)....28

2.15. TG hydrolase activity assay 29
2.16. ^{3}H-fatty acid uptake 29
2.17. Measurement of lipid droplet associated lipolysis 29
2.18. ASPA activity assay 30
2.19. Statistical analysis 30
3. RESULTS I - The role of NAT8L in brown adipocyte lipid, glucose, and energy metabolism – *in vitro* studies 32
3.1. *Nat8l* overexpression in iBACs increases UCP1 levels and oxygen consumption rate in a PPARα-dependent manner 32
3.2. Lipolysis in *Nat8l* o/e iBACs 34
3.3. Inhibition of Sirtuin activity reduces *Pparα* and *Ucp1* expression in *Nat8l* overexpressing iBACs 35
3.4. ASPA activity in iBACs 36
3.5. Silencing of Aspa in *Nat8l* o/e iBACs reduces *Ucp1* expression 37
3.6. FA uptake upon *Nat8l* o/e and silencing in iBACs 38
3.7. The impact of *Nat8l* deficiency in vitro 38
4. RESULTS II – NAT8L deficiency in vivo – characterization of the total body *Nat8l*-knock-out mouse regarding its metabolic phenotype 42
4.1. NAA levels in tissue and serum of *Nat8l*-ko mice 42
4.2. Survival rate of *Nat8l*-ko mice compared to wt littermates 43
4.3. Initial body weight and blood parameters at the age of 8-9 weeks 43
4.4. Body weight, weight gain, and blood parameters during chow and high-fat diet feeding 44
4.5. Glucose tolerance and insulin sensitivity 46
4.6. *Nat8l*-ko mice loose more weight during overnight fasting than wt mice 49
4.7. Body length of *Nat8l*-ko mice is slightly reduced 49
4.8. Indirect calorimetry of wt and *Nat8l*-ko mice 50
4.8.1. Food intake, water intake, and locomotor activity 50
4.8.2. Oxygen (O_2) consumption 51
4.8.3. Carbon dioxide (CO_2) production 52
4.8.4. Respiratory exchange ratio (RER) 53
4.8.5. Energy expenditure (EE) 55
4.9. Terminal experiments at room temperature (RT) 57
4.9.1. Blood parameters, tissue weight, tissue oxygen consumption, and fatty acid / glycerol release from adipose tissue 57
4.9.2. Marker gene expression, morphology, and UCP1 protein expression in BAT 60
4.10. Terminal experiments – cold challenge 62

4.10.1. Acute cold exposure (4 °C for 48 hours) of 5 months old wt and *Nat8l*-ko mice on chow diet....62
4.10.1.1. Blood parameters, weight loss, and tissue oxygen consumption....62
4.10.2. 5 days cold exposure (4 °C) of 5 months old wt and *Nat8l*-ko mice on high-fat diet....63
4.10.2.1. Blood parameters, weight loss, and tissue oxygen consumption....64
4.10.2.2. Marker gene expression, morphology, and UCP1 protein expression in BAT..64
4.10.3. 9 days cold exposure (4 °C) of wt and *Nat8l*-ko mice on CD and HFD at the age of 9 months....65
4.10.3.1. Weight loss during 9 days of cold exposure (4 °C)....66
4.10.3.2. Blood parameters, tissue weight, tissue oxygen consumption, and fatty acid / glycerol release from adipose tissue....66
4.10.3.3. Marker gene expression, morphology, and UCP1 expression in BAT....70
4.11. Cardiac parameters of wt and *Nat8l*-ko mice....71
4.12. Body temperature of wt versus *Nat8l*-ko mice....73
5. RESULTS III – Investigation of the physiological regulation of NAT8L and ASPA *in vitro* and *in vivo*....75
5.1. *Nat8l* and *Aspa* expression in brain and adipose tissue of C57Bl/6J mice during aging....75
5.2. Regulation of *Nat8l* and *Aspa* expression in BAT of wt and *Nat8l*-ko mice on HFD and during cold exposure (4 °C)....76
5.3. Regulation of *Nat8l* and *Aspa* expression in adipose tissue of C57Bl/6 mice upon chronic β3-adrenergic stimulation....77
5.4. *Nat8l* and *Aspa* expression in response to glucose availability in vitro and in vivo..79
6. Discussion....83
6.1. The NAA pathway in brown adipocyte metabolism in vitro....83
6.2. The role of the NAA pathway in vivo – physiological triggers and the effects of NAT8L deficiency on energy homeostasis....92
6.2.1. Is NAT8L the sole enzyme to produce NAA?....92
6.2.2. Physiological regulation of the NAA pathway....92
6.2.3. NAT8L deficiency and reduced life span in mice....97
6.2.4. NAT8L deficiency and energy homeostasis in mice....98
6.2.5. NAT8L-deficiency and histone / protein acetylation....104
6.3. Summary and Outlook....105
7. References....107
8. Abbreviations....118
8.1. Nomenclature....120
9. Appendix....122
9.1. Publication list....122

1 - Introduction

1. Introduction

1.1. Socio-economic significance: obesity, type II diabetes mellitus, and the metabolic syndrome

The world´s society nowadays is confronted with numerous social, economic, and environmental issues. Many of these issues have been classified according to the groups they affect, e.g. poor or rich people, developing or industrial countries, or ethnic groups. However, despite all inequalities in our society according to e.g. distribution of goods, access to proper health care, and capital, an increasing number of overweight and obese people can be observed as a worldwide phenomenon. We actually already passed the point where suffering from overnutrition outpaced that from undernutrition[1]. This obesity-epidemic has been reported for decades and it has also been accepted that obesity does not comply with artificial geographic or social boundaries[2–5].

Obesity is characterized by excess accumulation of body fat mass[1]. According to the guidelines of the world health organization (WHO), overweight and obesity are classified by a body mass index (BMI[1]) greater than 25 and 35, respectively. However, BMI does not account for shape nor comprises fat to lean mass ratio. Although generally applied for a long time, recommendations were given that either BMI should be adjusted according to the ethnicity or other indicators such as waist to hip circumference ratio should be taken into account. However, regardless of the applied measures, the number of people classified as obese and overweight massively increased during the last 50 years.

Obesity is a major prerequisite for the progression of medical conditions such as insulin resistance, dyslipidemia, and hypertension, finally leading to comorbidities such as type 2 diabetes mellitus (T2D) and cardiovascular disease. Altogether, the co-occurrence of one or more risk factors and comorbidities is called metabolic syndrome[6]. Furthermore, obesity and T2D have been associated with the development and progression of different cancers such as hepatocellular carcinoma, pancreatic cancer, and colorectal cancer[7,8].

Another alarming factor is the reported impact of maternal or childhood obesity on the development of the medical conditions mentioned above during adolescence and adulthood, although the underlying mechanisms definitely need further investigation[9–11].

Given all these facts, it has to be expected that the number of people suffering from obesity, T2D, cardiovascular disease, and cancer together with increased lifespan will undoubtedly increase the need for long term medical care all over the world. Thus, suffering from metabolic syndrome does not simply reflect a personal problem of the aggrieved party but constitutes a huge social and economic burden for our society[12–14].

[1] BMI = body weight (in kg) / (body height (in m))^2

Different approaches such as increasing energy dissipation *versus* intake (dietary restriction, exercise), healthy nourishment, and overall increasing health status (stop smoking, enough sleeping hours, etc.) have been reported as possibilities to counteract obesity. However, e.g. twin studies[15,16] and lastly the discovery of hormones such as leptin[17] impressively showed the significance of genes and genetics in the disposition to develop obesity. Hence, understanding the genetics of obesity is valuable to find new therapeutic approaches to sustainably counteract the global epidemic and with it the metabolic syndrome.

1.2. Different types and functions of adipose tissue – storage, thermogenesis, and beyond

Adipose tissue function is a central factor when it comes to assess the development, progression, and treatment of the metabolic syndrome. Different adipose tissue depots comprise diverse functions such as storage of nutrients, protection (detoxification) and insulation as well as release of hormones, thereby actively contributing to whole body lipid, glucose, and energy homeostasis[18]. The following section aims to give a brief overview on the different types of adipose tissues and their versatile functions.

1.2.1. White adipose tissue – a physiological snapshot

The first classical type of adipose tissue is the so called white adipose tissue (WAT). WAT plays a major role in nutrient homeostasis as it is the main site where nutrients are deposited as triglycerides (TG), when excess calories are available. WAT adipocytes are characterized by containing a single large lipid droplet and only few mitochondria (Figure 1). During periods of fasting, WAT serves as the main energy supply by providing free fatty acids released by breakdown of TG, a process referred to as lipolysis.[18–20]

Beyond the function as energy deposit, WAT serves as an endocrine organ for the secretion of autocrine, paracrine, and endocrine factors, collectively called adipokines. The discovery of major adipokines such as leptin[17], adiponectin[21], and tumor necrosis factor (TNF)-α[22] from the mid 1990´s led to an impressive interest in WAT endocrine function. It has become clear that adipokines are directly or indirectly engaged in a variety of physiological and pathophysiological processes such as inflammation, obesity, insulin resistance, cardiovascular disease, and cancers.[7,23–25]

Furthermore, WAT composition and morphology is dramatically remodeled in response to available nutrition, e.g. alterations in immune cell type and number, increasing adipocyte cell size (hypertrophy) and number (hyperplasia) during prolonged overnutrition. Adipocyte hypertrophy provides a safety mechanism to clear nutrients from the circulation and aims to prevent ectopic lipid accumulation in non-adipose tissues. Unfortunately, this safety mechanism is limited and an overload of WAT storage capacity in obese individuals leads to WAT

dysfunction. Consequently, increased circulating lipids (dyslipidemia) and glucose (hyperglycemia) can be observed, finally promoting the development of obesity related comorbidities such as insulin resistance, T2D, fatty liver disease, and atherosclerosis.[19,20]

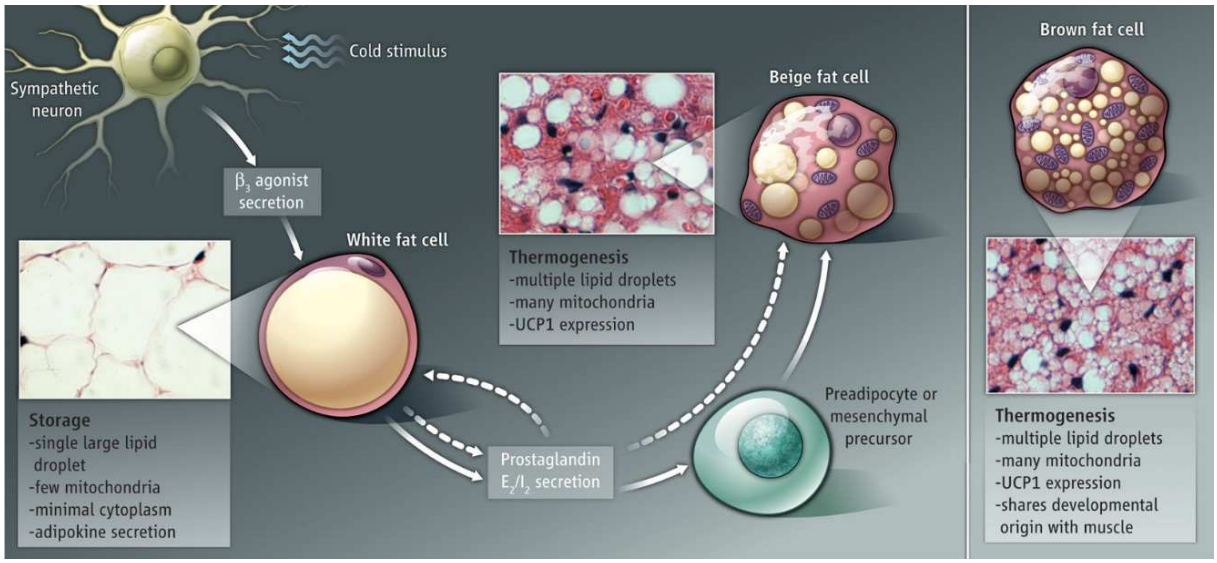

Figure 1. **The different types of fat cells.** Fat cells can be classified as white storage cells, brown thermogenic cells, or intermediate beige cells.[26]

Many different white adipose depots have been described in mice[27] and men[28]. The most common classification differs between visceral and subcutaneous white adipose tissue. This categorization might be oversimplified as there are more distinguishable depots within these two groups and there are substantial differences between fat depots in mice and their corresponding counterparts in humans. Recently, another model of adipose tissue has been proposed considering the different adipose depots as one interconnected adipose organ[29]. However, different adipose depots have been linked with different roles in energy homeostasis. In fact, visceral WAT such as mesenteric and epididymal / gonadal adipose tissue is well known for its association with metabolic disease. In contrast, subcutaneous WAT such as inguinal WAT has been reported to have even an inverse correlation with disease risk.[30] In this thesis, epididymal WAT (eWAT) and subcutaneous inguinal WAT (sWAT) from mice has been investigated as representative for visceral and subcutaneous WAT, respectively.

Taken together, WAT is not just simply a dynamic stockyard. It rather has to be seen as a center of energy homeostasis in health and disease.

1.2.2. Brown and beige adipose tissue

In addition to WAT, brown adipose tissue (BAT) has been reported as the second classical fat type. Similar to white adipose cells, brown adipocytes are also able to store and release lipids, but they contain many small lipid droplets (Figure 1). The major difference is that brown adipocytes have plenty of mitochondria highly enriched with uncoupling protein 1 (UCP1)[31]. UCP1 enables brown adipocytes to uncouple substrate oxidation from ATP synthesis thereby

producing heat, a process referred to as thermogenesis. Classic brown adipocytes are found in distinct depots of BAT located e.g. in the interscapular, axillary, and perirenal region in rodents[27]. BAT is highly innervated and norepinephrine released from neurons of the sympathetic nervous system activates thermogenesis during e.g. cold[32]. Furthermore, BAT is highly vascularized to provide sufficient and fast heat distribution into circulation[33].

The fact that BAT is an important tissue to regulate lipid, glucose, and energy metabolism in mice has been known for more than 10 years[34]. In addition to rodents, also human infants have significant amounts of BAT to support thermoregulation e.g. after birth[35,36]. Further, a discrete population of adults was shown to possess significant amounts of BAT, expectedly because of chronic cold exposure[37]. A very recent study also demonstrates BAT in children[38]. However, it was thought that BAT gets "lost" during adolescence and no functional BAT remains until adulthood[39].

In the year 2007, Cannon and Nedergaard published the first report on the existence of significant amounts of functional BAT in human adults[40]. Data from patient scans for cancer diagnosis using ^{18}F-fluoro-2-deoxy-d-glucose (^{18}F-FDG) positron emission tomography (^{18}F-FDG-PET) imaging finally led to the rediscovery of UCP1-positive adipose tissue consistent with brown fat in adult humans[41–44]. The most prominent BAT depots in adult humans are located in the supraclavicular and spinal region[42]. This might not necessarily reflect the whole entity of brown fat in humans, as ^{18}F-FDG-PET only detects glucose uptake and BAT is suggested to function as a "sink" for many more kinds of substrates. Recent studies also demonstrated high plasticity of human BAT. BAT mass e.g. increases during cold exposure[45,46], and negatively correlates with age[47] and BMI[48]. Hence, a comprehensive method to specifically detect all BAT depots in humans still has to be developed.

In addition to classical brown adipocytes, there is another brown-like fat cell type expressing UCP1 which can be found in WAT depots. These cells have been named "brite"[49] (for "brown-in-white") or "beige"[26] adipocytes (Figure 1). Beige adipocytes can be detected preferentially in subcutaneous WAT depots when animals have been exposed to cold or other inducers (Figure 2). Hence, beige adipocyte formation is a highly inducible process and the dependency on external stimuli for UCP1 induction is a distinct feature of these cells. The process of UCP1 induction in WAT depots is referred to as "browning" and was already reported in 1984 in rodents by Young et al.[50].

In contrast, brown adipocytes express high amounts of UCP1 even under unstimulated conditions. Upon stimulation, also classical BAT has an enormous ability to activate and increase its thermogenic capacity and mass. Therefore, the effect of browning of WAT *versus* increased thermogenesis in BAT on energy balance is highly debated. However, both brown and beige adipocyte activation / recruitment has been associated with improvements in e.g. diet induced obesity and T2D (reviewed in[19,51–53]).

Of note, whereas brown adipocytes in infants seem to be similar to classical brown adipocytes in mice[54,55], UCP1-positive cells in human adults have been reported to share more of their molecular signature with murine beige adipocytes[56,57]. However, this does not exclude the existence of classical BAT in human adults as fat depots containing UCP1-positive cells are likely to include both beige and brown adipocytes.

This work has been focused on BAT biology. Hence, the following sections comprise the most important facts about the molecular regulation of adipogenesis, metabolic function, and therapeutic potential of classical BAT.

1.2.2.1. Molecular regulation of brown adipocyte development and function

Adipogenesis, the developmental process from fibroblastic precursor cells to mature fat cells, is highly controlled and many molecular regulators have been identified until today. Although brown and white adipocytes have distinct developmental origins, they share some initial steps in differentiation (reviewed in[19,58]). One central and initial member of adipogenesis is peroxisome proliferator-activated receptor gamma (PPARγ), also referred to as the “master-regulator” of adipogenesis. PPARγ interacts with three CCAAT/enhancer-binding protein family members (C/EBP-α, -β, and –δ) to promote the transcriptional cascade needed for both brown and white fat cell development[59].

More important regulators to promote and maintain differentiation of precursor cells to mature brown adipocytes such as PPARα, PPARγ coactivator 1-alpha (PGC1α), PRD1-BF-1-RIZ1 homologous domain containing protein 16 (PRDM16), euchromatic histone-lysine N-methyltransferase 1 (EHMT1), Zinc finger protein 516 (Zfp516), and placenta specific 8 (PLAC8) protein, have been identified (reviewed in[20,58,60,61]). Despite these early developmental brown markers, expression analysis of brown vs. white adipocytes has been used to identify many more markers with enriched expression and of important function in brown adipocytes, e.g. cell death-inducing DNA fragmentation factor-α-like effector A (*Cidea*, a lipid droplet associated protein[62,63]) and type 2 iodothyronine deiodinase (*Dio2*, a component in the thyroid-sympathetic synergism required for thermal homeostasis in mice[64]).

The main function of mature brown adipocytes is to perform high rates of lipid and glucose oxidation upon thermogenic activation. So far, numerous studies identified a variety of signaling pathways and endocrine factors that increase BAT activity (Figure 2). Beside their role in brown adipogenesis, PPARα and PGC1α have special functions in regulating thermogenic activation in brown adipocytes. It has been shown that fatty acids derived from lipolysis activate PPARα, further leading to induction of oxidative genes such as *Pgc1α*, *Pdk4*, *Cpt1b* and most importantly *Ucp1*[65–68]. Recent studies also suggest PPARα activation by its agonist fenofibrate as a potent mechanism to promote browning of WAT[69] and to activate thermogenic gene expression in BAT[70]. PGC1α has been recognized as an essential player in activating

mitochondrial biogenesis and transcription during cold or β-agonist-induced thermogenic activation of brown adipocytes[71]. Specifically, PGC1α expression and activity is directly regulated by the β-adrenergic signaling pathway in brown adipocytes[72]. Activated PGC1α regulates the expression of thermogenic genes through its interactions with PPARα and PPARγ (reviewed in[51]) Hence, PGC1α provides a direct link between the physiological activator of thermogenesis and the transcriptional machinery in brown adipocytes. Therefore, PPARα and PGC1α have been referred to as master regulators of fatty acid oxidation and mitochondrial biogenesis, respectively.

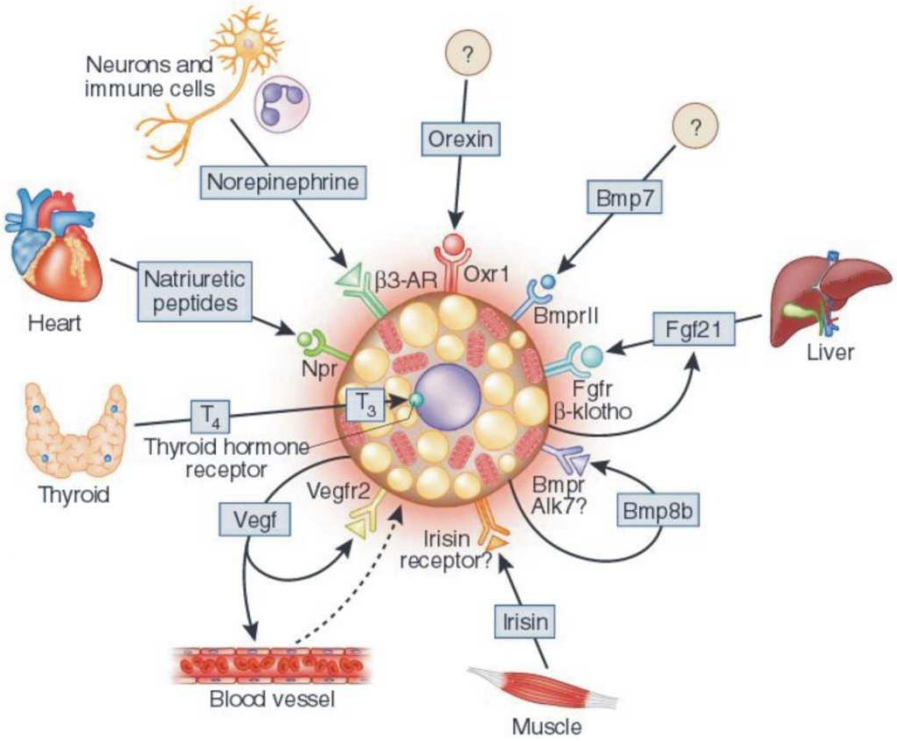

Figure 2. **Secreted factors that recruit brown adipocytes, beige adipocytes, or both (by Debbie Maizels).** In rodents, a number of tissues and cell types have been found to secrete factors that regulate brown and beige adipose activity through systemic, autocrine and paracrine mechanisms. Neurons and alternatively activated macrophages secrete norepinephrine; cardiac tissue secretes natriuretic peptides; liver and BAT secrete Fibroblast growth factor 21 (Fgf21); muscle secretes irisin; and thyroid secretes the hormone T4 (which is then converted to T3). BAT also produces bone morphogenic protein (Bmp)-8b and vascular endothelial growth factor (Vegf), which increase thermogenic function in an autocrine manner. Additionally, orexin and Bmp7 promote brown fat development, but their cellular source is unknown. Oxr1, oxidation resistance 1; Alk7 (also called Acvr1c, activin A receptor type 1C).[51]

1.2.2.2. Therapeutic potential of brown adipose tissue

With its re-discovery in adult humans, BAT has gained a lot of scientific interest in terms of its role in whole body lipid, glucose, and energy metabolism. The main question is if activation of BAT is feasible to prevent e.g. body weight gain and reverse metabolic abnormalities such as T2D? BAT has been reported to significantly contribute to whole body energy homeostasis in mice and men. Upon activation, BAT serves as a metabolic “sink” for many substrates including

glucose and fatty acids, thereby actively contributing to e.g. lipid and glucose clearance from the circulation (reviewed in[51,52,73]).

In rodents, several studies reported beneficial effects on whole body lipid, glucose, and energy metabolism by increasing BAT recruitment and activity (reviewed in[55,51]). Accordingly, it has been clearly demonstrated that cold acclimation promotes recruitment of BAT and increases postprandial insulin sensitivity also in adult humans[45,74,75]. Hence, β-adrenergic signaling upon cold exposure is the most prominent pathway to activate BAT thermogenesis in rodents and in humans. Consequently, different β-adreno receptor agonists such as natriuretic peptides, norepinephrine, and fibroblast growth factor (FGF) 21 have been tested for their ability to increase BAT activity in humans. However, adverse side effects on the cardiovascular system or sympathetic nervous system have hampered the clinical use of these activators (reviewed in[76]). Also nutritional compounds such as capsinoids have been shown to increase BAT mass and activity in humans[45,77].

Not only recruitment of BAT might be a valuable approach to increase energy expenditure in humans, but also directly targeting UCP1 using small molecules and synthetic agonists or inhibitors (reviewed in[73]). Further, identification of novel metabolic pathways in brown adipocytes provides opportunities to target and manipulate BAT metabolism on a molecular level. Hence, knowledge of the regulatory circuits controlling BAT recruitment and activity is constantly growing, but is not yet completed.

In conclusion, further investigation on BAT biology is needed to finally yield sustainable therapeutics. However, BAT is a valuable target to counteract obesity and its comorbidities such as insulin resistance, T2D, and cardiovascular disease.

1.3. The N-acetylaspartate (NAA) pathway from brain to brown fat

N-acetylaspartate (NAA) is the second most abundant metabolite in brain. The levels of NAA have been reported to reach 10 mM and higher in specific brain areas[78–80]. NAA has been used as a biomarker for brain health as NAA provides the largest single peak on spectra determined by proton magnetic resonance spectroscopy. NAA levels were found to be reduced in a majority of neuropathologies such as ischemic stroke, Alzheimer´s disease, epilepsy, multiple sclerosis, traumatic brain injury, and even brain cancer. Further, NAA serves as a precursor for the neurotransmitter N-acetylaspartylglutamate (NAAG). Several studies also reported NAA as an important metabolite in neuronal osmoregulation, lipid synthesis, and energy metabolism in neuronal mitochondria (reviewed in[81,82]).

1.3.1. NAA metabolism in brain

NAA is synthesized from L-aspartate (L-Asp) and acetyl coenzyme A (acetyl-CoA) by a membrane bound enzyme referred to as L-aspartate N-acetyltransferase[83–85] (Asp-NAT;

enzyme commission (EC) number: EC 2.3.1.17). In 2010, two studies reported that the gene *N-acetyltransferase 8-like* (*Nat8l* / *Shati*) encodes for Asp-NAT and that NAT8L protein is the enzyme responsible for NAA synthesis[86,87]. Therefore, the *Nat8l* / *Shati* gene will be referred to as *Nat8l* and NAT8L will be used to refer to Asp-NAT in this thesis. The coding sequence of *Nat8l* is comprised of 3 exons in the *Nat8l* gene (NM_001001985) located on mouse chromosome 5 (human chromosome 4)[86]. The *Nat8l* gene encodes a 33 kilo Dalton (kDa) protein (299 amino acids). A structural model proposed the presence of a membrane anchor domain and two hydrophilic arms that build up the sight for catalytic action of NAT8L[88]. Mammalian orthologues of NAT8L show high homology[89].

It is widely accepted that neurons are the primary place for NAA synthesis in brain. Interestingly, there is still controversy about the subcellular localization of NAT8L. It is highly debated whether NAT8L localizes to mitochondria and / or the ER and which cellular compartment is the main place of NAA synthesis in neurons[86,88,90–93]. A recent study by Toriumi et al.[94] reported Flag-NAT8L co-localization with endoplasmic reticulum. Another recent report determined higher NAA levels in mitochondria of neurons compared to cytosol measured by immune-electron microscopy, arguing for mitochondrial synthesis of NAA[95].

NAA is not metabolized in neurons but gets transported to oligodendrocytes (myelin forming cells) by a mechanism that may involve the sodium coupled high-affinity carboxylate transporter NaDC3 (SLC13A3[96,97]). Aspartoacylase (ASPA; EC 3.5.1.15; synonyms: aminoacylase II, N-acetyl-L-aspartate amidohydrolase), a nucleo-cytosolic protein in oligodendrocytes[98], specifically deacetylates NAA to yield acetate and L-Asp (enzymatic activity first described by Birnbaum et al.[99]). Of note, ASPA activity has also been found in purified myelin membrane fractions[100]. The *Aspa* gene is organized in 10 exons (NM_023113) located on mouse chromosome 11 (human: 9 exons, chromosome 17) (Source: http://ncbi.nlm.nih.gov/gene; February 2016). The *Aspa* gene encodes a 35 kDa protein (312 amino acids) (Source: http://www.uniprot.org; February 2016). The structure of ASPA has been described by Bitto et al.[101].

Finally, acetate released by ASPA is used to form acetyl-CoA[102] by acetyl coenzyme A synthetase (ACSS) activity[103]. This acetyl-CoA has been shown to be used for myelin lipid synthesis (reviewed in[82]). Acetyl-CoA is a universal metabolic carbon source and connects energy derivation, storage, and utilization. Further, acetyl-CoA dependent acetylation regulates protein function, enzyme activity, transcription factor signaling, and gene transcription (reviewed in[104]). So far, it is not entirely understood, how NAA and brain energy metabolism are connected, but it seems likely that this connection is established via NAA derived acetate / acetyl-CoA. A scheme of NAA metabolism and metabolic interconnection between neurons, oligodendrocytes, and astrocytes in brain is shown in Figure 3.

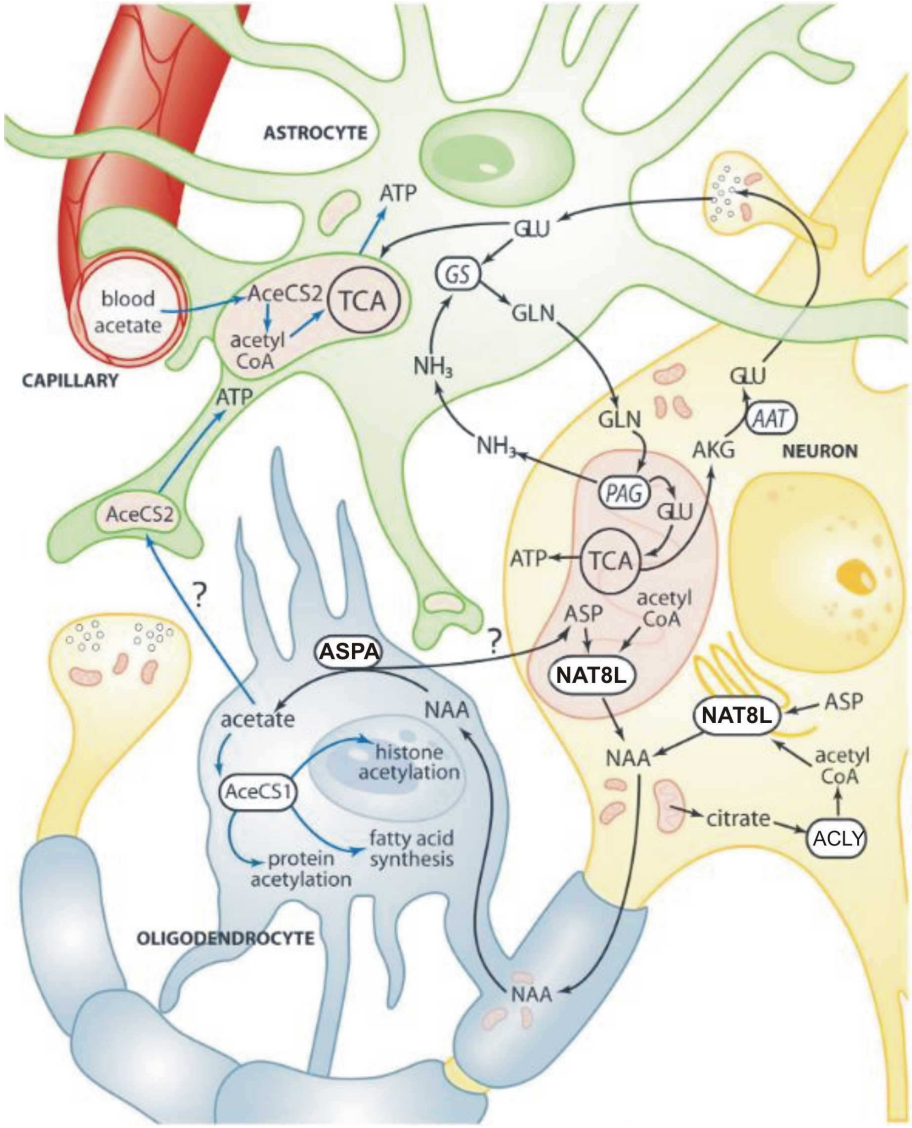

Figure 3. **Scheme of NAA metabolism and metabolic interconnection between neurons, oligodendrocytes, and astrocytes in brain**. A major metabolite cycle exists between neurons and oligodendrocytes via NAA that is transferred from axons to oligodendrocytes at axo-glial contact zones between the innermost oligodendrocyte plasma membrane in a myelin segment and the axonal membrane. ASPA in the oligodendrocytes generates free acetate which can then be converted to acetyl CoA by AceCS1, which can then go on to be utilized for fatty acid synthesis, cytoplasmic protein acetylation reactions, and nuclear histone acetylation (blue lines). It is possible that some acetate derived from NAA in oligodendrocytes is transferred to astrocytes for energy derivation through the enzyme AceCS2 present in mitochondria in astrocyte end feet and cellular contact zones. It is also possible that some NAA-derived aspartate in oligodendrocytes is recycled back to neurons. AAT, aspartate aminotransferase; AceCS1, acetyl CoA synthase-1; AceCS2, acetyl CoA synthase-2; AKG, α-ketoglutarate; ASP, aspartate; ASPA, aspartoacylase; ACLY, ATP citrate lyase; GLN, glutamine; GLU, glutamate; GS, glutamine synthase; NAT8L, N-acetyltransferase 8-like; NH3, ammonia; PAG, phosphate activated glutaminase. (adapted from Moffett et al.[82])

Defective NAA metabolism has also direct pathological consequences leading to two inborn diseases in humans. The first, deficiency of ASPA, leads to a leukodystrophy named Canavan disease (reviewed in[105]) which is characterized by dystonia (a neurological movement disorder), severe mental defects, blindness, megalencephaly, and death at an average age of 18 months[106]. Of note, NAA levels are increased in brain, cerebrospinal fluid and urine of these patients. The *Aspa*-knock out (*Aspa*-ko) mouse[107] and the tremor rat[108] are the two described

animal models of Canavan disease. Similar to humans, *Aspa*-ko mice lack ASPA activity, suffer from severe neuropathologies, show increased NAA levels in their urine, and die within the first 4 weeks of life[81,109].

The second disorder named hypoacetylaspartia is promoted by a mutation in the *Nat8l* gene leading to dysfunctional NAT8L, and consequently loss of NAA in brain[86]. Reduced myelination, truncal ataxia ("drunken sailor" syndrome), marked developmental delay, seizures, and secondary microcephaly are characteristics of this disease[110,111]. *Nat8l*-knock out (*Nat8l*-ko) mice described by Furukawa-Hibi et al.[112] are viable. These mice show reduced social interaction in unfamiliar environment, increased rearing and grooming time in the open field test, and increased exploration time of new objects. Interestingly, there was no reduced social interaction when *Nat8l*-ko mouse were tested in their homecage. Recently, Toriumi and colleagues reported that locomotor activity was increased in *Nat8l*-ko compared to wild-type (wt) mice[94]. It has been suggested for a long time that both loss and accumulation of NAA lead to demyelination and consequently promote neuropathologies (reviewed in[81]). However, *Nat8l*-ko mice show normal myelination whereas *Aspa* deficiency leads to demyelination and premature death of about 70 % of *Aspa*-ko mice compared to controls[109]. Further, *Nat8l* / *Aspa*-double-ko mice show normal myelination which indicates that defective NAA catabolism in brain is the major cause of myelination defects and premature death[109,113]. However, none of these reports give data on how defective NAA metabolism affects whole body energy homeostasis in mice.

1.3.2. NAA metabolism outside the central nervous system

Early studies reported that NAA synthesis was not detectable in peripheral tissues such as kidney and mammary gland, but specifically in brain[114]. Conversely, also other tissues than brain including kidney, liver, heart, and mammary gland were able to catabolize NAA[102,115]. It was further observed that NAA was taken up very fast and metabolized to CO_2 in kidney, whereas brain and mammary gland took up NAA and converted it into lipids. These studies were the first to support the idea, that NAA could be used for either energy production or lipid synthesis. Further, chromatographic analyses of different tissue extracts indicated that NAA concentration is at least 100-fold lower in non-neural tissues[79]. Hence, these data implied that NAT8L expression was highly specific to neurons, whereas ASPA is also expressed in peripheral tissues.

Against this hypothesis, our group reported similar expression levels of both *Nat8l* and *Aspa* in murine eWAT and BAT (Pessentheiner & Pelzmann et al.[116] and Prokesch & Pelzmann et al.[117]). In brown adipocytes, we found NAT8L and ASPA protein localized to mitochondria[116] and cytoplasm[117], respectively. We showed that *Nat8l* mRNA was downregulated in eWAT and BAT of genetically obese (ob/ob) mice. Furthermore, expression analyses of eWAT and BAT from *Atgl* and *Hsl* knock-out mice revealed that *Nat8l* was also downregulated when compared to

controls[118]. ATGL and HSL are the main enzymes for TG hydrolysis and deficiency of ATGL or HSL *in vivo* significantly impairs lipid, glucose and energy metabolism in these mice[119–121].
These results have been the first arguing for autonomous consecutive NAA synthesis and breakdown also in peripheral tissues. Recent studies further support the idea of an important role of NAT8L and NAA synthesis outside the CNS. Huang et al.[122] connected NAT8L to vascular endothelial cell autophagy. Two more reports by Lou et al.[123] and Zand et al.[124] linked increased *Nat8l* gene expression and NAA concentrations to lung and ovarian cancer, respectively. Hence, all these data further support the idea that a connection between NAA and energy homeostasis exists and might be established via NAA-derived acetate / acetyl-CoA.

1.3.3. NAA and mitochondrial energy metabolism in neurons and adipocytes.

Although the function of the NAA pathway in mitochondrial energy homeostasis is not clear, evidence for an important role of NAA metabolism in mitochondrial function in brain and adipose tissue is increasing. Namboodiri et al. proposed a multifunctional model of NAA metabolism involving its synthesis in neuronal mitochondria and endoplasmic reticulum[82]. This model is mainly based on the connection between NAA and acetyl-CoA metabolism in brain. For example, traumatic brain injury (TBI) provokes an energy crisis[125] and NAA, ATP, and acetyl-CoA levels have been shown to be reduced correlated with injury severity and their levels return with recovery[126,127]. Hence, acetyl-CoA available for NAA synthesis might be reduced or NAA as a storage form for acetate might be degraded due to need of acetyl-CoA for energy production and repair mechanisms. In addition, the synthesis of NAA also requires L-Asp. Aspartate aminotransferase (AAT) converts oxaloacetate and glutamate to L-Asp and α-ketoglutarate (α-KG). It has been reported that AAT activity is also reduced in response to TBI[128]. Hence, this would limit NAA synthesis from L-Asp and α-KG synthesis from glutamate, thus reducing the brain´s capacity to generate energy. This introduces glutamine availability as an additional parameter for providing metabolites for NAA synthesis.
Recently, Sumi et al. provided further evidence for a direct influence of NAA synthesis on neuronal energy metabolism, as they reported that adenoviral overexpression of *Nat8l* in cultured neurons increased ATP content[129].
In accordance with the proposed important connection of NAA and energy metabolism, we showed that NAT8L is highly expressed in mitochondria whereas ASPA is expressed in the cytoplasm of brown adipocytes[116,117]. Of note, it has been proposed that the metabolic connection between neurons and oligodendrocytes / astrocytes is similar to what is established between mitochondria and the cytoplasm in other cell types[130]. A scheme of NAA metabolism in mitochondria and the cytoplasm is shown in Figure 4.

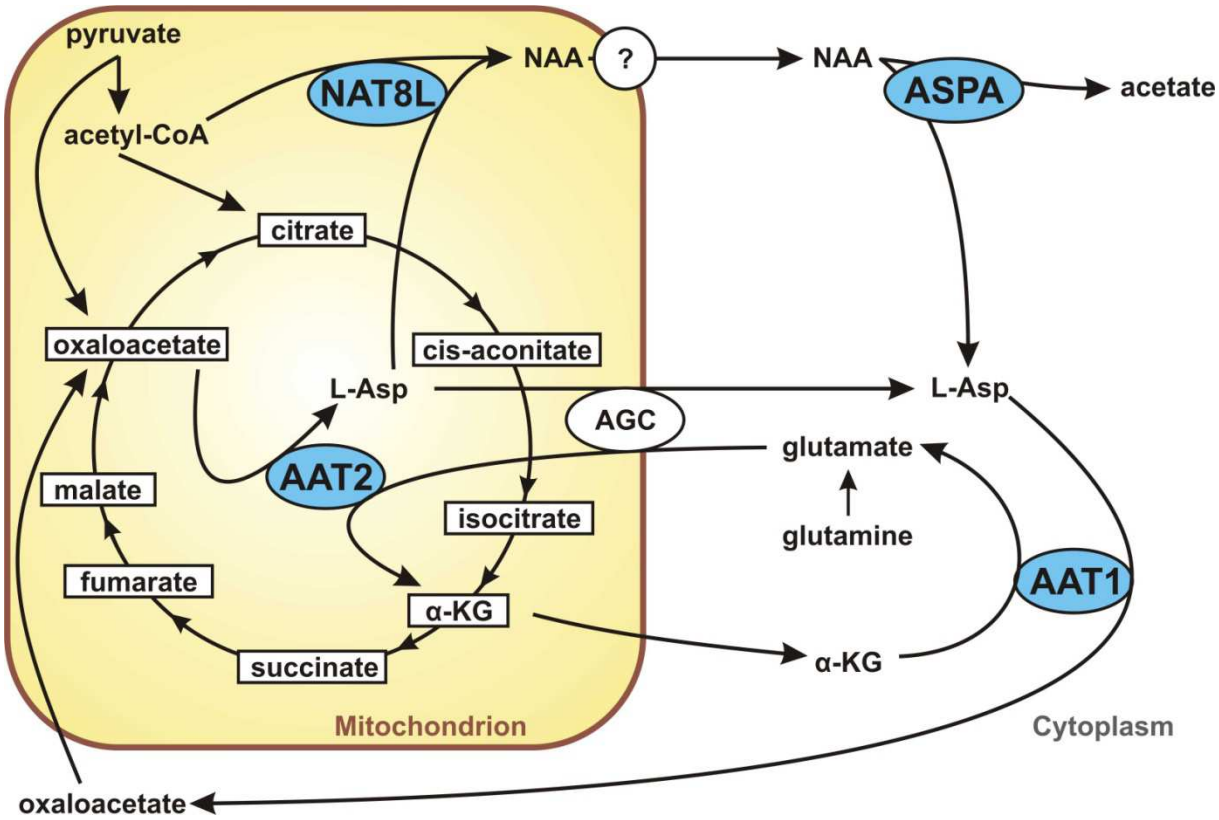

Figure 4. **Scheme of NAA metabolism and its connection to the TCA cycle.** NAA is synthesized from acetyl-CoA and aspartate (L-Asp). Aspartate aminotransferase (AAT) 2 utilizes glutamate and oxaloacetate to form L-Asp and α-ketoglutarate (α-KG) in mitochondria. Aspartoacylase (ASPA) catalyzes NAA breakdown in the cytoplasm to yield acetate and L-Asp. AAT1 utilizes α-KG and L-Asp to form oxaloacetate and glutamate in the cytoplasm. AGC, mitochondrial aspartate-glutamate carrier; NAT8L, N-acetyltransferase 8-like; NAA, N-acetylaspartate. (adapted from Moffett et al.[82])

1.3.4. NAA synthesis and breakdown and its connection to lipid metabolism in neurons and adipocytes

NAA is not a primary source of acetyl-CoA. The synthesis of NAA already requires the utilization of existing acetyl-CoA, therefore NAA might be a storage and transport form for acetate. Subsequently, this acetate moiety can be converted to acetyl-CoA, which could, amongst others, be further used for lipid synthesis. Chakraborty et al.[131] reported incorporation of radioactive [^{14}C]-NAA into myelin lipids after intraocular injection in rats. NAA was shown to supply ~1/3 of acetyl-CoA required for myelin lipid synthesis during brain development, the remaining 2/3 being supplied by citrate[132].

Adipogenesis is a process which also requires high amounts of lipid synthesis, similar to myelination in brain. Our group found expression of *Nat8l* upregulated during adipogenesis of murine and human white and brown adipocyte cell lines[116]. We demonstrated that overexpression of *Nat8l* in brown adipocytes increases lipid turnover in these cells. Mature brown adipocytes show high metabolic rates which can even be increased upon β-adrenergic stimulation. Therefore, these cells need to perform high rates of lipogenesis and lipolysis. The balance between these two processes is very important for adipocyte energy homeostasis.

One way to provide FAs for TG stores in adipocytes is FA acid uptake from the circulation (reviewed in[133]). The second way is to generate FAs by *de novo* lipogenesis (DNL; reviewed in[134]) from acetyl-CoA derived by glycolysis. However, acetyl-CoA cannot pass the mitochondrial membrane. The canonical pathway to provide cytosolic acetyl-CoA is the formation of citrate, followed by its transport to the cytosol via the tricarboxylic anion carrier and subsequent production of acetyl-CoA by ATP citrate lyase (ACLY). Our recent studies show that the NAA pathway is a second way to provide cytosolic acetyl-CoA in adipocytes[117]. A scheme of brown adipocyte lipid, glucose, and energy metabolism is given in Figure 5.

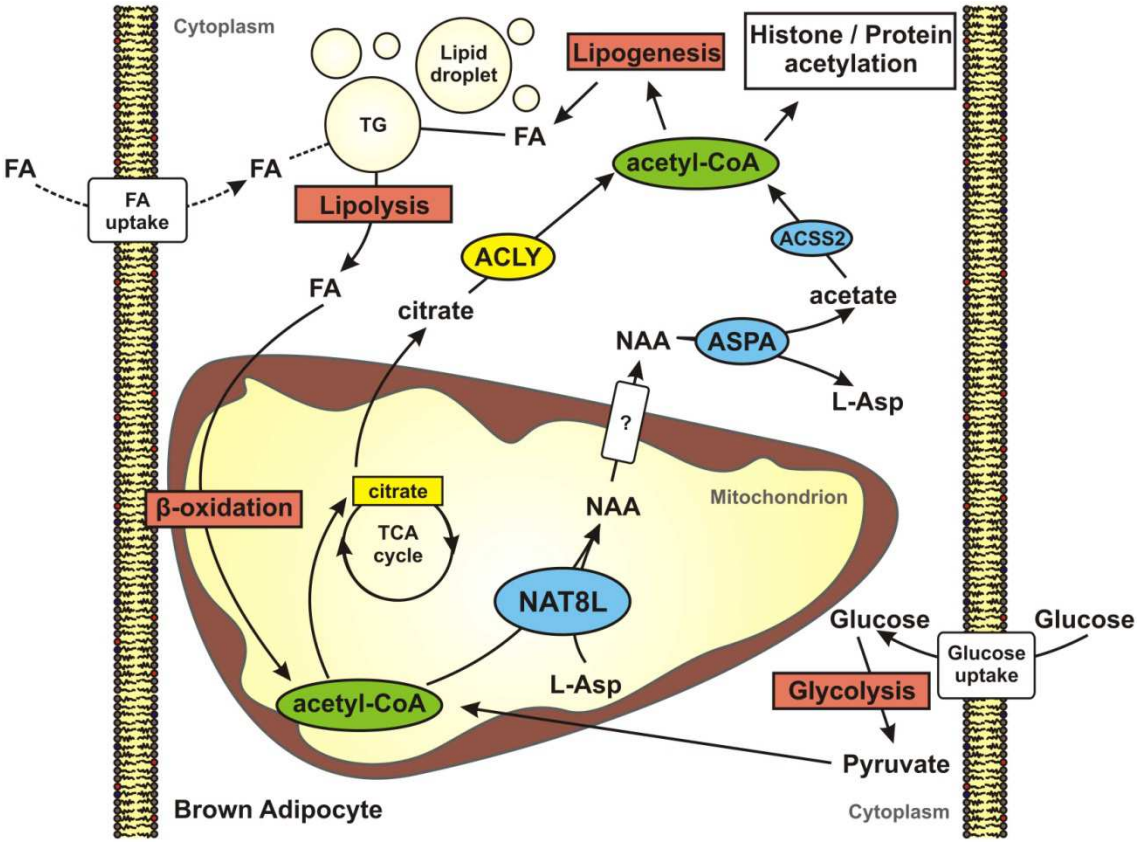

Figure 5. **Scheme of brown adipocyte lipid, glucose, and energy metabolism.** Mitochondrial acetyl-CoA is produced from glycolysis-derived pyruvate or from β-oxidation of fatty acids (FA) derived by lipolysis. Acetyl-CoA is used for citrate synthesis and can be used for energy production or transported to the cytoplasm. ATP citrate lyase (ACLY) produces cytoplasmic acetyl-CoA from citrate (highlighted in yellow). The NAA pathway (highlighted in blue) is a second pathway that provides cytoplasmic acetyl-CoA. Cytoplasmic acetyl-CoA can be used for *de novo* lipogenesis or histone and / or protein acetylation. Main anabolic / catabolic processes are highlighted in red. NAT8L, N-acetyltransferase 8-like; ASPA, Aspartoacylase; ACSS2, Acetyl coenzyme A synthetase 2; TG, triglyceride.

Upon β-adrenergic stimulation, adipocytes perform high rates of lipolysis. In each step of the lipolytic cascade, ATGL, HSL, and monoglyceride lipase (MGL) release one FA from TG, diacylglycerol, and monoacylglycerol, respectively[135]. As mentioned above, FA released by lipolysis can have signaling function (e.g. activation of transcription factors such as PPARα), be released into circulation (most important for white adipocytes), or re-esterified. Additionally and most important for brown adipocytes, FA can also be used for β-oxidation in mitochondria

yielding acetyl-CoA. Thus, acetyl-CoA for NAA synthesis might also be derived from oxidation of FA.

1.3.5. NAA catabolism and histone / protein acetylation

Histone acetylation controls chromatin-structure and DNA accessibility in eukaryotic cells, thereby regulating gene transcription. Wellen et al.[136] showed that histone acetylation impacts cellular metabolism. They reported that ACLY regulates acetyl-CoA availability, thereby impacting substrate supply and activity of histone acetyltransferases (HATs) and deacetylases (HDACs), respectively. Consequently, manipulation of HAT and HDAC enzyme activity regulates histone acetylation and gene transcription.

ACSS2 (EC 6.2.1.1), the enzyme converting acetate to acetyl-CoA has been reported to be localized in nuclei and cytoplasm of oligodendrocytes during brain development[137]. ACSS2 has been shown to provide acetyl-CoA for nuclear HATs involved in epigenetic gene regulation[138]. Of note, ASPA has also been reported to localize to the cytoplasm and the nucleus in oligodendrocytes[98]. Thus, ASPA and ACSS2 could be able to control acetyl-CoA availability used for histone and protein acetylation similar to ACLY. Importantly, our group recently linked NAA catabolism to epigenetic gene regulation[117] (see Figure 5). We showed that silencing of *Aspa* in brown adipocytes reduced histone acetylation and brown marker gene expression.

Acetylation and deacetylation of proteins is a reversible posttranslational modification which alters protein structure and function[139]. In return, these modifications can lead to changes of intermediary metabolites such as ATP, nicotinamide dinucleotide (NAD^+), and acetyl-CoA. These metabolites again function as direct substrates for posttranslational modifications. Lysine acetyltransferases (KATs) and deacetylases (KDACs) regulate reversible acetylation and deacetylation of proteins in mammals. Enzymatic activity of KATs and KDACs highly depend on cellular energy homeostasis (reviewed in[139]). A very prominent family of KDACs are the sirtuins (SIRTs) with its most prominent family member SIRT1 described to deacetylate and thereby activate important metabolic regulators such as PPARγ[140], PGC1α[141,142], and ACSS2[143].

Taken together, these data suggest that NAA-derived acetate provides acetyl-CoA for histone and / or protein acetylation.

1.4. Thesis aim and model system

The aim of this thesis is to describe the role of the N-acetylaspartate (NAA) pathway in adipocyte biology with special emphasis on brown adipose tissue glucose, lipid, and energy metabolism. Immortalized brown adipogenic cells (iBACs) overexpressing or silenced for *Nat8l* have been used as a model to investigate the impact *Nat8l* on energy metabolism *in vitro*. To investigate the effect of NAT8L on energy metabolism *in vivo, Nat8l*-knock-out (*Nat8l*-ko) mice have been characterized with regard to whole body lipid, glucose, and energy metabolism. The

physiological triggers for activation and / or inhibition of the NAA pathway will be discussed. Finally, our proposed model (Pessentheiner & Pelzmann et al.[116]; see also Figure 5) of the NAA pathway and its impact on adipocyte biology will be discussed and expanded to provide a good basis for further studies.

1.5. Hypothesis

We hypothesized that the NAA pathway provides an additional route to transport mitochondrial acetyl-CoA to the cytoplasm, thereby regulating mitochondrial / cytoplasmic acetyl-CoA availability and distribution in adipocytes. Acetyl-CoA is a central metabolite in energy homeostasis and metabolism. Therefore, it is reasonable that NAA synthesis and catabolism regulate adipose tissue physiology and thereby impacts whole body lipid, glucose, and energy homeostasis.

2 - Materials and Methods

2. Materials and Methods

2.1. Animal care

The *Nat8l*-ko mouse model has been originally described by Furukawa-Hibi et al.[112]. Unless otherwise specified, wt and *Nat8l*-ko mice (C57Bl/6J background) were kept in a standard temperature (23 – 25 °C) and humidity controlled environment with a 12 : 12 hour light-dark cycle. Mice had nesting material and *ad libitum* access to water and commercial chow diet (CD; CLEA Rodent Diet CE-2 for rearing and breeding – Japan; ssniff® #V1126 – Austria) or hight-fat diet (HFD; Research Diets Inc. #D12451 – Japan; ssniff® #E15744-34 acc. #D12451 – Austria) from indicated age.

All animal experiments were carried out according to national Japanese and EU ethical guidelines and approved by the local animal experimentation committee (Japan) and the Austrian Federal Ministry of Science, Research, and Economy, respectively.

2.2. Genotyping

DNA was extracted from tail-tips by adding 50 µL Direct-PCR Tail buffer (VWR International GmbH, Erlangen, GER) and 1.5 µL proteinase K (20 mg / mL stock, Carl Roth GmbH, Karlsruhe, GER) followed by incubation in thermomixer (56 °C / 1300 rpm / 90 minutes). Subsequently, samples were briefly vortexed and again incubated in thermomixer (85 °C / 600 rpm / 45 minutes). Tail-tip PCR reactions (were performed using PrimeSTAR® HS DNA Polymerase (TaKaRa Bio Inc., Kusatsu, JP) as shown in Table 1 and Figure 6.

Table 1. **Reaction composition for *Nat8l*-tail-tip PCR.**

Reagent	**Concentration**	**µL per reaction**
PrimeSTAR Buffer (Mg^{2+}) (supplied by TaKaRa)	5x	2.5
dNTP-Mixture (supplied by TaKaRa)	2.5 mM	1.0
PrimeSTAR® HS DNA Polymerase	1.25 units / 25 µL	0.125
Primer-Mix	20 µM	1.0
Sample		1.0
dH_2O		7.375
Total		13.0

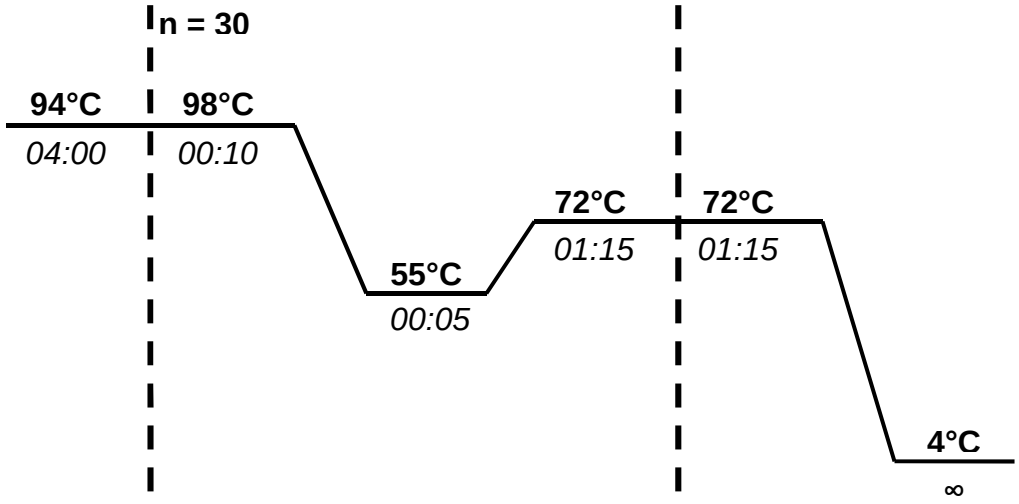

Figure 6. **PCR-program for tail-tip PCR of *Nat8l*-ko mice.**

Primer-mix was prepared from the following *Nat8l*-tail-tip-PCR (One part from primer 1 and 3 and two parts from primer 2; 20 µM final concentration):

Primer 1 (*Nat8l*-ko_WT_Fw):	CTATGAGTCACTGGGCTTCAGAC
Primer 2 (*Nat8l*-ko_WT_Rv):	TGTTGTAGAGGTTCTGTGCTTGAT
Primer 3 (*Nat8l*-ko_NEO_Fw):	CGGAGAACCTGCGTGCAATCCATCTTGTTC

Final PCR products were separated using a 1 % agarose gel (electrophoresis at 105 V / 400 mA for 45 minutes). Bands were detected at a length of 504 bp and 972 bp for wt and ko, respectively.

2.3. Cold Exposure

Animals on CD and HFD were challenged by cold exposure (4 – 8 °C) for a period of at least 48 hours and up to 9 consecutive days. Rectal body temperature was monitored every 30 minutes within the first 12 hours of cold challenge, followed by control measurements every 6 – 12 hours. Mice were removed from the experiment if they were not able to acclimate or sustain the cold challenge (drop of body temperature below 31°C).

2.4. Chronic adrenergic stimulation with CL 316,243

The β3-adreno receptor agonist CL 316,243 was administered to a one cohort of male C57Bl/6J at the age of 13 weeks by intraperitoneal injection on 8 consecutive days (1 mg / kg per day; 7.30 – 8.00 a.m.). Control mice were simultaneously injected same amounts of sterile saline. A second cohort at the age of 10 – 12 weeks was infused for 7 days using subcutaneously implanted osmotic minipumps (0.75 nmol / hour; Alzet 2001; Alzet® osmotic minipumps, Cupertina, CA, USA) and controls were left untreated.

2.5. Animal phenotyping

All clinical tests were carried out according to the guidelines from the Federation of European Laboratory Animal Science Associations (Felasa). Mice were weighted and food consumption was measured weekly on the same day. Oxygen consumption (VO_2), carbon dioxide production (VCO_2) and respiratory exchange ratio (RER) was monitored by indirect calorimetry using metabolic cages MK-5000RQ (Muromachi Kikai, Tokyo, JP) with a five minute measurement interval. Energy expenditure (EE) was estimated using VO_2 and VCO_2 values in the following equation: EE (cal / min) = (3.98 x VO_2) + (1.07 x VCO_2). Food intake and activity was also measured during a period of 24 hours. Glucose or insulin tolerance was assessed by intraperitoneal injection of 1.5 g / kg glucose or 0.5 U insulin / kg (human insulin 10 mg / mL, Carl Roth GmbH, Karlsruhe, GER) after 6 hours and 4 hours of fasting, respectively. For HFD-fed mice, the insulin dose was increased to 0.6 - 0.7 U insulin / kg. If not otherwise stated, blood samples were drawn by punctuation of the retro-orbital plexus or vena facialis and collected in tubes containing 0.5 M ETDA. Plasma was collected after centrifugation (3600 rpm / 10 min / 4 °C). Plasma free fatty acid, triglyceride, insulin, and ketone body concentrations were measured using commercial kits (NEFA C test kit, WAKO Diagnostics, Mountain View, CA, US; Triglyceride Reagent (TR22421), ThermoFisher Scientific, Waltham, MA, USA; Mouse Ultrasensitive Insulin ELISA (80-INSMSU-E01), ALPCO Diagnostics, Salem, NH, US; β-Hydroxybutyrate Assay Kit (MAK041), Sigma-Aldrich, St. Louis, MO, US).

2.6. Histological analyses and immunohistochemistry

Isolated tissue from BAT, sWAT, eWAT, and heart were fixed in 4 % paraformaldehyde for 24 hours and embedded in paraffin. 2 µm thick sections were cut, deparaffinized with xylene, and stained with hematoxylin and eosin (HE). Immunohistochemistry was performed using a specific UCP1 antibody (ab10983, Abcam, Cambridge, GB) and F4/80 (MCA 497 GA, Bio-Rad AbD Serotec GmbH, Puchheim, GER). Antigen retrieval was done with EDTA-sodium buffer (1.0 mM, pH 8.0) for 40 minutes. For incubation and detection, the Dako Real Envision System (K5007, Dako Österreich GmbH, Vienna, AUT) was used. For lipid droplet area and diameter quantification, 100 – 170 droplets of each genotype were counted.

2.7. Measurement of lipolysis from organ explants

BAT, sWAT, and eWAT was surgically removed, washed with phosphate buffered saline (PBS, pH 7.4; GIBCO, ThermoFisher Scientific, Waltham, MA, US), incubated in prewarmed DMEM (4.5 g / L glucose; GIBCO, ThermoFisher Scientific, Waltham, MA, US), and all further measurements were performed on the same day. Tissue pieces of about 20 mg were preincubated for 1 hour in 200 µL of DMEM containing 2 % BSA (fatty acid-free) in absence or

presence of 10 µM isoproterenol at 37 °C / 5 % CO_2 / 95 % humidity atmosphere. Preincubation was not necessary for measurement of basal lipolysis. After preincubation, fat explants were transferred into 200 µL of identical, fresh medium and incubated for further 60 minutes. Incubation media was collected and lipid extraction at 37 °C was done for 1 hour using 1 mL chloroform : methanol (2 : 1, vol : vol) containing 1 % acetic acid. Subsequently, tissues were lysed by overnight vigorous shaking in 500 µL NaOH / SDS (0.3 N / 0.1 %) at 55 °C. Protein content was measured using Pierce™ BCA Protein Assay Kit (ThermoFisher Scientific, Waltham, MA, US). Free fatty acid- and glycerol release was determined as described in 2.10 and values were normalized to protein levels.

2.8. Cell culture

If not otherwise stated, immortalized brown adipogenic cells[144] (iBACs) were grown in DMEM (4.5 g / L glucose; GIBCO, ThermoFisher Scientific, Waltham, MA, US) supplemented with 10 % FBS (Biochrom GmbH, Berlin, GER), 2 mM L-glutamine (L-glut; ThermoFisher Scientific, Waltham, MA, US), 50 µg / mL streptomycin, 50 units / mL penicillin (P/S; ThermoFisher Scientific, Waltham, MA, US), and 20mM Hepes (ThermoFisher Scientific, Waltham, MA, US) at 37 °C, 5 % CO_2. iBACs were induced to differentiate at the day of confluence with 0.5 mM 3-isobutyl-1-methylxanthine (IBMX, Sigma-Aldrich, St. Louis, MO, US), 0.5 µM dexamethasone (Dex, Sigma-Aldrich, St. Louis, MO, US), 20 nM insulin (Carl Roth GmbH, Karlsruhe, GER), 1 nM triiodothyronine (T3, Sigma-Aldrich, St. Louis, MO, US), and 125 µM indomethacin (Sigma-Aldrich, St. Louis, MO, US). Two days after induction, medium was changed to maintenance medium containing 20 nM insulin and 1 nM T3 and cells were kept in this medium until harvest. iBACs stably overexpressing *Nat8l* or stably silenced for *Nat8l* and *Aspa* were generated using retroviral transduction particles as described previously[116,117].

To stimulate β3-adrenergic receptors, cells were incubated with 1 µM isoproterenol (iso) for 4 hours. iBACs were treated with 10 µM *PPARα* antagonist GW6471 (Tocris Bioscience, Bristol, GB) from day 4 until harvest. Supernatants and cells (scraped from the culture dish with PBS) were harvested at the indicated time points. To inhibit lipolytic activity, iBACs were incubated with either 50 µM Atglistatin[145] or 50 µM Hi 76-0079 (HSL-Inhibitor, Novo-Nordisk, NNC 0076-0000-0079, DK) for 7 hours prior to harvest on day 7 of differentiation. To inhibit acetyl-CoA carboxylase and thereby FA synthesis, iBACs were incubated with 10 µM 5-(tetradecyloxy)-2-furoic acid (TOFA; Tocris Bioscience, Bristol, GB Respiration) for 12 hours prior to harvest on day 7 of differentiation. To inhibit CPT1b and thereby FA β-oxidation, iBACs were treated with 0.1, 1.0, 10, and 40 µM of Etomoxir (Sigma-Aldrich, St. Louis, MO, US) for 12 hours prior to harvest on day 7 of differentiation.

2.9. Respiration

Tissue respiration was performed using a Clark electrode (Strathkelvin Instruments, Motherwell, GB) as described previously by Cohen et al.[146]. Briefly, freshly isolated tissues were isolated from wild-type and *Nat8l*-ko mice, minced, and placed in 100 % air saturated respiration buffer (PBS, 2 % BSA, 0.45 % D-glucose, 6 mg sodium-pyruvate – prepare a 100 mM stock and use 545 µL in 50 mL respiration buffer). O_2 consumption was normalized to tissue weight and calculated as µg O_2 / min / mg tissue.

For assays on cultured cells, Clark electrode (Strathkelvin Instruments, Motherwell, GB) as well as XF96 extracellular flux analyzer (Seahorse Bioscience, North Billerica, MA, US) was used to determine respiration rates.

For XF96 extracellular flux analyzer, oxygen consumption rate measurement was performed as described.[116] Briefly, iBACs overexpressing *Nat8l* and controls were used on day 6 of differentiation, counted and plated in XF96 polystyrene cell culture microplates (Seahorse Bioscience, North Billerica, US) at a density of 40000 cells per well. The next day, cells were washed and preincubated for 30 minutes in unbuffered XF assay medium (Seahorse Bioscience, North Billerica, US) supplemented with 5.5 mM D-glucose (Carl Roth GmbH, Karlsruhe, GER) and 1 mM sodium pyruvate (Sigma-Aldrich, St. Louis, MO, US) at 37 °C in a CO_2-free environment. OCR was subsequently obtained in a time interval of 7 minutes using the XF96 extracellular flux analyzer. Prior to the experiments, optimal concentrations of specific inhibitors / accelerators of the electron transport chain were determined by titration. The following working concentrations were used: 1 µM oligomycin, 2 µM FCCP (carbonyl cyanide-p-trifluoromethoxyphenylhydrazone), and 2.5 µM antimycin A.

2.9.1. Set-Up for respiration measurement using the Strathkelvin Instruments 782 System

To measure OCR using the Strathkelvin, the Clark electrode system was set up as described in manuals for the SI782 Single / Dual Channel Meter, MT200A respirometer cell, and the SI130 electrode.[2] However, some critical steps for the setup process should be mentioned here to provide reproducibility.

Before assembly of the system, a membrane had to be fitted to the electrode (Figure 7B). For closed cell respirometry (e.g. tissue oxygen consumption), which was used for experiments described in this thesis, polypropylene membranes were used. If the system should be used to measure very fast changes of oxygen (e.g. isolated mitochondria), it would be necessary to use FEP membranes. The unprotected electrode is very vulnerable and has to be handled very

[2] http://www.strathkelvin.com/wp-content/uploads/2014/11/782-manual.pdf
http://www.strathkelvin.com/wp-content/uploads/2015/04/mt200-mt200A-manual.pdf
http://www.strathkelvin.com/wp-content/uploads/2015/04/electrode-manual.pdf

carefully. The membrane jacket was filled with electrolyte solution (provided in the electrode service kit) up to the inscribed line. It is critical to remove all air bubbles by tapping of the jacket and inspecting it under strong light. The electrode has to be slowly inserted into the membrane jacket and screwed until tight. An air bubble should remain inside the jacket. Otherwise, the electrode pressure might be too high and lead to measurement failure.

After fitting the membrane jacket to the electrode, the MT200A respirometer cell can be assembled (Figure 7A). The electrode has to be inserted from the bottom and the clamp ring is used to fix the glass top on the respirometer and close the respiration chamber. The plunger can be adjusted to define the respiration chamber volume (1 mL, 0.5 mL, and 0.3 mL for the MT200A system). A water supply has to be connected at the backside of the respirometer cell. After respirometer assembly, the electrode can be connected to the SI782 Single / Dual Channel Meter.

When the electrode is first connected or re-connected to the SI782 meter, the electrode has to be polarized. Therefore, system assembly has to be done some hours before measurement, as this might take some time. The system was always used with computer connection, as the software interface provides easier handling.

First, the basic setup has to be adjusted (Figure 7C). The parameters for the measurements performed in this thesis were set as follows:

Type of experiment:	closed cell respirometry
Oxygen units:	µg / mL
Respiration rate:	µg / min

The number of electrodes will be recognized automatically by the system. Second, the oxygen solubility has to be entered (Figure 7D). The oxygen concentration for the 100 % air-saturated water at 37 °C corresponds to 6.72 µg / mL. The concentration can also be directly calculated in the software according to the buffer parameters and temperature ("*Calculate concentration*").

Third, electrodes have to be calibrated (Figure 7E). A "Zero"-calibration and a "High"(100 %)-calibration point have to be defined. Therefore, 100 % air-saturated and 0 % oxygen containing water have to be pre-warmed to 37 °C. 100 % air saturation can be achieved by bubbling air through a hose. 0 % oxygen saturation can be achieved by adding a small amount of sodium-sulfite (WAKO Diagnostics, Mountain View, CA, US) to water. The output current of the electrode is displayed at the SI782 Meter. The "High" output should be in the range of 600 – 900 pA and the "Zero" output should be ideally 0 pA (all below 20 pA is fine). Values can be accepted after electrode output is stable. Note, that after using the "Zero" calibration solution, the chamber has to be washed thoroughly to avoid a decreasing signal in the "High" solution due to residual sodium-sulfite. Calibration has to be confirmed by pushing the "*Calibration*

complete"-button (Figure 7E). Finally, respiration buffer has to be loaded to the respirometer cell to make sure that the output is stable also with respiration buffer.

Right before measurement, experimental values, most importantly biomass (e.g. mg tissue, but this can be also adjusted during analysis) and water volume, have to be set (Figure 7F).

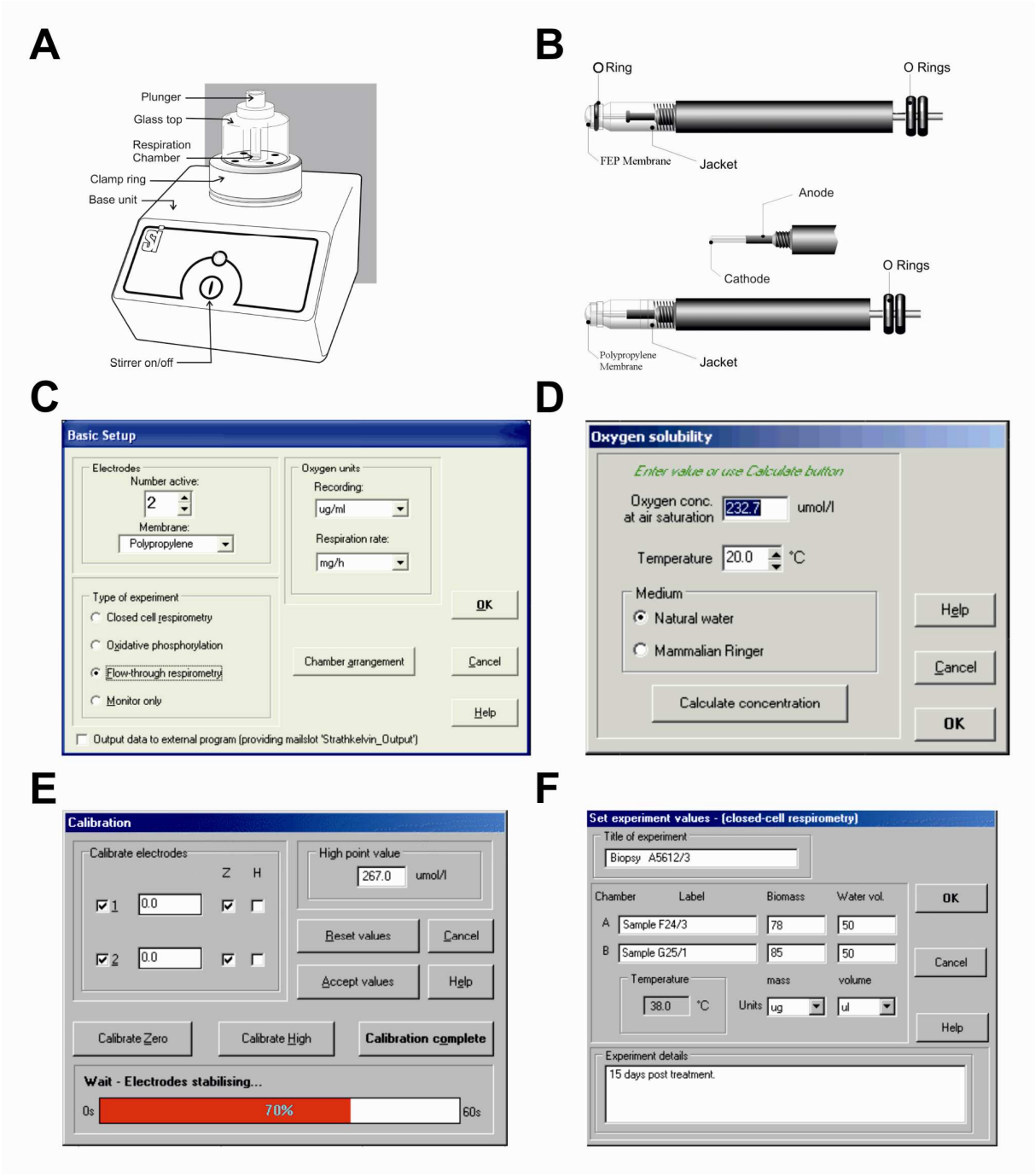

Figure 7. **Experimental setup for respiration measurement using the Clark electrode from Strathkelvin Instruments.** (A) MT200A respirometer cell. (B) SI130 electrode with FEP and polypropylene membrane jacket. Graphic user interface for (C) basic setup, (D) oxygen solubility, (E) calibration of electrodes, and (F) experimental values in the Strathkelvin Instruments 782 System data analysis module version 4.1.0.11.

2.9.2. Data analysis using the Strathkelvin Instruments 782 System

After recording the oxygen concentration in the measurement chamber over time, a respiration report can be produced. A decrease of oxygen is recorded as measure of respiration rate (Figure 8A, blue line). Upper and lower analysis limit has to be set (Figure 8A, red bars 1 & 2). As soon as the calculation limits have been set, a dashed line indicates the fitted function for the respiration rate. Finally, the calculation and report format has been selected as shown in Figure 8B. The final respiration report (press the "*Calc*"-Button) is shown in Figure 8C. The duration of analysis should be chosen as long as possible, but an analysis time of at least 1 minute is highly desirable.

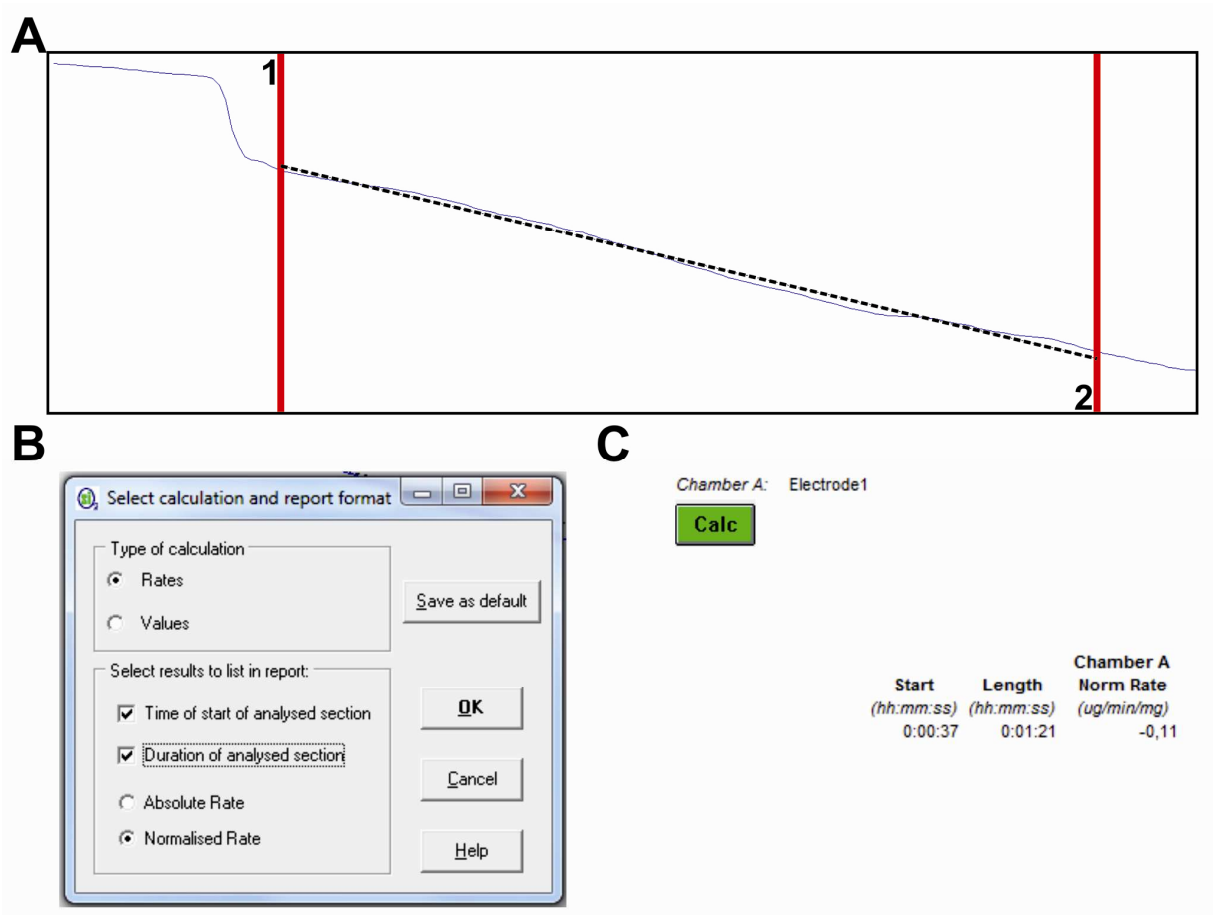

Figure 8. **Data analysis using the Strathkelvin Instruments 782 System.** (A) Scheme of respiration record; blue line: recorded oxygen consumption over time, red bars 1 & 2: borders for rate calculation, dashed black line: fitted function for rate calculation. (B) Calculation and report preference window. (C) Final respiration report.

2.10. Lipid staining and quantification

Cells were fixed (10 % formalin in PBS for 30 minutes), rinsed in PBS, and stained with oil red O (0.25 % in 60 % isopropyl alcohol stock solution diluted 3 : 2, vol : vol with distilled H_2O for 30 minutes). Cellular triglyceride content was determined from cells and supernatants using the Infinity Triglyceride Reagent (ThermoFisher Scientific, Waltham, MA, US). Free fatty acid

content was measured using the NEFA C test kit (WAKO Diagnostics, Mountain View, CA, US). Values were normalized to protein content, measured in the cell lysate using the Pierce™ BCA Protein Assay Kit (ThermoFisher Scientific, Waltham, MA, US).

2.11. RNA isolation, reverse transcription, and gene expression analysis

Total RNA from cells was isolated using the Total RNA isolation kit (Sigma-Aldrich, St. Louis, MO, US) and the peqGOLD Total RNA kit (VWR International GmbH, Erlangen, GER), respectively. Tissue RNA was isolated with TRIzol® reagent (Invitrogen™, ThermoFisher Scientific, Waltham, MA, US) according to the manufacturer's protocol. cDNA was generated using Superscipt II reverse transcriptase (Invitrogen™, ThermoFisher Scientific, Waltham, MA, US) and the OneStep RT-PCR kit (Qiagen, Venlo, NL), respectively. mRNA expression was measured using the StepOnePlus real-time PCR System and ABI Prism 7700 Sequence Detector system with SYBR Green PCR master mix (all from Applied Biosystems, ThermoFisher Scientific, Waltham, MA, US). Gene expression was normalized to expression of *TfIIß* and *18S rRNA* in murine tissues and cells.Relative mRNA expression levels were calculated using averaged $2^{-\Delta\Delta Ct}$ values for each biological replicate as described previously[147]. Primer sequences are listed in Table 2.

Table 2. **Primer pairs used for qRT-PCR.** All primers were designed for and used with murine cDNA.

Target gene	Forward primer 5' → 3'	Reverse primer 5' → 3'
18S rRNA	CACGGCCGGTACAGTGAAAC	AGCGAGCGACCAAAGGAA
Acly	AGGAAGTGCCACCTCCAACAGT	CGCTCATCACAGATGCTGGTCA
Acsl1	TCCTACAAAGAGGTGGCAGAACT	GGCTTGAACCCCTTCTGGAT
Acss2-ct	CTGAGTGGATGAAAGGAGCAAC	CAGGAGTTCACGGTATGTGATC
Aspa	CCATATGAAGTGAGAAGGGCTC	CCTCAAGAATAAGAGTGCAACC
Cidea	TGACATTCATGGGATTGCAGAC	GGCCAGTTGTGATGACTAAGAC
Cox1-mt	TGAGCCCACCACATATTCACAG	AGGGTTGCAAGTCAGCTAAATAC
Cpt1b	TGTATCGCCGCAAACTGGACCG	TCTGGTAGGAGCACATGGGCAC
Fabp4 / aP2	CGACAGGAAGGTGAAGAGCATC	ACCACCAGCTTGTCACCATCTC
Fasn	GCTGTAGCACACATCCTAGGCA	TCGTGTTCTCGTTCCAGGATC
Nat8l	TGTGCATCCGCGAGTTCCGC	GCGGAAAGCCGTGTTGGGGA
Pdk4	TTTCTCGTCTCTACGCCAAG	GATACACCAGTCATCAGCTTCG
Pgc1α	TCTCTGGAACTGCAGGCCTAAC	TCAGCTTTGGCGAAGCCTT
Pparα	CCTGAACATCGAGTGTCGAATATG	GCGAATTGCATTGTGTGACATC
Pparγ2	TGCCTATGAGCACTTCACAAGAAAT	CGAAGTTGGTGGGCCAGAA
Scd1	ATCGCCTCTGGAGCCACAC	ACACGTCATTCTGGAACGCC
TfIIβ	GTCACATGTCCGAATCATCCA	TCAATAACTCGGTCCCCTACAA
Ucp1	ACACCTGCCTCTCTCGGAAA	TAGGCTGCCCAATGAACACT

2.12. Western blot analysis

iBACs (at indicated time points) were harvested for protein analysis by scraping with SDS-lysis buffer (50 mM Tris-HCl, pH 6.8, 10 % glycerol, 2.5 % SDS, cOmplete™ protease inhibitor cocktail) and samples were digested by benzonase (Merck Millipore, Darmstadt, GER).
Tissues on ice were homogenized in RIPA buffer (150 mM Tris-HCl pH 8.0, 50 mM NaCl, 1 % TritonX-100, 0.5 % Na-Deoxycholate, 0.1 % SDS) and incubated on ice for 20 minutes. After centrifugation at 16000 g / 10 min / 4 °C, intermediate phase was carefully collected into a new Eppendorf tube by puncture of the tube wall with a hot needle.
Protein concentrations were determined with the PierceTM BCA Protein Assay Kit (ThermoFisher Scientific, Waltham, MA, US). 70 µg of sample were subjected to a 10 % BisTris gel (NuPAGE, Invitrogen™, ThermoFisher Scientific, Waltham, MA, US), and gels were blotted to nitrocellulose membranes. The following antibodies were used: anti-UCP1 (1 : 750) (ab10983, Abcam, Cambridge, GB), anti-aspartoacylase (1 : 1000) (ab112530, Abcam, Cambridge, GB), αTUBULIN (1 : 100) (#RB-9281, ThermoFisher Scientific, Waltham, MA, US), and anti β-ACTIN (1 : 25000 for tissue, and 1 : 250000 for cells, respecitvely) (A5316, Sigma-Aldrich, St. Louis, MO, US). For chemiluminescent detection, horseradish peroxidase-conjugated secondary antibodies were used (anti-rabbit 1 : 5000 and anti-mouse 1 : 5000, respectively) (Dako Österreich GmbH, Vienna, AUT). SuperSignal™ West Pico Chemiluminescent Substrate (ThermoFisher Scientific, Waltham, MA, US) and ECL prime substrate (RPN2232, GE Healthcare, Little Chalfont, GB) served as substrates. Before re-probing, blots were stripped with Restore™ Western Blot Stripping Buffer (ThermoFisher Scientific, Waltham, MA, US) for 15 – 20 minutes.

2.13. HPLC / HRMS

Cells (cultivated in 6-well plates) were washed once with 10 mM ammonium acetate buffer and washing solution was thoroughly removed before plates were frozen at -80 °C. For extraction, 10 µL of internal standard mix ($^{13}C_6$-N-acetylaspartic acid + $^{13}C_2$-acetyl-CoA Mix: 990 µL $^{13}C_2$-acetyl-CoA (120 µM stock in water, Sigma-Aldrich, St. Louis, MO, US) + 10 µL $^{13}C_6$-NAA (10 mM stock in water, Sigma)) were added per sample. Extraction procedure was performed according to Ritter et al[148]. Two ml of 75 % boiling ethanol were added to each sample immediately after the plate was placed in a water bath (90 °C) and incubated for 2 minutes. Subsequently, plates were cooled on dry ice, supernatants were collected and centrifuged for 10 min / 17000 g at room temperature. Supernatants were collected and plates and centrifuged pellet were kept for protein determination. Samples were dried using a nitrogen evaporator and stored at -80 °C until analysis.
For animal tissues, extraction was performed as described by Marino et al.[149]. Briefly, flash-frozen tissue fragments of 60 to 80 mg were placed into dry ice pre-cooled homogenization

tubes (2.0 mL SC Micro Tube PCR-PT, Sarstedt, Nümbrecht, GER) containing ceramic beads (Circonia beads, N038.1, Carl Roth GmbH, Karlsruhe, GER). 5 µL of lysis buffer (methanol / water (80 / 20, vol / vol, -20 °C, supplemented with internal standard ($^{13}C_6$-N-acetylaspartic acid, 1 mg / L, Sigma-Aldrich, St. Louis, MO, US) was added to the tubes for each mg of tissue. Tissues were homogenized twice for 20 seconds at 5500 rpm using the Precellys 24 tissue homogenator (Bertin Technologies). Once homogenized, tissue extracts were centrifuged 10 minutes at 12000 g (4 °C), and supernatants were collected and transferred to 1.5 mL Eppendorf tubes. Tubes containing supernatants were lyophilized in a DNA 120 SpeedVac® concentrator (ThermoSavant, Bartelt GmbH, Graz, Austria) for 2 hours at 35 ºC (medium drying rate). If necessary, dried samples were stored at -80 °C. For analysis, frozen samples were re-suspended in 100 µL of analytical-grade water, transferred to HPLC vials and injected into the HPLC-MS system.

Eight calibration standards containing the same amount of internal standards were prepared. Highest concentration of NAA (80 µM) and acetyl-CoA (72 µM) in water were consecutively diluted in a serial 1 : 3 dilution.

A Dionex Ultimate 3000 HPLC setup, equipped with an Atlantis T3 C18 analytical column (Waters), was used for compound separation prior to high resolution mass spectrometric detection with an Exactive™ Orbitrap (ThermoFisher Scientific, Waltham, MA, US). A reversed-phase ion-pairing HPLC method was used for metabolite separation[150]. A 40 minute gradient was applied and 2-propanol and an aqueous phase (5 % methanol (vol : vol), 10 mM tributylamine, 15 mM acetic acid, pH 4.95) were used as eluents. The injection volume was 10 µL per sample and calibration standard. Negative ionization of metabolites was carried out via heated electrospray ionization prior to mass spectrometric analysis. For the untargeted online detection of analytes, a full scan of all masses between 70 and 1100 m / z with a resolution (R) of 50000 (at m / z 200) was used.

LC/MS-data acquisition was conducted with Xcalibur software (vers. 2.2 SP1, ThermoFisher Scientific, Waltham, MA, US). Targeted compound analysis for NAA, $^{13}C_6$-NAA, acetyl-CoA, and $^{13}C_2$-acetyl-CoA were carried out with TraceFinder™ software (version 3.1, ThermoFisher Scientific, Waltham, MA, US). Relative metabolite levels (fold change) were calculated from the absolute concentrations calculated from the peak area ratio of compound and internal standard by a linear calibration function.

2.14. ^{14}C-glucose incorporation and lipid extraction (DNL – de novo lipogenesis)

^{14}C-glucose uptake was performed as described[116]. Briefly, iBACs were incubated overnight with DMEM supplemented with 1 nM T3, 20 nM insulin, 0.5 g / L glucose, and 0.1 µCi D[^{14}C(U)]-glucose / mL (ARC). Thereafter, cells were washed four times with ice-cold PBS and neutral

lipids were extracted with hexane / isopropanol (3 / 2, vol / vol). Thin layer chromatography was performed with hexane / diethylether / acetic acid (70 / 29 / 1, vol) as mobile phase. Lipids were visualized with iodine vapour and cut out. Extracted lipids were transferred into scintillation cocktail and shaken overnight. The incorporated radioactivity was measured by liquid scintillation counting in the Tri-Carb 2300TR (Packard HP) or the LS6500 (Beckman) scintillation-counter. Total glucose incorporation into each lipid class was calculated and values were normalized to protein content.

2.15. TG hydrolase activity assay

Briefly, fully differentiated iBACs were harvested in PBS and centrifuged at 500 g / 7 min / 4 °C. The resulting pellet was subsequently re-suspended in HSL buffer (0.25 M sucrose, 1 mM EDTA, 1 mM DTT, pH 7.0 with acetic acid, c protease inhibitor cocktail) and cells were disrupted using sonication. After a centrifugation step at 16000 g / 30 min / 4 °C the infranatant was collected (punctuate tube with a hot needle to ensure no contamination of fatty acids. Protein concentration was determined by Bradford Protein Assay (Bio-Rad Protein Assay, Bio-Rad Laboratories, Hercules, CA, US) and 20 – 40 µg protein lysate per sample was used for TG hydrolase assay as described previously[119,151].

2.16. ^{3}H-fatty acid uptake

^{3}H-fatty acid uptake was performed according to the method described by Zimmermann et al.[152]. Briefly, iBACs were incubated for 2, 5, and 10 minutes with 1 g / L glucose - maintenance medium (see 2.8) containing 400 µM oleic acid (OA) and 0.15 µCi [^{3}H-9,10]-OA / mL, respectively. Cells were washed 3 times with PBS, harvested in PBS and radioactivity was measured in 2 mL of scintillation cocktail.

2.17. Measurement of lipid droplet associated lipolysis

For labeling of triglyceride stores, fully differentiated iBACs were incubated for 12 hours in the presence of 0.4 mM oleic acid (OA) complexed to BSA, containing 0.1 mCi [^{3}H-9,10]-OA / mL as tracer. Cells were washed 3 times with PBS, harvested in HSL buffer (see 2.15), and disrupted by sonication. Cell lysates were transferred to siliconized tubes (13.2 mL total volume), overlaid with overlay buffer (50 mM potassium phosphate buffer (KPB) pH 7.4, 100 mM KCl, 1 mM EDTA, cOmplete^{TM} protease inhibitor cocktail), and centrifuged at 100000 g / 2 hours / 4 °C. Floating lipid droplets (LD) were collected and resuspended in overlay buffer by brief sonication. TG and protein content was determined using Infinity Triglyceride Reagent (ThermoFisher Scientific, Waltham, MA, US) and Bradford Protein Assay (Bio-Rad Protein Assay, Bio-Rad Laboratories, Hercules, CA, US), respectively. 0.2 mM TG from isolated LD was prepared in 100 µL overlay buffer. 100 µL of 50 mM KPB containing 1 % BSA (FA-free) and

EDTA, cOmplete™ protease inhibitor cocktail was added and samples were incubated for 1 hour at 37 °C under constant shaking. 100 µL overlay buffer was used as blank. The reaction was terminated by addition of 3.25 mL extraction solution I (methanol / chloroform / n-heptane 10 / 9 / 7, vol). 1.05 mL extraction solution II (0.1 M potassium carbonate, 0.1 M boric acid, pH 10.5) was added and samples were vigorously vortexed for 5 seconds. After final centrifugation at 1000 g / 10 min / RT, 200 µL of the upper aqueous phase were measured in 2 mL of scintillation cocktail.

2.18. ASPA activity assay

Differentiated iBACs (day 7 of differentiation) were harvested in homogenization buffer (PBS pH 8.5, 1 mM DTT, 10 % glycerol) and sonicated three times for 5 seconds. Cell homogenates were centrifuged at 10000 g / 10 min / 4 °C and supernatants were collected. Equal amount of 2x reaction buffer (dH2O pH 8.5, TrisHCl 100 mM, NaCl 100 mM, CaCl2 5 mM, DTT 0.2 mM, IGEPAL CA-630 (1 %, Sigma-Aldrich, St. Louis, MO, US) 0.5 %, N-acetylaspartic acid (Sigma-Aldrich, St. Louis, MO, US) 40 mM) was added to the samples and a defined volume per sample was collected to provide the same background matrix for the aspartate standard curve. The background matrix was heated at 95 °C for 10 minutes and subsequently centrifuged at 16000 g / 3 min / 4 °C. The background supernatant was collected and all samples and the background sample were incubated for 18 hours at 38 °C in a thermomixer (constant agitation at 350 rpm). After incubation, all samples were inactivated at 95 °C for 10 minutes and subsequently centrifuged at 16000 g / 3 min / 4 °C. Supernatants were used for analyzing released aspartate content using a commercially available aspartate assay kit (BioVision, Milpitas, CA, USA).

2.19. Statistical analysis

If not otherwise stated, results are mean values (± standard deviation, SD) of at least three independent experiments, or results show one representative experiment out of at least three independent experiments. All data are shown as means ± SD. Single comparisons between two groups were assessed by two-tailed, unpaired student's t-test. Two-way analysis of variance (ANOVA) with repeated measures was used for analysis of timeline studies, e.g. weight gain, ipGTT, and energy expenditure. Analysis of covariance (ANCOVA) was used to analyse energy expenditure as a function of body weight. Significance levels: * $p \leq 0.05$, ** $p \leq 0.01$, *** $p \leq 0.001$

3 - Results I – The role of NAT8L in brown adipocyte lipid, glucose, and energy metabolism – *in vitro* studies

3. RESULTS I - The role of NAT8L in brown adipocyte lipid, glucose, and energy metabolism – *in vitro* studies

Previous results showed that stable overexpression of N-acetyltransferase 8-like (*Nat8l*) in immortalized brown adipocytes (iBACs) significantly increased the brown phenotype, in particular brown marker gene expression, oxygen consumption, and lipid turnover[116]. Peroxisome proliferator-activated receptor (PPAR) α has been shown to be activated by lipolytic products and a regulator of fatty acid catabolism and gene transcription in brown adipocytes[68,153]. We found *Pparα* expression upregulated on day 3 and day 7 of differentiation[116]. Therefore, I wanted to investigate whether the observed effects are mediated by PPARα.

3.1. Nat8l overexpression in iBACs increases UCP1 levels and oxygen consumption rate in a PPARα-dependent manner

I treated *Nat8l*-overexpressing (*Nat8l* o/e) iBACs with a peroxisome PPARα antagonist (10 µM GW6471) from day 4 of differentiation until day 7. GW6471 treatment slightly reduced mRNA expression of cytochrome c oxidase subunit 1 *(Cox1*, involved in mitochondrial oxidative phosphorylation[154]) and pyruvate dehydrogenase kinase 4 (*Pdk4,* regulating glucose oxidation[155]) and did not change PPARγ coactivator 1α (*Pgc1α,* regulation of mitochondrial biogenesis[156]) and adipocyte protein 2 (*aP2*[157]) expression, but the direct PPARα target genes *Ucp1*[67] and carnitine palmitoyltransferase 1B (*Cpt1b,* key enzyme of fatty acid oxidation[158,159]) were significantly reduced (Figure 9A). Further, the massive *Nat8l*-mediated induction of UCP1 protein expression (Figure 9B) and oxygen consumption rate was nearly reduced to control cell level in *Nat8l* o/e cells after GW6471 treatment (Figure 9C). Triglyceride content was not changed upon GW6471 treatment (Figure 9E) indicating no detrimental effects on differentiation capacity. Increased lipogenesis as well as elevated basal and isoproterenol-stimulated fatty acid release evoked by *Nat8l* overexpression were not affected by GW6471 treatment. Thus, we conclude that PPARα activation is needed to increase *Ucp1* and *Cpt1b* transcription in *Nat8l* o/e iBACs, ultimately leading to increased fatty acid oxidation and oxygen consumption. In contrast, increased lipid turnover is independent of PPARα activation.

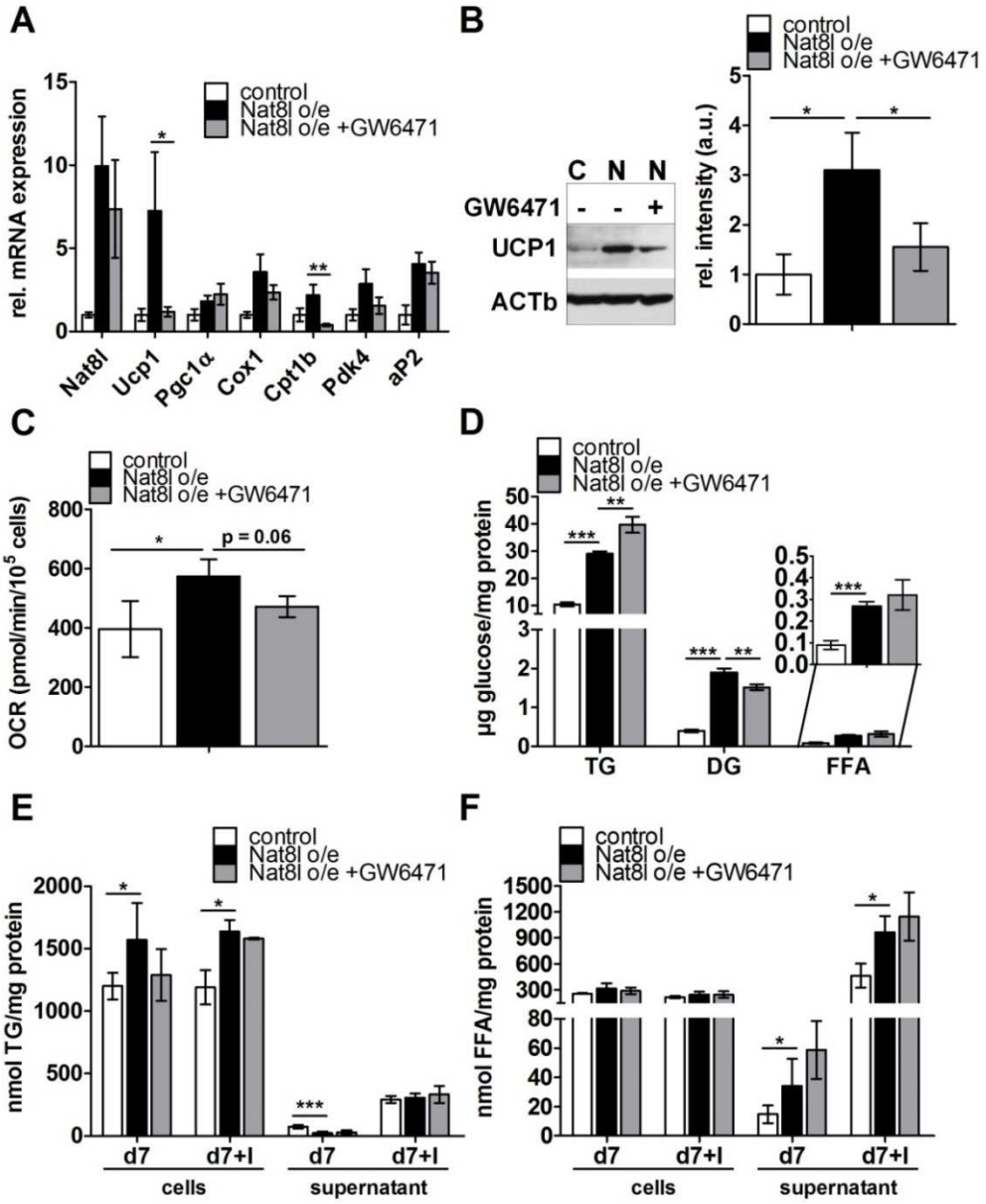

Figure 9. ***Nat8l*-mediated induction of UCP1 and oxygen consumption rate is PPARα-dependent, whereas lipid turnover is not.** iBACs were incubated with 10 µM of the PPARα antagonist GW6471 from day 4 until day 7 of differentiation. All experiments were performed with mature adipocytes (differentiated until day 7). (A) mRNA expression of adipogenic marker genes (*aP2*, *Ucp1*, and *Pgc1α*) and genes involved in mitochondrial oxidative phosphorylation (*Cox1*) and β-oxidation (*Cpt1b* and *Pdk4*) (n = 3). *Tfllβ* was used for normalization. (B) UCP1 protein expression. One representative blot of n = 3 is shown. Relative band intensity was calculated from n = 3 and normalized to β-ACTIN (ACTb). (C) Oxygen consumption rate (OCR) measured with the Seahorse™ Extracellular Flux Analyzer (n = 3). (D) incorporation of [^{14}C-]glucose into neutral lipids (n = 3). (E) Triglyceride (TG) and (F) fatty acid content in cells and supernatants in the absence or presence of 10 µM isoproterenol (4 hours; +I) (n ≥ 3). All data are presented as mean ± standard deviation. Statistical significance was assessed by two-tailed Student´s t test. *p < 0.05; **p < 0.01; ***p < 0.001.

3.2. Lipolysis in Nat8l o/e iBACs

ATGL-mediated lipid catabolism has been identified to provide essential mediators involved in the generation of lipid ligands such as fatty acids for PPARα activation[65]. Therefore, we investigated if ATGL-mediated lipolysis is increased in *Nat8l* o/e iBACs. Triglyceride hydrolase activity measured in the cytosol was not changed (Figure 10A) whereas fatty acid release from the lipid droplet fraction was highly increased in *Nat8l* o/e cells compared to control cells (Figure 10B). Treatment of mature *Nat8l* o/e iBACs with 50 µM Atglistatin[145] or 50 µM HSL inhibitor (76-0079; Novo Nordisk) revealed that inhibition of ATGL reduced fatty acid release whereas HSL inhibition did not (Figure 10C). Thus, these data show that increased lipolytic activity in *Nat8l* o/e iBACs is mediated by ATGL.

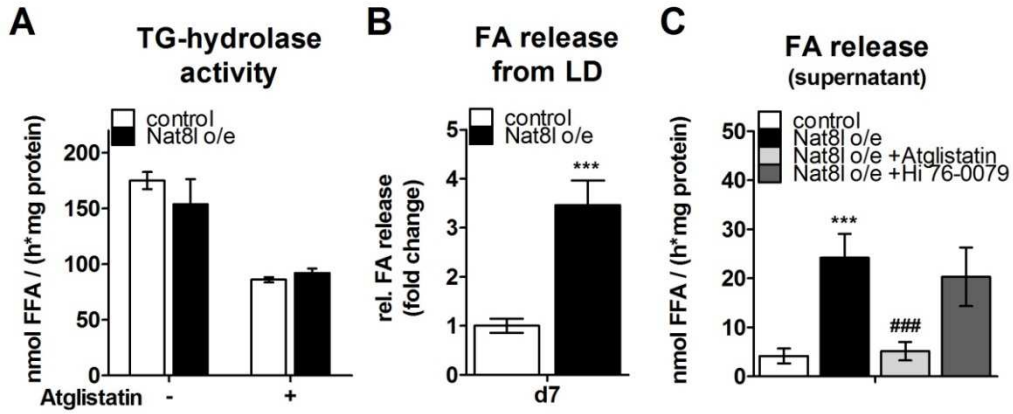

Figure 10. **LD-associated ATGL mediates increased lipolytic activity in *Nat8l*-overexpressing iBACs.** All experiments were performed with mature adipocytes (differentiated until day 7; d7). (A)Triglyceride (TG-) hydrolase activity in the absence or presence of 40 µM Atglistatin (n = 3). (B) Fatty acid (FA) release from lipid droplet fraction (n = 4). FA content in the supernatant of control and *Nat8l*-overexpressing cells treated with 50 µM Atglistatin or 50 µM HSL inhibitor (Hi 76-0079) (n = 3). All data are presented as mean ± standard deviation. Statistical significance was assessed by two-tailed Student´s t test. ***$p < 0.001$; $^{###}p < 0.001$ for Nat8l o/e vs. *Nat8l* o/e +Atglistatin.

We hypothesized that Nat8l overexpression could drain acetyl-CoA from energy production to DNL, thereby making it necessary to increase lipolysis and β-oxidation of FAs for energy production[160]. TOFA (5-(tetradecyloxy)-2-furoic acid) has been shown to inhibit acetyl-CoA carboxylase activity, the initial step in FA synthesis[161]. I wanted to test if inhibiting FA synthesis in *Nat8l* o/e iBACs would decrease lipolysis and lipid turnover. Therefore I treated *Nat8l* o/e and control iBACs with 10 µM TOFA for 12 hours (from day 6 to day 7 of differentiation) and measured FA release into the supernatant. TOFA treatment did not reduce basal and isoproterenol (Iso) stimulated FA release in *Nat8l* o/e iBACs (Figure 11A), but also did not affect FA release in control cells. Of note, this treatment is lacking a positive control. Thus, it is possible that the treatment did not work efficiently and the experiment setup should be revised. However, these data might also indicate that increased DNL and lipolysis are independent effects caused by *Nat8l* o/e in iBACs. Next, I wanted to test whether inhibiting FA β-oxidation

would decrease lipolysis or even increase FA release into the supernatant to prevent lipotoxicity in *Nat8l* o/e iBACs. In a preliminary experiment, I used different concentrations of CPT1b inhibitor Etomoxir[162] and measured FA release into the supernatant. Etomoxir treatment for 12 hours did not change FA release in *Nat8l* o/e and control iBACs (Figure 11B). Again, this experiment lacks proof of principle for efficient inhibition of CPT1b. Hence, it would be important to validate efficient Etomoxir treatment during e.g. oxygen consumption measurement using the Seahorse™ Extracellular Flux Analyzer to life image the expected decrease in cellular respiration.

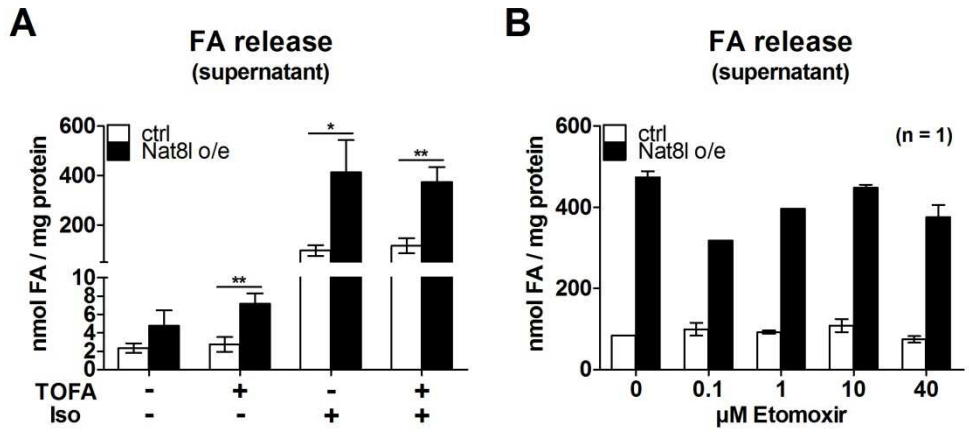

Figure 11. **FA release into the supernatant in *Nat8l* o/e iBACs upon TOFA and Etomoxir treatment.** All experiments were performed with mature adipocytes (differentiated until day 7; d7). (A) FA release in *Nat8l* o/e compared to control iBACs in the absence or presence of 10 µM TOFA for 12 hours (n = 3). (B) FA release in *Nat8l* o/e compared to control iBACs treated with different concentrations of Etomoxir for 12 hours (n = 1; SD shown from technical replicates). All data are presented as mean ± standard deviation. Statistical significance was assessed by two-tailed Student´s t test. *p < 0.05; **p < 0.01; ***p < 0.001.

3.3. Inhibition of Sirtuin activity reduces Pparα and Ucp1 expression in Nat8l overexpressing iBACs

Sirtuin 1 (SIRT1) is a NAD^+-dependent deacetylase which is activated upon caloric restriction and exercise[163]. SIRT1 has been shown to deacetylate PPARγ, thereby increasing its activity similar to known PPARγ ligands (e.g. rosiglitazone)[140]. It is known that chronic PPARγ activation leads to induction of marker gene expression and mitochondrial biogenesis (reviewed in[58]) in brown adipocytes. Thus, I wanted to test if SIRT1 participates in the cascade leading to increased brown marker gene expression and mitochondrial biogenesis in *Nat8l* overexpressing iBACs. Therefore, I treated *Nat8l* overexpressing iBACs with 20 mM of nicotinamide (NA; inhibitor of sirtuin activity), from day 4 to day 7 (similar to the experiments performed with the PPARα antagonist GW6471 (see section 3.1)) and from day 0 to day 7 of differentiation. In accordance with our previous results, *Ucp1*, *Pparα*, and *Pparγ2* were increased in *Nat8l* o/e iBACs compared to controls (Figure 12). NA was able to significantly reduce *Pparα* and *Ucp1* expression in *Nat8l* o/e iBACs. Of note, *Pparγ2* expression was not decreased by NA treatment.

Hence, these data indicate that SIRT1 might participate in activation of brown marker gene expression upon *Nat8l* overexpression in iBACs.

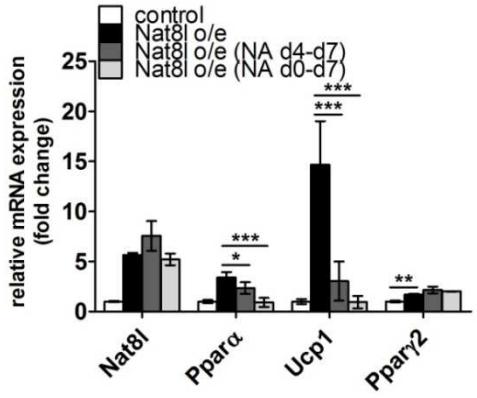

Figure 12. ***Nat8l*-mediated induction of *Pparα* and *Ucp1* can be attenuated when sirtuin activity is inhibited by nicotinamide (NA).** Experiment was performed with mature adipocytes (differentiated until day 7; d7). iBACs were incubated with 20 mM NA (inhibitor of sirtuin activity) from day 4 until day 7 and from day 0 until day 7 of differentiation. mRNA expression analysis by qRT-PCR is shown for *Nat8l*, *Pparα*, *Ucp1*, and *Pparγ2. TfIIβ* was used for normalization (n = 4 for *Nat8l*, *Pparα*, *and Ucp1*; n = 3 for *Pparγ2*). All data are presented as mean ± standard deviation. Statistical significance was assessed by two-tailed Student´s t test. *p < 0.05; **p < 0.01; ***p < 0.001.

3.4. ASPA activity in iBACs

We recently showed that ASPA is expressed in the cytoplasm of brown adipocytes and in BAT of C57Bl/6 mice[116]. As it has not been shown that ASPA is also active in brown adipocytes, I performed ASPA activity assays (see 2.18) using control and *Aspa*-silenced iBACs. Briefly, this assay detects released aspartate from NAA during 18 hours of incubation. ASPA activity was detectable in iBACs and silencing of *Aspa* markedly reduced ASPA acitivity (Figure 13A).

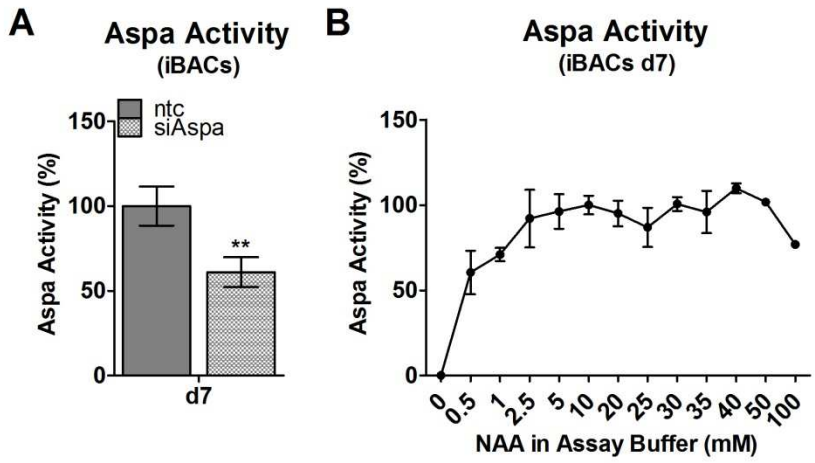

Figure 13. **ASPA is active in iBACs and ASPA activity is not inhibited by NAA.** Experiment was performed with mature adipocytes (differentiated until day 7; d7). (A) ASPA activity in control (ntc) and *Aspa*-silenced iBACs (n=4). (B) ASPA activity in iBACs with different concentrations of NAA in assay buffer (n ≥ 2). All data are presented as mean ± standard deviation. Statistical significance was assessed by two-tailed Student´s t test. **p < 0.01.

Next, I wanted to test if how ASPA activity is affected by different concentrations of NAA in the assay buffer. Of note, ASPA activity was not detectable when NAA was absent in the assay buffer and increased rapidly with increasing NAA concentrations (Figure 13B). Importantly, even very high concentrations of NAA up to 100 mM were not able to significantly decrease ASPA activity in iBACs compared to physiological concentrations around 10 mM. Simple linear regression analyses of the data in Figure 13B using a Lineweaver Burk plot revealed a K_m for ASPA of around 3 mM. Of note, Wang et al.[92] reported a K_m of 1.69 mM and 3.75 mM in cytosol and myelin in brain, respectively. Thus, these data show that ASPA is active in brown adipocytes and that ASPA activity is increased by NAA.

3.5. Silencing of Aspa in Nat8l o/e iBACs reduces Ucp1 expression

We recently showed that NAA accumulation caused by *Aspa* silencing or exogenous supplementation reduces the brown adipogenic phenotype[117]. Interestingly, unpublished data of Katharina Huber also indicate that NAA accumulates in *Nat8l* o/e iBACs compared to controls. Importantly, we also observed increased *Aspa* expression in *Nat8l* o/e iBACs. Thus, I tested if silencing of *Aspa* attenuates the effects caused by *Nat8l* o/e in iBACs. I transduced *Nat8l* o/e iBACs and corresponding controls with lentiviral particles coding for *Aspa* shRNA or non-target shRNA (ntc) as a control. Silencing of *Aspa* markedly reduced *Ucp1* mRNA and protein expression compared to *Nat8l* o/e - ntc iBACs (Figure 14A and B). *Aspa* expression in *Nat8l* o/e - si*Aspa* iBACs was reduced to control - ntc level (Figure 14A). These data suggest that increased flux of acetyl-CoA through the NAA pathway is important to increase lipid turnover, marker gene expression, and oxygen consumption in iBACs.

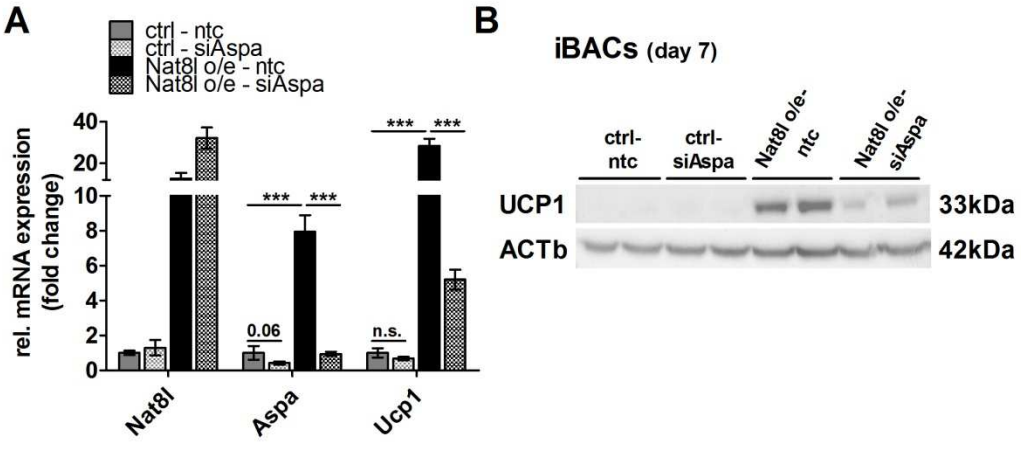

Figure 14. **Silencing of *Aspa* in *Nat8l* o/e iBACs reduces *Ucp1* expression.** Experiments were performed with mature adipocytes (differentiated until day 7; d7). Control and *Nat8l* o/e iBACs were transduced using lentiviral particles coding for non-target control (ntc) shRNA (ctrl - ntc, *Nat8l* o/e - ntc) or *Aspa* shRNA (ctrl - si*Aspa*, *Nat8l* o/e - si*Aspa*) (A) mRNA expression of *Nat8l*, *Aspa*, and *Ucp1* (n=3). *TfIIβ* was used for normalization. (B) Protein expression of UCP1. β-ACTIN (ACtb) serves as a loading control (n = 2). All data are presented as mean ± standard deviation. Statistical significance was assessed by two-tailed Student´s t test. *p < 0.05; **p < 0.01; ***p < 0.001.

3.6. FA uptake upon Nat8l o/e and silencing in iBACs

We previously showed that *Nat8l* o/e increases DNL from glucose, lipolysis, FA release into the supernatant, and oxygen consumption in brown adipocytes[160]. Therefore, I tested the hypothesis that *Nat8l* o/e might lead to an overload of intracellular FA, thereby leading to decreased FA uptake in *Nat8l* o/e iBACs. I performed uptake assays (see 2.16) using radiolabeled ^{3}H-oleic acid (OA) and found FA uptake reduced in *Nat8l* o/e iBACs compared to controls (Figure 15A) whereas silencing of *Nat8l* did not lead to changes in FA uptake (Figure 15B).

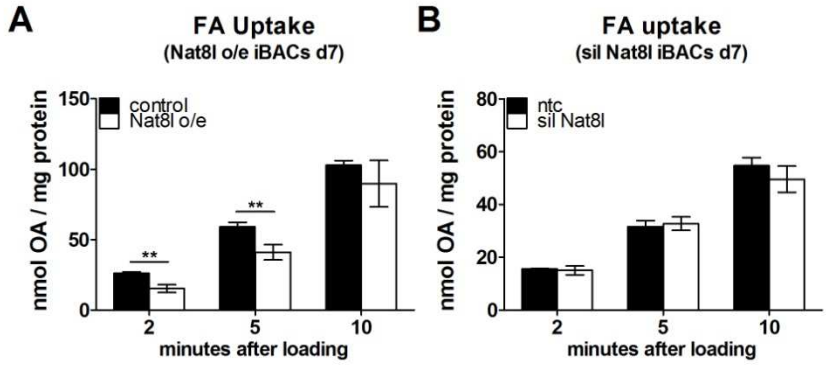

Figure 15. **FA uptake is reduced upon *Nat8l* o/e but unchanged upon silencing of *Nat8l* in iBACs.** Experiments were performed with mature adipocytes (differentiated until day 7; d7). ^{3}H-oleic acid (OA) uptake determined at 2, 5, and 10 minutes after loading is shown for (A) *Nat8l* o/e and (B) *Nat8l*-silenced iBACs compared to corresponding controls (n = 3). All data are presented as mean ± standard deviation. Statistical significance was assessed by two-tailed Student´s t test. **p < 0.01.

3.7. The impact of Nat8l deficiency in vitro

To analyze the influence of *Nat8l* knockdown on lipid and energy metabolism in brown adipocytes, I generated iBACs stably silenced for *Nat8l* using shRNA containing retroviral particles and single cells were selected for *Nat8l* silencing as described by Pessentheiner et al.[116]. Finally, three monoclonal *Nat8l*-silenced cell lines and five control lines were pooled for performing experiments. Of note, NAA determination in *Nat8l*-silenced and control iBACs (Figure 16C) includes measurements performed in the monoclonal expanded cells as well as a second set of *Nat8l*-silenced cells produced by neomycin selection. Protein and mRNA expression was ~ 50 % decreased in *Nat8l*-silenced cells on day 3 and day 7 of differentiation, respectively (Figure 16A and G). *Nat8l* silencing did not affect neutral lipid synthesis (Figure 16B) whereas N-acetylaspartate (NAA) levels were highly reduced in *Nat8l*-silenced cells (Figure 16C). *Nat8l* silencing did not affect differentiation capacity as shown by cellular TG content (Figure 16D) whereas lipolysis was significantly increased in basal and isoproterenol-stimulated conditions, as reflected by free fatty acid and glycerol release on day 7 when compared to control cells (Figure 16D and E).

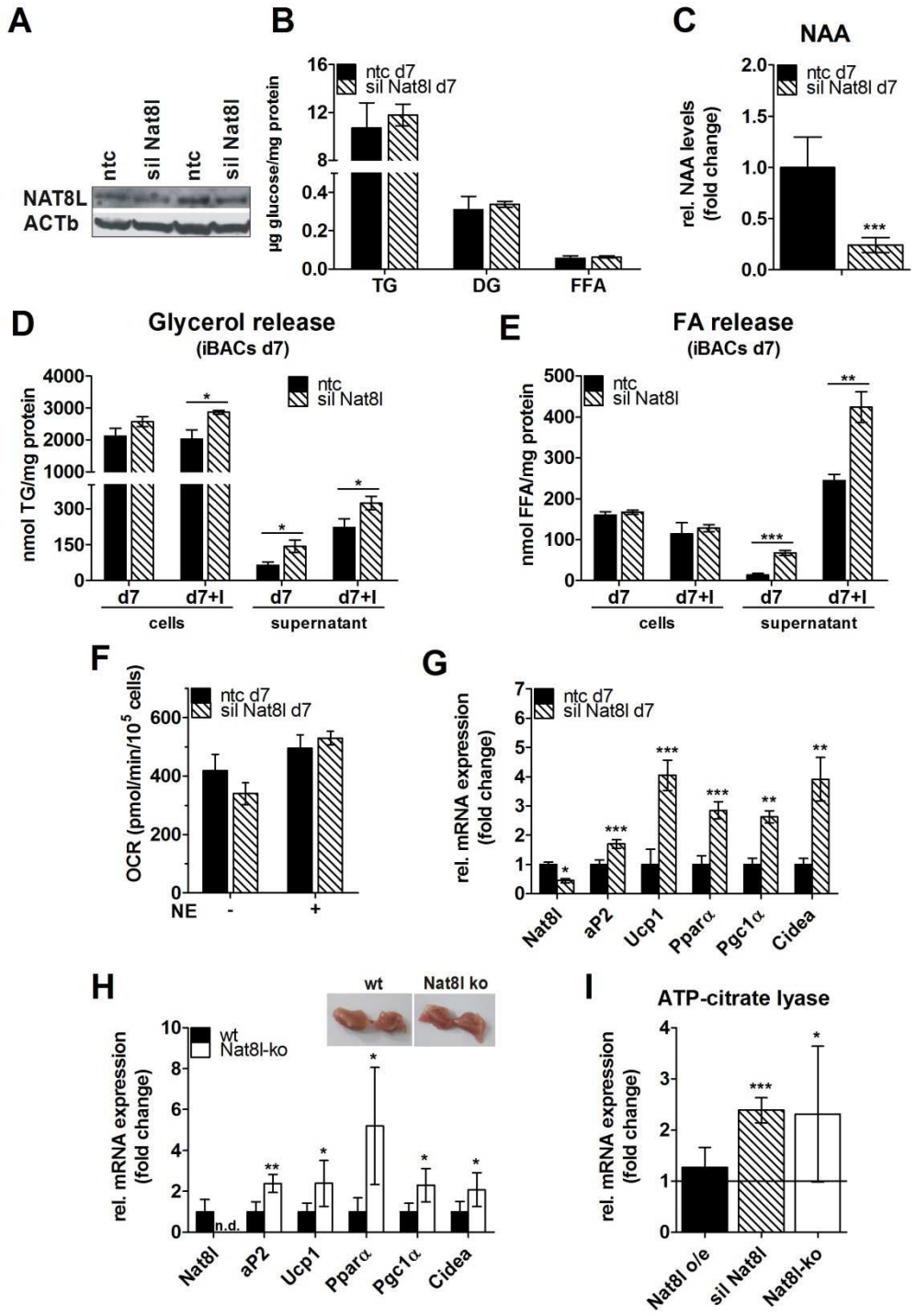

Figure 16. ***Nat8l* silencing in iBACs and mRNA expression of BAT from *Nat8l*-ko mice.** If not otherwise stated, all experiments were performed with mature adipocytes (differentiated until day 7; d7). *Nat8l*-ko and control mice (wt) were fed *ad libitum*, and tissues were harvested at the age of 3-4 months. (A) Protein expression of *Nat8l* in day 3 iBACs. β-ACTIN (ACtb) serves as a loading control (n = 2). (B) Incorporation of [^{14}C-]glucose into neutral lipids (n = 3). (C) NAA concentrations measured by HPLC/HRMS (n = 6 for ntc, n = 8 for sil *Nat8l*. (D) Triglyceride (TG) content and (E) FA content in cells and supernatants in the absence or presence of 10 µM isoproterenol (4 hours; +I) (n = 3). (F) OCR measured with the Seahorse™ Extracellular Flux Analyzer (n = 3). (G) Expression of adipogenic marker genes in *Nat8l*-silenced iBACs (n = 3) and (H) BAT of *Nat8l*-ko and wt mice (n ≥ 5). *Inset*. pictures of BAT of *Nat8l*-ko and wt mice. (I) ATP-citrate lyase (*Acly*) mRNA expression in *Nat8l o/e* iBACs (n = 3), *Nat8l*-silenced iBACs (n = 3), and BAT of *Nat8l*-ko and wt mice (n ≥ 5). All data are presented as mean ± standard deviation. Statistical significance was assessed by two-tailed Student´s t test. *p < 0.05; **p < 0.01; ***p < 0.001.

Interestingly, *Nat8l*-silenced cells did not show a difference in OCR, neither under basal nor under norepinephrine-stimulated conditions (Figure 16F), although expression of adipogenic marker genes such as *aP2*, *Ucp1*, *Pparα*, *Pgc1α*, and *Cidea*, was significantly increased in *Nat8l*-silenced iBACs compared to controls (Figure 16G). However, to validate these *in-vitro* results, we investigated BAT of 3 – 4 month old *Nat8l*-knock-out (*Nat8l*-ko) mice. These data was provided by our Japanese collaborators from the University of Toyama. BAT from *Nat8l*-ko mice and wt-mice was similar in weight (0.13 ± 0.04 g for *Nat8l*-ko *versus* 0.12 ± 0.06 g for wt mice, respectively; n = 3; see also Table 7) and morphology (Figure 16H, *inset*). We analyzed gene expression in BAT of *Nat8l*-ko mice and found *aP2*, *Ucp1*, *Pparα*, *Pgc1α*, and *Cidea* significantly increased (Figure 16H) which is in agreement with our *in vitro* results. Further, we found ATP-citrate lyase (*Acly*) mRNA expression significantly increased in *Nat8l*-silenced iBACs as well as in BAT of *Nat8l*-ko mice whereas it was unchanged upon *Nat8l*-o/e compared to control cells.

4 - Results II – NAT8L deficiency *in vivo* – characterization of the total body *Nat8l*-knock-out mouse regarding its metabolic phenotype

4. RESULTS II – NAT8L deficiency in vivo – characterization of the total body *Nat8l*-knock-out mouse regarding its metabolic phenotype

Total body *Nat8l*-knock-out (*Nat8l*-ko) mice were produced in the lab of Prof. Atsumi Nitta (University of Toyama, Japan). Her group has investigated the impact of *Nat8l* deficiency on brain metabolism and its behavioral consequences[94,112,164–167]. I characterized *Nat8l*-ko mice in comparison to wt C57Bl/6J controls regarding lipid, glucose, and energy metabolism between the age of 8-9 weeks and 9 months. Mice were fed either chow diet (CD; 4.5 % calories in fat) or high-fat diet (HFD; 45 % calories in fat) starting from the age of 8-9 weeks. In total, three cohorts of mice were used: cohort 1 (6 wt / 6 *Nat8l*-ko mice; CD and HFD), cohort 2 (6 wt / 6 *Nat8l*-ko mice, CD / HFD), cohort 3 (6 wt / 6 *Nat8l*-ko mice on CD, 9 wt / 9 *Nat8l*-ko mice on HFD). If not otherwise stated (see footnotes), the following data comprises values of all three cohorts of mice.

4.1. NAA levels in tissue and serum of Nat8l-ko mice

NAT8L has been described as the N-acetylaspartate (NAA) synthesizing enzyme in the brain[86,91]. As we found NAT8L also expressed in white and brown adipose tissue[116], I investigated if NAA can be measured in these tissues and whether any residual NAA was detectable in *Nat8l*-ko mice. HPLC/HRMS was used to measure NAA in brain, BAT, sWAT, and serum of *Nat8l*-ko mice. NAA was not detectable in brain of *Nat8l*-ko mice (Figure 17A). Although the levels were very low, NAA was still detectable in BAT and sWAT of *Nat8l*-ko compared to wt mice (Figure 17A). Interestingly, serum NAA was only reduced to 30% of wt level (Figure 17B).

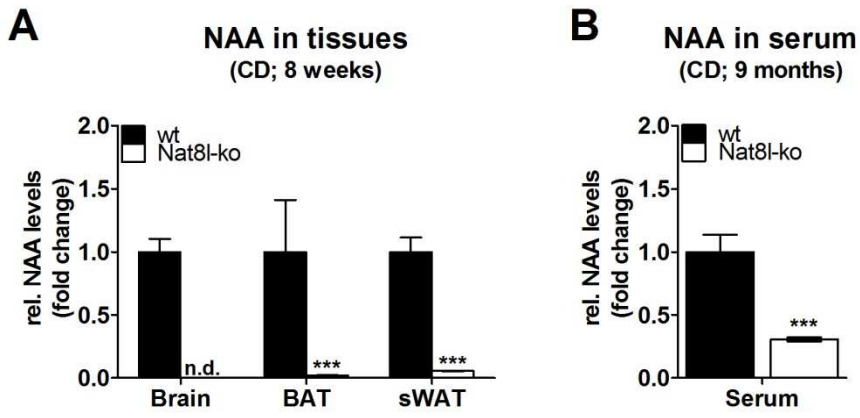

Figure 17. **NAA levels are highly reduced in tissues and serum of *Nat8l*-ko mice.** NAA was measured using HPLC/HRMS. (A) NAA in brain, BAT, and sWAT of wt and *Nat8l*-ko mice at the age of 8 weeks (n = 3). (B) NAA in serum of wt and *Nat8l*-ko mice at the age of 9 months (n = 6 / 5). Data presented as mean ± standard deviation. Statistical significance was assessed by two-tailed Student´s t test. *p < 0.05; **p < 0.01;***p < 0.001.

4.2. Survival rate of Nat8l-ko mice compared to wt littermates

Regardless of the diet, we observed spontaneous death in *Nat8l*-ko mice whereas wt mice survived the whole period of experimental observation (Figure 18). These results might indicate that NAT8L deficiency has severe detrimental effects, although the causes finally leading to lethality remain unclear.

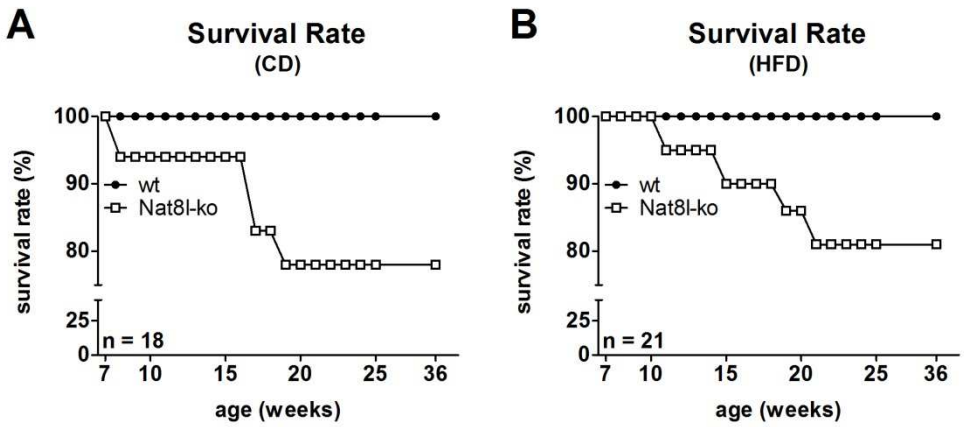

Figure 18. **Survival rate is reduced in *Nat8l*-ko mice.** Number of wt and *Nat8l*-ko mice was monitored from 7 - 36 weeks of age. (A) Survival rate on chow diet (CD) (n = 18). (B) Survival rate on high-fat diet (HFD) (n = 21). Survival rate was calculated as % from initial.

4.3. Initial body weight and blood parameters at the age of 8-9 weeks

Initially, we determined body weight and blood parameters of wt and *Nat8l*-ko mice (age 8-9 weeks) in the fed *ad libitum* and fasted state (overnight – 12 hours). *Nat8l*-ko mice showed reduced body weight when compared to wt littermates. Blood Glucose and plasma free fatty acids (FFA) were unchanged whereas plasma triglyceride (TG) concentrations were significantly reduced in *Nat8l*-ko mice in the fed and fasted state.

Table 3. **Body weight and blood parameters of wt and *Nat8l*-ko mice on chow diet at the age of 8-9 weeks.** (n ≥ 6). Data are presented as mean ± standard deviation. Statistical significance was assessed by two-tailed Student´s t test. Light grey highlighted results show a trend ($p < 0.1$), statistical significant results are highlighted in dark grey. *$p < 0.05$; **$p < 0.01$; ***$p < 0.001$.

Parameter	**fed**			**fasted (overnight – 12h)**		
Chow diet (age 8-9 weeks)[3]	**wt**	***Nat8l*-ko**	**p-value**	**wt**	***Nat8l*-ko**	**p-value**
Weight (g)	24.5 ±0.7	23.3 ±1.1**	0.0077	21.5 ±0.7	21.3 ±1.3	0.7876
Glucose (mg/dL)	161.1 ±17.7	163.6 ±10.1	0.6868	77.7 ±8.1	79.0 ±9.7	0.8017
FFA (mM)	0.762 ±0.10	0.716 ±0.20	0.4839	1.551 ±0.21	1.483 ±0.10	0.6205
TG (mg/dL)	121.2 ±23.8	79.6 ±36.5**	0.0037	149.7 ±34.9	120.9 ±16.8	0.0986

[3] Data fed state from cohort 2. Data fasted state from cohort 3.

4.4. Body weight, weight gain, and blood parameters during chow and high-fat diet feeding

Absolute body weight (fed *ad libitum*) of wt and *Nat8l*-ko mice was monitored weekly after starting CD and HFD feeding. *Nat8l*-ko mice showed significantly reduced body weight at the age of 9 weeks (Table 3, Figure 19A and B). Figure 19A shows that *Nat8l*-ko mice on CD caught up but never had a higher body weight than their wt littermates, reflected by highly significant p-value calculated by ANOVA analysis. Further, weight gain was not significantly different between *Nat8l*-ko an wt mice on CD. On HFD, the decreased body weight of *Nat8l*-ko mice was even more pronounced. In addition, weight gain was significantly lower when *Nat8l*-ko mice were compared to wt littermates (Figure 19B).

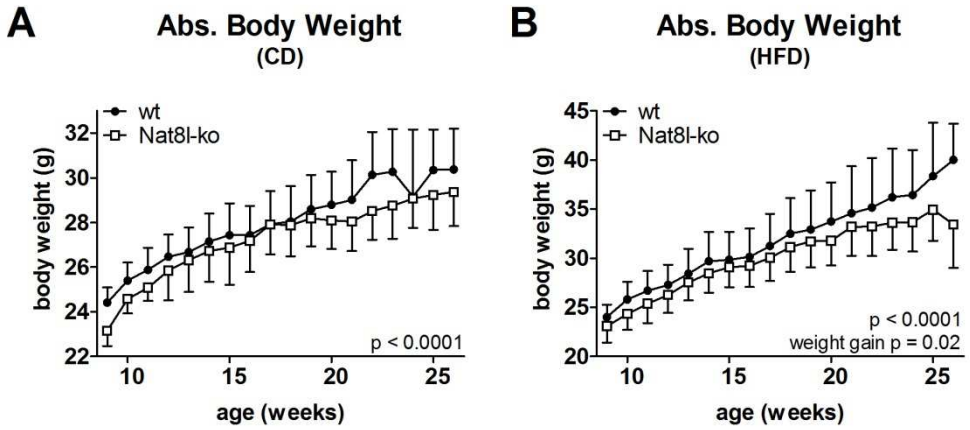

Figure 19. **Body weight and weight gain is reduced in *Nat8l*-ko mice.** Absolute body weight of wt *versus Nat8l*-ko mice was monitored weekly during (A) chow diet (CD) and (B) high-fat diet feeding (HFD) ($n \geq 11$). Data are presented as mean ± standard deviation. Statistical significance was assessed using 2-way ANOVA and $p < 0.05$ was considered as statistically significant.

After 8 weeks on the according diet (age 16 weeks), we again measured body weight and blood parameters. Table 4 shows that there was no body weight difference any more in the CD group whereas HFD fed *Nat8l*-ko mice were still lighter than their wt littermates. Upon fasting, plasma TG concentrations are significantly reduced on CD and there was also a trend to reduction on HFD fed *Nat8l*-ko compared to wt mice. Additionally, fasting blood glucose was significantly reduced on CD and on HFD. Plasma FFA showed no difference.

Table 4. **Body weight and blood parameters of wt and *Nat8l*-ko mice on chow and high-fat diet at the age of 16 weeks.** (n ≥ 10). Data are presented as mean ± standard deviation. Statistical significance was assessed by two-tailed Student´s t test. Light grey highlighted results show a trend ($p < 0.1$), statistical significant results are highlighted in dark grey. *$p < 0.05$; **$p < 0.01$; ***$p < 0.001$.

Parameter	**Fed**			**fasted (overnight – 12h)**		
Chow diet (age 16 weeks)	**wt**	***Nat8l*-ko**	**p-value**	**wt**	***Nat8l*-ko**	**p-value**
Weight (g)	26.89 ±0.96	26.7 ±1.27	0.6534	-	-	-
Glucose (mg/dL)	157.1 ±22.5	143.2 ±12.9*	0.0421	88.2 ±7.1	77.1 ±8.8**	0.0046
FFA (mM)	0.880 ±0.20	0.922 ±0.23	0.5696	1.580 ±0.34	1.599 ±0.21	0.8817
TG (mg/dL)	140.9 ±51.2	138.5 ±60.8	0.9014	108.7 ±21.5	78.8 ±12.7**	0.0015
High-fat diet (age 16 weeks)[4]	**wt**	***Nat8l*-ko**	**p-value**	**wt**	***Nat8l*-ko**	**p-value**
Weight (g)	30.63 ±2.16	28.74 ±1.83*	0.0350	-	-	-
Glucose (mg/dL)	159.1 ±12.3	165.1 ±10.7	0.2229	100.5 ±12.0	86.7 ± 13.6*	0.0200
FFA (mM)	0.919 ±0.16	0.869 ±0.19	0.5107	1.487 ±0.34	1.421 ±0.35	0.6616
TG (mg/dL)	183.7 ±57.7	157.3 ±47.8	0.2625	131.7 ±37.2	102.5 ±31.0	0.0621

Finally, body weight and blood parameter measurements were performed at the age of 34 weeks. Body weight of *Nat8l*-ko mice on CD and HFD was reduced in fed and fasted state (Table 5). Further, blood glucose was significantly lower in *Nat8l*-ko mice in every condition when compared to controls. Plasma TG concentrations were not different between genotypes. As plasma FFA again did not show any differences on CD, we refrained from analyzing FFA levels on HFD. Interestingly, fasting β-hydroxybutyrate (β-OHB) representing one category of ketone bodies, were significantly reduced in *Nat8l*-ko compared to wt mcie on HFD.

Table 5. **Body weight and blood parameters of wt and *Nat8l*-ko mice on chow and high-fat diet at the age of 34 weeks.** (n ≥ 10). Data are presented as mean ± standard deviation. Statistical significance was assessed by two-tailed Student´s t test. Light grey highlighted results show a trend ($p < 0.1$), statistical significant results are highlighted in dark grey. *$p < 0.05$; **$p < 0.01$; ***$p < 0.001$.

Parameter	**fed**			**Fasted (overnight – 12h)**		
Chow diet (34 weeks)[5]	**wt**	***Nat8l*-ko**	**p-value**	**wt**	***Nat8l*-ko**	**p-value**
Weight (g)	30.77 ±1.57	29.53 ±1.09	0.0583	28.03 ±1.47	26.74 ±1.03*	0.0367
Glucose (mg/dL)	161.6 ±21.3	140.9 ±9.52*	0.01431	81.83 ±6.08	68.3 ±9.22***	0.0008
FFA (mM)	0.500 ±0.08	0.477 ±0.06	0.6409	0.843 ±0.17	0.938 ±0.14	0.3940
TG (mg/dL)	73.1 ±12.8	71.9 ±15.3	0.8589	86.3 ±14.7	78.9 ±7.28	0.1847
β-OHB (ng/µL)	-	-	-	174.1 ±24.1	170.9 ±28.5	0.8505
High-fat diet[6] **(34 weeks)**	**wt**	***Nat8l*-ko**	**p-value**	**wt**	***Nat8l*-ko**	**p-value**
Weight (g)	41.27 ±6.00	37.23 ±4.35	0.0746	39.32 ±5.78	34.78 ±4.05*	0.0383
Glucose (mg/dL)	183.3 ±23.4	159.8 ±23.4*	0.0163	108.9 ±20.4	85.73 ±20.2*	0.0122
FFA (mM)	-	-	-	-	-	-
TG (mg/dL)	74.8 ±10.8	77.76 ±13.9	0.5625	94.4 ±19.8	99.02 ±16.4	0.5391
β-OHB (ng/µL)	-	-	-	246.8 ±61.8	165.6 ±61.5*	0.0223

[4] Data from cohorts 1 & 2.
[5] Data from cohorts 2 & 3.
[6] Data from cohorts 2 & 3

4.5. Glucose tolerance and insulin sensitivity

As blood glucose was reduced in *Nat8l*-ko mice compared to controls, I wanted to investigate if glucose tolerance and / or insulin sensitivity are affected by NAT8L deficiency. Therefore, intraperitoneal glucose (ipGTT) and insulin tolerance tests (ipITT) were performed at the age of 16 and 34 weeks, respectively.

In 16 week old CD fed *Nat8l*-ko mice, glucose concentrations were significantly lower during ipGTT whereas glucose tolerance was not changed compared to controls (Figure 20A). Same aged *Nat8l*-ko mice on HFD showed decreased glucose concentrations but also a strong trend to increased glucose tolerance, additionally supported by decreased AUC (Figure 20C). Insulin tolerance was unchanged in 16 week old *Nat8l*-ko when compared to wt mice on CD and HFD (Figure 20B and D).

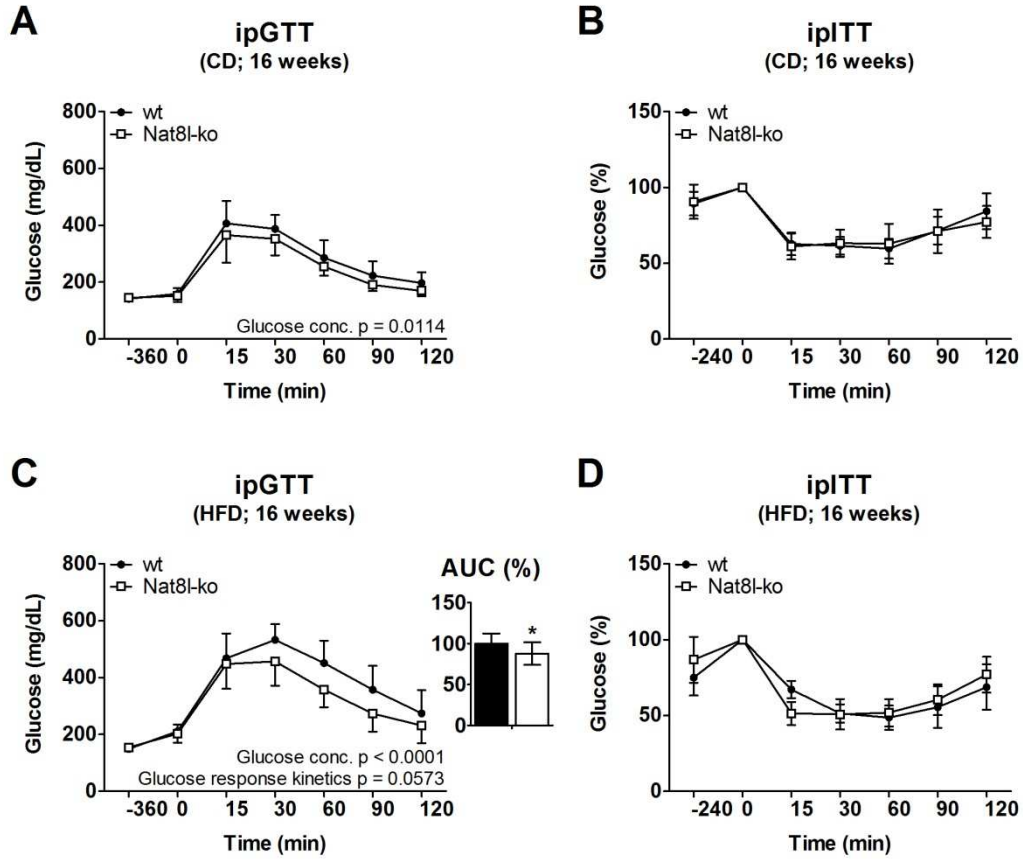

Figure 20. **Glucose tolerance and insulin sensitivity of wt and *Nat8l*-ko mice on chow diet (CD) and high-fat diet (HFD) at an age of 16 weeks.** Intraperitoneal (A) glucose (ipGTT; 1.5 g / kg glucose) and (B) insulin tolerance test (ipITT; 0.5 U / kg insulin) is shown from wt and *Nat8l*-ko mice on CD (n = 10 / 8). (C) ipGTT (1.5 g / kg glucose; n = 12 / 11) and (D) ipITT (0.6 U / kg insulin; n = 12 / 11) is shown from wt and *Nat8l*-ko mice on HFD. AUC was calculated using sum of squares method. ipGTT and ipITT were performed after a 6 and 4 hour fasting period, respectively. Data are presented as mean ± standard deviation. ipGTT and ipITT: Statistical significance was assessed using 2-way ANOVA and $p < 0.05$ was considered as significant. AUC: Statistical significance was assessed by two-tailed Student´s t test. *$p < 0.05$.[7]

[7] Data from cohorts 1 & 2.

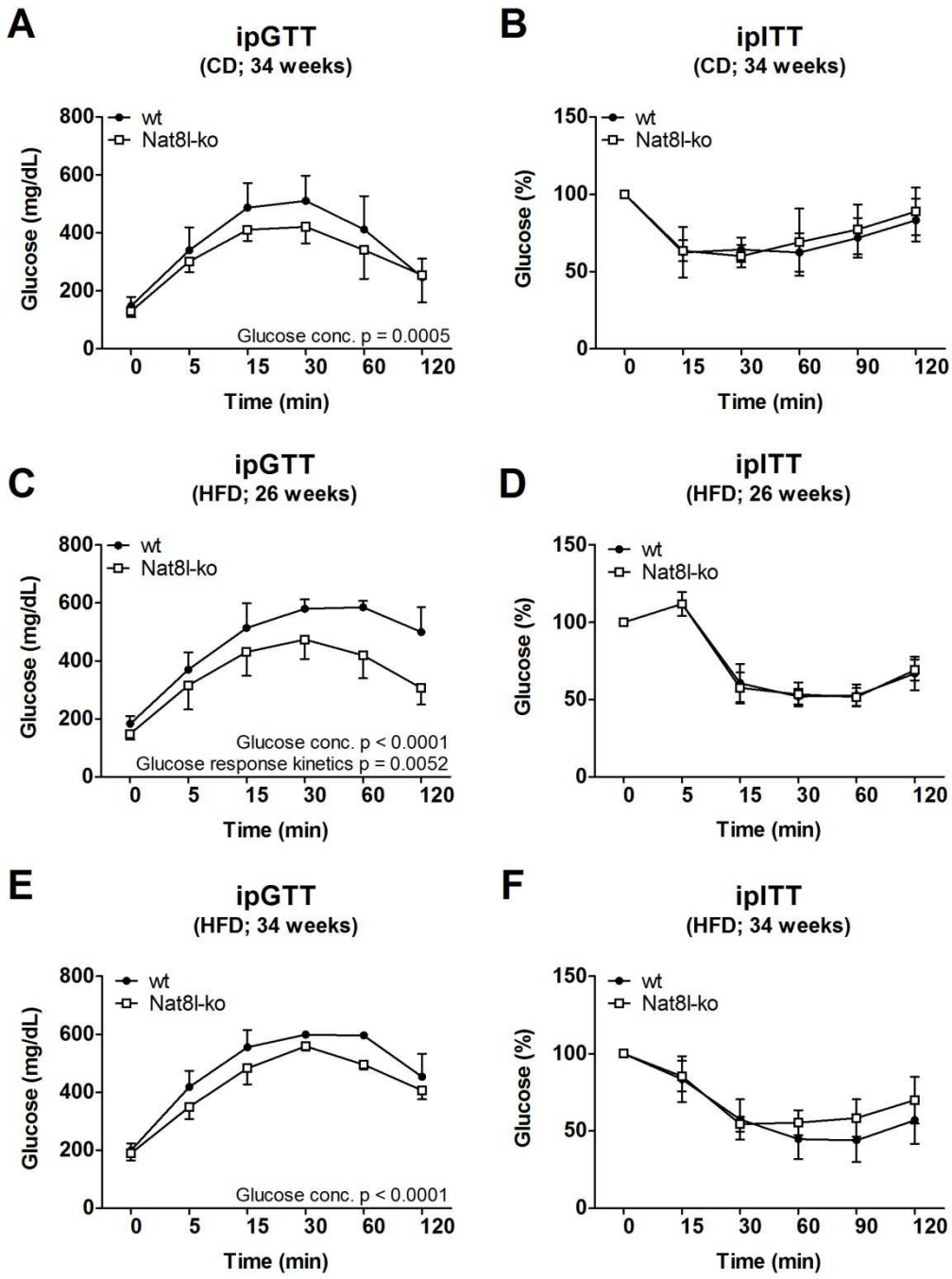

Figure 21. **Glucose tolerance and insulin sensitivity of wt and *Nat8l*-ko mice on chow diet (CD; age 34 weeks) and high-fat diet (HFD; age 26 & 34 weeks).** Intraperitoneal (A) glucose (ipGTT; 1.25 g / kg glucose) and (B) insulin tolerance test (ipITT; 0.5 U / kg insulin) is shown from wt and *Nat8l*-ko mice on CD (n = 10 / 10). (C) ipGTT (1.5 g / kg glucose; n = 12 / 11) and (D) ipITT (0.6 U / kg insulin; n = 7 / 8) is shown from 6 hours fasted wt and *Nat8l*-ko mice on HFD at the age 26 weeks. (E) ipGTT (1.0 g / kg glucose and (F) ipITT (0.7 U / kg insulin) of HFD fed 34 week old wt and *Nat8l*-ko mice (n = 6 / 4). Data are presented as mean ± standard deviation. ipGTT and ipITT were performed after a 6 and 4 hours fasting period, respectively. Statistical significance was assessed using 2-way ANOVA and $p < 0.05$ was considered as significant.[8]

At the age of 34 weeks, *Nat8l*-ko mice on CD showed significantly lower glucose concentrations during ipGTT but neither significant changes in glucose response kinetics nor in insulin

[8] Figure 21A and B: data from cohorts 2 & 3. Figure 21C and D: data from cohort 3. Figure 21E and F: data from cohort 2.

sensitivity (Figure 21A and B). ipGTT and ipITT for HFD fed mice was performed in 26 and 34 weeks old *Nat8l*-ko and wt mice. *Nat8l*-ko mice on HFD also show significantly lower blood glucose during ipGTT (Figure 21C and E) and at the age of 26 weeks, glucose tolerance was also increased in comparison to wt mice (Figure 21C). Of note, more than 50% of values for time point 30 and 60 minutes post glucose injection of 34 weeks old wt mice (Figure 21E) were out of the glucometer measurement range (glucose > 600 mg / dL). These data points were set to 600 mg / dL. Therefore, the difference between wt and *Nat8l*-ko mice can be assumed bigger than depicted in Figure 21E. According to results from 16 weeks old mice (Figure 20B and D), insulin sensitivity is also not changed in 26 or 34 weeks old *Nat8l*-ko mice compared to wt littermates (Figure 21D and F).

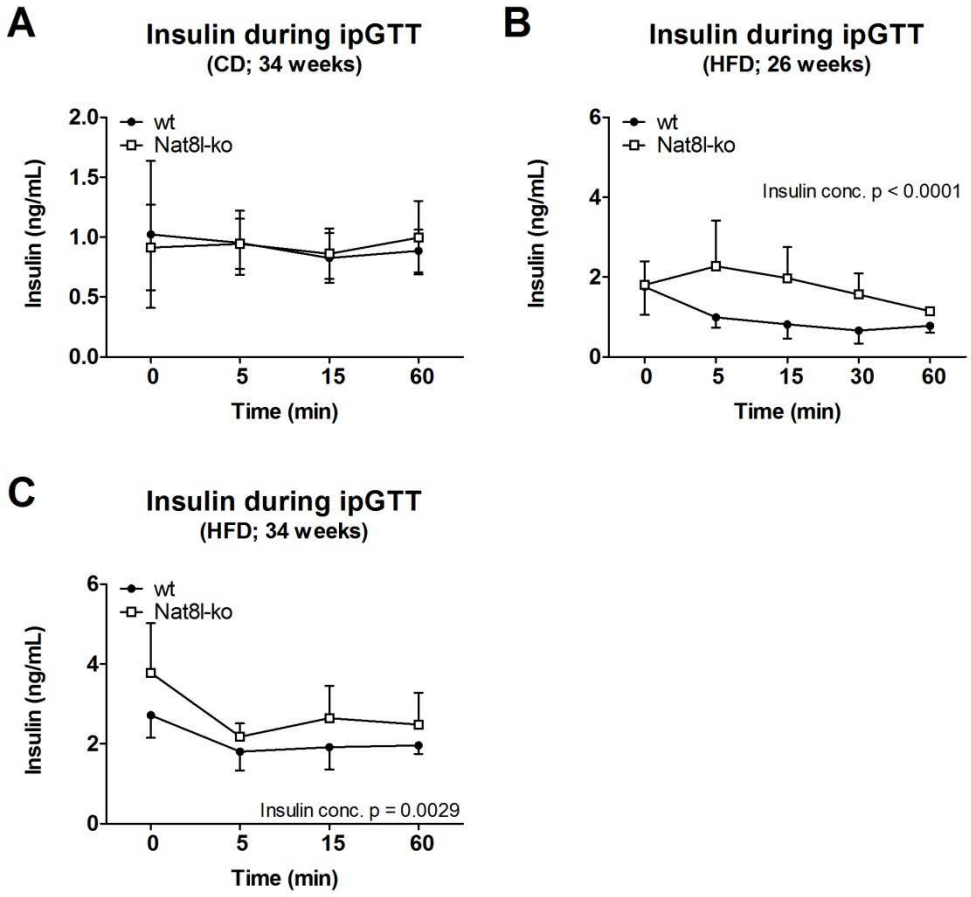

Figure 22. **Plasma insulin during ipGTT in wt and *Nat8l*-ko mice.** (A) Plasma insulin during ipGTT in 34 weeks old wt and *Nat8l*-ko mice on CD. Plasma insulin during ipGTT in (B) 26 weeks old and (C) 34 weeks old wt and *Nat8l*-ko mice on HFD. Insulin concentrations were determined by ELISA immunoassay. Data are presented as mean ± standard deviation. Statistical significance was assessed using 2-way ANOVA and $p < 0.05$ was considered as significant.[9]

We also wanted to assess changes in plasma insulin upon glucose challenge. Therefore, blood was taken by puncture of the facial vein at 0, 5, 15, 30, and 60 minutes during ipGTT and insulin concentration was measured using ELISA immunoassay. Figure 22A shows that insulin levels were not significantly different during ipGTT of *Nat8l*-ko compared to wt mice on CD. It should

[9] Figure 22A: data from cohorts 2 & 3. Figure 22B: data from cohort 3. Figure 22C: data from cohort 2.

be noted that I was not able to show a significant increase of insulin levels after glucose injection in wt mice, as e.g. shown by Miles et al.[168], but absolute insulin concentrations were in a comparable range. However, *Nat8l*-ko mice on HFD had higher plasma insulin concentrations during ipGTT (Figure 22B and C), which corresponds well to the increased glucose tolerance (Figure 21C and E).

4.6. Nat8l-ko mice loose more weight during overnight fasting than wt mice

We analyzed weight data of 26 and 34 week old wt and *Nat8l*-ko mice after overnight fasting (12h; see Table 5). Absolute weight loss within 12 hours over night fasting was significantly higher in *Nat8l*-ko mice on HFD (1.95 ±0.38 g in wt *versus* 2.49 ±0.39 g in *Nat8l*-ko mice; p = 0.0002) and showed the same trend on CD (2.58 ±0.47 g in wt *versus* 2.79 ±0.18 g in *Nat8l*-ko mice; p = 0.1861) (Figure 23A). Relative weight loss upon overnight fasting was significantly higher in *Nat8l*-ko mice when compared to wt littermates on CD and HFD (Figure 23B).

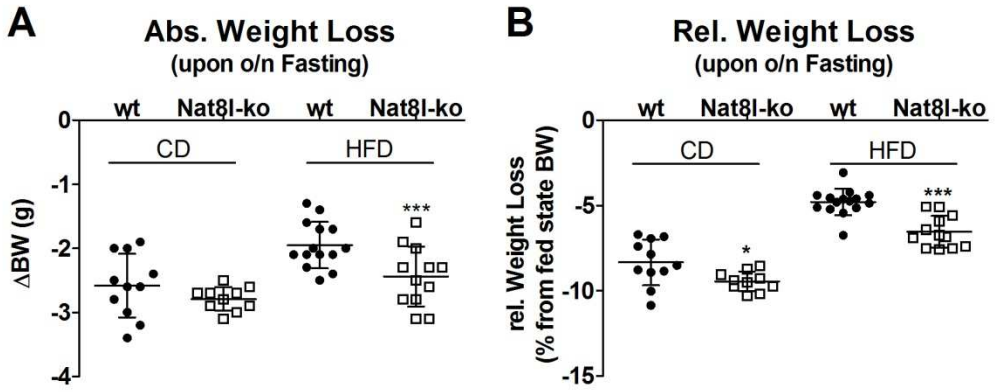

Figure 23. W**eight loss is increased during overnight (o/n) fasting in *Nat8l*-ko compared to wt mice.** CD age: 34 weeks, HFD age: 26 and 34 weeks. (A) Absolute weight loss. (B) Relative weight loss as % from fed state body weight (BW). Data are presented as mean ± standard deviation. (Statistical significance was assessed by two-tailed Student´s t test. *p < 0.05; **p < 0.01; ***p < 0.001.[10]

4.7. Body length of Nat8l-ko mice is slightly reduced

We wanted to analyze, if body length is different between wt and *Nat8l*-ko mice. Therefore, nose to anus length (in mm) was measured as described[169] using a linear ruler. *Nat8l*-ko mice on CD showed a trend to reduced body length on CD (91.23 ±3.52 mm in wt *versus* 88.90 ±4.93 mm in *Nat8l*-ko mice; p = 0.0631) at the age of 34 weeks. Body length was not significantly different between wt and *Nat8l*-ko mice on HFD at the age of 26 (p = 0.1505) and 34 weeks (p = 0.5849), respectively. Therefore, the HFD group in Figure 24 was averaged for mice at both ages. Compared to CD, body length of *Nat8l*-ko compared to wt mice was similar on HFD (92.40 ±3.52 mm in wt *versus* 90.67 ±5.12 mm in *Nat8l*-ko mice; p = 0.1438) (Figure 24).

[10] Data from cohorts 2 & 3.

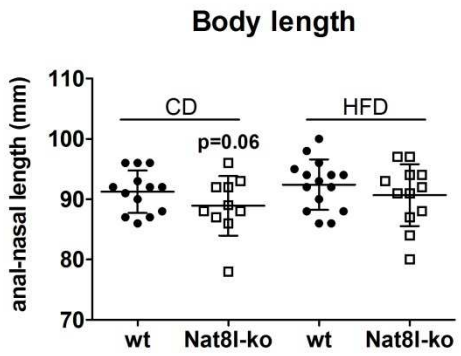

Figure 24. **Body length of wt and *Nat8l*-ko mice.** CD age: 34 weeks, HFD age: 26 and 34 weeks. Data are presented as mean ± standard deviation. Statistical significance was assessed by two-tailed Student´s t test.[11]

4.8. Indirect calorimetry of wt and Nat8l-ko mice

As shown above, blood glucose was reduced whereas glucose tolerance and relative weight loss upon fasting was increased in *Nat8l*-ko compared to wt mice. Therefore, we aimed to characterize 26 weeks old *Nat8l*-ko and wt mice on CD and HFD housed in single metabolic cages (MK-5000RQ; Muromachi Kikai[170], Tokyo, Japan) to perform indirect calorimetric measurements. All data from indirect calorimetry are derived from cohort 2.

Due to high occupancy of metabolic cages, the measurement period was limited to 72 hours per mouse. This is rather short as mice have to acclimate to single housing and probably different drinking and / or feeding apparatus[171]. Longer periods (at least 3 – 4 days) of acclimatization have been suggested by Stechman et al.[172]. In contrast, Kalliokoski et al. reported that BALB/c mice never acclimate to single housing[173].

For these analyses, the first 48 hours were excluded as acclimatization phase. Analysis of the last 24 hours of 12 : 12 hours light : dark cycle was performed. Zeitgeber time 0 corresponds to start of the light cycle (7 a.m.) and Zeitgeber time 12 corresponds to the beginning of the dark cycle (7 p.m.). As group numbers were quite small (CD: n = 5 wt and 4 *Nat8l*-ko mice; HFD n = 6 wt and 4 *Nat8l*-ko-mice), it would be of great interest to repeat these studies to increase the number of mice per group. However, the obtained results give a good first glance on the metabolic status of *Nat8l*-ko *versus* wt mice.

4.8.1. Food intake, water intake, and locomotor activity

First, food and water intake were calculated as gram per mouse per day. Food intake was not different between *Nat8l*-ko and wt mice on CD. On HFD, *Nat8l*-ko mice showed a strong trend to increased food intake (Figure 25A). Water intake was unchanged when *Nat8l*-ko were compared to wt mice. Locomotor activity (LA) was analyzed as counts per mouse per 12h.

[11] Data from cohorts 2 & 3.

Nat8l-ko mice showed similar LA on CD and HFD (Figure 25C and D) when compared to controls.

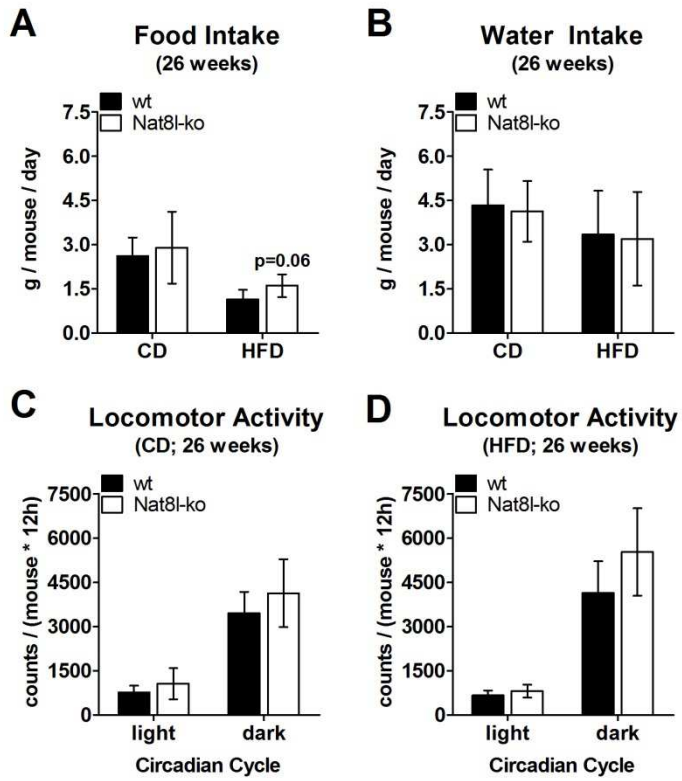

Figure 25. **Food intake, water intake, and locomotor activity from wt and *Nat8l*-ko mice at the age of 26 weeks.** (n = 5 / 4 for CD; n = 6 / 5 for HFD). (A) Food and (B) drink intake as gram / mouse / day (24 hours) on CD and HFD. Locomotor activity in the light and dark cycle is shown on (C) CD and (D) HFD. Data are presented as mean ± standard deviation. Statistical significance was assessed by two-tailed Student´s t test.

Second, metabolic parameters reflected by oxygen (O_2) consumption, carbon dioxide (CO_2) production, respiratory exchange ratio (RER), and energy expenditure (EE) were analyzed.

4.8.2. Oxygen (O_2) consumption

Oxygen consumption was determined and shown as progression curve during one circadian cycle as well as mean O_2 consumption during light and dark cycle calculated for wt and *Nat8l*-ko mice on CD and HFD. O_2 consumption is shown as ml O_2 / min / $kg^{0.75}$, where $kg^{0.75}$ corresponds to the metabolic body weight after Kleiber´s law[174]. O_2 consumption was increased in Nat8l-ko mice fed a CD, at least in the dark cycle (Figure 26A and B). Additionally, O_2 consumption of *Nat8l*-ko mice on HFD was significantly increased in the light and higher in the dark cycle (Figure 26C and D).

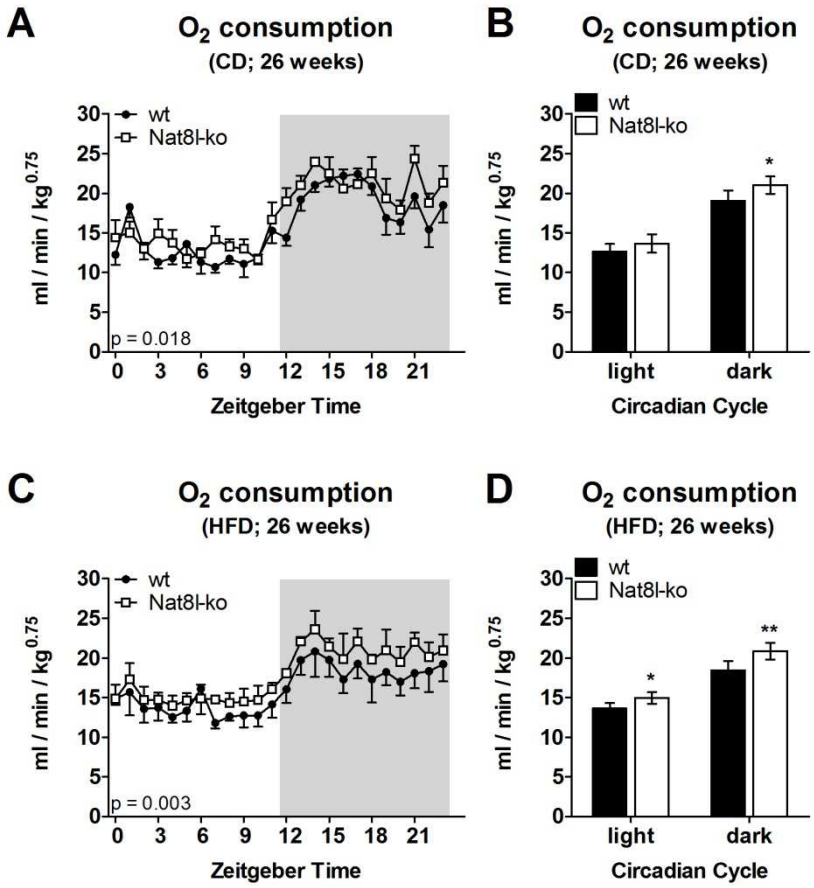

Figure 26. **Oxygen consumption rate is increased in *Nat8l*-ko compared to wt mice at the age of 26 weeks.** (n = 5 / 4 for CD; n = 6 / 5 for HFD). (A) Progression curve and (B) mean oxygen consumption rate per circadian cycle of wt and *Nat8l*-ko mice on CD. (C) Progression curve and (D) mean oxygen consumption rate per circadian cycle of wt and *Nat8l*-ko mice on HFD. Data are presented as mean ± standard deviation. Statistical significance was assessed by 2-way ANOVA (p-value < 0.05 was considered as significant) and two-tailed Student´s t test (*p < 0.05; **p < 0.01; ***p < 0.001), respectively.

4.8.3. Carbon dioxide (CO_2) production

CO_2 production was analyzed and is shown as progression curve during one circadian cycle as well as mean CO_2 production during light and dark cycle calculated for wt and *Nat8l*-ko mice on CD and HFD. CO_2 production is shown as ml CO_2 / min / $kg^{0.75}$. CO_2 production was unchanged in *Nat8l*-ko mice fed CD (Figure 27A and B). In contrast, CO_2 production of *Nat8l*-ko mice on HFD was significantly increased in the light and in the dark cycle (Figure 27C and D).

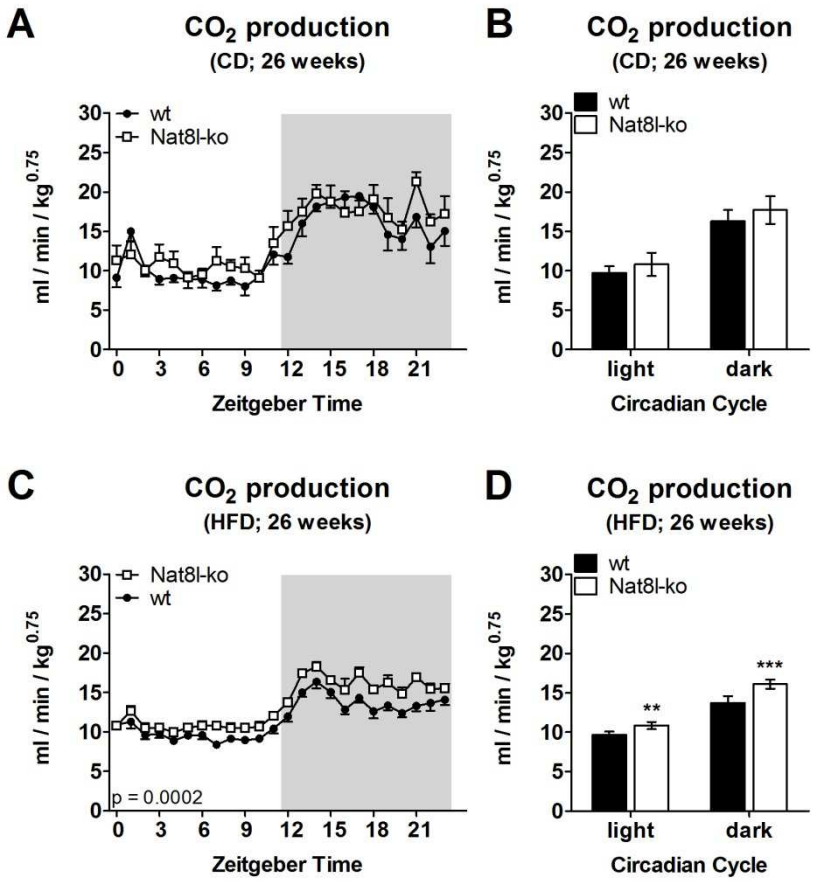

Figure 27. **Carbon dioxyde (CO_2) production rate of wt and *Nat8l*-ko mice at the age of 26 weeks.** (n = 5 / 4 for CD; n = 6 / 5 for HFD). (A) Progression curve and (B) mean CO_2 production rate per circadian cycle of wt and *Nat8l*-ko mice on CD. (C) Progression curve and (D) mean CO_2 production rate per circadian cycle of wt and *Nat8l*-ko mice on HFD. Data are presented as mean ± standard deviation. Statistical significance was assessed by 2-way ANOVA (p-value < 0.05 was considered as significant) and two-tailed Student´s t test (*p < 0.05; **p < 0.01; ***p < 0.001), respectively.

4.8.4. Respiratory exchange ratio (RER)

Respiratory exchange ratio (RER) is defined as the ratio between volume of CO_2 produced and volume of oxygen consumed (RER = VCO_2 / VO_2). A RER close to 1 reflects a high rate of carbohydrate oxidation whereas a RER of 0.7 indicates fatty acids as oxidation substrates. In contrast, the so called respiratory quotient (RQ), which is often synonymously used, reflects the actual substrate oxidation at tissue level and is reflected in the RER, but not necessarily the same.[171]

RER was analyzed and is shown as progression curve during one circadian cycle and as mean RER during light and dark cycle calculated for wt and *Nat8l*-ko mice on CD and HFD. RER was unchanged in Nat8l-ko mice fed CD (Figure 28A and B). In HFD feeding, RER of *Nat8l*-ko mice on HFD was significantly increased in the dark cycle (Figure 28C and D).

When wt and *Nat8l*-ko mice were compared according to diet dependent changes in RER, a significant decrease of the RER could be observed when mice were fed a HFD (Table 6). This

reflects the effect that, due to HFD feeding, more fatty acids are available and used as energy substrate.

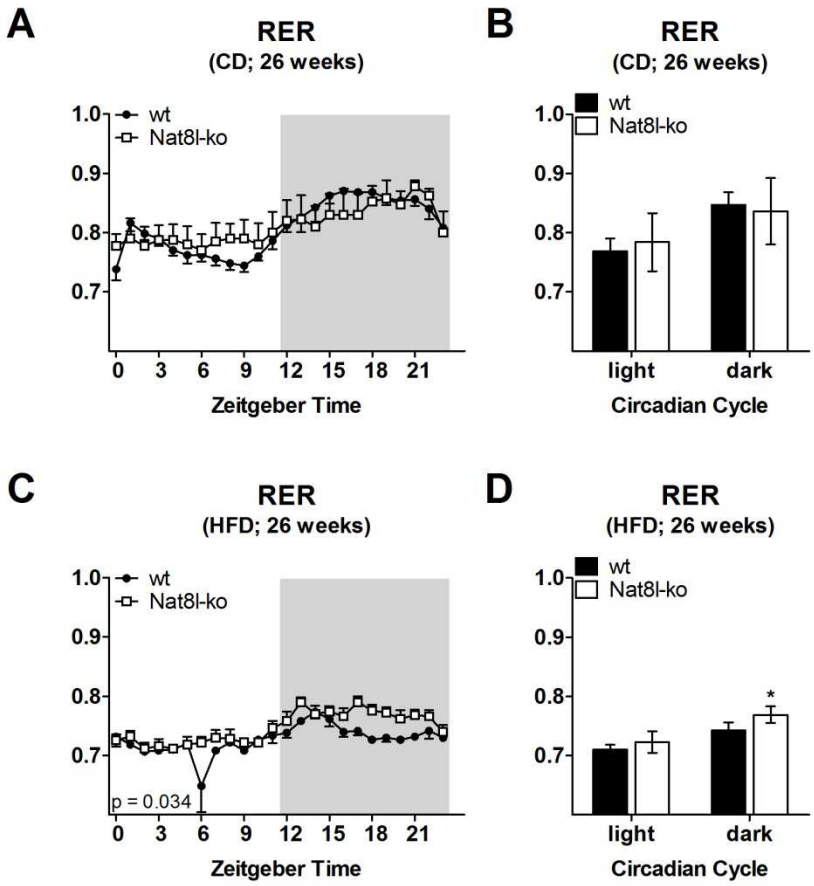

Figure 28. **Respiratory exchange ratio (RER) of wt and *Nat8l*-ko mice at the age of 26 weeks.** (n = 5 / 4 for CD; n = 6 / 5 for HFD). (A) Progression curve and (B) mean RER per circadian cycle of wt and *Nat8l*-ko mice on CD. (C) Progression curve and (D) mean RER per circadian cycle of wt and *Nat8l*-ko mice on HFD. Data are presented as mean ± standard deviation. Statistical significance was assessed by 2-way ANOVA (p-value < 0.05 was considered as significant) and two-tailed Student´s t test (*p < 0.05; **p < 0.01; ***p < 0.001), respectively.

Table 6. **Respiratory exchange ratio (RER) of wt and *Nat8l*-ko mice at the age of 26 weeks comparing CD and HFD.** (n = 5 / 4 for CD; n = 6 / 5 for HFD). RER changes due to the diet were compared between wt and *Nat8l*-ko mice. Data are presented as mean ± standard deviation. Statistical significance was assessed by two-tailed Student´s t test and is highlighted in dark grey. *p < 0.05; **p < 0.01; ***p < 0.001.

Parameter	**light**			**dark**		
RER (26 weeks)	**CD**	**HFD**	**p-value**	**CD**	**HFD**	**p-value**
wt	0.77 ±0.02	0.71 ±0.01***	0.0001	0.85 ±0.02	0.74 ±0.01***	<0.0001
Nat8l-ko	0.78 ±0.05	0.72 ±0.02*	0.0362	0.84 ±0.06	0.77 ±0.01*	0.0347

4.8.5. Energy expenditure (EE)

Total energy expenditure (EE) in cal / min / $kg^{0.75}$ was calculated according to Suzuki et al.[170] using the following equation:

$$EE = (1.07 \cdot RER + 3.98) \cdot VO_2$$

The coefficients in this equation are predefined by the operating parameters of the calorimetry system (e.g. cage size, flow rate, etc.).

It has been reported that normalization of EE to metabolic body weight is more suitable for comparison of rates between different species rather than comparing within one species. Analysis of covariance (ANCOVA)[171,175] was recommended as a proper method, where total EE is displayed per mouse (in kcal / mouse / hour) as a function of body weight and linear regression calculations for each genotype are compared. Figure 29 shows three different ways for displaying EE.

First, energy expenditure is displayed as cal / min / $kg^{0.75}$ for a period of 24 hours (Figure 29A and C). Zeitgeber time 0 corresponds to the beginning of the light phase and Zeitgeber time 12 corresponds to the beginning of the dark phase. Statistical significance was assessed by ANOVA by comparing EE between genotypes over time. From these analyses we can conclude that EE was significantly increased in *Nat8l*-ko mice on CD and HFD when compared to controls (Figure 29A and C).

Second, mean values for EE were calculated during light and dark cycle. On CD, *Nat8l*-ko mice showed a trend to an increased EE (Figure 29B), but Figure 29D shows that EE was significantly increased in *Nat8l*-ko compared to wt mice on HFD. Student´s t test was performed to test statistical significance.

Finally, EE was plotted as function of body weight and linear regression analysis was performed on individual data sets. Of note, if EE was the same function of body weight for wt and *Nat8l*-ko mice, the linear regression lines would overlap. EE was significantly increased in *Nat8l*-ko compared to wt mice on CD as the two regression lines showed significantly different values for the intercept ($p = 0.0069$; Figure 29E). On HFD, the same trend could be observed although the correlation coefficient for the wt group is very poor ($R^2 = 0.18$) (Figure 29F).

In summary, an increased number of mice would be highly desirable, especially to provide a better basis for the data analysis by ANCOVA. However, it can be concluded that total EE of *Nat8l*-ko mice is increased compared to wt littermates.

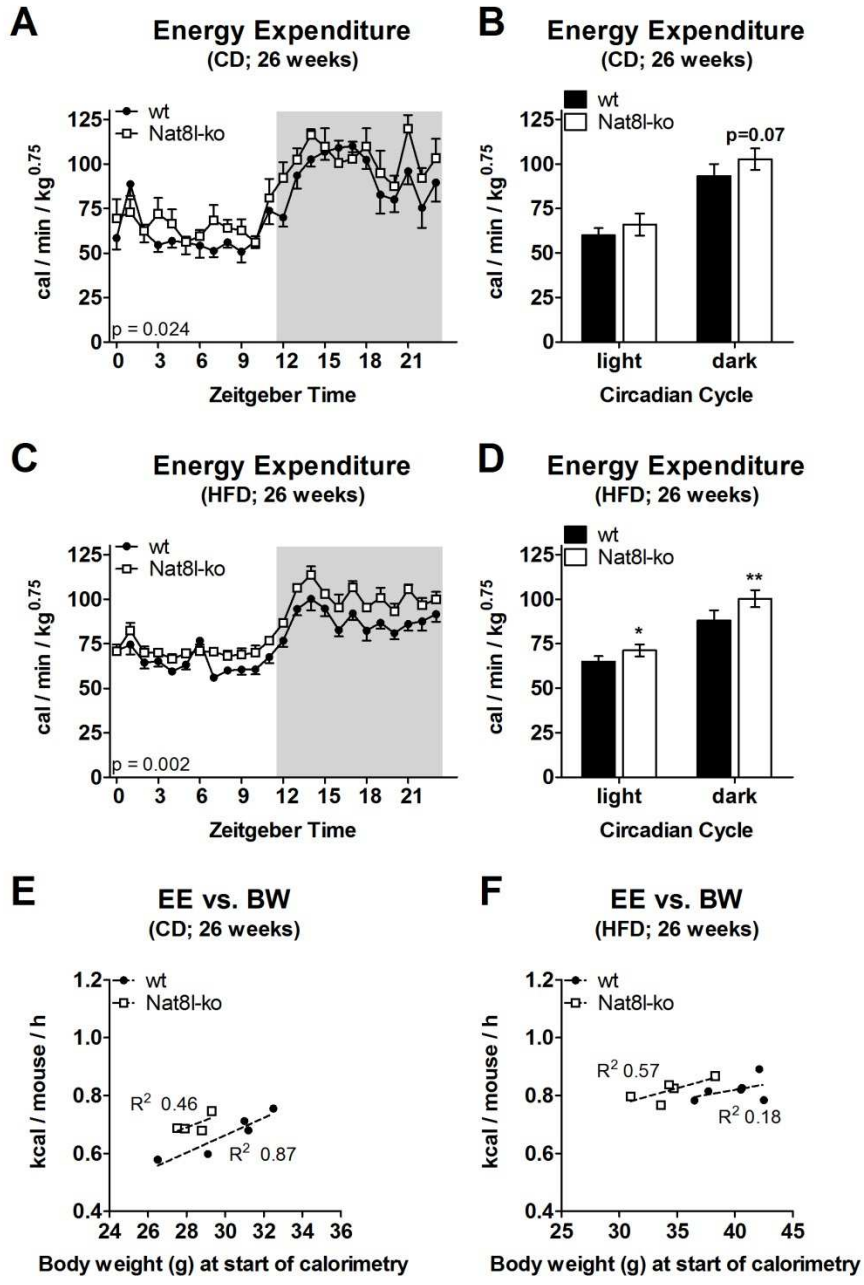

Figure 29. **Total energy expenditure (EE) is increased in *Nat8l*-ko mice compared to wt littermates at the age of 26 weeks.** (n = 5 / 4 for CD; n = 6 / 5 for HFD). (A) Progression curve and (B) mean EE (cal / min / $kg^{0.75}$) per circadian cycle of wt and *Nat8l*-ko mice on CD. (C) Progression curve and (D) mean EE (cal / min / $kg^{0.75}$) per circadian cycle of wt and *Nat8l*-ko mice on HFD. EE in kcal / mouse / hour is shown for (E) CD and (F) HFD. Linear regression analysis was performed for data points from wt and *Nat8l*-ko mice, respectively. Data are presented as mean ± standard deviation. Statistical significance was assessed by 2-way ANOVA (A and C; p-value < 0.05 was considered as significant.), two-tailed Student´s t test (B and D; *p < 0.05; **p < 0.01; ***p < 0.001), and ANCOVA (E and F; p-value < 0.05 was considered as significant), respectively.

4.9. Terminal experiments at room temperature (RT)

Finally, we decided to perform final experiments at the age of 9 months. Mice on CD and HFD were harvested between 8 a.m. and 12 a.m. in the fed *ad libitum* state. Blood was drawn from the facial vein and analyses were performed in serum. Further analyses of tissue weight, tissue oxygen consumption, fatty acid (FA) and glycerol release from adipose tissues, and molecular characterization of BAT (marker gene expression, morphology, and UCP1 expression) was performed. All data presented in this section were acquired from cohort 2.

4.9.1. Blood parameters, tissue weight, tissue oxygen consumption, and fatty acid / glycerol release from adipose tissue

Body weight and final blood parameters of wt and *Nat8l*-ko mice on CD and HFD at an age of 9 months are shown in Table 7. Body weight of *Nat8l*-ko mice at the age of 9 months was lower compared to wt animals, but only the difference of the HFD group was significant. On CD, blood glucose showed a trend to reduction as previously observed in younger cohorts (see Table 4 & Table 5) while no more reduction of glucose could be observed in the aged *Nat8l*-ko mice on HFD. Also in contrast to younger cohorts, serum TG levels were significantly higher in *Nat8l*-ko mice compared to controls fed a HFD.

Table 7. **Body weight and blood parameters of wt and *Nat8l*-ko mice on chow and high-fat diet at the age of 9 months.** (n = 6 / 5 for CD; n = 6 / 4 for HFD). Data are presented as mean ± standard deviation. Statistical significance was assessed by two-tailed Student´s t test. Light grey highlighted results show a trend ($p < 0.1$), statistical significant results are highlighted in dark grey. *$p < 0.05$; **$p < 0.01$; ***$p < 0.001$.

Weight / blood parameters (RT)			
Chow diet (age 9 months)	**Wt**	***Nat8l*-ko**	**p-value**
Weight (g)	30.37 ±1.69	29.04 ±0.75	0.1746
Glucose (mg/dL)	139.5 ±7.2	130.0 ±6.2	0.0649
FFA (mM)	0.741 ±0.06	0.554 ±0.13*	0.0185
TG (mg/dL)	110.6 ±29.4	122.8 ±43.2	0.6291
High-fat diet (age 9 months)	**Wt**	***Nat8l*-ko**	**p-value**
Weight (g)	44.95 ±1.64	40.78 ±1.58**	0.0072
Glucose (mg/dL)	149.2 ±12.8	138.5 ±7.7	0.2173
FFA (mM)	0.525 ±0.15	0.494 ±0.07	0.7264
TG (mg/dL)	60.2 ±13.0	92.6 ±16.9*	0.0240

After sacrificing mice, tissue weight of eWAT, sWAT, BAT, and heart was determined for wt and *Nat8l*-ko mice (Table 8). No significant differences of tissue weight could be observed in the CD group, although there was a trend towards a reduction of eWAT mass in *Nat8l*-ko compared to wt mice. On HFD, sWAT mass was about 30 – 40 % reduced in *Nat8l*-ko compared to wt mice. After excision, tissues have also been checked for any morphological differences, but no obvious differences were noticed.

Table 8. **Tissue weight of eWAT, sWAT, BAT and heart of wt and *Nat8l*-ko mice on chow and high-fat diet at the age of 9 months.** (n = 6 / 5 for CD; n = 6 / 4 for HFD). Tissue weight was calculated as absolute weight (g) and as percentage of body weight (% BW). Data are presented as mean ± standard deviation. Statistical significance was assessed by two-tailed Student´s t test. Light grey highlighted results show a trend (p < 0.1), statistical significant results are highlighted in dark grey. *p < 0.05; **p < 0.01; ***p < 0.001.

Tissue weight (RT)				
Chow diet (age 9 months)		**wt**	***Nat8l*-ko**	**p-value**
eWAT	(mg)	579.3 ±143.0	418.8 ±59.2	0.0626
	% BW	1.89 ±0.38	1.44 ±0.18	0.0556
sWAT	(mg)	287.0 ±45.5	266.2 ±29.2	0.4458
	% BW	0.94 ±0.11	0.91 ±0.08	0.6959
BAT	(mg)	93.7 ±14.8	93.4 ±12.1	0.9774
	% BW	0.307 ±0.036	0.321 ±0.038	0.5792
Heart	(mg)	121.8 ±5.1	118.2 ±11.2	0.5362
	% BW	0.402 ±0.019	0.407 ±0.034	0.7956
High-fat diet (age 9 months)		**wt**	***Nat8l*-ko**	**p-value**
eWAT	(mg)	1993.3 ±426.3	1848.8 ±275.0	0.6060
	% BW	4.43 ±0.95	4.55 ±0.76	0.8548
sWAT	(mg)	1875.2 ±240.7	1366.3 ±107.9**	0.0075
	% BW	4.16 ±0.43	3.35 ±0.16*	0.0113
BAT	(mg)	165.0 ±28.3	148.5 ±24.8	0.4205
	% BW	0.366 ±0.052	0.363 ±0.050	0.9438
Heart	(mg)	127.0 ±16.1	116.5 ±10.1	0.3308
	% BW	0.283 ±0.036	0.286 ±0.021	0.8987

Subsequently, adipose tissues were divided into five parts. Tissue oxygen consumption measurement and analysis of FA / glycerol release was performed immediately. On CD, *Nat8l*-ko mice showed increased oxygen consumption rates in BAT, sWAT, and eWAT (Figure 30A). On HFD, oxygen consumption in *Nat8l*-ko eWAT was reduced while it was unchanged in BAT and sWAT when compared to wt (Figure 30B).

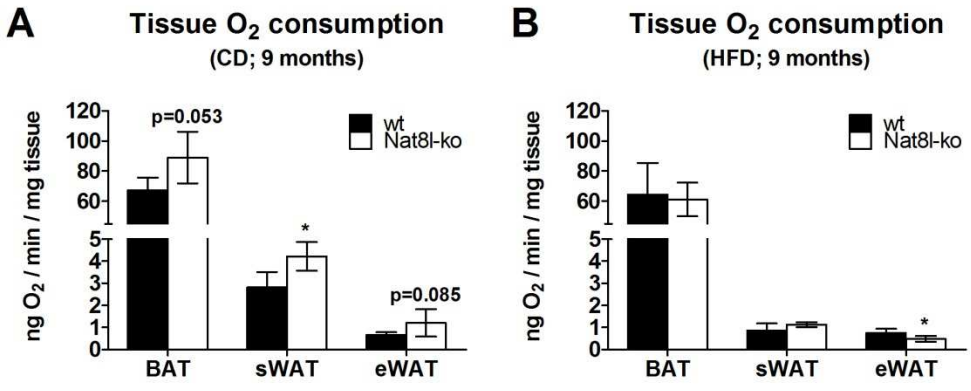

Figure 30. **Tissue oxygen (O_2) consumption of BAT, sWAT, and eWAT from wt and *Nat8l*-ko mice at the age of 9 months.** (n = 6 / 5 for CD; n = 6 / 4 for HFD). Data are presented as mean ± standard deviation. Tissue oxygen consumption rate of BAT, sWAT, and eWAT from wt and *Nat8l*-ko mice shown for (A) CD and (B) HFD was measured using a Clark electrode (Strathkelvin Instruments). Statistical significance was assessed by two-tailed Student´s t test. *p < 0.05; **p < 0.01; ***p < 0.001.

As read out for adipose tissue lipolytic activity, FA and glycerol release was measured (Figure 31) after incubation of tissues for 1 hour in DMEM containing 2 % fatty acid-free BSA to

scavenge FAs. Basal and β-adrenergic-stimulated release (10 µM isoproterenol (Iso) preincubation for 1 hour) was determined and normalized to tissue protein after lipid extraction. Triacsin C, an inhibitor of acyl-CoA synthetase long-chain family member (ACSL) enzyme activity, preventing re-esterification of FAs[176], was not used in these experiments. FA release from eWAT and sWAT under basal conditions was strongly reduced in *Nat8l*-ko mice on CD and HFD when compared to controls (Figure 31A). Isoproterenol-stimulated FA release on CD was decreased in BAT but unchanged in sWAT and eWAT of *Nat8l*-ko compared to wt mice (Figure 31B). On HFD, FA release from BAT, sWAT, and eWAT was not different between wt and *Nat8l*-ko mice upon isoproterenol stimulation. Basal and isoproterenol-stimulated glycerol release from BAT, sWAT and eWAT was similar when *Nat8l*-ko mice were compared to wt (Figure 31C and D).

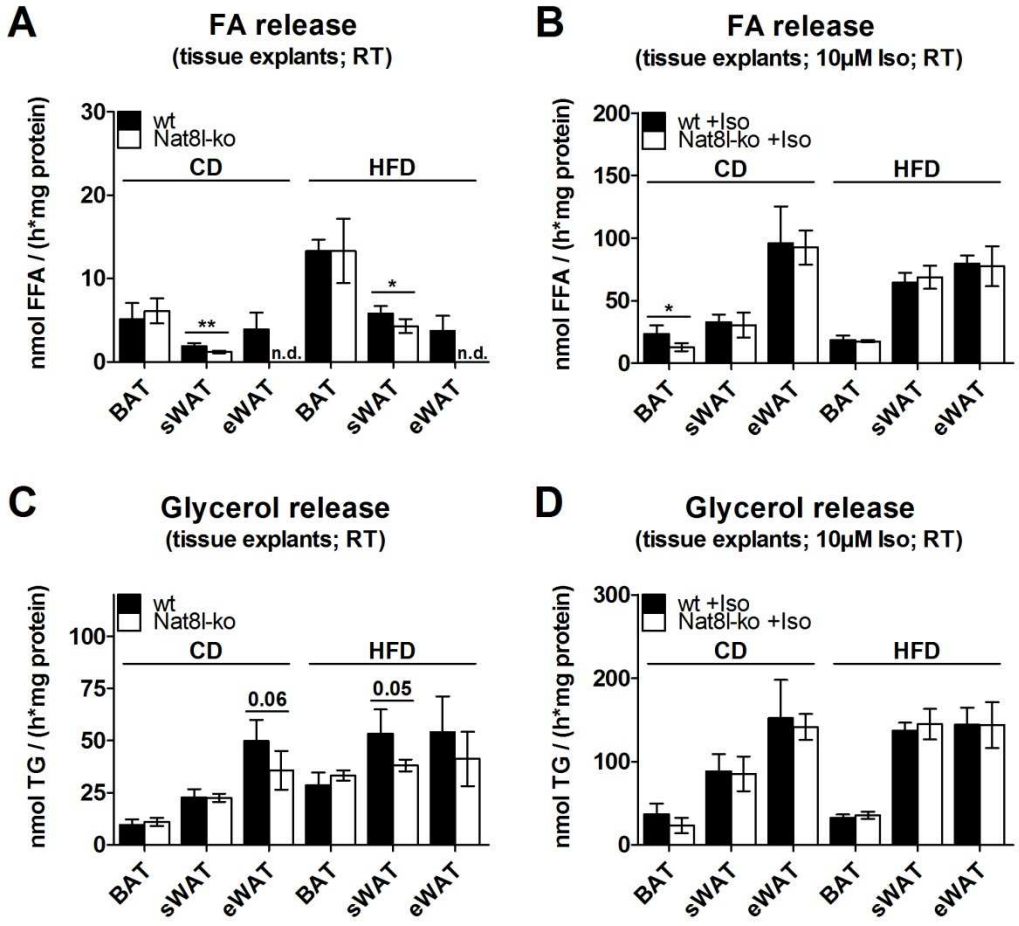

Figure 31. **Fatty acid (FA) and glycerol release in BAT, sWAT, and eWAT of wt and *Nat8l*-ko mice on chow (CD) and high-fat diet (HFD) at the age of 9 months.** (n = 6 / 5 for CD; n = 6 / 4 for HFD). Data are presented as mean ± standard deviation. (A) Basal and (B) β-adrenergic-stimulated (10 µM isoproterenol (+Iso) for 1 hour) FA release from BAT, sWAT, and eWAT. (C) Basal and (D) β-adrenergic-stimulated (10 µM isoproterenol (+Iso) for 1 hour) glycerol release from BAT, sWAT, and eWAT. Statistical significance was assessed by two-tailed Student´s t test. *p < 0.05; **p < 0.01; ***p < 0.001.

4.9.2. Marker gene expression, morphology, and UCP1 protein expression in BAT

We investigated marker gene expression, morphology, and UCP1 protein expression in BAT of 9 month old wt and *Nat8l*-ko mice. RNA was extracted from BAT, followed by cDNA synthesis and gene expression analysis by qRT-PCR: On CD, *Ucp1*, *Pgc1α*, and *Pparγ2* were significantly increased in BAT of *Nat8l*-ko mice (Figure 32A). We also observed a trend to increased expression of *Pparα* and *Cidea* (Figure 32A), corroborating the expression profile we received with *Nat8l*-ko mice at the age of 3 - 4 months (Figure 16H). *Acly* mRNA expression was not changed at the age of 9 months (Figure 32A). On HFD, *Cidea* and *Acly* expression was significantly increased in *Nat8l*-ko compared to wt mice, while *aP2* and *Ucp1* showed a trend to increased expression in BAT of *Nat8l*-ko mice (Figure 32B).

Next, Hematoxylin & Eosin (HE) and UCP1 immunohistochemistry staining was performed for BAT of *Nat8l*-ko and wt mice on CD and HFD. HE staining revealed decreased lipid droplet (LD) area and diameter in *Nat8l*-ko mice compared to controls on CD and HFD (Figure 32C, quantified in Figure 32D and E). Further, UCP1 protein staining was increased in BAT of *Nat8l*-ko compared to wt mice on both diets (Figure 32C). We also investigated sWAT morphology by HE and UCP1 staining and did not find any differences (data not shown).

Interestingly, we found increased UCP1 protein expression already in BAT of 8 week old *Nat8l*-ko mice on CD as shown by western blot analysis and quantification (Figure 32F).

In summary, these results show increased expression of UCP1 mRNA / protein in BAT of *Nat8l*-ko mice on CD and HFD accompanied by decreased lipid droplet area and diameter. Other BAT marker genes such as *Pparα* and *Pgc1α* seem to have diet specific expression patterns. I also wanted to investigate expression of genes involved in *de novo* lipogenesis DNL and FA oxidation. Therefore, I measured mRNA expression of *Acss2*, *Acsl1*, *Scd1*, and *Cpt1b* (Figure 33). *Acss2* encodes for cytosolic actely-CoA synthetase (ACSS2), the enzyme acetylating coenzyme A using free acetate to yield acetyl-CoA which can be used for lipid synthesis[103]. Acyl-CoA synthetase long-chain family member 1 (*Acsl1*) encodes for a protein which activates free FA for esterification or β-oxidation[177]. Stearoyl-CoA desaturase (SCD1) produces monounsaturated fatty acids from saturated fatty acids and its activity is upregulated with increasing dietary carbohydrate content[178]. CPT1b is the rate limiting enzyme of FA transport into mitochondria for β-oxidation[158,159]. Overall, expression of *Acss2*, *Acsl1*, *Scd1*, and *Cpt1b* was not different between *Nat8l*-ko and wt mice on CD (Figure 33A) and HFD (Figure 33B).

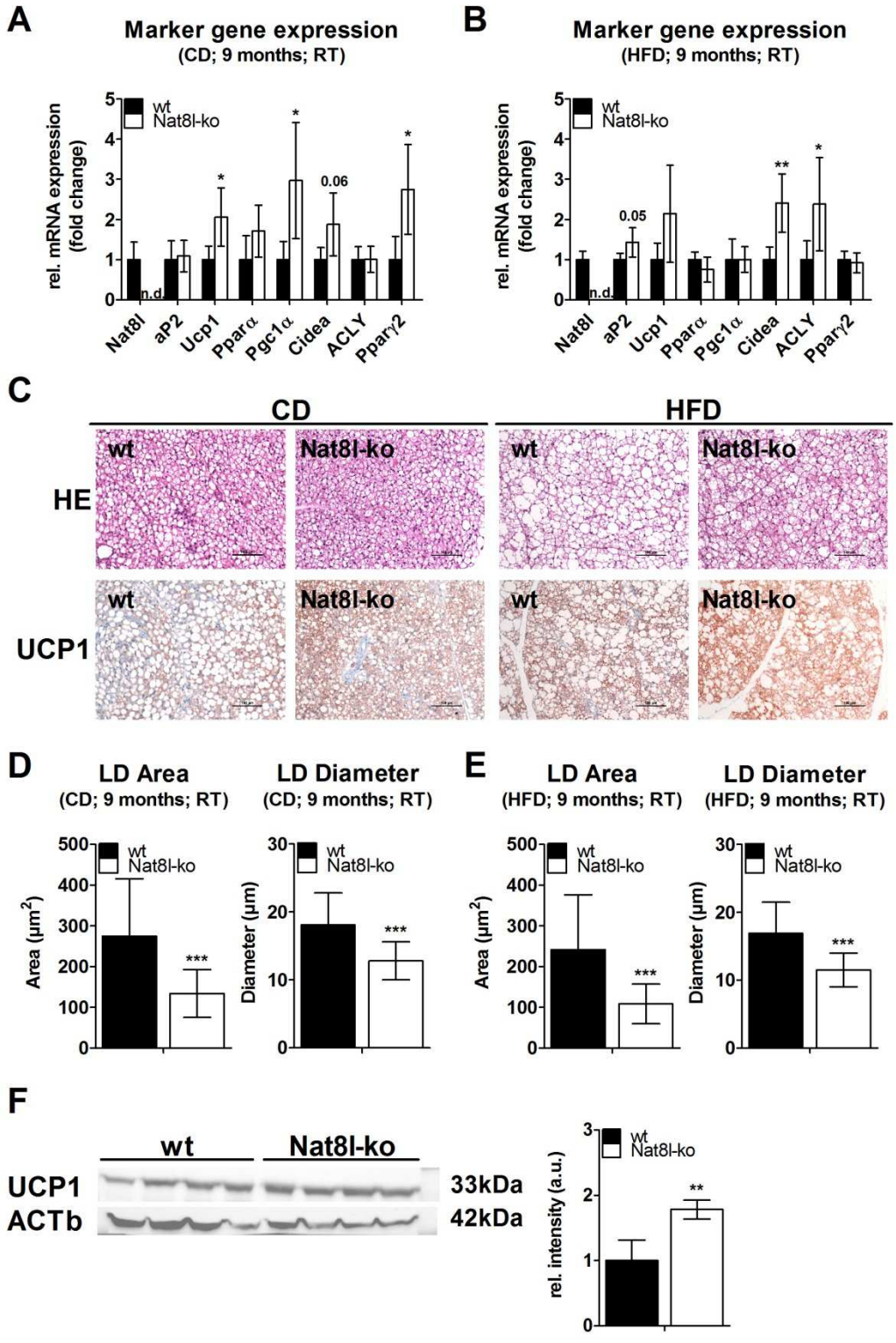

Figure 32. **Marker gene expression, morphology, and UCP1 protein expression in BAT of wt and *Nat8l*-ko mice at room temperature (RT).** (n = 6 / 5 for CD; n = 6 / 4 for HFD; age 9 months). Data are presented as mean ± standard deviation. mRNA expression of *Nat8l*, *aP2*, *Ucp1*, *Pparα*, *Pgc1α*, *Cidea*, *Acly*, and *Pparγ2* in BAT on (A) CD and (B) HFD. *18S rRNA* was used for normalization. (C) Hematoxylin & Eosin (HE) and UCP1 staining of BAT. (D) Quantification of lipid droplet (LD) area and diameter in BAT on (D) CD and (E) HFD. (F) UCP1 western blot of BAT of wt and *Nat8l*-ko mice at the age of 8 weeks on CD (n = 4). Quantification was performed using Image J software. β-ACTIN (ACTb) serves as reference. Statistical significance was assessed by two-tailed Student´s t test. *p < 0.05; **p < 0.01; ***p < 0.001.

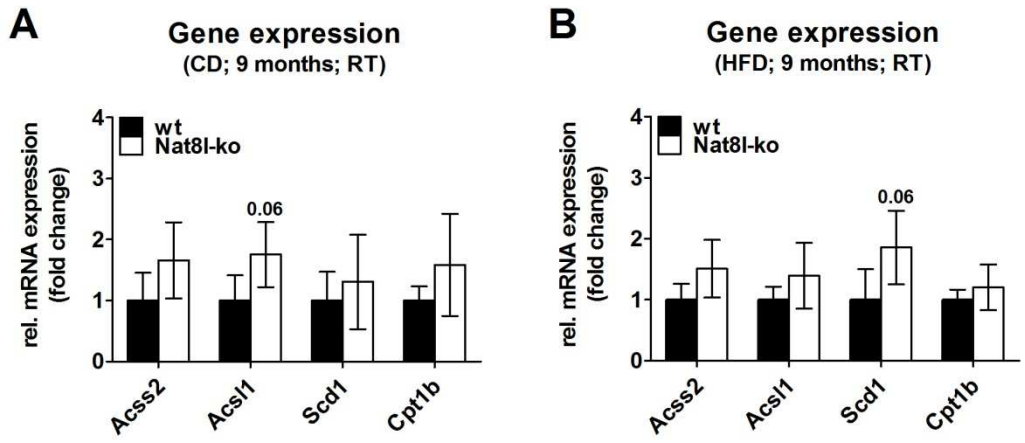

Figure 33. **Expression of genes involved in *de novo* lipogenesis and fatty acid oxidation in BAT of wt and *Nat8l*-ko mice at room temperature (RT).** (n = 6 / 5 for CD; n = 6 / 4 for HFD; age 9 months). Data are presented as mean ± standard deviation. mRNA expression of actely-CoA synthetase *2 (Acss2*), acyl-CoA synthetase long-chain family member 1 (*Acsl1*), stearoyl-CoA desaturase (*Scd1*), and carnitine palmitoyltransferase 1B (*Cpt1b*) on (A) CD and (B) HFD. *18S rRNA* was used for normalization. Statistical significance was assessed by two-tailed Student´s t test. *p < 0.05; **p < 0.01; ***p < 0.001.

4.10. Terminal experiments – cold challenge

As we observed increased weight loss upon overnight fasting (Figure 23) and increased total energy expenditure (Figure 29) in *Nat8l*-ko mice compared to wt, we wanted to investigate how *Nat8l*-ko mice react to thermal stress compared to their wt littermates. Therefore, mice were weighted and transferred from RT into a cold chamber (4 °C) at 12 a.m. Core body temperature was monitored every 30 minutes for the first 12 hours of cold exposure followed by an interval of 6 hours. All wt and *Nat8l*-ko mice survived the cold challenge and no mouse had to be excluded during the experiments due to a life-threatening decrease in body temperature.

4.10.1. Acute cold exposure (4 °C for 48 hours) of 5 months old wt and Nat8l-ko mice on chow diet

As a first trial, I subjected 5 months old mice to acute cold exposure (48 hours / 4 °C). The mice were single housed to ensure the effects are not attenuated by mice reciprocal warming each other. To increase the metabolic challenge, mice were fasted for 4 hours (8 a.m. to 12 a.m.) in the cold before performing final experiments. FA and glycerol release from adipose tissues was measured, but the BSA used was not fatty acid-free due to manufacturers´ problems. Therefore, these data could not be analyzed. All data presented in this section were acquired from the CD group of cohort 1.

4.10.1.1. Blood parameters, weight loss, and tissue oxygen consumption

After 48 hours of cold exposure, body weight and blood parameters of *Nat8l*-ko mice were not different when compared to controls (Table 9). Furthermore, we did not detect differences in

weight loss (Figure 34A) and tissue oxygen consumption of BAT, sWAT, and eWAT (Figure 34B) from wt and *Nat8l*-ko mice.

Table 9. **Body weight and blood parameters of wt and *Nat8l*-ko mice on chow diet at the age of 5 months after acute cold exposure (48 hours / 4 °C).** (n = 6 / 4). "Initial" corresponds to values before cold exposure and "final" corresponds to 48 hours cold exposure (4 hours fasted from 8 a.m. to 12 a.m.). Data are presented as mean ± standard deviation. Statistical significance was assessed by two-tailed Student´s t test.

Weight / blood parameters (4 °C; 48 hours)				
Chow diet (age 5 months)		**wt**	***Nat8l*-ko**	**p-value**
Weight (g)	Initial	27.85 ±0.49	27.75 ±1.15	0.9123
	Final	25.35 ±0.72	25.35 ±0.88	0.9359
Glucose (mg/dL)	Initial	190.2 ±40.5	184.3 ±36.5	0.8781
	Final	156.7 ±12.0	153.5 ±25.9	0.6093
FFA (mM)	Final	0.696 ±0.26	0.544 ±0.11	0.3099
TG (mg/dL)	Final	38.3 ±10.9	44.6 ±15.2	0.4948

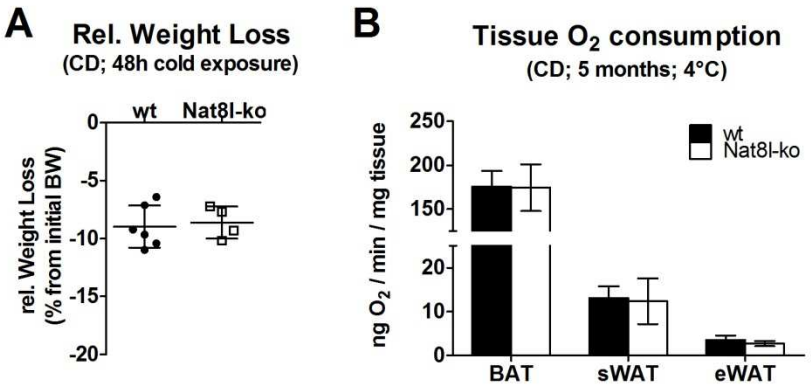

Figure 34. **Weight loss and tissue oxygen (O_2) consumption after acute cold exposure (48 hours / 4 °C) is similar in *Nat8l*-ko compared to wt mice on CD.** (A) Weight loss during 48 hours cold exposure. (B) Tissue oxygen consumption of BAT, sWAT, and eWAT from wt and *Nat8l*-ko mice on CD at the age of 5 months was measured using a Clark electrode (Strathkelvin Instruments) (n = 6 / 4). Mice were fasted for 4 hours prior to harvest (8 a.m. to 12 a.m.). Data are presented as mean ± standard deviation. Statistical significance was assessed by two-tailed Student´s t test.

4.10.2. 5 days cold exposure (4 °C) of 5 months old wt and Nat8l-ko mice on high-fat diet

The results in section 4.10.1 did not reveal differences between wt and *Nat8l*-ko mice upon 48 hours of cold exposure. Therefore, we wanted to test whether increasing cold exposure time to prolong acclimatization of the animals to low temperatures provokes differences between wt and *Nat8l*-ko mice. Mice were kept in the cold for 5 days in total and again fasted for 4 hours (8 a.m. to 12 a.m.) prior to final experiments. FA and glycerol release from adipose tissues was measured, but the BSA used was not fatty acid-free due to manufacturers´ problems. Therefore, these data could not be analyzed. All data presented in this section were acquired from the HFD group of cohort 1.

4.10.2.1. Blood parameters, weight loss, and tissue oxygen consumption

We determined body weight and blood parameters of 5 months old wt and *Nat8l*-ko mice on HFD after 5 days of cold exposure (Table 10). Body weight was generally lower when Nat8l-ko mice were compared to controls, although variation was high. Further, *Nat8l*-ko mice showed a slight trend to decreased weight loss during cold exposure when compared to wt littermates (Figure 35A). We detected significantly lower TG concentrations in plasma, similar to what was observed in 8 – 9 and 16 weeks old mice fed a HFD at RT (Table 3 and Table 4, respectively). Tissue oxygen consumption rate of BAT, sWAT, and eWAT was not different between wt and *Nat8l*-ko mice (Figure 35B).

Table 10. **Body weight and blood parameters of wt and *Nat8l*-ko mice on HFD at the age of 5 months after 5 days cold exposure (4 °C).** (n = 6 / 4). "Initial" corresponds to values before cold exposure and "final" corresponds to 5 days cold exposure (4 hours fasted from 8 a.m. to 12 a.m.). Data are presented as mean ± standard deviation. Statistical significance was assessed by two-tailed Student´s t test. Statistical significance is highlighted in dark grey. **p < 0.01.

Weight / blood parameters (4 °C; 5 days)				
High-fat diet (age 5 months)		**wt**	***Nat8l*-ko**	**p-value**
Weight (g)	Initial	36.00 ±1.25	33.70 ±3.28	0.2859
	Final	32.20 ±1.68	31.15 ±2.10	0.8437
Glucose (mg/dL)	Initial	189.7 ±33.9	179.3 ±24.0	0.6120
	Final	157.2 ±21.4	144.5 ±33.8	0.4837
FFA (mM)	Final	0.705 ±0.24	0.686 ±0.18	0.8943
TG (mg/dL)	Final	65.4 ±9.9	44.5 ±6.1**	0.0057

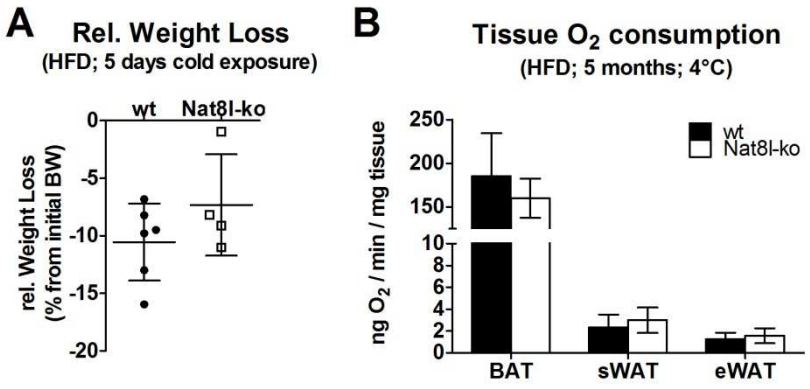

Figure 35. **Weight loss and tissue oxygen consumption (O_2) after 5 days cold exposure (4 °C) in 5 months old wt and *Nat8l*-ko mice.** (A) Relative weight loss to initial body weight. (B) Tissue oxygen consumption of BAT, sWAT, and eWAT from wt and *Nat8l*-ko mice on HFD at the age of 5 months after 5 days of cold exposure (4 °C) was measured using a Clark electrode (Strathkelvin Instruments) (n = 6 / 4). Mice were fasted for 4 hours prior to harvest (8 a.m. to 12 a.m.). Data are presented as mean ± standard deviation. Statistical significance was assessed by two-tailed Student´s t test.

4.10.2.2. Marker gene expression, morphology, and UCP1 protein expression in BAT

We investigated marker gene expression, morphology, and UCP1 protein expression in BAT of 5 months old HFD fed wt and *Nat8l*-ko mice after 5 days of cold exposure. *Ucp1*, *Pparα*, and

Pgc1α mRNA expression was similar in BAT of wt and *Nat8l*-ko mice under these conditions (Figure 36A). Morphological analysis by Hematoxylin & Eosin (HE) staining showed that BAT of *Nat8l*-ko seems to have increased lipid droplet size. Although *Ucp1* mRNA expression was not altered, UCP1 staining showed a decreased intensity in BAT of *Nat8l*-ko compared to wt mice. F4/80 staining as a measure of macrophage infiltration into adipose tissue[179] was unchanged between genotypes (Figure 36B).

We also investigated sWAT and eWAT by HE, F4/80, and UCP1 staining. We neither observed morphological differences nor any differences in UCP1 or F4/80 staining in sWAT and eWAT between wt and *Nat8l*-ko mice (data not shown).

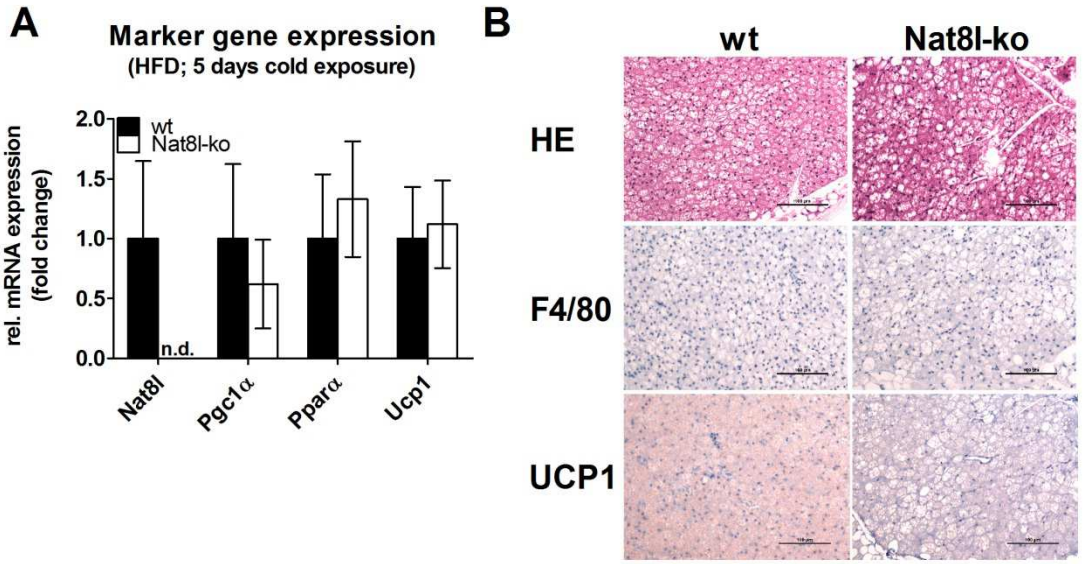

Figure 36. **Marker gene expression, morphology, and UCP1 protein expression in BAT of 5 months old HFD-fed wt and *Nat8l*-ko mice after 5 days cold exposure (4 °C).** (n = 6 / 4). Data are presented as mean ± standard deviation. (A) mRNA expression of *Nat8l*, *Pgc1α*, *Pparα*, and *Ucp1* in BAT. *18S rRNA* was used for normalization. (B) Hematoxylin & Eosin (HE), F4/80, and UCP1 staining of BAT. Statistical significance was assessed by two-tailed Student´s t test.

In summary, 5 days of cold exposure revealed a trend to decreased weight loss and increased LD size accompanied by decreased UCP1 expression in BAT of *Nat8l*-ko compared to wt mice. In addition, it has been shown that at least 1 week of cold exposure is needed to induce maximal UCP1 induction[180], reflecting a strong increase in BAT activity. Hence, shorter treatments might not recruit full thermogenic capacity in BAT. Therefore, we decided to repeat these experiments with mice on CD and HFD and extended the period if cold exposure to 9 days.

4.10.3. 9 days cold exposure (4 °C) of wt and Nat8l-ko mice on CD and HFD at the age of 9 months

As mentioned above, I repeated cold exposure experiments with a CD and a HFD fed group of wt and *Nat8l*-ko mice for a period of 9 days. Consistent with previous experimental settings,

mice were fasted for 4 hours (8 a.m. to 12 a.m.) prior to final experiments. Final blood was drawn by puncture of the facial vein and analyses were performed in serum. The CD mice were harvested at an age of 9 months, the HFD group at the age of 7 months. All data presented in this section were acquired from cohort 3.

4.10.3.1. Weight loss during 9 days of cold exposure (4 °C)

First, I measured weight loss in *Nat8l*-ko compared to wt mice. On CD, *Nat8l*-ko mice showed a trend to increased absolute weight loss during 9 days of cold exposure compared to controls (1.40 ±0.42 g in wt *versus* 2.08 ±0.51 g in *Nat8l*-ko mice; p = 0.0760). On HFD, *Nat8l*-ko mice showed reduced absolute weight loss during 9 days of cold exposure (3.47 ±1.13 g in wt *versus* 2.13 ±1.05 g in *Nat8l*-ko mice; p = 0.0402) (Figure 37A). Further, we found weight loss relative to initial BW increased for *Nat8l*-ko mice fed a CD whereas weight loss was decreased in *Nat8l*-ko mice fed a HFD (Figure 37B). A similar trend in the HFD group has already been noticed in 4.10.2.1 (see Figure 35A).

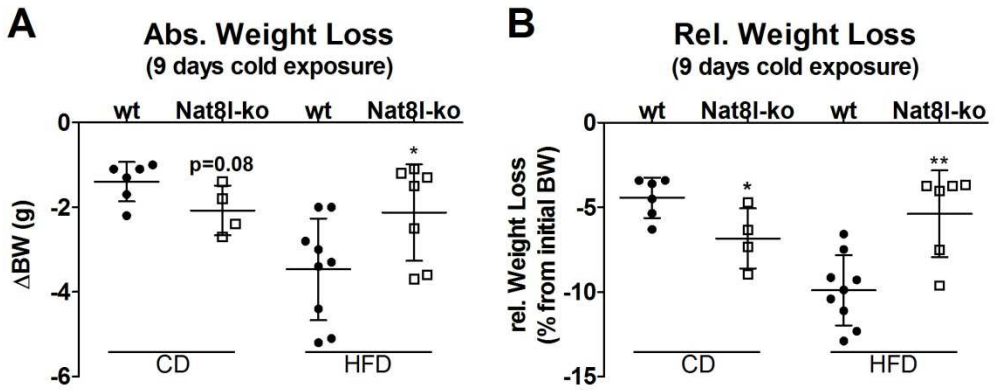

Figure 37. **Weight loss after 9 days cold exposure (4 °C) of wt and *Nat8l*-ko mice.** (n = 6 / 5 for CD, age 9 months; n = 9 / 8 for HFD; age 7 months). (A) Absolute weight loss. (B) Relative weight loss Relative weight loss was calculated as % from initial body weight before cold exposure. Mice were fasted for 4 hours prior to harvest (8 a.m. to 12 a.m.). Data are presented as mean ± standard deviation. Statistical significance was assessed by two-tailed Student´s t test. *p < 0.05; **p < 0.01; ***p < 0.001.

4.10.3.2. Blood parameters, tissue weight, tissue oxygen consumption, and fatty acid / glycerol release from adipose tissue

Body weight and blood parameters after 9 days of cold exposure were measured for wt and *Nat8l*-ko mice on CD and HFD (age of 9 and 7 months, respectively; Table 11). On CD, blood glucose concentrations were significantly decreased, whereas both serum FFA and TG concentrations were increased in *Nat8l*-ko mice compared to controls. Of note, FFA and TG concentrations were similar when wt and *Nat8l*-ko mice at RT were compared at the same age (see Table 7). Mean body weight was lower for *Nat8l*-ko mice, but not significantly different when compared to controls. On HFD, no significant differences could be detected after 9 days

of cold exposure. Interestingly serum TG concentrations in 9 months old *Nat8l*-ko mice were increased compared to controls at RT (see Table 7).

Table 11. **Body weight and blood parameters of wt and *Nat8l*-ko mice on CD and HFD after 9 days cold exposure (4 °C).** (n = 6 / 5 for CD, age 9 months; n = 9 / 8 for HFD; age 7 months). "Initial" corresponds to values before cold exposure and "final" corresponds to 9 days cold exposure (4 hours fasted from 8 a.m. to 12 a.m.). Data are presented as mean ± standard deviation. Statistical significance was assessed by two-tailed Student´s t test. Statistical significant results are highlighted in dark grey. *p < 0.05; **p < 0.01; ***p < 0.001.

Weight / blood parameters (4 °C; 9 days)				
Chow diet (age 9 months)		**wt**	***Nat8l*-ko**	**p-value**
Weight (g)	Initial	31.27 ±2.01	30.02 ±1.46	0.3223
	Final	29.87 ±1.69	28.34 ±1.29	0.1687
Glucose (mg/dL)	Final	124.0 ±11.0	96.4 ±9.0**	0.0028
FFA (mM)	Final	0.939 ±0.14	1.289 ±0.08**	0.0013
TG (mg/dL)	Final	53.1 ±9.3	70.6 ±11.57*	0.0326
High-fat diet (age 7 months)		**wt**	***Nat8l*-ko**	**p-value**
Weight (g)	Initial	34.16 ±4.85	34.48 ±3.13	0.8832
	Final	30.69 ±3.77	32.63 ±2.80	0.2816
Glucose (mg/dL)	Final	128.1 ±15.2	122.4 ±15.6	0.4822
FFA (mM)	Final	0.685 ±0.05	0.733 ±0.19	0.9719
TG (mg/dL)	Final	58.9 ±10.3	60.7 ±13.2	0.7801

Table 12. **Tissue weight of eWAT, sWAT, BAT and heart of wt and *Nat8l*-ko mice on CD and HFD after 9 days cold exposure (4 °C).** (n = 6 / 5 for CD, age 9 months; n = 9 / 8 for HFD; age 7 months). Tissue weight was measured as absolute weight (mg) and calculated relative to body weight (in % BW). Data are presented as mean ± standard deviation. Statistical significance was assessed by two-tailed Student´s t test. Light grey highlighted results show a trend (p < 0.1), statistical significant results are highlighted in dark grey. *p < 0.05; **p < 0.01; ***p < 0.001.

Tissue weight (4 °C; 9 days)				
Chow diet (age 9 months)		**wt**	***Nat8l*-ko**	**p-value**
eWAT	(mg)	482.5 ±115.6	448.2 ±76.7	0.6201
	% BW	1.61 ±0.33	1.58 ±0.25	0.8943
sWAT	(mg)	264.2 ±36.5	261.8 ±33.7	0.9224
	% BW	0.88 ±0.10	0.92 ±0.10	0.5558
BAT	(mg)	96.3 ±15.2	103.2 ±16.3	0.5302
	% BW	0.325 ±0.065	0.363 ±0.043	0.3438
Heart	(mg)	141.0 ±7.4	154.3 ±10.3	0.0681
	% BW	0.473 ±0.023	0.537 ±0.039*	0.0190
High-fat diet (age 7 months)		**wt**	***Nat8l*-ko**	**p-value**
eWAT	(mg)	1221.7 ±278.7	1347.8 ±422.4	0.5013
	% BW	3.93 ±0.50	4.07 ±1.02	0.7447
sWAT	(mg)	733.1 ±353.9	666.9 ±242.6	0.6821
	% BW	2.30 ±0.83	2.01 ±0.55	0.4408
BAT	(mg)	113.1 ±23.3	139.1 ±23.1*	0.0471
	% BW	0.366 ±0.037	0.426 ±0.060*	0.0316
Heart	(mg)	128.7 ±11.0	157.5 ±19.2**	0.0026
	% BW	0.424 ±0.058	0.425 ±0.028	0.9424

After sacrificing wt and *Nat8l*-ko mice, tissue weight of eWAT, sWAT, BAT, and heart was determined (Table 12). On CD, adipose tissue weight was not different between wt and *Nat8l*-ko mice, but heart weight was increased in *Nat8l*-ko compared to wt mice. On HFD, BAT mass showed an increase of about 20 % in *Nat8l*-ko mice compared to controls. Interestingly,

absolute heart weight was increased whereas heart weight relative to body weight was not significantly different between genotypes. After excision, tissues have also been checked for any morphological differences, but no obvious differences have been noticed. Subsequently, adipose tissues were divided into five parts. Tissue oxygen consumption and analysis of FA / glycerol release were performed immediately. As expected, oxygen consumption rates in BAT, sWAT, and eWAT (Figure 38) of wt and *Nat8l*-ko mice on CD and HFD were higher when compared to age-matched mice of the corresponding phenotype at RT (see Figure 30A). However, the rates from adipose tissue of CD fed wt and *Nat8l*-ko mice were similar after 9 days cold exposure (Figure 38A).

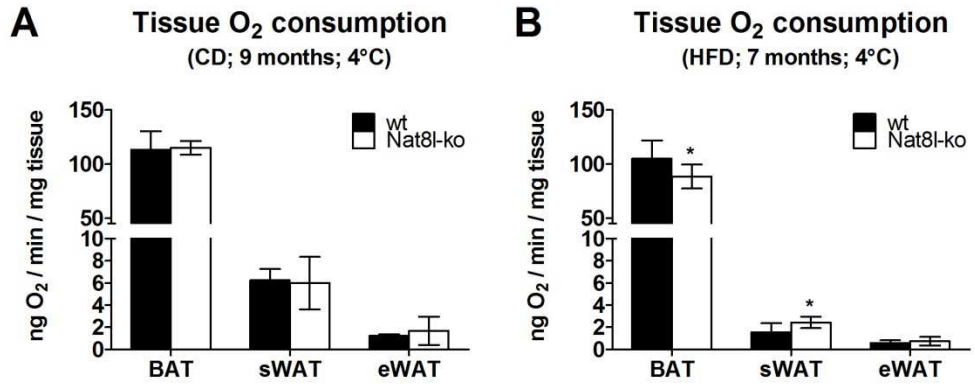

Figure 38. **Tissue oxygen (O_2) consumption of BAT, sWAT, and eWAT in wt and *Nat8l*-ko mice on chow (CD) and high-fat diet (HFD) after 9 days cold exposure (4 °C).** (n = 6 / 5 for CD, age 9 months; n = 9 / 8 for HFD; age 7 months). Data are presented as mean ± standard deviation. Tissue oxygen consumption rate measured by Clark electrode (Strathkelvin Instruments) of BAT, sWAT, and eWAT on (A) CD and (B) HFD). Statistical significance was assessed by two-tailed Student´s t test. *p < 0.05; **p < 0.01; ***p < 0.001.

On HFD, BAT of *Nat8l*-ko mice showed significantly decreased oxygen consumption rates compared to wt whereas sWAT of *Nat8l*-ko mice showed increased rates (Figure 38B). The same trends for BAT and sWAT respiration rate have already been observed after 5 days of cold exposure (see Figure 35B). *Nat8l*-ko eWAT oxygen consumption was similar to wt littermates on HFD (Figure 38B).

FA and glycerol release from adipose tissues (Figure 39) was measured after 1 hour of incubation in DMEM containing 2 % fatty acid-free BSA to scavenge FAs. Basal and β-adrenergic stimulated release (10 µM isoproterenol (Iso) preincubation for 1 hour) was determined and normalized to tissue protein after lipid extraction. FA re-esterification was not inhibited by Triacsin C in this experiment.

On CD, FA release from sWAT and eWAT was increased whereas FA release from BAT was similar when *Nat8l*-ko mice were compared to wt littermates (Figure 39A). Basal FA release in all adipose tissues was increased compared to same aged mice of both genotypes on RT (see Figure 31A). Stimulation with isoproterenol was able further increase FA release from sWAT and eWAT but not from BAT (compare Figure 39A and B, left panels). FA release after

isoproterenol stimulation was similar in adipose tissues of *Nat8l*-ko and wt mice (Figure 39B). Glycerol release was unchanged in all tissues, except *Nat8l*-ko BAT showed increased glycerol release after isoproterenol stimulation compared to wt BAT on CD (Figure 39C and D).

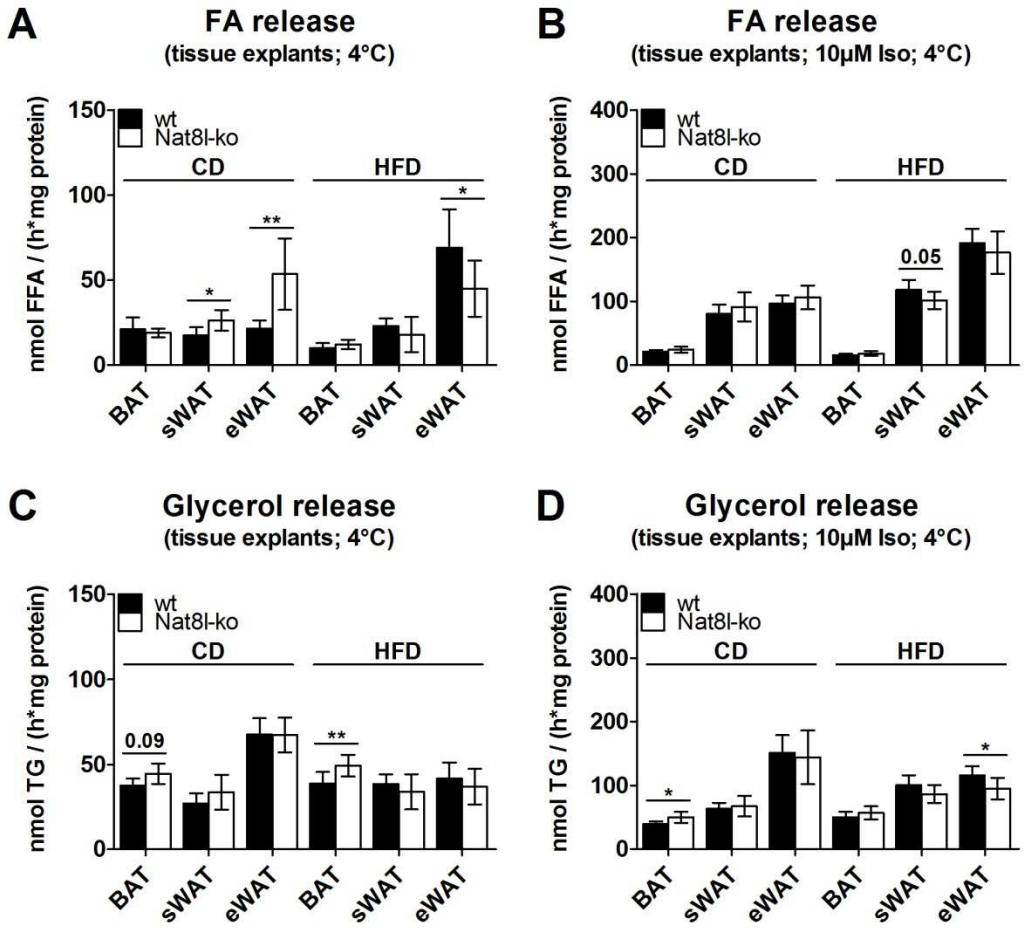

Figure 39. **Fatty acid (FA) and glycerol release in BAT, sWAT, and eWAT of wt and *Nat8l*-ko mice CD and HFD after 9 days cold exposure (4 °C).** (n = 6 / 5 for CD, age 9 months; n = 9 / 8 for HFD; age 7 months). Data are presented as mean ± standard deviation. (A) Basal, and (B) β-adrenergic-stimulated (10 µM isoproterenol (+Iso) for 1 hour) FA release from BAT, sWAT, and eWAT. (C) Basal, and (D) β-adrenergic-stimulated (10 µM isoproterenol (+Iso) for 1 hour) glycerol release from BAT, sWAT, and eWAT. Statistical significance was assessed by two-tailed Student´s t test. *p < 0.05; **p < 0.01; ***p < 0.001.

On HFD, the opposite could be detected. FA release from eWAT was significantly reduced in *Nat8l*-ko mice under basal conditions (Figure 39A), but not different after isoproterenol stimulation (Figure 39B). FA release from BAT was not significantly altered between *Nat8l*-ko and wt mice under basal and isoproterenol stimulated conditions, whereas sWAT FA release showed a trend to reduction (Figure 39A and B). Glycerol release from BAT was increased in *Nat8l*-ko compared to wt mice on HFD under basal conditions (Figure 39C), but equalized after stimulation with isoproterenol (Figure 39D). Glycerol release from sWAT and eWAT was slightly reduced in *Nat8l*-ko mice in both conditions.

4.10.3.3. Marker gene expression, morphology, and UCP1 expression in BAT

I investigated marker gene expression, morphology, and UCP1 protein expression in BAT of wt and *Nat8l*-ko mice (CD, age 9 months; HFD, age 7 months). On CD, *aP2*, *Ucp1*, *Pparα*, *Pgc1α*, *Cidea*, and *Acly* mRNA expression was significantly increased in BAT of *Nat8l*-ko mice compared to controls (Figure 40A). On HFD, *aP2*, *Ucp1*, *Cidea*, and *Acly* mRNA expression was also significantly increased, but the fold changes are much smaller compared to CD (Figure 40B).

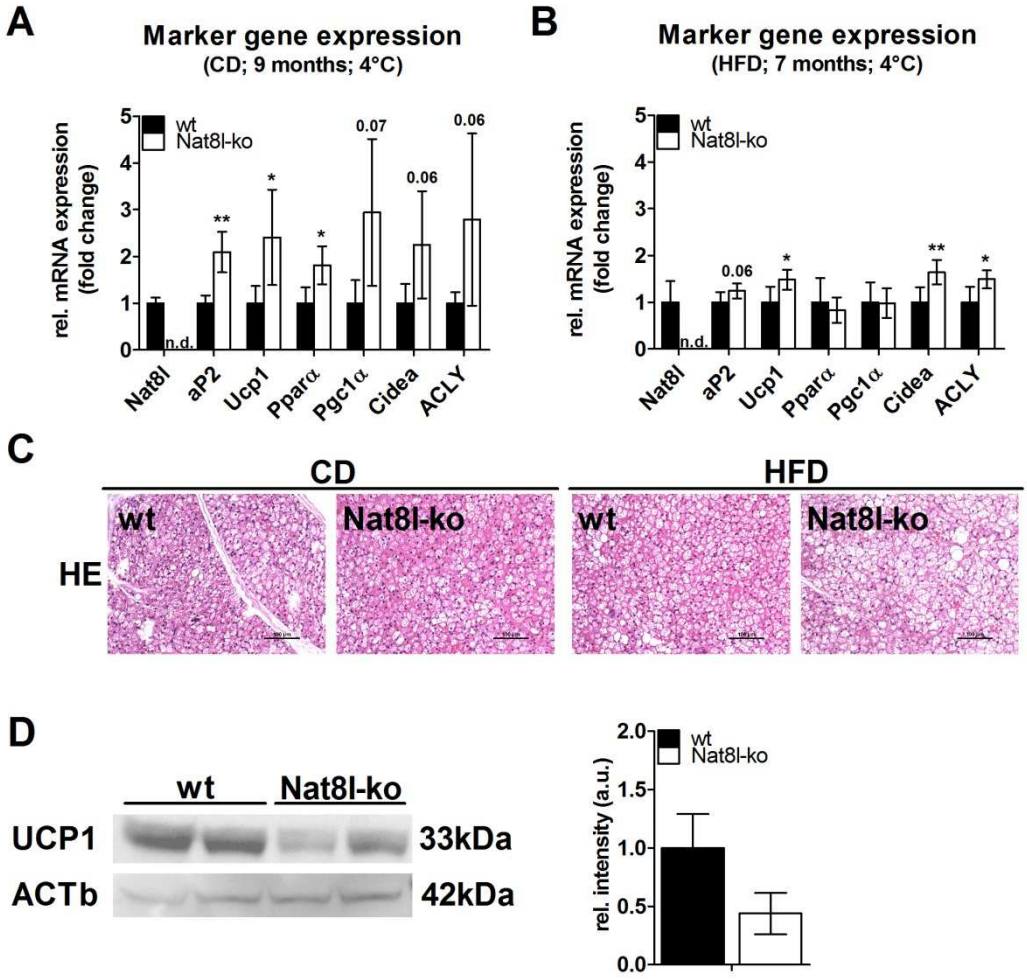

Figure 40. **Marker gene expression, morphology, and UCP1 protein expression in BAT of wt and *Nat8l*-ko mice after 9 days cold exposure (4 °C).** (n = 6 / 5 for CD, age 9 months; n = 9 / 8 for HFD; age 7 months). Data are presented as mean ± standard deviation. mRNA expression of *Nat8l*, *aP2*, *Ucp1*, *Pparα*, *Pgc1α*, *Cidea*, and *Acly* in BAT on (A) CD and (B) HFD. *18S rRNA* was used for normalization. (C) Hematoxylin & Eosin (HE) staining of BAT. (D) UCP1 western blot in BAT of wt and *Nat8l*-ko on HFD (n = 2). Quantification was performed using Image J software. B-ACTIN (ACTb) serves as reference. Statistical significance was assessed by two-tailed Student´s t test. *p < 0.05; **p < 0.01; ***p < 0.001.

Next, Hematoxylin & Eosin (HE) immunohistochemistry staining was performed for BAT of *Nat8l*-ko and wt mice on CD and HFD. HE staining revealed similar BAT morphology on CD, whereas it seems that lipid droplet (LD) area and diameter is increased in BAT of *Nat8l*-ko mice on HFD after 9 days of cold exposure (Figure 40C).

Weight loss and tissue oxygen consumption rate was decreased in *Nat8l*-ko compared to wt mice on HFD after 9 days of cold exposure. Contrarily, *Ucp1* mRNA expression was increased in BAT (see Figure 40B). UCP1 staining of BAT slices revealed regions within BAT of *Nat8l*-ko mice with less UCP1 staining than the surrounding tissue (data not shown). As this indicated reduced UCP1 expression, I performed UCP1 western blot in BAT of HFD fed wt and *Nat8l*-ko mice and found reduced UCP1 protein expression in *Nat8l*-ko mice (Figure 40D).

We also investigated sWAT morphology by HE and UCP1 immunohistochemistry staining in sWAT slices. HE and UCP1 staining in sWAT of wt and *Nat8l*-ko mice did not show any differences (data not shown) between genotypes.

These results show diet-specific effects after 9 days cold exposure. On CD, BAT function appears unchanged in *Nat8l*-ko compared to wt mice as tissue oxygen consumption and morphology is similar after 9 days of cold exposure (Figure 38A and Figure 40C). However, a reasonable set of brown fat marker genes including *Ucp1* and *Pgc1α* was upregulated in BAT of *Nat8l*-ko mice on CD (Figure 40A). In contrast, cold exposure of mice fed a HFD led to decreased oxygen consumption rate (Figure 38B), increased lipid accumulation (Figure 40C), and reduced UCP1 protein expression in BAT (Figure 40D) of *Nat8l*-ko compared to wt mice.

4.11. Cardiac parameters of wt and Nat8l-ko mice

As spontaneous cardiac failure could be a cause for spontaneous death of *Nat8l*-ko mice (see Figure 18), we measured blood pressure and heart rate of *Nat8l*-ko mice. Values for systolic, diastolic, and mean arterial blood pressure as well as heart rate were similar when *Nat8l*-ko mice were compared to wt littermates (Table 13 and Figure 41). We further determined heart weight and analyzed cardiac muscle fiber morphology by HE staining. Heart weight of *Nat8l*-ko mice was not different compared to wt when mice were housed at RT (Figure 42A; Table 8). Interestingly, 9 days of cold exposure led to heart hypertrophy in *Nat8l*-ko mice (Figure 42B; see also Table 12). However, there was no difference in fiber morphology as shown in Figure 42C and D.

Table 13. **Cardiac Parameters are similar in wt and *Nat8l*-ko mice on CD and HFD at the age of 30 weeks.** Systolic blood pressure (systol. BP), mean arterial blood pressure (mean art. BP), diastolic blood pressure (diast. BP), and heart rate on CD (n = 6 / 5) and HFD (n = 6 / 4). Data are presented as mean ± standard deviation. Statistical significance was assessed by two-tailed Student´s t test. Light grey highlighted results show a trend ($p < 0.1$).

Parameter	CD			HFD		
	wt	*Nat8l*-ko	p-value	wt	*Nat8l*-ko	p-value
systol. BP (mmHg)	100.1 ±8.4	107.4 ±4.6	0.0927	111.2 ±7.5	116.7 ±9.9	0.5194
mean art. BP (mmHg)	75.4 ±7.4	71.4 ±8.3	0.4697	86.1 ±9.4	88.0 ±8.2	0.7199
diastol. BP (mmHg)	60.4 ±8.8	67.0 ±10.7	0.2922	72.4 ±11.3	74.3 ±6.4	0.6424
heart rate (bpm)	655.6 ±77.8	683.8 ±40.7	0.4853	725.1 ±13.4	739.5 ±23.3	0.1516

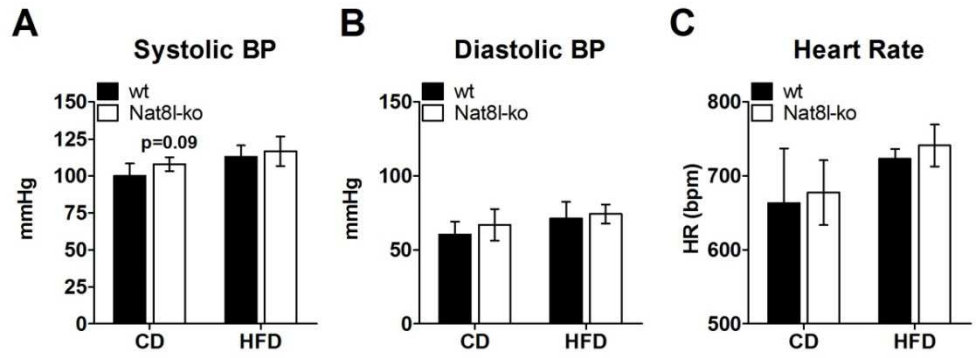

Figure 41. **Cardiac Parameters are similar in wt and *Nat8l*-ko mice on CD and HFD at the age of 30 weeks. (**A) Systolic blood pressure, (B) diastolic blood pressure, and (C) heart rate of wt and *Nat8l*-ko mice on chow diet (CD; n = 6 / 5) and high-fat diet (HFD; n = 6 / 4) at an age of 30 weeks. Data presented as mean ± standard deviation. Statistical significance was assessed by two-tailed Student´s t test.

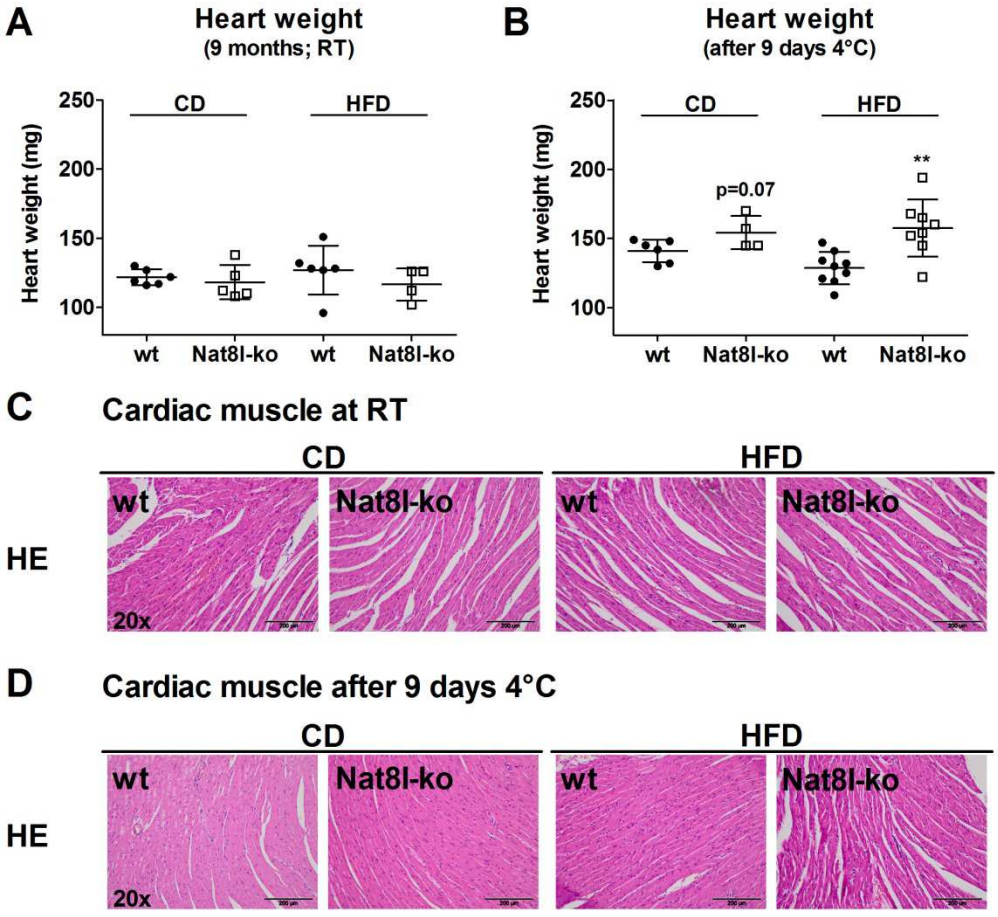

Figure 42. **Heart weight and morphology in wt and *Nat8l*-ko mice on RT and after 9 days cold exposure (4 °C).** Data are presented as mean ± standard deviation. Absolute heart weight of wt and *Nat8l*-ko mice at (A) RT (age 9 months), and (B) after 9 days cold exposure (4 °C; age 9 months for CD; age 7 months for HFD). Hematoxylin & Eosin (HE) staining of cardiac muscle of wt and *Nat8l*-ko mice at (C) RT, and (D) after 9 days cold exposure (4 °C). Statistical significance was assessed by two-tailed Student´s t test. *p < 0.05; **p < 0.01; ***p < 0.001.

In summary, these data show that *Nat8l*-ko mice do not have a severe cardiac phenotype which could explain the phenomenon of sudden death observed in these mice (see Figure 18).

4.12. Body temperature of wt versus Nat8l-ko mice

We also measured core body temperature (BT) using a rectal probe (RET-3; Physitemp Instruments, New Jersey, USA). We measured BT in wt and *Nat8l*-ko mice on CD and HFD at different ages and before final experiments at the age of 9 and 7 months, respectively (Table 14). We were not able to detect consistent changes in BT on CD and HFD. The significant differences on HFD even contradicted each other. Performing rectal measurements in rodents has been reported to have significant stress-related effects on thermal homeostasis[181] and leads to high variations depending on handling time. Therefore, other methods such as thermal imaging[182] and subcutaneously implanted thermosensors[183] might be more valuable to determine body temperature in mice. However, these data suggest that there is no difference in BT of wt and *Nat8l*-ko mice.

Table 14. **Body temperature in wt *versus* *Nat8l*-ko mice on CD and HFD.** Core body temperature was determined in wt and *Nat8l*-ko mice using a rectal probe (RET-3; Physitemp Instruments). "Initial" corresponds to values before cold exposure and "final" corresponds to 9 days cold exposure (4 hours fasted from 8 a.m. to 12 a.m.). All data are presented as mean ± standard deviation. Statistical significance was assessed by two-tailed Student´s t test. Light grey highlighted results show a trend ($p < 0.1$), statistical significant results are highlighted in dark grey. *$p < 0.05$; **$p < 0.01$; ***$p < 0.001$.

Body temperature (°C)					
Chow diet Age[12]:	**time**		**wt**	***Nat8l*-ko**	**p-value**
16 weeks	12 a.m.		35.43 ±1.08 (n = 6)	36.18 ±0.75 (n = 4)	0.2700
34 weeks	10 a.m.		36.30 ±0.85 (n = 12)	35.82 ±0.74 (n = 10)	0.1761
9 months (RT)	8 a.m. to 12 a.m.		35.27 ±0.19 (n = 6)	35.76 ±0.29* (n = 5)	0.0129
9 months (9 days 4 °C)	12 a.m. to 2 p.m.	Initial	36.62 ±0.27 (n = 6)	36.60 ±0.23 (n = 5)	0.9229
		Final	34.63 ±1.04 (n = 6)	33.96 ±1.14 (n =5)	0.3791
High-fat diet Age[13]:	**time**		**wt**	***Nat8l*-ko**	**p-value**
16 weeks	12 a.m.		34.74 ±0.396 (n = 12)	35.36 ±0.558** (n = 8)	0.0066
26 weeks	10 a.m.		36.18 ±0.44 (n = 9)	36.48 ±0.37 (n = 8)	0.1780
34 weeks	10 a.m.		36.45 ±0.35 (n = 6)	35.78 ±0.36* (n = 4)	0.0291
9 months (RT)	8 a.m. to 12 a.m.		36.13 ±0.36 (n = 6)	36.20 ±0.83 (n = 4)	0.8807
7 months (9 days 4 °C)	12 a.m. to 2 p.m.	Initial	36.56 ±0.23 (n = 9)	36.20 ±0.51 (n = 8)	0.0982
		Final	34.38 ±1.04 (n = 9)	34.49 ±0.59 (n = 8)	0.8082

[12] Age 16 weeks: data from cohort 1. Age 34 weeks: data from cohorts 2 & 3. Age 9 months (RT): data from cohort 2. Age 9 months (9 days 4 °C): cohort 3.
[13] Age 16 weeks: data from cohorts 1 & 2. Age 26 weeks: data from cohorts 3. Age 34 weeks: data from cohorts 2. Age 9 months (RT): data from cohort 2. Age 7 months (9 days 4 °C): cohort 3.

5 - Results III – Investigation of the physiological regulation of NAT8L an ASPA *in vitro* and *in vivo*

5. RESULTS III – Investigation of the physiological regulation of NAT8L and ASPA *in vitro* and *in vivo*

Our previous results showed that *Nat8l* expression was reduced in BAT and eWAT of genetically obese (ob/ob) mice compared to controls whereas expression was not changed in brain[116]. Further, a potential PPAR binding site in intron 2 of *Nat8l* was identified by *in silico* analyses performed by Ariane R. Pessentheiner[14] (2610-3081 downstream from TSS). Co-transfection of this *Nat8l*-fragment with PPARγ and RXRα into cos7 cells followed by luciferase reporter assays revealed increased luciferase activity compared to controls. Luciferase activity was even further increased when cells were treated with the PPARγ agonist rosiglitazone 24 hours prior to luciferase assay. She also showed that *Nat8l* expression was nearly blunted when iBACs were treated with the PPARα antagonist GW6471. In summary, these results indicate that *Nat8l* is connected and responding to PPARγ and PPARα, the respective master regulators of adipogenesis (reviewed by Lefterova et al.[59]) and adipocyte metabolism[68,153,184].
However, the physiological triggers activating or inhibiting the NAA pathway have not been identified. Therefore, I aimed to investigate the regulation of *Nat8l* and *Aspa* expression *in vitro* and *in vivo*.

5.1. Nat8l and Aspa expression in brain and adipose tissue of C57Bl/6J mice during aging

As a first approach to assign *Nat8l* and *Aspa* regulation *in vivo*, I measured the mRNA expression profile in brain, BAT, sWAT and eWAT of C57Bl/6J mice during aging. Tissues were harvested from 1 day up to 10.5 month-old mice in the fed *ad libitum* state (n = 4 each time point). In brain, *Nat8l* and *Aspa* expression was increased with aging (Figure 43A and B, black circles). *Nat8l* and *Aspa* expression was also increased during aging in BAT, but at the age of 1 month a drop in expression could be observed and expression levels were comparable to those observed right after birth (Figure 43A and B, white circles). In sWAT and eWAT, *Nat8l* and *Aspa* expression diametrically reached its highest values at the age of 1 month compared to BAT (Figure 43C and D).

[14] Doctoral thesis; Ariane R. Pessentheiner, Ph.D.; “Elucidation of genes influencing adipogenic development and energy metabolism”; August 2014; Graz University of Technology

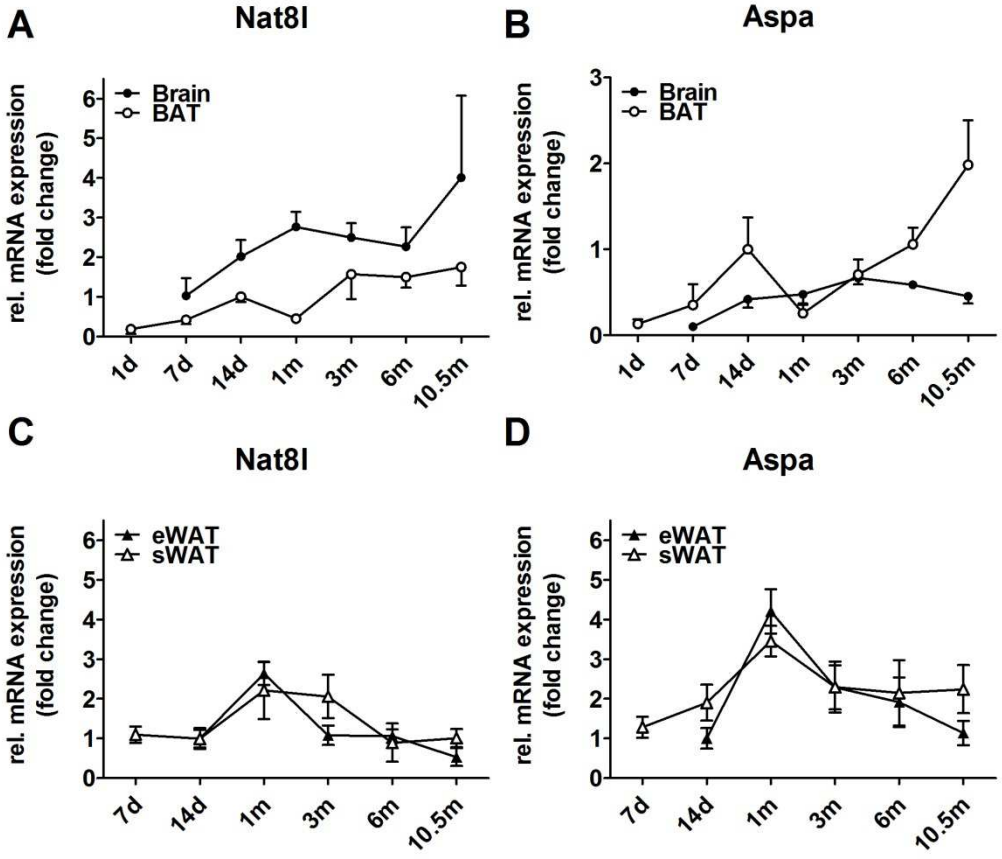

Figure 43. ***Nat8l* and *Aspa* mRNA expression during aging in C57Bl/6J mice.** Data are presented as mean ± standard deviation (n = 4 for each time point). (A) *Nat8l*, and (B) *Aspa* mRNA expression in BAT and brain (14d BAT value was set to 1). *18S rRNA* was used for normalization. (C) *Nat8l*, (D) *Aspa* mRNA expression in eWAT and sWAT (14d eWAT valuewas set to 1). TFIIβ was used for normalization.

5.2. Regulation of Nat8l and Aspa expression in BAT of wt and Nat8l-ko mice on HFD and during cold exposure (4 °C)

Next, I aimed to elucidate what happens to *Nat8l* and *Aspa* expression upon HFD feeding and cold exposure. Therefore, expression levels in BAT of wt and *Nat8l*-ko mice described in chapters 4.9 (RT) and 4.10.3 (9 days cold exposure – 4°C), were analyzed regarding expression changes in these conditions. *Nat8l* expression was increased upon HFD when compared to CD and also upon 9 days of cold exposure (Figure 44A). A combination of both HFD and cold exposure was not able to further increase *Nat8l* expression. As a control for the treatment, *Ucp1* expression was analyzed. *Ucp1* expression was increased in BAT upon HFD feeding as well as on cold exposure (Figure 44B) which has been described before (reviewed in[180,185]). *Aspa* mRNA expression was also significantly increased upon HFD feeding as well as cold exposure (Figure 44C). Furthermore, ASPA expression was significantly increased in BAT of *Nat8l*-ko mice on CD at the age of 8 weeks (Figure 44D).

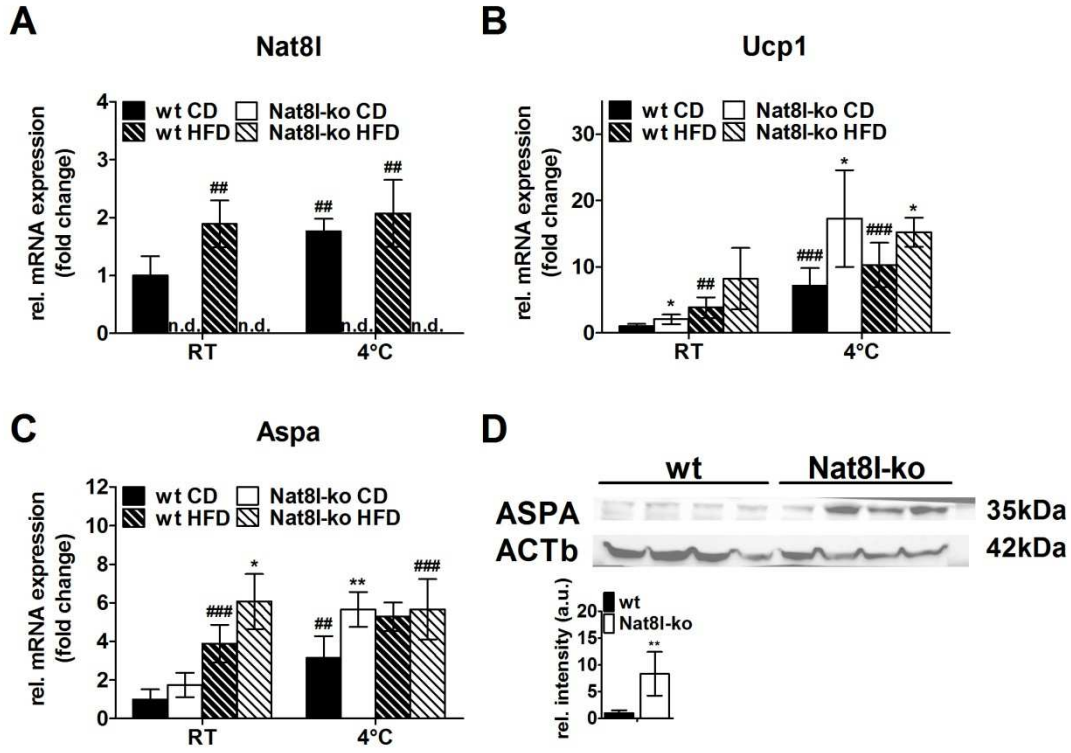

Figure 44. **Expression of *Nat8l*, *Ucp1*, and *Aspa* in BAT of wt and *Nat8l*-ko mice on CD and HFD at RT and after 9 days cold exposure (4 °C).** Data are presented as mean ± standard deviation. (A) *Nat8l*, (B) *Ucp1*, and (C) *Aspa* mRNA expression. *18S rRNA* was used for normalization. (D) ASPA protein expression in BAT of wt and *Nat8l*-ko mice on CD at the age of 8 weeks. Quantification was performed using Image J software. β-ACTIN (ACTb) serves as reference. Statistical significance was assessed by two-tailed Student´s t test. *p < 0.05; **p < 0.01; ***p < 0.001 for wt *versus Nat8l*-ko. $^{\#}$p < 0.05; $^{\#\#}$p < 0.01; $^{\#\#\#}$p < 0.001 for comparison to wt CD (RT).

5.3. Regulation of Nat8l and Aspa expression in adipose tissue of C57Bl/6 mice upon chronic β3-adrenergic stimulation

Granneman et al.[186] showed that fatty acid synthesis and fatty acid oxidation in adipocytes are coupled during chronic adrenergic stimulation using CL 316,243 (CL), a specific activator of the β3-adrenergic receptor. We previously proposed the NAT8L – ASPA axis might be an additional way to provide acetyl-CoA for lipid synthesis in adipocytes[116]. Therefore, we aimed to elucidate the influence of chronic β3-adrenergic stimulation by CL on *Nat8l* and *Aspa* expression in adipose tissue of C57Bl/6J mice.

First, I intraperitoneally injected 13 weeks old mice with either 1 mg / kg of sterile saline or CL for 8 consecutive days (injection always between 7.30 – 8.00 a.m.). I observed reduced *Nat8l* (~50% to control) expression whereas *Acss2*, *Aspa*, *Fasn*, *Pparγ2*, and *Pparα* mRNA was not significantly changed in BAT of CL-treated mice (Figure 45A). *Ucp1* expression was used as a control for effective CL treatment. *Ucp1* mRNA expression was increased in BAT and eWAT of CL-treated mice (Figure 45A and B). In addition, we confirmed increased UCP1 and unchanged ASPA protein expression in BAT by western blot (Figure 45C). Interestingly, *Nat8l*, *Aspa*, and *Acss2* expression was increased whereas *Pparγ2* expression was decreased in eWAT of CL-

treated mice compared to controls (Figure 45B). Consistent with the results of Motillo et al.[186], *Fasn* was increased in eWAT of CL-treated mice.

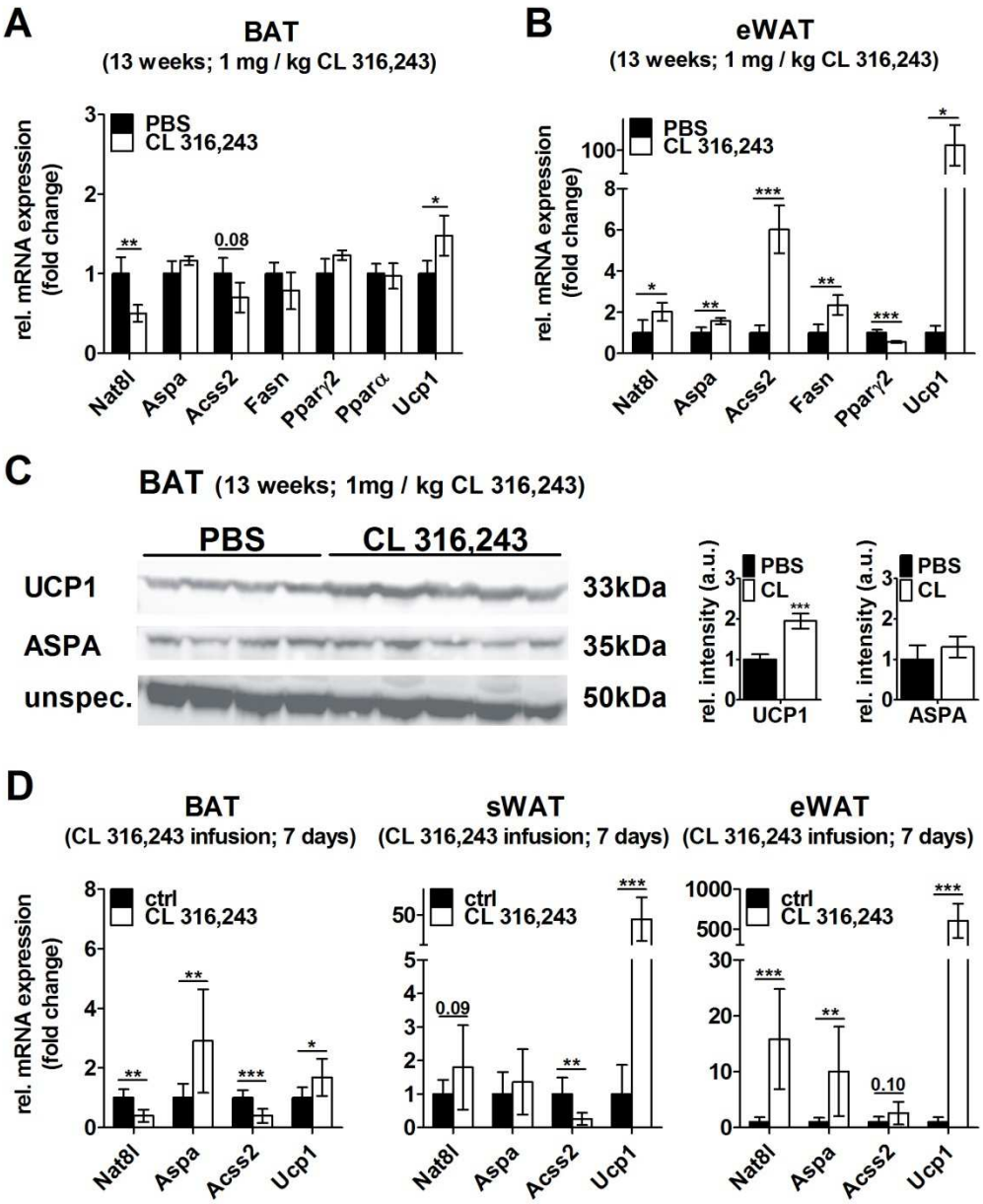

Figure 45. **Chronic β3-adrenergic stimulation by CL 316,243 and expression analysis in adipose tissue of C57Bl/6J mice.** Data are presented as mean ± standard deviation. mRNA expression of *Nat8l*, *Aspa*, and adipogenic marker genes in (A) BAT, and (B) eWAT of C57Bl/6J mice (age 13 weeks) injected with either 1 mg / kg saline or CL 316,243 for 7 days (n = 4 / 5). TFIIβ was used for normalization. (C) UCP1 and ASPA protein expression in BAT of C57Bl6J mice (age 13 weeks).injected with either 1 mg / kg saline of CL 316,243 for 7 days (n = 4 / 5). Quantification was performed using Image J software. An unspecific band was used for normalization. (D) *Nat8l*, *Aspa*, *Acss2*, and *Ucp1* expression in BAT, sWAT and eWAT of C57Bl/6J mice (age 10-12 weeks) infused with 0.75 nmol CL 316,243 / hour using osmotic minipumps (n = 5) and control mice (n = 10). Data in (D) was provided by Martin Bilban (Medical University of Vienna). Acidic ribosomal protein (*Arp*) was used for normalization. Statistical significance was assessed by two-tailed Student´s t test. *p < 0.05; **p < 0.01; ***p < 0.001.

Second, 10 – 12 weeks old C57Bl/6 mice were infused with 0.75 nmol CL / hour using osmotic minipumps for 7 days. Similar to the results from repeated intraperitoneal CL injection, expression of *Nat8l* was decreased in BAT, but increased in eWAT of CL-infused compared to

control mice (Figure 45D; compare Figure 45A and B). Interestingly, CL treatment increased *Aspa* in BAT and eWAT whereas both *Nat8l* and *Aspa* expression was not changed in sWAT when compared to controls. As mentioned above, *Ucp1* served as a control for CL treatment and was increased in BAT, sWAT, and eWAT of CL-treated mice when compared to controls. Consistent to Figure 45B, a trend for increased *Acss2* expression could be observed in eWAT of CL-treated mice compared to controls. Further, *Acss2* expression was reduced in BAT and sWAT of CL-treated compared to control mice. Overall, CL treatment reduces *Nat8l* and *Acss2* expression whereas Aspa expression seems to be upregulated in BAT of CL-treated mice compared to controls. Furthermore, CL treatment does not affect *Nat8l*, *Aspa*, and *Acss2* expression in sWAT but seems to activate the NAA pathway in eWAT.

In summary, these data show that the NAA pathway in adipose tissues is regulated by chronic β3-adrenergic stimulation with CL 316,243. The results further suggest different roles for NAA metabolism in brown and white adipose tissue.

5.4. Nat8l and Aspa expression in response to glucose availability in vitro and in vivo

To test whether the expression of *Nat8l* and *Aspa* is influenced by glucose availability, we differentiated iBACs in 4.5 (high) or 1.0 (low) g / L glucose differentiation media until day 7. Fully differentiated brown adipocytes were then incubated with maintenance media containing 4.5, 1.0, or 0 g / L of glucose for another 24 hours (Figure 46A) or harvested directly on day 7 of differentiation (Figure 46B). *Nat8l* expression was reduced in every condition, in which glucose was reduced from high (4.5 g / L) to lower concentrations and vice versa.

Aspa expression was massively induced upon changing from high to low glucose, but decreased when glucose was completely removed. However, the increase in *Aspa* expression to low glucose differentiation could only be shown in one data set (Figure 46B vs. Figure 46A, *Aspa* expression in condition 4.5 / 4.5 compared to 1.0 / 1.0 g / L glucose). Further, both *Nat8l* and *Aspa* mRNA expression showed a trend to increase when cells were differentiated in low glucose media and then treated with high glucose for another 24 hours (Figure 46A, condition 4.5 / 4.5 *versus* 1.0 / 4.5 g / L glucose).

Therefore, we tested if and how NAT8L and ASPA respond to a glucose bolus *in vivo*. We injected C57Bl/6 mice with 1.5 g / kg glucose (similar to what is used for ipGTT, see materials and methods section 2.5) and harvested adipose tissue after 30 minutes. *Nat8l* and *Aspa* expression was nearly doubled in BAT of glucose-injected mice compared to saline controls (Figure 46C). NAT8L and ASPA protein expression was not changed 30 minutes after glucose injection (data not shown). In eWAT, *Nat8l* expression also showed a trend to increase whereas *Aspa* was reduced to ~50 % of controls (Figure 46D).

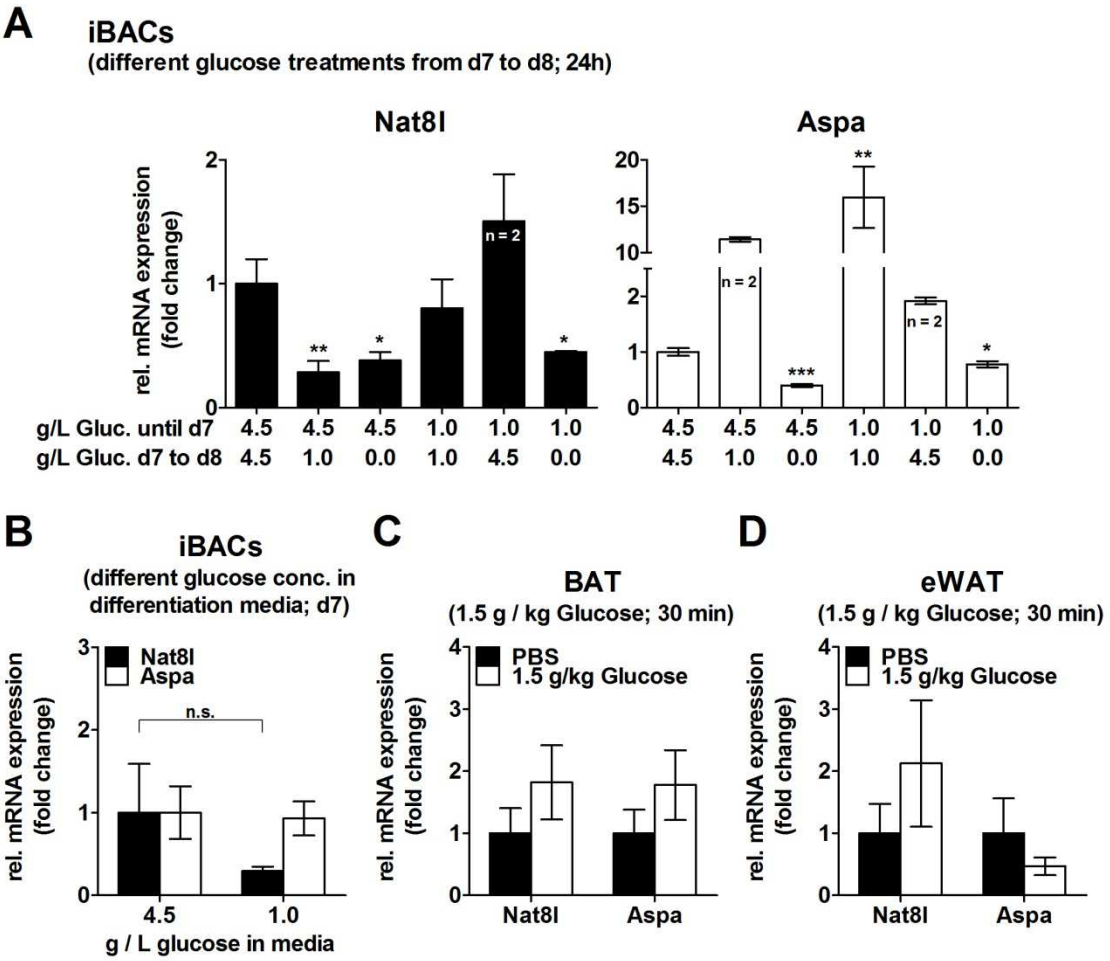

Figure 46. ***Nat8l* and *Aspa* expression response to glucose availability in vitro and in vivo.** Data are presented as mean ± standard deviation. (A) *Nat8l* and *Aspa* mRNA expression in iBACs on day 8 of differentiation treated under different conditions of glucose availability (if not otherwise indicated, n = 3). (B) *Nat8l* and *Aspa* mRNA expression in iBACs on day 7 of differentiation, differentiated in the presence of 4.5 or 1.0 g / L glucose in the media (n = 3). Expression in (A) and (B) was normalized to *TfIIβ*. *Nat8l* and *Aspa* mRNA expression in (C) BAT and (D) eWAT of C57Bl/6J mice 30 minutes after glucose bolus compared to saline controls (n = 4 for PBS, n = 3 for 1.5 g / kg glucose). Expression was normalized to *18S rRNA*. Statistical significance was assessed by two-tailed Student´s t test. *p < 0.05; **p < 0.01 for comparison of *Nat8l* and $^{\#}p < 0.05$; $^{\#\#}p < 0.01$; $^{\#\#\#}p < 0.001$ for comparison of *Aspa* expression between different glucose conditions.

Finally, I wanted to test how NAT8L and ASPA expression in adipose tissue was affected by nutritional status *in vivo*. As a first approach, I analyzed brain, BAT, sWAT, and eWAT of C57Bl/6J mice in the fed *ad libitum*, 12 hours fasted, and 12 hours fasted / 1 hour refed nutritional state (age 6 – 7 months). *Nat8l* expression was decreased in sWAT and eWAT upon overnight fasting (Figure 47A). One hour refeeding was able to recover and even further increased *Nat8l* expression in sWAT and eWAT compared fed state. Nutritional status did not influence *Nat8l* expression in Brain and BAT. *Aspa* expression in sWAT was also reduced in the fasted state and recovered upon refeeding (Figure 47B). *Aspa* expression was not altered upon fasting and refeeding in brain, BAT, and eWAT.

When the fasting period was prolonged to 24 hours, we found *Nat8l* and *Aspa* expression downregulated in BAT (Figure 47C). Refeeding recovered *Nat8l* but not *Aspa* expression. In addition, we confirmed downregulation of ASPA protein upon 24 hours of fasting (Figure 47D). In summary, these data show that the NAA pathway responds to dietary challenges and is primarily downregulated by energy deprivation.

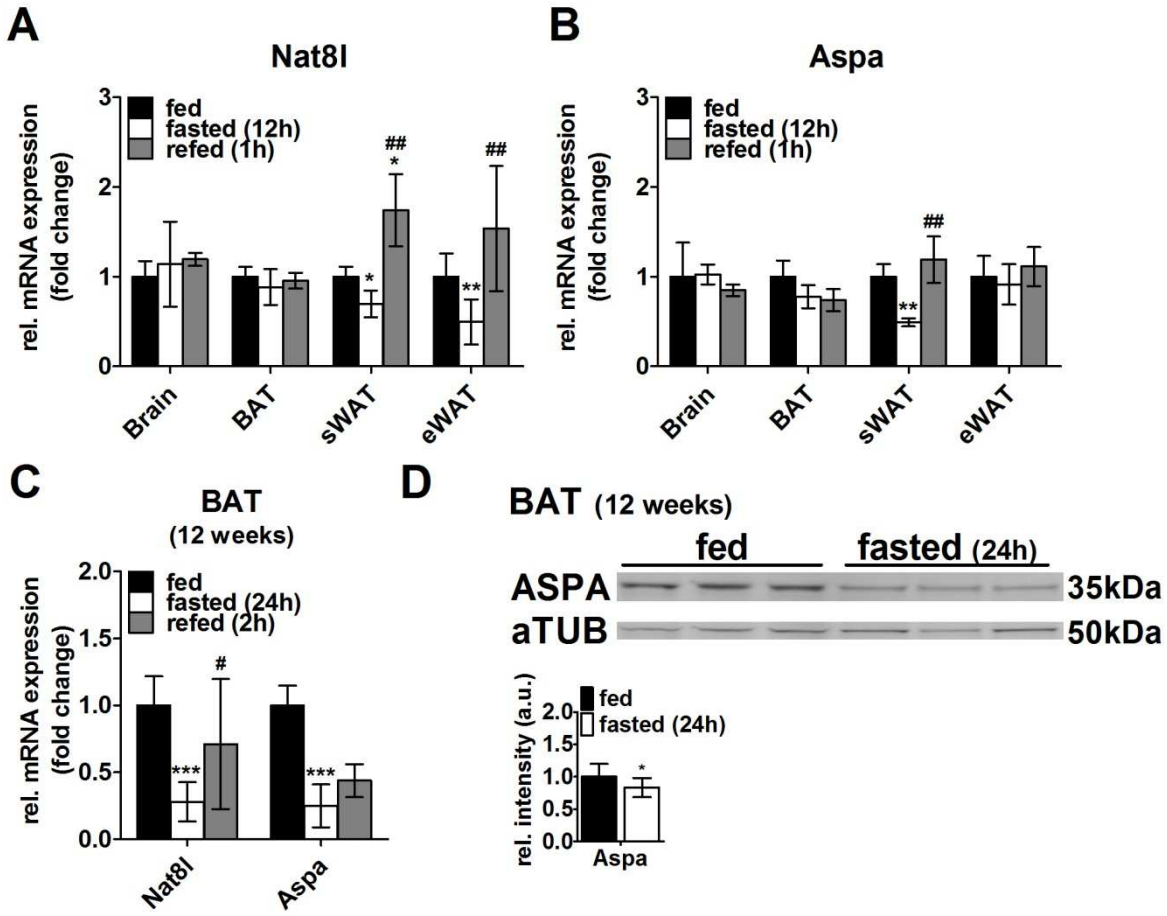

Figure 47. **Feeding / fasting regulation of *Nat8l* and *Aspa in vivo*.** Data are presented as mean ± standard deviation. (A) *Nat8l* and (B) *Aspa* mRNA expression in brain, BAT, sWAT, and eWAT of C57Bl/6J mice 16 weeks of age in fed ad libitum; fasted overnight (12h), and fasted overnight (12h) followed by 1 hour refed state (n ≥ 4;). *18S rRNA* was used for normalization. (C) *Nat8l* and *Aspa* mRNA expression in BAT of C57Bl/6J mice in fed ad libitum; fasted (24h), and fasted overnight (24h) followed by 2 hours refed state at the age of 12 weeks (n = 7). TFIIβ was used for normalization. (D) ASPA protein expression in BAT of C57Bl/6 mice at the age of 12 weeks (n = 3). Data in (C) and (D) was provided by Andreas Prokesch. Quantification was performed using Image J software. αTUBULIN (aTUB) was used for normalization. All data presented as mean ± standard deviation. Statistical significance was assessed by two-tailed Student´s t test. *p < 0.05; **p < 0.01; ***p < 0.001 for comparison to fed state. $^{\#}$p < 0.05; $^{\#\#}$p < 0.01; $^{\#\#\#}$p < 0.001 for comparison to fasted state.

6 - Discussion

6. Discussion

The N-acetylaspartate (NAA) pathway has been extensively described in brain. N-acetyltransferase 8-like (NAT8L) and aspartoacylase (ASPA) are the two main enzymes in NAA metabolism, responsible for NAA synthesis and breakdown, respectively. NAT8L utilizes acetyl-CoA and L-aspartate (L-Asp) to synthesize NAA. NAA has been described as the second most abundant metabolite in brain and has been established as a biomarker for NMR-spectroscopy-based determination of neuronal health. In addition, NAA metabolism has been shown to be important for neuronal lipid and energy metabolism (reviewed by Ariyannur et al.[187]).

Our group recently showed that NAT8L and ASPA are highly expressed in WAT and BAT (Pessentheiner & Pelzmann et al.[116]). Hence, we were the first to introduce the NAA pathway in adipocyte biology. Of note, NAT8L expression is very low in other metabolic tissues such as cardiac muscle, skeletal muscle, and liver when compared to adipose tissues and brain. Importantly, we also showed that *Nat8l* expression is increased during differentiation of human and murine white and brown adipocytes.

6.1. The NAA pathway in brown adipocyte metabolism in vitro

The first part of my thesis focused on providing more detail on the role of NAT8L in brown adipocyte metabolism *in vitro*. Based on our recent studies, we developed a working model of the NAA pathway as a novel route to provide cytoplasmic acetyl-CoA and its contribution to brown adipocyte metabolism (Figure 48)[15]. Briefly, glycolysis and β-oxidation of FFAs are the two main processes to derive mitochondrial acetyl-CoA in brown adipocytes. Mitochondrial acetyl-CoA can be used for energy production in the TCA cycle or transported to the cytoplasm. The canonical pathway to transport acetyl-CoA to the cytoplasm is provided by the formation of citrate and its export from mitochondria. Subsequently, ATP citrate lyase (ACLY) catalyzes the formation of cytoplasmic acetyl-CoA from citrate. The formation of NAA via NAT8L provides a novel route for mitochondrial acetyl-CoA to be transported to the cytoplasm. Cytoplasmic ASPA catalyzes the breakdown of NAA to L-Asp and acetate. Finally, ACSS2 uses acetate to provide cytoplasmic acetyl-CoA. Hence, the NAA pathway is able to regulate acetyl-CoA distribution and availability between mitochondria and cytoplasm and might thereby impact lipid metabolism and energy homeostasis in brown adipocytes. This model will be expanded based on the data of this thesis.

We demonstrated that overexpression of *Nat8l* led to increased lipid turnover, increased mitochondrial biogenesis and oxygen consumption in brown adipocytes[116]. Further, we found increased expression of brown marker genes such as *Pgc1α*, *Pparα*, and *Prdm16*. It has been shown that these genes induce mitochondrial biogenesis and the expression of *Ucp1*[67,68].

[15] Doctoral thesis; Ariane R. Pessentheiner, Ph.D.; "Elucidation of genes influencing adipogenic development and energy metabolism"; August 2014; Graz University of Technology

Indeed, we observed strikingly increased UCP1 expression in *Nat8l* o/e iBACs compared to controls. In conclusion, these data indicated that *Nat8l* o/e iBACs represent brown adipocytes with a higher energy turnover compared to control cells.

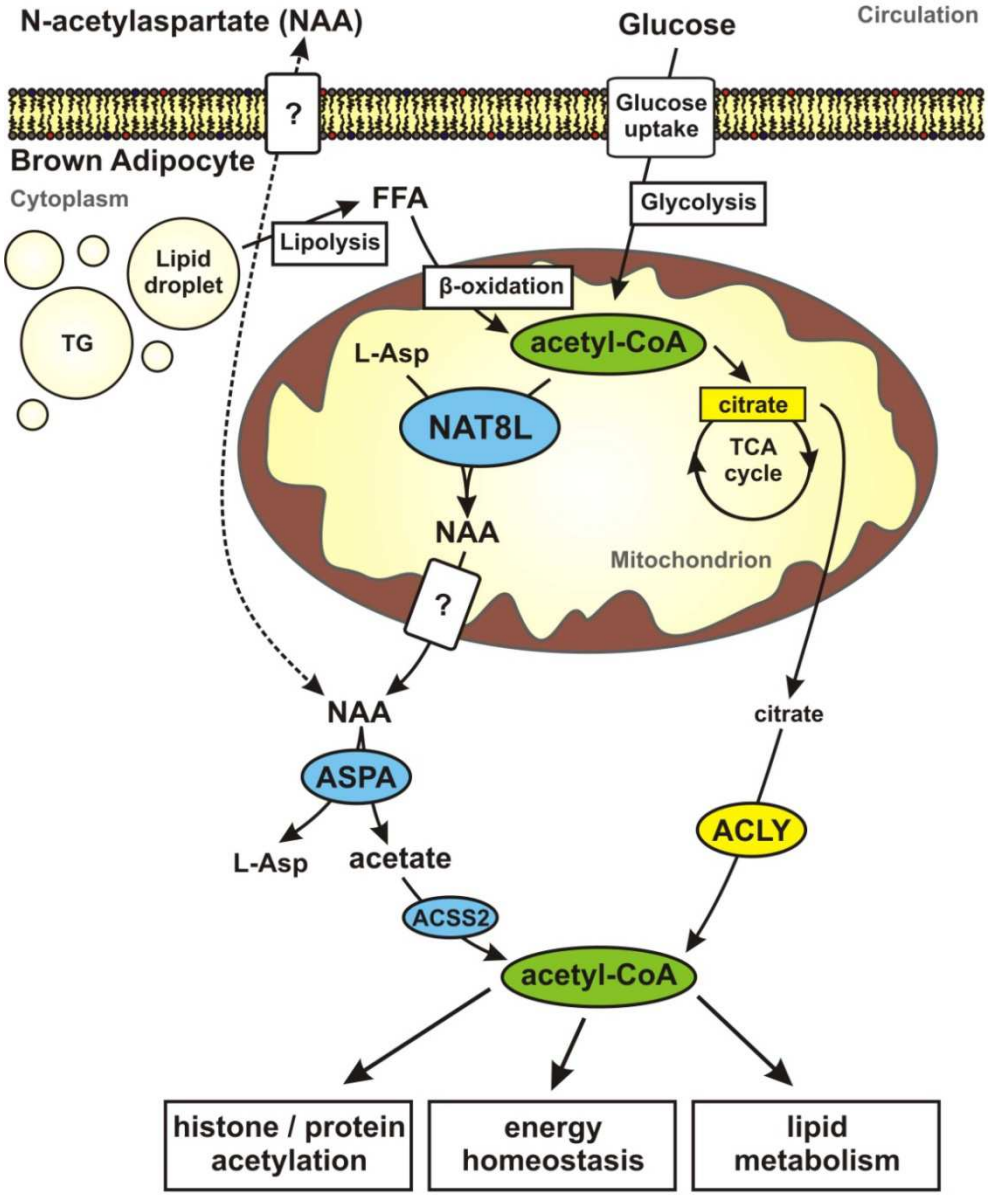

Figure 48. **Working model of the NAA pathway in brown adipocytes.** β-oxidation of free fatty acids (FFAs) and glycolysis are the two main processes to derive mitochondrial acetyl-CoA in brown adipocytes. Mitochondrial acetyl-CoA can be used for energy production in the TCA cycle or transported to the cytoplasm. The canonical pathway to provide cytosolic acetyl-CoA is via the formation and export of citrate. ATP citrate lyase (ACLY) uses citrate to provide cytoplasmic acetyl-CoA. The formation of N-acetylaspartate (NAA) via N-acetyltransferase 8-like (NAT8L) provides a novel route for mitochondrial acetyl-CoA to be transported to the cytoplasm. Cytoplasmic aspartoacylase (ASPA) catalyzes the breakdown of NAA to L-aspartate (L-Asp) and acetate. Finally, acetyl-CoA synthetase 2 (ACSS2) catalyzes the formation of cytoplasmic acetyl-CoA from acetate. TG, triglycerides.

As it is not clear how *Nat8l* o/e causes the observed effects, I will now provide more detail on parts of this molecular cascade based on the data of my thesis.

The transcription factor PPARα, a regulator of fatty acid catabolism and gene transcription in brown adipocytes, has been shown to be activated by lipolytic products such as fatty acids[68,153]. We found *Pparα* expression upregulated in *Nat8l* o/e iBACs on day 3 and day 7 of differentiation

whereas the majority of brown marker genes was increased exclusively on day 7[116]. Therefore, I used the PPARα antagonist GW6471 to investigate whether the observed effects are mediated by PPARα. Indeed, *Nat8l*-induced UCP1 expression and the concomitant oxygen consumption were reduced to control cell levels upon GW6471 treatment. Of note, increased lipid turnover was not affected by GW6471 treatment. Thus, this indicates that the effects of forced *Nat8l* expression and increased NAA synthesis on lipid turnover are upstream of PPARα action.

Brown adipocytes perform high rates of *de novo* lipogenesis (DNL) and lipolysis to fuel and maintain thermogenic activity (reviewed in[188]). We observed increased DNL assessed by [^{14}C]-glucose incorporation into neutral lipid stores. Also, lipolysis was elevated as indicated by increased FA release from *Nat8l* o/e cells. ATGL and HSL are the two main TG hydrolases in adipose tissue[119]. Therefore, I tested whether the increased FA release in *Nat8l* o/e iBACs was mediated by ATGL, HSL or both lipases. We did not detect increased TG hydrolase activity in the cytoplasm, but FA release from isolated lipid droplets was increased in *Nat8l* o/e iBACs compared to controls. When *Nat8l* o/e iBACs were treated with specific inhibitors for ATGL (Atglistatin[145]) or HSL (Hi 76-0079; Novo Nordisk), only the ATGL inhibitor was able to decrease FA release to levels comparable to control cells. These results are supported by studies showing that specifically ATGL-mediated lipolysis is substantial for maintaining adaptive thermogenesis in BAT[189] and provides FA for activation of UCP1[190] and PPARs[65,191]. Thus, these data show that ATGL-mediated lipolysis activates PPARα, further leading to increased UCP1 expression in *Nat8l* o/e iBACs (Figure 49). The underlying mechanism for altered lipid metabolism during *Nat8l* overexpression and silencing will be discussed in the next paragraphs.

Mottillo et al. showed that DNL and lipolysis are highly coupled processes in brown adipocytes[186]. As mentioned above, we found that DNL was increased in *Nat8l* o/e iBACs whereas *Nat8l* silencing did not lead to changes in DNL. The differential effects on DNL might be explained by the results of d'Adamo and Yatsu[115] who showed that NAA-derived acetate is preferentially used for lipid synthesis in brain when compared to free acetate. Further, we found *Acly* mRNA expression upregulated in *Nat8l*-silenced iBACs and BAT of *Nat8l*-ko mice compared to controls[160]. This indicates a compensation reaction to reduced delivery acetyl-CoA by the NAA pathway. Thus, these data suggest that the NAA pathway is able to drain acetate / acetyl-CoA into DNL. FA release was increased in both *Nat8l* o/e and *Nat8l*-silenced iBACs whereas glycerol release was reduced in *Nat8l* o/e, but increased in *Nat8l*-silenced iBACs when compared to controls, respectively. In addition, FA β-oxidation was strongly increased during *Nat8l* o/e whereas *Nat8l* silencing did not change FA β-oxidation in *Nat8l*-silenced iBACs compared to controls. This raised the questions why glycerol released by lipolysis is not exported in *Nat8l* o/e iBACs and why FA release is increased during both overexpression and silencing of *Nat8l* in brown adipocytes.

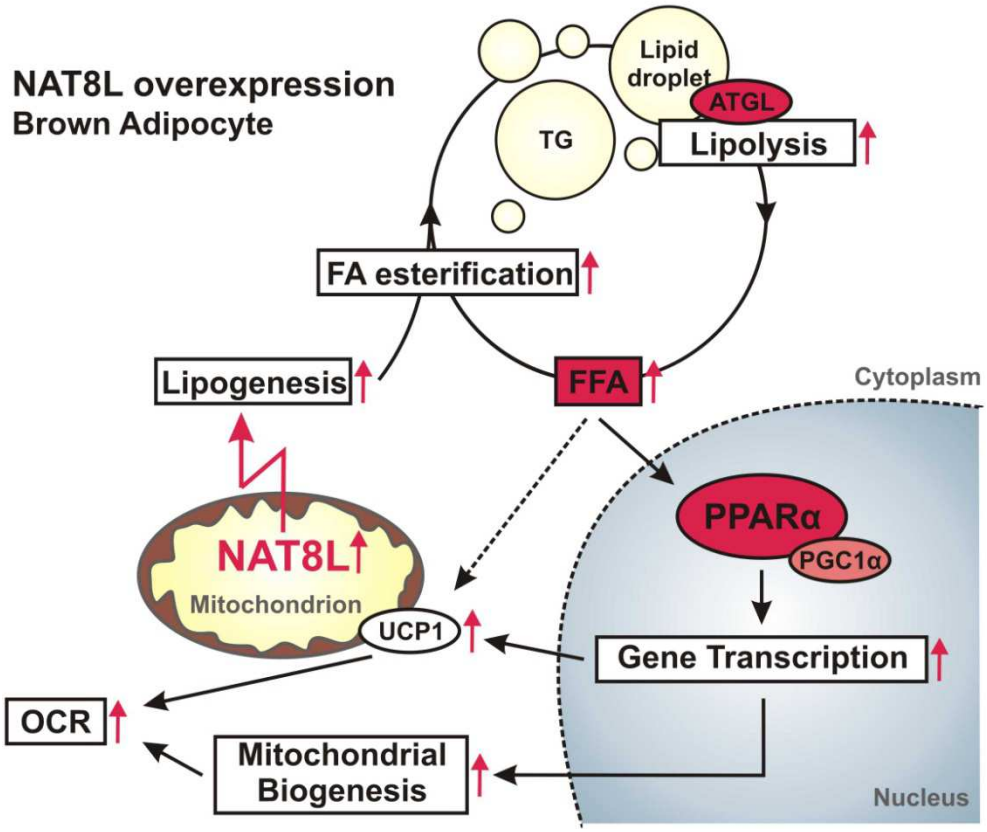

Figure 49. **ATGL-mediated PPARα activation increases *Ucp1* transcription and oxygen consumption rate (OCR) in *Nat8l* overexpressing brown adipocytes.** *Nat8l* overexpression in mitochondria of brown adipocytes leads to increased lipid turnover. Increased lipolytic activity of ATGL on the lipid droplet releases FFAs as ligands for PPARα activation. PPARα recruits PGC1α and activates gene transcription, mitochondrial biogenesis and FA oxidation, finally leading to increased OCR in *Nat8l* o/e iBACs. TG, triglycerides.

Building triglyceride (TG) stores in adipocytes requires two components, activated free fatty acids (FFA) and glycerol-3-phosphate (G3P). FFAs for TG stores can be provided by *de novo* synthesis, uptake, or reuse after their release by lipolysis. Acyl-CoA synthetase long-chain family member 1 (ACSL1) is the enzyme activating FFAs for incorporation into TG stores or mitochondrial β-oxidation in adipocytes[177]. If FFAs cannot be used in one of these processes, they will be exported to the circulation to prevent lipotoxicity. G3P is generated during glycolysis to provide the backbone for TG synthesis. Lipolysis of one molecule TG generates three molecules FFAs and one free glycerol. It has been reported that adipocytes do not reuse but rather release free glycerol into the circulation[192]. Conversely, Festuccia et al.[188] showed that brown adipocytes express glycerokinase (GYK), the enzyme catalyzing the formation of G3P from free glycerol. Hence, reduced glycerol release in *Nat8l* o/e iBACs indicates that glycerol might be reutilized to G3P and reused for building TGs. Interestingly, we found *Acsl1* expression not changed in *Nat8l* o/e iBACs compared to controls[16]. Hence, this argues against increased re-esterification of FFAs in these cells. However, mRNA might not reflect activity. Further, it has been described that metabolic signals such as norepinephrine and insulin also

[16] Doctoral thesis; Ariane R. Pessentheiner, Ph.D.; "Elucidation of genes influencing adipogenic development and energy metabolism"; August 2014; Graz University of Technology

trigger phosphorylation of ACSL1, thereby regulating its activity (reviewed in[193]). Importantly, FA β-oxidation is strongly increased in *Nat8l* o/e iBACs arguing for increased ACSL1 activity. However, increased FA release during *Nat8l* o/e might reflect an overload of FFAs due to high rates of both lipogenesis and lipolysis. Supportive to that, FA uptake in *Nat8l* o/e iBACs was reduced, indicating usage of intracellular FA for both esterification and β-oxidation. Of note, FA uptake was not changed in *Nat8l*-silenced cells compared to controls. Hence, it would be important to analyze GYK and ACSL1 protein in *Nat8l* o/e iBACs compared to controls. It would be also interesting to test whether inhibiting ACSL1 with Triacsin C would further increase FA release in *Nat8l* o/e iBACs or even induce lipotoxicity as FFA esterification would be inhibited.

As mentioned above, silencing of *Nat8l* in iBACs did not alter DNL compared to controls, but increased FA and glycerol release. These data indicate that free glycerol is rather exported than re-utilized in *Nat8l*-silenced cells. A possible explanation might be that DNL is strongly increased by *Nat8l* o/e iBACs, making it necessary to reuse free glycerol for esterification whereas this is not the case in *Nat8l*-silenced cells. Unfortunately, this does not answer question how silencing of *Nat8l* increases FA release in these cells? However, the common denominator between *Nat8l* overexpression and silencing is that manipulations of the NAA pathway are likely to impact acetyl-CoA availability and usage in mitochondria and the cytoplasm of brown adipocytes. Thus, it seems likely that the connection between the NAA pathway and glucose, lipid, and energy metabolism is established via NAA-derived acetate / acetyl-CoA. Therefore, the next paragraphs aim to establish different hypotheses, how manipulation of the NAA pathway impacts acetyl-CoA shuttling and consequently energy homeostasis in brown adipocytes.

Acetyl-CoA is a central metabolite and carbon source and is derived and produced in various cellular processes and compartments (Figure 50). It is important to emphasize that total intracellular acetyl-CoA has to be divided into a (nucleo-) cytoplasmic and a mitochondrial pool. In mammals, the most important pathways to derive mitochondrial acetyl-CoA are glycolysis and β-oxidation of FA. The distribution and availability of acetyl-CoA in mitochondria, cytoplasm, and the nucleus impacts cellular energy homeostasis and influences the balance between anabolic and catabolic actions such as DNL, lipolysis, autophagy, FA β-oxidation, and others. Further, acetyl-CoA regulates gene transcription, transcription factor signaling, and enzyme activity.[82,149,194,139]

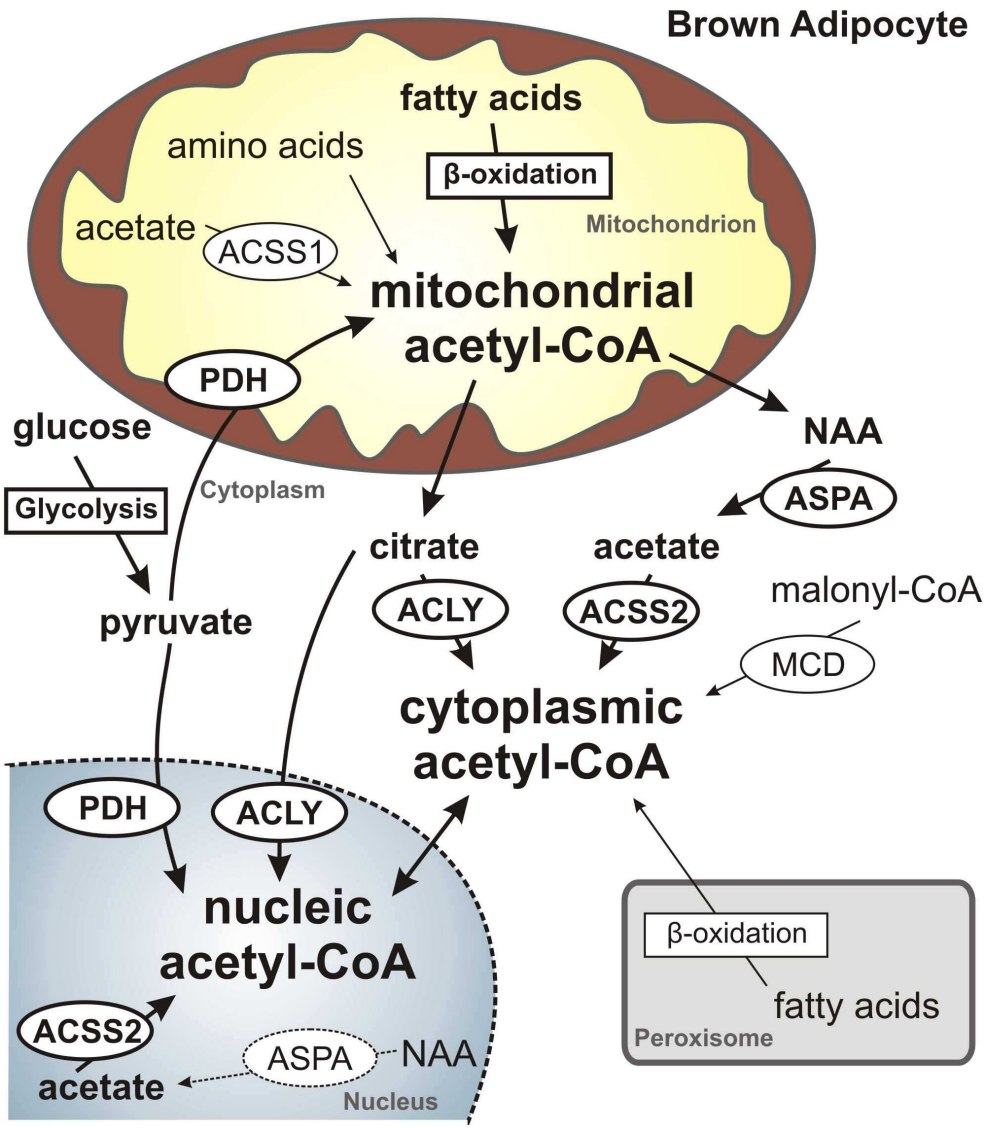

Figure 50. **Brown adipocyte intracellular acetyl-coenzyme A (acetyl-CoA) sources and distribution.** Fatty acids and pyruvate are the main sources to provide mitochondrial acetyl-CoA beside amino acids and acetate. Citrate and acetate represent the main sources of cytoplasmic acetyl-CoA. Acetate might either be taken up from the circulation[195] or derived from NAA. Acetyl-CoA in the nucleus is provided by pyruvate, citrate, and acetate or direct diffusion from the cytoplasm. Peroxisomes also provide cytoplasmic acetyl-CoA by β-oxidation of fatty acids[196]. ACSS1 / 2, acetyl-CoA synthetase 1 / 2; PDH, pyruvate dehydrogenase; ACLY, ATP citrate lyase; ASPA, aspartoacylase; MCD, malonyl-CoA decarboxylase.

One hypothesis on the underlying mechanism how manipulation of the NAA pathway might activate lipid turnover is via Sirtuin1 (SIRT1) dependent deacetylation of PPARγ (Figure 51). SIRT1 is a NAD^+-dependent deacetylase which is activated upon caloric restriction and exercise[163]. We found *Sirt1* mRNA expression upregulated in differentiating *Nat8l* o/e iBACs when compared to controls. *Sirt1* mRNA expression has been linked to energy expenditure and mitochondrial function in insulin-sensitive tissues[197]. We measured increased incorporation of ^{14}C-labeled glucose into neutral lipids in *Nat8l* o/e iBACs compared to controls[160]. Thus, forced NAA synthesis might drain acetyl-CoA into DNL. This can be supported by the results of d'Adamo and Yatsu[115] who showed that NAA-derived acetate is three times better incorporated into FAs in brain when compared to free acetate. Hence, *Nat8l* o/e in brown adipocytes might

prevent use of acetyl-CoA for energy production in the TCA cycle, thereby causing an energy crisis (probably increased NAD^+ / NADH ratio). Consequently, this would activate SIRT1-dependent deacetylation of PPARγ and increase its activity similar to known PPARγ ligands (e.g. rosiglitazone)[140]. It is known that chronic PPARγ activation leads to induction of marker gene expression and mitochondrial biogenesis (reviewed in[58]) in brown adipocytes. Further, Festuccia et al.[198] showed that rosiglitazone-mediated PPARγ activation increased lipolysis in WAT of rats. Kershaw et al.[199] reported that PPARγ regulates ATGL expression in adipocytes *in vitro* and *in vivo*. Hence, PPARγ-mediated activation of ATGL might increase lipolysis, thus providing ligands for PPAR-activation and creating a feed-forward loop for e.g. activation of gene transcription and mitochondrial biogenesis. Of note, SIRT1 is also known to deacetylate and activate PGC1α, the so called master regulator of mitochondrial biogenesis[141,142]. Thus, it might be important to analyze PGC1α protein acetylation upon overexpression of *Nat8l*.

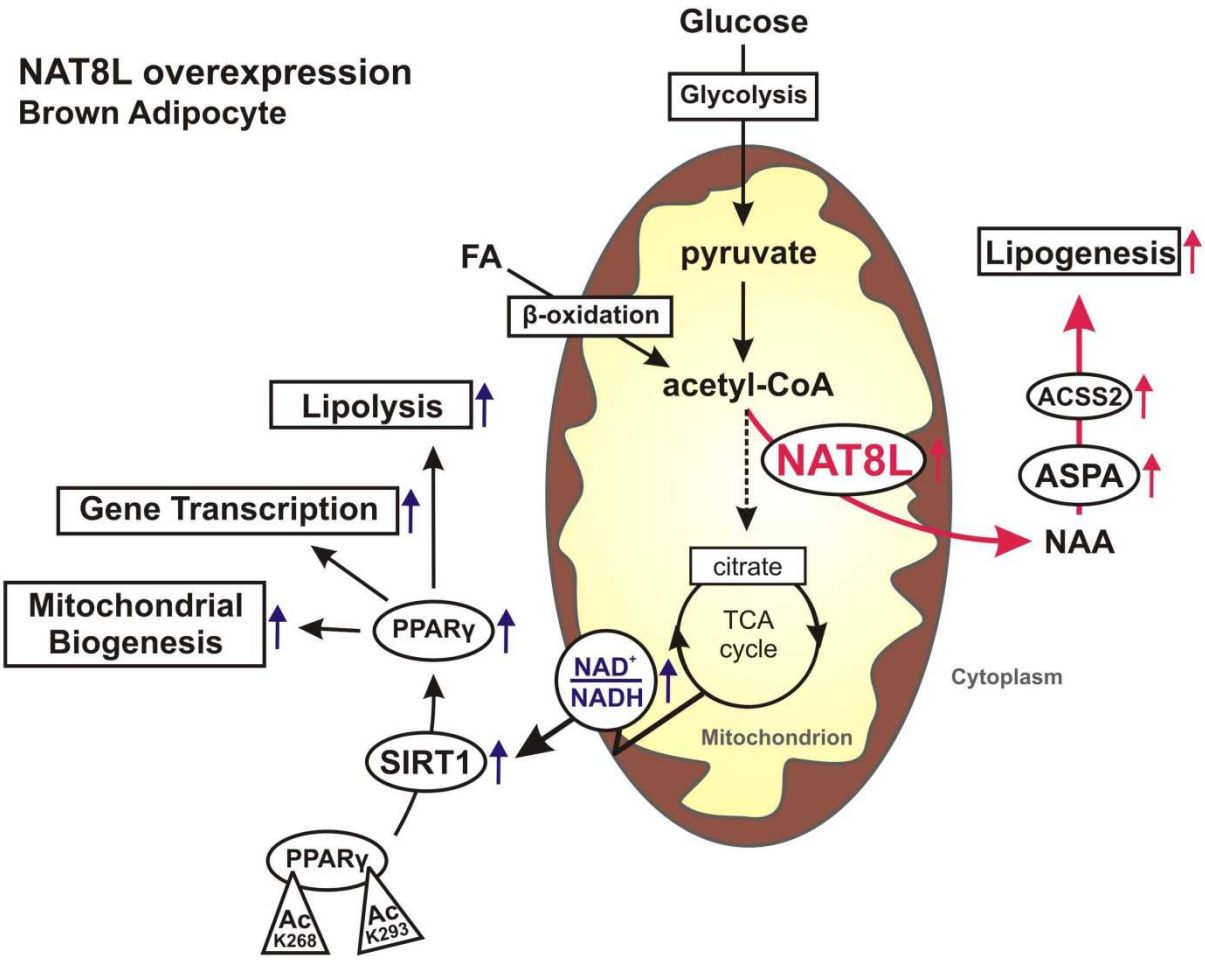

Figure 51. **SIRT1-dependent deacetylation of PPARγ in *Nat8l* o/e iBACs.** *Nat8l* o/e in mitochondria drains acetyl-CoA from energy production to *de novo* lipogenesis. As a result, nicotinamide adenine dinucleotide (NAD^+) to NADH ratio increases and activates SIRTUIN 1 (SIRT1) deacetylase activity. SIRT1 activates PPARγ by deacetylation and leads to increased mitochondrial biogenesis, gene transcription, and lipolysis. NAA, N-acetylaspartate; ASPA, aspartoacylase; ACSS2, Acetyl-CoA synthetase 2; Ac, acetylation site.

Nicotinamide (NA), a product of sirtuin deacetylase activity, has been reported to noncompetitively inhibit SIR2P, the yeast SIRT1 orthologue[200–202]. Hence, NA is not a specific

SIRT1 inhibitor in mammals, but targets general sirtuin activity. However, when *Nat8l* o/e iBACs were treated with NA, an inhibitor of sirtuin activity, the induction of *Pparα* and *Ucp1* was inhibited. Therefore, SIRT1-dependent deacetylation of PPARγ might be a possible explanation for increased lipolysis in *Nat8l* o/e iBACs compared to controls. Together with increased DNL this might account for increased lipid turnover and its downstream effects on gene transcription and oxygen consumption. To further strengthen this hypothesis, it will be necessary to investigate PPARγ and / or PGC1α protein acetylation in *Nat8l* o/e iBACs in the absence or presence of a specific SIRT1 inhibitor such as selisistat[203].

Another hypothesis is based on our recent study where we showed that reducing ASPA activity by silencing of *Aspa* led to a marked reduction of cytoplasmic acetyl-CoA and decreased histone acetylation in iBACs, thereby connecting NAA catabolism to epigenetic gene regulation (Prokesch & Pelzmann et al.[117]). Thus, we hypothesized that manipulation of NAT8L might also alter acetyl-CoA distribution in brown adipocytes. As a consequence, changes in acetyl-CoA availability for histone acetyltransferases (HATs) might directly regulate gene transcription. We showed that both *Nat8l* o/e and silencing led to increased expression of brown marker genes such as *Ucp1*, *Pparα*, and *Pgc1α* in brown adipocytes[116]. Concomitantly, these genes were increased in BAT of *Nat8l*-ko mice compared to controls. Of note, we found decreased NAA levels and increased *Acly* mRNA expression in *Nat8l*-silenced iBACs and BAT of *Nat8l*-ko mice when compared to controls. Wellen et al.[136] reported that ACLY regulates gene expression via histone acetylation in mammalian cells. Therefore, ACLY might compensate the supply for cytoplasmic acetyl-CoA upon NAT8L deficiency, but also alter acetyl-CoA shuttling and histone acetylation in iBACs. Taken together, this might lead to altered histone acetylation and activation of gene transcription in *Nat8l*-silenced iBACs.

Another interesting possibility is that modulating intracellular NAA concentrations directly affects histone and / or protein acetylation, thereby regulating gene transcription. We have shown that differentiation of iBACs in the presence of NAA also reduces marker gene expression similar to *Aspa* silencing[117]. Therefore, I tested whether an overload of NAA would probably inhibit ASPA activity. Importantly, I found that ASPA activity was high even when NAA concentrations were far beyond physiological levels. Furthermore, addition of exogenous NAA did not change cytosolic acetyl-CoA in iBACs, but reduced gene transcription[117]. Thus, NAA supplementation during differentiation might not inhibit ASPA, but increase cytoplasmic acetate / acetyl-CoA derived from NAA. Interestingly, we found *Acly* expression decreased in iBACs differentiated in the presence of NAA[117]. However, *Acly* expression was also reduced in *Aspa*-silenced iBACs compared to controls. Therefore, it might be interesting to investigate if ACLY activity is directly inhibited by NAA or by increased NAA-derived cytoplasmic acetyl-CoA. This could again alter ACLY-mediated acetyl-CoA delivery for HATs and subsequently affect histone acetylation and gene transcription.

Further, we wanted to investigate if other deacetylases such as sirtuins might be able to deacetylate NAA, thereby using NAA as a direct source for acetate moieties for histone and / or protein acetylation. However, *in silico* analyses of protein structure and substrate specificity by Monika Oberer revealed that NAA is no possible substrate for sirtuins. Finally, I want to discuss if ASPA and ACSS2 could be directly involved in providing nuclear acetyl-CoA. It has been shown that ASPA and ACSS2 localize to the cytoplasm and nucleus and are likely to regulate acetyl-CoA availability and thereby histone and protein acetylation in brain[98,138]. Hence, it cannot be ruled out that unknown triggers also promote translocation of ASPA and ACSS2 to the nucleus in brown adipocytes (see Figure 50). Thus, manipulation of intracellular NAA might directly regulate nuclear acetyl-CoA availability for HATs.

Taken together, these data indicate that brown adipocytes precisely sense if cytoplasmic acetyl-CoA is provided by citrate or NAA and control the corresponding pathways depending on this relation. Accordingly, this could change the fate of acetyl-CoA in metabolic processes and their regulation.

As mentioned above, we observed that intracellular accumulation of NAA by either silencing of *Aspa* or exogenous addition of NAA reduced *Nat8l* expression and reduced the brown adipogenic phenotype in iBACs[117]. Conversely, unpublished data from Katharina Huber shows that NAA also accumulates in *Nat8l* o/e iBACs, where we observed increased lipid turnover, UCP1 expression, mitochondrial biogenesis, and oxygen consumption rate when compared to controls. Of note, we also found markedly increased *Aspa* expression in *Nat8l* o/e iBACs compared controls, indicating increased ASPA activity. Further, I found that ASPA activity is high when intracellular NAA concentrations are high. Madhavarao et al.[91] showed that enzymatic activity of NAT8L is activated by high concentrations of acetyl-CoA and L-Asp, but inhibited by its product NAA. Hence, accumulation of NAA probably decreases NAA synthesis. However, this would not necessarily exclude increased ASPA activity but could decrease NAA-mediated flux of mitochondrial acetyl-CoA to the cytoplasm. Thus, NAA accumulation during *Aspa* silencing and exogenous NAA supplementation might be able to decrease endogenous NAT8L activity in brown adipocytes whereas NAA accumulation during *Nat8l* o/e might not be able to decrease net NAT8L activity, as much more protein is present. Hence, these data suggest that forced NAA synthesis and full ASPA activity together increase the metabolic flux through the NAA pathway during *Nat8l* o/e in iBACs. Indeed, silencing of *Aspa* in *Nat8l* o/e iBACs recovered *Aspa* expression to control cell level and *Ucp1* expression was also massively decreased when compared to control *Nat8l* o/e cells. Although mitochondrial biogenesis, lipid turnover, and oxygen consumption need to be investigated in detail in these cells, these data strongly suggest that increased flux through the NAA pathway is a prerequisite to increase the brown adipogenic phenotype during *Nat8l* o/e in brown adipocytes.

In summary, the detailed mechanism on how the NAA pathway impacts lipid, glucose, and energy homeostasis in brown adipocytes remains unclear. Furthermore, the consequences of manipulating NAA metabolism regarding histone and protein acetylation and its downstream effects on gene transcription remain matter of further investigation. However, the *in vitro* data obtained in this thesis further strengthen the hypothesis that the NAA pathway is a novel route to regulate cytoplasmic acetyl-CoA, is connected to PPARα signaling, and able to regulate lipid, glucose, and energy metabolism in brown adipocytes.

6.2. The role of the NAA pathway in vivo – physiological triggers and the effects of NAT8L *deficiency on energy homeostasis*

The second and third part of my thesis addressed the question how the NAA pathway impacts energy homeostasis (and vice versa) *in vivo*. C57Bl/6J wild-type (wt) and *Nat8l* knock-out[112] (*Nat8l*-ko) mice were used as a model system.

6.2.1. Is NAT8L the sole enzyme to produce NAA?

First, I tested if NAT8L is the only enzyme to produce NAA *in vivo*. Of note, Toriumi et al.[167] reported that deletion of NAT8L strongly reduced NAA in different brain regions of C57Bl/6J mice, but did not eliminate NAA. In contrast, I did not detect NAA in total brain homogenates of *Nat8l*-ko when using mice at the same age as in the study of Toriumi and colleagues. Interestingly, residual NAA was detected in BAT, sWAT, and serum of *Nat8l*-ko compared to wt mice. This raised the question if external sources of NAA may exist? It has been described that NAA is part of many foods[204] and bioavailable based on studies of Karaman et al.[205,206]. We found expression of two out of three proposed NAA transporters in small intestine[117]. Hence, residual NAA detected in *Nat8l*-ko mice might be taken up from the diet. However, this does not explain the residual NAA in brain of *Nat8l*-ko mice shown by Toriumi et al. as NAA cannot cross the blood brain barrier[206,207]. One major difference in sample preparation was that Toriumi and colleagues immediately extracted metabolites from the tissue samples whereas I used flash frozen samples for analysis. Although NAA is a very stable metabolite compared to e.g. acetyl-CoA, I cannot rule out that some NAA was lost during the additional freeze-thaw cycle before homogenization and extraction. However, these data provide strong evidence that NAT8L is the main enzyme to produce NAA in mice and NAA uptake from nutrients is feasible.

6.2.2. Physiological regulation of the NAA pathway

The physiological triggers activating or inhibiting the NAA pathway in adipose tissues have not been identified. We reported an important role of the NAA pathway in lipid and glucose metabolism[160]. Therefore, I will discuss the physiological regulation and importance of NAA

metabolism in brown and white adipose tissue in the next paragraphs. Namboodiri and colleagues reported that the NAA pathway is upregulated after birth to support myelination in brain[81,208]. Further, a variety of conditions including traumatic brain injury (TBI), neuronal energy production, and neurodegenerative diseases have been reported to influence NAA synthesis and catabolism in brain (reviewed in[81,82]). Based on the hypothesis that the NAA pathway is important to provide acetyl-CoA for lipid synthesis (see Figure 48), I studied the regulation of *Nat8l*, and *Aspa* mRNA expression in adipose tissues *in vivo* and *in vitro*. A graphical summary of these results is given in Figure 52.

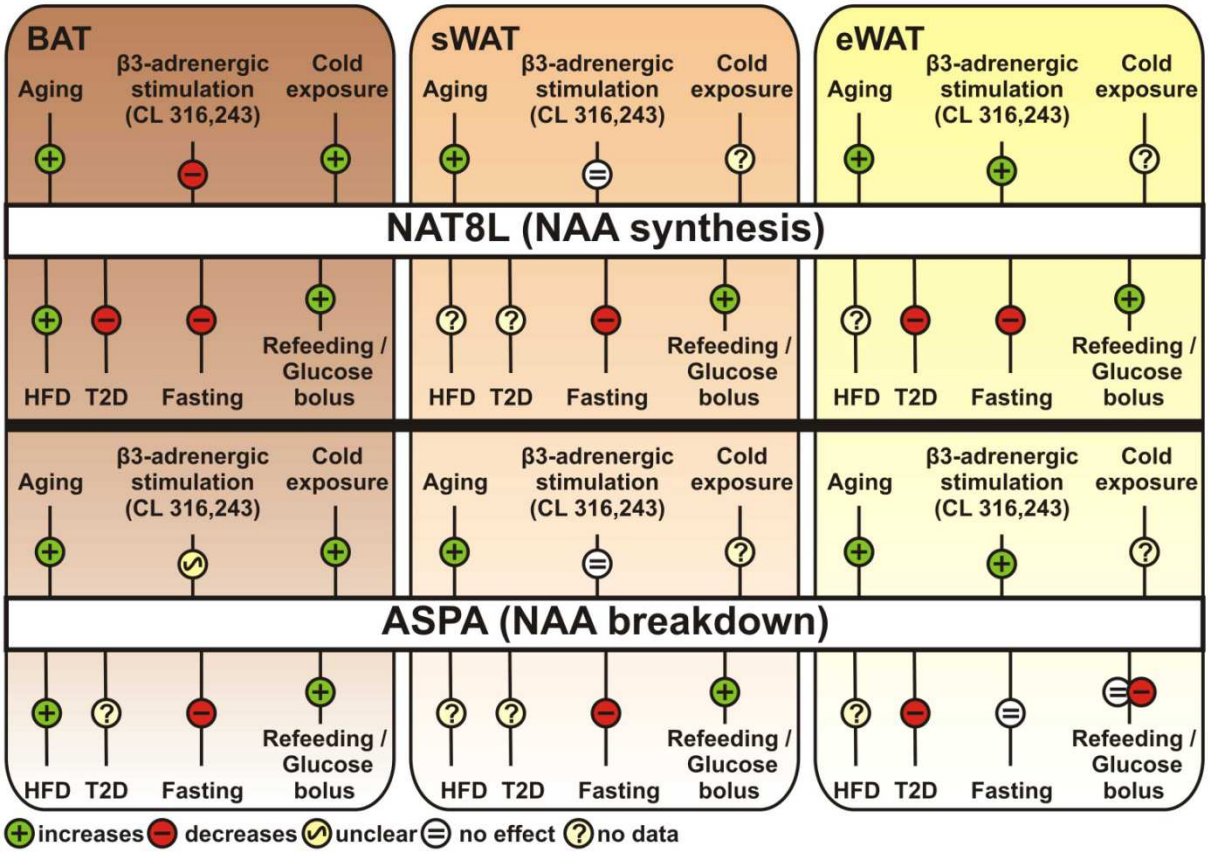

Figure 52. **Physiological regulation of N-acetylaspartate (NAA) metabolism in adipose tissues in C57Bl/6 mice.** The influence of aging, β3-adrenergic stimulation by CL 316,243, cold exposure, high-fat diet (HFD) feeding, type 2 diabetes, fasting, and refeeding / glucose bolus on NAT8L (representing NAA synthesis) and ASPA (representing NAA breakdown) is shown.

In accordance with a proposed role of the NAA pathway during developmental lipid synthesis, I found *Nat8l* and *Aspa* mRNA expression upregulated in brain but also BAT, sWAT, and eWAT of aging C57Bl/6J mice. Interestingly, I detected a drop in expression of both *Nat8l* and *Aspa* mRNA expression in BAT at the age of one month. In sWAT and eWAT, the opposite was found and *Nat8l* and *Aspa* had an expression peak at the age of one month. The main function of BAT in newborns is to perform high rates of thermogenesis to support the adaptive thermal response which is necessary to prevent hypothermia[209]. Further, BAT in newborn mice is functional but not fully developed and activated at the time of birth. Of note, murine BAT gets activated and maturates very fast within the first postnatal days. Thermoneutral conditions and huddling in

nests decelerate the thermogenic response of BAT, but standard housing temperatures (23 – 25 °C) lead to a massive increase of BAT mass (including lipid accumulation) and activity in newborn mice[210]. Accordingly, BAT has to perform high rates of glycolysis, lipogenesis, lipolysis, and FA β-oxidation. Increased flux through the NAA pathway might thereby provide acetyl-CoA for lipid synthesis to provide FAs for β-oxidation. With increasing age and decreasing surface to volume ratio, thermogenic demand decreases which might explain the downregulation of the NAA pathway in BAT. On the other hand, the main white adipose depots (eWAT and sWAT) are expanding in young rodents to provide energy storage[211]. Although this is speculation, *Nat8l* / *Aspa* upregulation during weaning might support DNL in healthy white adipose tissue. Thus, it might be interesting to investigate how and if thermoneutral housing affects the regulation of the NAA pathway in adipose tissues. In addition, Moffett et al. described that NAA synthesis in neurons is activated when there is plenty of energy available[81]. Mother milk is a high fat and high carbohydrate diet[212]. Hence, changing diet from mother milk to normal CD at the age of 3 to 4 weeks might constitute a challenge to energy homeostasis in mice. Unfortunately, this does not explain why the NAA pathway should be upregulated in sWAT and eWAT as switching from mother milk to CD seems to mimic a fasting state.

Another interesting observation was that I found *Nat8l* and *Aspa* mRNA expression upregulated in BAT of wt mice fed a HFD. BAT has been described as a sink for both circulating glucose and lipids[133]. HFD contains 45 % fat and 20 % protein, but also 35 % carbohydrates. Therefore, the NAA pathway in BAT might support lipid turnover and energy expenditure on HFD as long as excess glucose can be provided by and taken up from the circulation. We previously showed that *Nat8l* was downregulated in BAT and eWAT of genetically obese ob/ob mice[116]. Of note, ob/ob mice are diabetic and highly insulin-resistant whereas the HFD-fed mice used in my experiments were obese but still responded to an insulin bolus in ipITT. Thus, decreased glucose uptake resulting from insulin resistance might decrease NAA synthesis in ob/ob mice. Consistently, NAA concentrations in serum and urine of ob/ob mice were reported to be reduced[213]. In addition, micro array expression analyses revealed reduced expression[17] of *Nat8l* and *Aspa* in subcutaneous and visceral white adipose tissue of insulin-resistant compared to insulin-sensitive obese individuals, respectively[214]. Conversely, it has been shown that urinary NAA was increased in diabetic rats and humans[215]. Although inconsistent, these data indicate that insulin-dependent glucose uptake and glucose availability might control NAA synthesis downstream of glycolysis. Further, the NAA pathway might be important to regulate insulin-dependent glucose disposal in adipose tissues during overnutrition. Supportive to that, I found *Nat8l* mRNA expression decreased when glucose concentration was reduced in the differentiation media of brown adipocytes, indicating a direct link between glucose availability and NAA synthesis. However, the *in vitro* data on *Aspa* mRNA expression in brown adipocytes

[17] Data analyzed byGEO2R (http://www.ncbi.nlm.nih.gov.gate2.inist.fr/geo/geo2r/?acc=GSE20950)

in response to changing glucose concentrations is not conclusive yet and needs further investigation. Importantly, *Nat8l* and *Aspa* mRNA expression was upregulated in BAT when mice were injected with 1.5 g / kg glucose (similar to what is used for ipGTT) (see Figure 46). These data suggest that glucose is able to increase the flux through the NAA pathway in BAT. In eWAT, *Nat8l* mRNA expression was upregulated whereas expression of *Aspa* was reduced after intraperitoneal glucose bolus, indicating increased NAA synthesis but not breakdown. Hence, it could be speculated that NAA might store energy in eWAT. Further, these data indicate that NAA synthesis is regulated by circulating glucose and insulin as injection of glucose provokes an anabolic response similar to the normal feeding situation and increases insulin secretion in healthy mice. Conversely, fasting induces a catabolic state in mice[216], reduces circulating insulin and glucose concentrations and increases FA release from white adipose tissue to be used for energy production[19]. Therefore, I tested how fasting influences the NAA pathway *in vivo*. *Nat8l* and *Aspa* expression are reduced in adipose tissues of fasted mice compared to *ad libitum* fed controls. Importantly, refeeding was able to increase *Nat8l* and *Aspa* expression again. Thus, high levels of circulating FAs might inhibit whereas high levels of glucose activate the NAA pathway.

Adaption to cold induces thermogenesis and consequently the production of heat in BAT of rodents[19]. Further, cold exposure increases the usage of both fatty acids and glucose as substrates for heat production[133]. I found *Nat8l* and *Aspa* mRNA expression upregulated during cold exposure in BAT. Mice adapt to cold by increasing their food consumption compared to normal temperatures[217]. Hence, cold exposure increases energy dissipation from both FAs and carbohydrates, but also increases food intake and nutrient supply. Thus, increased glucose availability combined with an increased lipid turnover might increase *Nat8l* / *Aspa* expression during cold exposure. Chronic β3-adrenergic stimulation with the β3-adrenoreceptor agonist CL 316,243 (CL) has also been shown to increases energy dissipation and glucose disposal in BAT and eWAT[133]. Of note, CL does not increase food intake[218]. Grujic et al.[219] even reported reduced food intake in CL-treated mice compared to controls. Thus, a main energy source for BAT thermogenesis during CL treatment is provided by circulating FFAs derived from lipolysis of WAT. Motillo et al.[186] showed that lipolysis and DNL are coupled processes in adipose tissue. Briefly, DNL is inhibited by acute β3-adrenergic stimulation and lipolysis is activated to provide FAs for β-oxidation. On the other hand, chronic β3-adrenergic stimulation is able to increase DNL again. Thus, increased DNL is necessary to supply novel FAs to TGs to compensate the increase in lipolysis and FA β-oxidation[186]. Accordingly, we found *Nat8l*, *Aspa*, and *Acss2* mRNA upregulated in eWAT of CL-treated mice when compared to controls. This indicates that the NAA pathway supports lipogenesis upon chronic CL-mediated adrenergic stimulation (see Figure 45). Conversely, *Nat8l* and *Acss2* mRNA expression was downregulated in BAT of mice treated with CL for at least 7 days. It has been reported that glucose uptake into BAT during β-

adrenergic stimulation is insulin-independent[220]. Hence, the downregulation of *Nat8l* and *Acss2* in BAT could be explained by decreased insulin-mediated glucose-uptake and increased FAs in the circulation. Thus, it could be important to determine if insulin is required to increase *Nat8l* and *Aspa* expression upon glucose administration. In two independent experiments, *Aspa* mRNA expression was found unchanged or increased in BAT of CL-treated mice compared to controls (Figure 45). Thus, *Aspa*-mediated breakdown of NAA might provide acetate which could be shuttled to mitochondria for energy production.

From these data, the question has to be raised if NAA could function as a “long-term” storage form for acetyl-CoA in adipose tissue? NAA breakdown provides L-Asp and acetate. Acetate can be used for lipid synthesis or transported back into the mitochondria where mitochondrial acetyl-CoA synthetase (ACSS) 1 uses acetate to provide acetyl-CoA for energy production. Thus, it seems feasible that certain amounts of NAA are produced as a backup for immediate energy needs. A similar role has been reported in brain, where acute reductions of neuronal NAA after TBI could provide fast supply of acetyl-CoA for energy production and repair mechanisms[82]. Thus, stored NAA might be catabolized to L-Asp and acetate to fuel thermogenesis rather than lipogenesis in brown adipocytes as soon as insulin-mediated glucose uptake is limited.

In summary, these data demonstrate that the NAA pathway in adipose tissues is highly regulated depending on glucose and FA availability and utilization, respectively. Therefore, measurement of NAA uptake, release, production, and breakdown in different tissues and fluids during metabolic challenges such as fasting, HFD, cold exposure, high-glucose diet, and thermoneutrality is of great interest to gain deeper knowledge of the role of NAA metabolism *in vivo*. Further, NAA transport between cellular compartments and different organs remains matter of future investigation, as we did not detect expression of reported NAA transporters in adipose tissues[117]. In accordance with a role in lipid synthesis during development, I show that the NAA pathway is upregulated in adipose tissue after birth and during adolescence. Further, NAA metabolism seems to be activated whenever high energy supply is needed (cold exposure) and disposal of circulating carbohydrates is necessary (HFD, glucose injection). Of note, continuous supply with dietary nutrients seems to be a prerequisite for the activation of the NAA pathway as shown by CL treatment and fasting / refeeding experiments. Most importantly, defective lipid and glucose metabolism strongly reduces *Nat8l* and *Aspa* expression in adipose tissues of mice and men[118,160,214]. Thus, although the collected data are partly inconsistent, I want to hypothesize that NAA metabolism plays an important role in the development of obesity and T2D via insulin-mediated glucose disposal in adipose tissues.

6.2.3. NAT8L deficiency and reduced life span in mice

Next, I started to determine the metabolic phenotype of *Nat8l*-ko mice at the age of 8 weeks. It was reported that either loss or accumulation of NAA causes myelination deficits and severe neuropathologies in humans[105,110]. *Nat8l*-ko mice are viable without any early developmental impairment and show normal myelination whereas *Aspa* deficiency leads to demyelination and premature death of about 70 % of *Aspa*-ko mice compared to controls[109]. Interestingly, *Nat8l* / *Aspa*-double-ko mice have a normal myelination phenotype and survival time was increased when compared to *Aspa*-ko mice, but still about 50 % of these mice died earlier than their wt littermates[109,113]. These data suggest that the NAA pathway is not required to provide acetyl-CoA with regard to myelination. More likely, NAA accumulation in brain promotes myelination defects and premature death. Of note, also peripheral accumulation of NAA has to be considered in the lethal cascade in *Aspa*-ko mice. As a consequence of NAA accumulation in brain and other tissues, acetyl-CoA might be sequestered in NAA, therefore not available as an energy source. It might be valuable to determine NAA concentrations in *Aspa*-ko mice to get information about which tissues actually take up / accumulate NAA. Further, increased urinary NAA has been observed upon ASPA deficiency[105,106]. Hence, this could simply mean that acetyl-CoA gets “lost” as an energy source and might thereby lead to an energy crisis and death in *Aspa*-ko mice. This would not be the case when also NAA synthesis is blocked by knock-out of *Nat8l*. Maier et al.[109] also reported that *Nat8l*-ko mice have reduced life span compared to controls (about 20 % of these mice died in an observation period of 1 year). I observed similar rates of sudden death of *Nat8l*-ko mice on CD and HFD without any obvious signs of illness, weight loss, or seizures. As a first approach to identify the cause of death, I assessed cardiac function in *Nat8l*-ko mice. I found similar heart rate, systolic, diastolic, and mean arterial blood pressure in *Nat8l*-ko mice when compared to controls. It is known that cold exposure increases blood pressure and induces cardiac hypertrophy in rodents (reviewed in[221]). Of note, hearts of *Nat8l*-ko mice compared to controls became more hypertrophic when mice were exposed to cold (4 °C) for 9 days (see Table 12). Before, I hypothesized that the NAA pathway might be important in insulin-mediated glucose disposal in adipose tissues (see 6.2.2). Cold exposure induces thermogenesis in BAT and food intake[19,217]. Hence, glucose availability and glucose utilization is high under these conditions. Thus, NAT8L deficiency might lead to an inability to activate the NAA pathway as observed during cold exposure in BAT of wt mice. It is also known that insulin resistance can cause hypertrophy in rodents[222]. Of note, I measured increased insulin levels during intraperitoneal glucose tolerance test in plasma of *Nat8l*-ko compared to wt mice on HFD at room temperature (RT). However, insulin sensitivity was not altered in *Nat8l*-ko compared to wt mice. Further, no mouse died during cold exposure and I could not detect morphological differences when fiber structure was compared in tissue sections of cardiac muscle from wt and *Nat8l*-ko mice.

In summary, both NAT8L and ASPA deficiency lead to decreased life expectancy in mice. Until now, CNS-mediated loss or accumulation of NAA has been accounted for sudden death in these mice. Importantly, these data show that NAA metabolism in peripheral tissues should also be considered. Further, the data obtained in this thesis show that cardiovascular system and heart function seem normal in *Nat8l*-ko mice at RT, but cold-induced cardiac hypertrophy was increased when compared to wt mice. However, it is difficult to ascertain if this effect is mediated by sympathetic nervous signaling or caused by metabolic changes due NAT8L deficiency in peripheral tissues.

6.2.4. NAT8L deficiency and energy homeostasis in mice

Our recent *in vitro* studies showed that manipulation of the NAA pathway has significant impact on brown adipocyte energy homeostasis[116,117]. *Nat8l* expression is strongly reduced in adipose tissue of genetically obese mice and humans[118,160,214]. NAT8L deficiency in mice leads to behavioral deficits and reduced survival compared to wt mice[167,223], but there is no data on the metabolic phenotype of these mice. Therefore, I determined the metabolic phenotype of *Nat8l*-ko compared to wt mice with special emphasis on changes in adipose tissue lipid, glucose, and energy metabolism in accordance to the guidelines described by Tschöp et al.[175]. When starting the experiments at the age of 8 weeks, body weight (BW) of *Nat8l*-ko mice was reduced and *Nat8l*-ko mice never caught up with their wt littermates neither on chow diet (CD) nor on high-fat diet (HFD). In addition, weight gain of *Nat8l*-ko mice on HFD was reduced compared to controls. Above, I proposed that the NAA pathway might be important for adipose tissue development as *Nat8l* is upregulated after birth and during aging in mice (see 6.2.2). In addition, we and others showed that NAA provides acetate / acetyl-CoA for lipid synthesis in brain[131] and BAT[160]. Thus, NAT8L deficiency might impair adipose tissue development and remodeling during adolescence and HFD feeding, thereby leading to the observed differences in BW.

I also hypothesized that NAA synthesis is activated by insulin-mediated glucose uptake into adipocytes (see 6.2.2). Thus, it might be possible that defective NAA synthesis might have consequences for cellular and systemic glucose metabolism. Circulating glucose concentrations increase during a meal and activate insulin secretion from β-cells in the pancreas promoting glucose uptake into metabolic tissues (reviewed in[224]). Glucose uptake is mediated by the glucose transporter (GLUT) protein family (reviewed in[225]). Most importantly, GLUT4 is the main glucose transporter expressed in metabolic tissues such as WAT, BAT, cardiac muscle, and skeletal muscle, where it facilitates insulin-dependent glucose uptake. Conversely, GLUT1 mediates the basal insulin-independent uptake of glucose into many tissues with its most prominent role to provide glucose for the brain[226]. Katz et al.[227] reported that *Glut4*-ko mice are growth-retarded and have markedly reduced fat mass. *Nat8l*-ko mice also show reduced BW accompanied by a trend to reduced body length compared to wt mice, resembling a kind of

growth retardation. In addition, eWAT mass was significantly reduced in *Nat8l*-ko mice on CD and sWAT mass was reduced in *Nat8l*-ko on HFD when compared to controls at the age of 9 months. Further, *Glut4*-ko mice develop cardiac hypertrophy and have a shortened lifespan[227]. Life span was also reduced in *Nat8l*-ko mice compared to controls. As mentioned above, I observed that cold exposure led to increased cardiac hypertrophy in *Nat8l*-ko compared to wt mice (see 6.2.3). Cold exposure increases FA release from WAT but also increases food intake, thereby leading to high levels of circulating FAs but also glucose[133,217]. Concomitantly, both insulin-dependent as well as insulin-independent glucose transport by GLUT4 and GLUT1, respectively, gets activated in BAT[220]. I showed that cold exposure also increased expression of *Nat8l* and *Aspa* in BAT. Hence, NAT8L deficiency might impair GLUT4 insulin-mediated glucose uptake into BAT and WAT and thus probably evoke i) that circulating glucose would have to be cleared by uptake into other metabolic tissues such as cardiac or skeletal muscle and / or ii) lead to increased insulin secretion and insulin resistance. As a consequence, this could lead to the observed cardiac hypertrophy in *Nat8l*-ko mice during cold exposure. Of note, adipose tissue specific *Glut4*-ko mice do not suffer from cardiac hypertrophy and show increased life span when compared to controls[228].

Another interesting fact is that *Glut4*-ko mice do not develop diabetes[227]. Male *Glut4*-ko mice show even mild hypoglycemia and do not show changes in plasma FFA, similar to what I observed in *Nat8l*-ko mice on CD and HFD when compared to controls. In contrast, more than 50 % of heterozygous *Glut4*-ko mice develop diabetes by 6 months of age[229]. Of note, *Glut1* mRNA in cardiac muscle and *Glut2* mRNA in the liver have been found upregulated in *Glut4*-ko mice as a compensatory mechanism to GLUT4 deficiency[227]. Hence, it is also possible that this is the case in *Nat8l*-ko mice. Further, we recently showed that the NAA pathway regulates cytosolic acetyl-CoA concentrations[117]. Hence, a compensatory reaction in BAT of *Nat8l*-ko mice would include forced formation of citrate and provision of acetyl-CoA by ACLY. Indeed, we observed compensatory upregulation of ACLY in BAT of *Nat8l*-ko mice[160]. Therefore, it is possible that heterozygous *Nat8l*-ko mice do not provoke these compensatory effects and might reveal a better view on the importance of NAA metabolism in glucose homeostasis. Thus, it might be important to investigate if heterozygous *Nat8l*-ko mice have a different phenotype compared to the homozygous mice. Further, it might be valuable to investigate mRNA and protein expression of GLUTs in various tissues of *Nat8l*-ko mice compared to controls.

Glut4-ko mice showed postprandial hyperinsulinemia and decreased insulin sensitivity during ipITT whereas glucose clearance assessed by oral glucose tolerance test (oGTT) was similar to wt[227]. In contrast, *Nat8l*-ko mice on CD did not show differences in insulin sensitivity and glucose tolerance. On HFD; insulin sensitivity was also not changed, but glucose tolerance was increased in *Nat8l*-ko mice. Interestingly, analyses of insulin levels during ipGTT indicated higher insulin concentrations in *Nat8l*-ko compared to wt mice. Thus, *Nat8l*-ko mice might not be

insulin resistant at all but rather glucose-induced insulin secretion from pancreas might be increased on HFD, leading to increased glucose clearance. Therefore, it would be important to determine postprandial (e.g. after oral glucose gavage) and fasting insulin levels in *Nat8l*-ko compared to wt mice. It is highly speculative, but these data suggest that NAA could possibly regulate insulin secretion. Briefly, NAA synthesis activated by glucose disposal / uptake into adipose tissue could finally result in NAA release into the circulation. Concomitantly, increasing NAA concentrations sensed by β-cells in the pancreas could provide a feedback loop for reducing insulin secretion. Thus, if NAT8L deficiency prevents NAA synthesis, one feedback mechanism to attenuate insulin secretion might be lost. Hence, it could be important to test the influence of NAA on β-cell function.

Taken together, these data indicate that the NAA pathway plays an important role in insulin-mediated glucose uptake in adipose tissue and that NAA might have the potential to regulate insulin secretion from pancreas.

Another interesting observation was that *Nat8l*-ko mice showed increased weight loss upon overnight fasting and increased energy expenditure (EE), when they were housed at standard RT conditions. Of note, it is not trivial how to analyze EE in mice according to BW. Total body mass, lean body mass, and an adjusted value termed metabolic body mass ($BW^{0.75}$) have been used for normalization[230]. Three types of analyses have been used here (Figure 29). First, 24 hour EE was normalized to metabolic BW and displayed as a function of time. Second, EE during 12 : 12 hour light and dark cycle has been averaged (also normalized to metabolic BW). Third, EE has been analyzed as a function of body weight. Although the number of mice should be increased to provide a better basis for these analyses, the obtained results clearly show that EE is increased in *Nat8l*-ko compared to wt mice on CD and HFD. Recently, Toriumi and colleagues[94] reported that locomotor activity (LA) was increased in *Nat8l*-ko compared to wt mice. We did not detect significant changes in LA between wt and *Nat8l*-ko mice. However, it cannot be excluded that increases in LA might, at least partly, contribute to increase EE in *Nat8l*-ko mice. Another important point is to emphasize that differences in fat mass also significantly contribute to EE[230].As mentioned above, I found eWAT mass reduced in CD-fed and sWAT mass reduced in HFD-fed *Nat8l*-ko compared to wt mice at the age of 9 months. These results just represent a final measurement but it would be interesting to determine lean and fat mass more accurately and over time. Therefore, it would be valuable to compare body composition of *Nat8l*-ko and wt mice on CD and HFD during aging using proton magnetic resonance (NMR) spectroscopy[231]. However, this does not explain increased EE in *Nat8l*-ko compared to wt mice. The respiratory exchange ratio RER is a measure of which energy substrates are used in an organism, with a RER of 0.7 indicating lipid utilization, and a RER of 1.0 indicating carbohydrate utilization, respectively[175]. Of note, (RER) was not significantly changed in *Nat8l*-ko mice on CD but significantly increased on HFD when compared to controls.

Therefore, if insulin-independent glucose uptake is increased in *Nat8l*-ko mice, this might explain the mild hypoglycemia observed, as these animals would use more carbohydrates (glucose) as an energy substrate. Activated BAT has been described as a metabolic sink of both FAs and glucose[133]. Further, we reported that brown marker gene expression was increased in *Nat8l*-silenced brown adipocytes and BAT of *Nat8l*-ko mice compared to controls[160]. Hence, BAT thermogenesis could be activated by NAT8L deficiency. BAT is able to burn significant amounts of FA and glucose, thereby impacting lipid, glucose, and energy metabolism in mice and men[51,52,195]. Of note, expression of brown marker genes such as *Ucp1*, *Pparα*, *Pgc1α*, and *Cidea* was increased in *Nat8l*-ko BAT on CD and HFD when compared to wt littermates. Further, lipid droplet size and diameter was decreased while UCP1 protein in BAT of *Nat8l*-ko on CD and HFD was increased compared to wt mice. Thus, these data suggested that increased BAT thermogenesis might account for increased EE in *Nat8l*-ko mice. However, tissue oxygen consumption of BAT was neither significantly increased on CD nor on HFD when *Nat8l*-ko mice were compared to controls. The development of brown-like adipocytes in WAT has also been described as a potent driver to increase whole body EE in mice[26,73]. Of note, tissue oxygen consumption was increased in sWAT of *Nat8l*-ko mice on CD, but not altered on HFD when compared to controls. Furthermore, I did not detect increased number of adipocytes containing multilocular lipid droplets or increased UCP1 staining in sWAT and eWAT of *Nat8l*-ko mice. These data suggest that browning of WAT does not contribute to increase EE in *Nat8l*-ko mice. Thus, I want to conclude that BAT and browning of WAT is not likely to increase EE in *Nat8l*-ko mice. In summary, all these data support the hypothesis that other metabolic tissues such as cardiac muscle, skeletal muscle, and probably liver might be affected by NAT8L deficiency and should be taken into account to plan further experiments. Interestingly, *Nat8l*-ko mice on CD showed increased weight loss during cold exposure, similar to what was observed during fasting at RT. Conversely, *Nat8l*-ko mice fed a HFD showed decreased weight loss when compared to controls. In addition, I found decreased UCP1 protein expression and tissue oxygen consumption, but increased lipid droplet size in BAT of *Nat8l*-ko mice on HFD after cold exposure. Thus, I want to hypothesize that *Nat8l*-ko mice probably have deficits in handling or reduce disposal of circulating lipids.

The so called Randle-cycle describes that if FA oxidation is performed in a tissue, glucose oxidation is reduced, and vice versa[232]. This is achieved by the fact that FA oxidation finally yields mitochondrial acetyl-CoA. Hence, high rates of FA oxidation are able to increase mitochondrial acetyl-CoA / coenzyme A ratio. As a consequence, the pyruvate dehydrogenase (PDH) complex which catalyzes the final step in glycolysis to yield acetyl-CoA is inhibited (reviewed in[233]). I mentioned before that NAT8L deficiency might impair insulin-dependent glucose uptake by GLUT4 and lead to a compensatory upregulation of insulin-independent GLUT1-mediated glucose uptake, related to what has been observed in *Glut4*-ko mice[227].

Hence, increased insulin-independent glucose utilization might be performed in cardiac muscle, skeletal muscle, and liver of *Nat8l*-ko mice. In contrast, also circulating FFA concentrations have to be controlled to prevent dyslipidemia. Thus, there might be a permanent competition whether FAs or glucose is used as energy substrate by these tissues. Figure 53 gives a graphical summary of the results discussed below and the resulting questions.

Mice are more active during the night and consume the majority of their daily food during this period. During sleeping in the light phase, food intake is low and FAs released from WAT are mainly used as an energy substrate. This is normally reflected by a high RER during the dark and a lower RER during the light phase resembling carbohydrate and FA utilization, respectively. Interestingly, this regulation of the RER is attenuated in *Nat8l*-ko mice on CD (see Figure 28A). As mentioned above, this indicates a perturbation of FA or glucose utilization as energy substrate. Conversely, *Nat8l*-ko mice on HFD get a lot of FAs from the diet but seem to use more carbohydrates compared to their wt littermates, as indicated by increased RER (see Figure 28C). Thus, FA utilization might be limited and an increase in GLUT1-mediated basal glucose uptake could consequently lead to mild hypoglycemia as long as FA concentrations can be controlled. Indeed, *Nat8l*-ko mice housed at RT show mild hypoglycemia but normal plasma FFA when compared to wt littermates fed either CD or HFD. Importantly, FA release from eWAT and sWAT was significantly reduced in *Nat8l*-ko fed CD and HFD when compared to wt littermates. Thus, this indicates that FA utilization is impaired in *Nat8l*-ko mice and FA release from WAT might be reduced to prevent hyperlipidemia. Of note, I also found reduced FA uptake when *Nat8l* was overexpressed in brown adipocytes, indicating a preference in glucose utilization when NAA synthesis is increased.

In contrast, cold exposure increases FA release from WAT and FA utilization in BAT, skeletal muscle, and cardiac muscle. In addition, cold exposure also leads to increased glucose utilization in these tissues but also increases food intake (reviewed in[133,217]). Cold-exposed *Nat8l*-ko mice on CD still have mild hypoglycemia but FA release from eWAT and sWAT was significantly increased compared to controls. Accordingly, FFA and TG concentrations in the serum of *Nat8l*-ko mice were significantly increased compared to controls. As mentioned above, *Nat8l*-ko mice might have problems to utilize FAs as an energy substrate or FA release from WAT might not be enough to reach the threshold of the Randle hypothesis to switch from glucose to FA utilization in these mice. Finally, cold exposure of mice fed a HFD increases circulating FAs by i) release of FAs from adipose tissue and ii) dietary FAs, but also circulating carbohydrates[133,217]. Of note, FA release from eWAT was induced in cold-exposed *Nat8l*-ko mice on HFD whereas it was undetectable in *Nat8l*-ko mice at room temperature. Thus, excess dietary FAs from HFD in combination with FAs released from WAT might be able to decrease glucose utilization in *Nat8l*-ko mice during cold exposure in accordance with the Randle hypothesis.

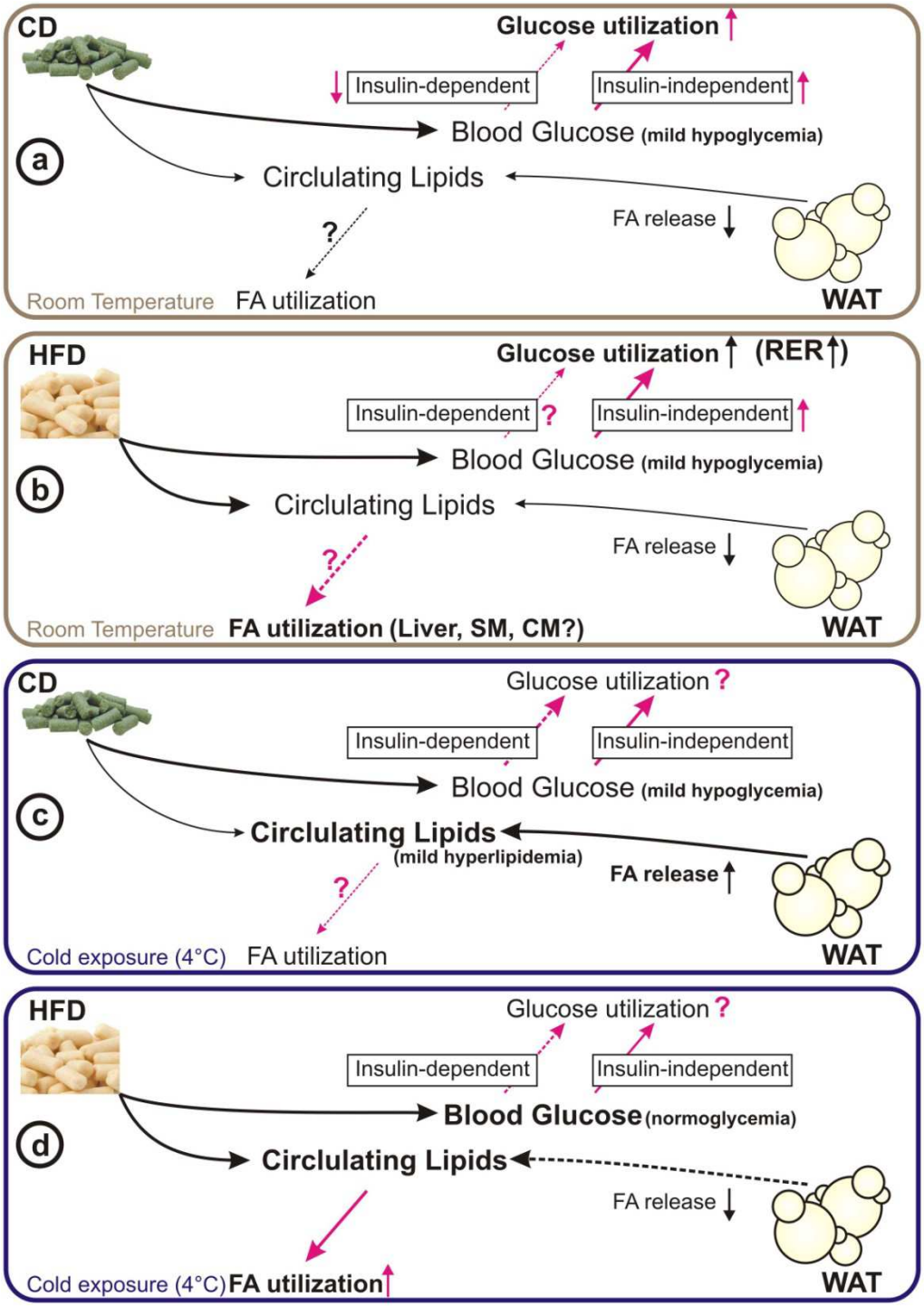

Figure 53. **NAT8L deficiency and the Randle-hypothesis.** Vertical Arrows indicate differences between wt and *Nat8l*-ko mice. Pink arrows indicate a hypothesis but are not supported by data yet. Hypotheses: (A) On chow diet (CD), *Nat8l*-ko mice have deficits in insulin-mediated glucose uptake and compensate by increasing insulin-independent glucose uptake leading to mild hypoglycemia. FA release from white adipose tissue (WAT) is reduced to prevent hyperlipidemia. (B) On high-fat diet (HFD), more lipids are supplied by the diet but *Nat8l*-ko mice still use more glucose (indicated by mild hypoglycemia and increased respiratory exchange ratio (RER)). FA utilization in other tissues is a possible mechanism to prevent hyperlipidemia here. (C) Cold exposure of *Nat8l*-ko mice on CD leads to both mild hypoglycemia and hyperlipidemia, indicating a normal response of WAT to cold but defective FA utilization. (D) Cold exposure of *Nat8l*-ko mice on HFD leads to highest FA / glucose ratio in the circulation compared to (A), (B), and (C), as fatty acids are supplied by diet and WAT lipolysis. This might reach a certain threshold to switch from glucose to FA utilization according to the Randle hypothesis (indicated by normoglycemia and normal circulating lipids).

Indeed, HFD-fed *Nat8l*-ko mice did not show hypoglycemia but serum FFA and TG levels were also unchanged compared to wt littermates. However, FA release from eWAT was still reduced in *Nat8l*-ko mice on HFD when compared to controls. Thus, sufficient FA supply from the diet together with decreased FA release from eWAT might prevent weight loss of *Nat8l*-ko mice during cold exposure. In summary, *Nat8l*-ko mice might have increased basal insulin-independent glucose uptake leading to mild hypoglycemia as long as a certain threshold in the ratio of circulating lipids to carbohydrates is reached, leading to increased FA and decreased glucose utilization.

Taken together, the NAA pathway might be important to regulate substrate utilization *in vivo* in accordance with the idea of the Randle cycle. Further, these data show that NAT8L deficiency seems to regulate insulin-dependent *versus* insulin-independent glucose uptake in adipose tissue, thereby affecting whole body lipid, glucose, and energy homeostasis. Further, the results obtained in this thesis suggest a role of NAA in insulin signaling, thereby directly connecting NAA metabolism to obesity-induced insulin resistance and diabetes.

6.2.5. NAT8L-deficiency and histone / protein acetylation

Manipulation of nucleo-cytoplasmic acetyl-CoA availability has been shown to regulate histone and protein acetylation, thereby impacting cellular metabolism[139,194]. Acetyl-CoA is predominantly produced in mitochondria and then transported to the cytoplasm. The formation of citrate in mitochondria and its subsequent transport to the cytoplasm has been described as the canonical pathway to provide cytoplasmic acetyl-CoA by the action of ATP citrate lyase (ACLY). Of note, Wellen et al. reported that ACLY regulates acetyl-CoA availability and links cellular metabolism to histone acetylation.[136] In addition, we recently introduced the NAA pathway as an additional way to provide cytoplasmic acetyl-CoA. NAA is synthesized in mitochondria, cleaved in the cytoplasm by aspartoacylase (ASPA) and the product acetate is used by acetyl-CoA synthetase (ACSS) 2[160] for acetyl-CoA synthesis[117]. We showed that *Acly* mRNA expression is upregulated in BAT of *Nat8l*-ko mice compared to controls, arguing for a compensatory upregulation of the ACLY-dependent acetyl-CoA production when the NAA pathway is missing.

In addition we and others showed that NAA-derived acetate / acetyl-CoA also plays a role in histone and / or protein acetylation[82,117]. Of note, ASPA has been reported to localize to the cytoplasm and the nucleus in oligodendrocytes in brain[98]. However, we found ASPA localized to the cytoplasm in brown adipocytes[117]. ACSS2, the enzyme downstream of ASPA which facilitate the formation of acetyl-CoA from acetate, has been shown to provide acetyl-CoA to nuclear histone-acetyltransferases (HATs) involved in epigenetic gene regulation[138]. Hence, cytoplasmic ASPA could deliver acetate for ACSS2, thereby regulating acetyl-CoA availability for HATs and histone acetylation as well as lysine acetyltransferases (KATs) and protein acetylation[139]. I

found ASPA expression highly increased in BAT of *Nat8l*-ko compared to wt mice (Figure 44). This might also be a compensatory upregulation upon loss of NAT8L.

Taken together, these data show that the modulating NAA pathway might have significant impact on histone and protein acetylation in adipose tissue. However, *Nat8l*-ko mice show significant differences regarding energy homeostasis. Therefore, it might be valuable to first analyze histone / protein acetylation upon manipulation of the NAA pathway *in vitro* before overinterpreting mouse data.

6.3. Summary and Outlook

N-acetylaspartate (NAA) is synthesized by mitochondrial N-acetyltransferase 8-like (NAT8L) and catabolized by cytoplasmic aspartoacylase (ASPA) in brown adipocytes. These two enzymes build the so called NAA pathway. NAA synthesis requires mitochondrial acetyl-CoA and L-aspartate. Acetyl-CoA is a universal metabolite linking energy derivation to virtually all major cellular functions (reviewed in[104]). Based on the data obtained in this thesis I was able to show that NAA metabolism contributes to lipid and glucose metabolism in brown adipocytes by regulating lipolysis and transcription factor signaling. Further, these data suggest that NAA-metabolism is able to regulate acetyl-CoA availability for histone and / or protein acetylation, thereby impacting DNA accessibility, gene transcription, enzyme activity, and energy homeostasis. *In vivo*, the NAA pathway is highly regulated by metabolic triggers such as high / low nutrient availability, circulating fatty acids, insulin secretion, and β-adrenergic stimulation. Most importantly, investigation of lipid, glucose, and energy metabolism in *Nat8l*-knock-out mice revealed a possible connection of NAA metabolism to insulin signaling and insulin-dependent glucose uptake. Thus, although the function of the NAA pathway in adipose tissue is not clear yet, this thesis provides fundamental evidence for the importance of NAA metabolism in adipocyte energy homeostasis.

For future research, it will be most important to determine the physiological role of the NAA pathway using tissue-specific knock-out models for *Nat8l* (and *Aspa*) and its comparison to the full knock-out mouse model described here. Further, investigation of the regulation of circulating NAA and NAA concentration in tissues as well as their changes during metabolic challenges will provide a better understanding of the physiological role of NAA. It will also be important to address the question how NAA transport is facilitated from tissues to the circulation (and vice versa) as well as which tissues take up, metabolize, or sense circulating NAA. All these attempts will help to integrate the NAA pathway into the big picture of adipose tissue metabolism and its role in whole body physiology.

7 - References

7. References

1. Haslam, D. W. & James, W. P. T. Obesity. *The Lancet* **366,** 1197–1209 (2005).
2. VanItallie, T. B. Worldwide epidemiology of obesity. *PharmacoEconomics* **5,** 1–7 (1994).
3. Popkin, B. M. & Doak, C. M. The Obesity Epidemic Is a Worldwide Phenomenon. *Nutr. Rev.* **56,** 106–114 (1998).
4. Seidell, J. C. Obesity, insulin resistance and diabetes — a worldwide epidemic. *Br. J. Nutr.* **83,** S5–S8 (2000).
5. Popkin, B. M. & Slining, M. M. New dynamics in global obesity facing low- and middle-income countries. *Obes. Rev. Off. J. Int. Assoc. Study Obes.* **14,** 11–20 (2013).
6. O'Neill, S. & O'Driscoll, L. Metabolic syndrome: a closer look at the growing epidemic and its associated pathologies. *Obes. Rev.* **16,** 1–12 (2015).
7. Font-Burgada, J., Sun, B. & Karin, M. Obesity and Cancer: The Oil that Feeds the Flame. *Cell Metab.* **23,** 48–62 (2016).
8. Arnold, M. *et al.* Obesity and cancer: An update of the global impact. *Cancer Epidemiol.* **41,** 8–15 (2016).
9. Gaillard, R. Maternal obesity during pregnancy and cardiovascular development and disease in the offspring. *Eur. J. Epidemiol.* **30,** 1141–1152 (2015).
10. Simmonds, M., Llewellyn, A., Owen, C. G. & Woolacott, N. Predicting adult obesity from childhood obesity: a systematic review and meta-analysis. *Obes. Rev.* **17,** 95–107 (2016).
11. Faienza, M. F., Wang, D. Q. H., Frühbeck, G., Garruti, G. & Portincasa, P. The dangerous link between childhood and adulthood predictors of obesity and metabolic syndrome. *Intern. Emerg. Med.* 1–8 (2016). doi:10.1007/s11739-015-1382-6
12. Wang, Y. C., McPherson, K., Marsh, T., Gortmaker, S. L. & Brown, M. Health and economic burden of the projected obesity trends in the USA and the UK. *The Lancet* **378,** 815–825 (2011).
13. Rtveladze, K. *et al.* Obesity prevalence in Mexico: impact on health and economic burden. *Public Health Nutr.* **17,** 233–239 (2014).
14. Gupta, S., Richard, L. & Forsythe, A. The humanistic and economic burden associated with increasing body mass index in the EU5. *Diabetes Metab. Syndr. Obes. Targets Ther.* **8,** 327–338 (2015).
15. Bouchard, C. *et al.* The Response to Long-Term Overfeeding in Identical Twins. *N. Engl. J. Med.* **322,** 1477–1482 (1990).
16. Stunkard, A. J., Harris, J. R., Pedersen, N. L. & McClearn, G. E. The Body-Mass Index of Twins Who Have Been Reared Apart. *N. Engl. J. Med.* **322,** 1483–1487 (1990).
17. Zhang, Y. *et al.* Positional cloning of the mouse obese gene and its human homologue. *Nature* **372,** 425–432 (1994).
18. Rosen, E. D. & Spiegelman, B. M. Adipocytes as regulators of energy balance and glucose homeostasis. *Nature* **444,** 847–853 (2006).
19. Rosen, E. D. & Spiegelman, B. M. What We Talk About When We Talk About Fat. *Cell* **156,** 20–44 (2014).
20. Peirce, V., Carobbio, S. & Vidal-Puig, A. The different shades of fat. *Nature* **510,** 76–83 (2014).
21. Oh, D. K., Ciaraldi, T. & Henry, R. R. Adiponectin in health and disease. *Diabetes Obes. Metab.* **9,** 282–289 (2007).
22. Hotamisligil, G. S., Shargill, N. S. & Spiegelman, B. M. Adipose expression of tumor necrosis factor-alpha: direct role in obesity-linked insulin resistance. *Science* **259,** 87–91 (1993).
23. Lago, F., Dieguez, C., Gómez-Reino, J. & Gualillo, O. Adipokines as emerging mediators of immune response and inflammation. *Nat. Clin. Pract. Rheumatol.* **3,** 716–724 (2007).
24. Lehr, S., Hartwig, S. & Sell, H. Adipokines: A treasure trove for the discovery of biomarkers for metabolic disorders. *PROTEOMICS – Clin. Appl.* **6,** 91–101 (2012).
25. Kammoun, H. L., Kraakman, M. J. & Febbraio, M. A. Adipose tissue inflammation in glucose metabolism. *Rev. Endocr. Metab. Disord.* **15,** 31–44 (2013).
26. Ishibashi, J. & Seale, P. Beige can be slimming. *Science* **328,** 1113–1114 (2010).

27. Waldén, T. B., Hansen, I. R., Timmons, J. A., Cannon, B. & Nedergaard, J. Recruited vs. nonrecruited molecular signatures of brown, 'brite,' and white adipose tissues. *Am. J. Physiol. - Endocrinol. Metab.* **302,** E19–E31 (2012).
28. Shen, W. *et al.* Adipose Tissue Quantification by Imaging Methods: A Proposed Classification. *Obes. Res.* **11,** 5–16 (2003).
29. Giordano, A., Smorlesi, A., Frontini, A., Barbatelli, G. & Cinti, S. MECHANISMS IN ENDOCRINOLOGY: White, brown and pink adipocytes: the extraordinary plasticity of the adipose organ. *Eur. J. Endocrinol.* **170,** R159–R171 (2014).
30. Lee, M.-J., Wu, Y. & Fried, S. K. Adipose Tissue Heterogeneity: Implication of depot differences in adipose tissue for Obesity Complications. *Mol. Aspects Med.* **34,** 1–11 (2013).
31. Nicholls, D. G., Bernson, V. S. & Heaton, G. M. The identification of the component in the inner membrane of brown adipose tissue mitochondria responsible for regulating energy dissipation. *Experientia. Suppl.* **32,** 89–93 (1978).
32. Bartness, T., Vaughan, C. & Song, C. Sympathetic and sensory innervation of brown adipose tissue. *Int. J. Obes. 2005* **34,** S36–S42 (2010).
33. Cao, Y. Adipose tissue angiogenesis as a therapeutic target for obesity and metabolic diseases. *Nat. Rev. Drug Discov.* **9,** 107–115 (2010).
34. Lowell, B. B. *et al.* Development of obesity in transgenic mice after genetic ablation of brown adipose tissue. *Nature* **366,** 740–742 (1993).
35. Heaton, J. M. The distribution of brown adipose tissue in the human. *J. Anat.* **112,** 35–39 (1972).
36. Merklin, R. J. Growth and distribution of human fetal brown fat. *Anat. Rec.* **178,** 637–645 (1974).
37. Huttunen, P., Hirvonen, J. & Kinnula, V. The occurrence of brown adipose tissue in outdoor workers. *Eur. J. Appl. Physiol.* **46,** 339–345 (1981).
38. Rockstroh, D. *et al.* Direct Evidence of Brown Adipocytes in Different Fat Depots in Children. *PLoS ONE* **10,** (2015).
39. Cunningham, S. *et al.* The characterization and energetic potential of brown adipose tissue in man. *Clin. Sci.* **69,** 343–348 (1985).
40. Nedergaard, J., Bengtsson, T. & Cannon, B. Unexpected evidence for active brown adipose tissue in adult humans. *Am. J. Physiol. - Endocrinol. Metab.* **293,** E444–E452 (2007).
41. Cypess, A. M. *et al.* Identification and Importance of Brown Adipose Tissue in Adult Humans. *N. Engl. J. Med.* **360,** 1509–1517 (2009).
42. Saito, M. *et al.* High Incidence of Metabolically Active Brown Adipose Tissue in Healthy Adult Humans Effects of Cold Exposure and Adiposity. *Diabetes* **58,** 1526–1531 (2009).
43. van Marken Lichtenbelt, W. D. *et al.* Cold-Activated Brown Adipose Tissue in Healthy Men. *N. Engl. J. Med.* **360,** 1500–1508 (2009).
44. Virtanen, K. A. *et al.* Functional Brown Adipose Tissue in Healthy Adults. *N. Engl. J. Med.* **360,** 1518–1525 (2009).
45. Yoneshiro, T. *et al.* Recruited brown adipose tissue as an antiobesity agent in humans. *J. Clin. Invest.* **123,** 3404–3408 (2013).
46. Blondin, D. P. *et al.* Increased Brown Adipose Tissue Oxidative Capacity in Cold-Acclimated Humans. *J. Clin. Endocrinol. Metab.* **99,** E438–E446 (2014).
47. Ouellet, V. *et al.* Outdoor Temperature, Age, Sex, Body Mass Index, and Diabetic Status Determine the Prevalence, Mass, and Glucose-Uptake Activity of 18F-FDG-Detected BAT in Humans. *J. Clin. Endocrinol. Metab.* **96,** 192–199 (2011).
48. Vijgen, G. H. E. J. *et al.* Brown Adipose Tissue in Morbidly Obese Subjects. *PLoS ONE* **6,** e17247 (2011).
49. Petrovic, N. *et al.* Chronic Peroxisome Proliferator-activated Receptor γ (PPARγ) Activation of Epididymally Derived White Adipocyte Cultures Reveals a Population of Thermogenically Competent, UCP1-containing Adipocytes Molecularly Distinct from Classic Brown Adipocytes. *J. Biol. Chem.* **285,** 7153–7164 (2010).
50. Young, P., Arch, J. r. s. & Ashwell, M. Brown adipose tissue in the parametrial fat pad of the mouse. *FEBS Lett.* **167,** 10–14 (1984).

51. Harms, M. & Seale, P. Brown and beige fat: development, function and therapeutic potential. *Nat. Med.* **19,** 1252–1263 (2013).
52. Schrauwen, P., Lichtenbelt, W. D. van M. & Spiegelman, B. M. The future of brown adipose tissues in the treatment of type 2 diabetes. *Diabetologia* **58,** 1704–1707 (2015).
53. Nedergaard, J. & Cannon, B. The Browning of White Adipose Tissue: Some Burning Issues. *Cell Metab.* **20,** 396–407 (2014).
54. Lidell, M. E. *et al.* Evidence for two types of brown adipose tissue in humans. *Nat. Med.* **19,** 631–634 (2013).
55. Lidell, M. E., Betz, M. J. & Enerbäck, S. Two types of brown adipose tissue in humans. *Adipocyte* **3,** 63–66 (2014).
56. Shinoda, K. *et al.* Genetic and functional characterization of clonally derived adult human brown adipocytes. *Nat. Med.* **21,** 389–394 (2015).
57. Cannon, B. & Nedergaard, J. Cell biology: Neither brown nor white. *Nature* **488,** 286–287 (2012).
58. Seale, P. Transcriptional Regulatory Circuits Controlling Brown Fat Development and Activation. *Diabetes* **64,** 2369–2375 (2015).
59. Lefterova, M. I., Haakonsson, A. K., Lazar, M. A. & Mandrup, S. PPARγ and the global map of adipogenesis and beyond. *Trends Endocrinol. Metab.* **25,** 293–302 (2014).
60. Dempersmier, J. & Sul, H. S. Shades of brown: a model for thermogenic fat. *Exp. Endocrinol.* 71 (2015). doi:10.3389/fendo.2015.00071
61. Cohen, P. & Spiegelman, B. M. Brown and Beige Fat: Molecular Parts of a Thermogenic Machine. *Diabetes* **64,** 2346–2351 (2015).
62. Puri, V. *et al.* Cidea is associated with lipid droplets and insulin sensitivity in humans. *Proc. Natl. Acad. Sci. U. S. A.* **105,** 7833–7838 (2008).
63. Jong, J. M. A. de, Larsson, O., Cannon, B. & Nedergaard, J. A stringent validation of mouse adipose tissue identity markers. *Am. J. Physiol. - Endocrinol. Metab.* **308,** E1085–E1105 (2015).
64. de Jesus, L. A. *et al.* The type 2 iodothyronine deiodinase is essential for adaptive thermogenesis in brown adipose tissue. *J. Clin. Invest.* **108,** 1379–1385 (2001).
65. Haemmerle, G. *et al.* ATGL-mediated fat catabolism regulates cardiac mitochondrial function via PPAR-α and PGC-1. *Nat. Med.* **17,** 1076–1085 (2011).
66. Mottillo, E. P., Bloch, A. E., Leff, T. & Granneman, J. G. Lipolytic Products Activate Peroxisome Proliferator-activated Receptor (PPAR) α and δ in Brown Adipocytes to Match Fatty Acid Oxidation with Supply. *J. Biol. Chem.* **287,** 25038–25048 (2012).
67. Barberá, M. J. *et al.* Peroxisome Proliferator-activated Receptor α Activates Transcription of the Brown Fat Uncoupling Protein-1 Gene A LINK BETWEEN REGULATION OF THE THERMOGENIC AND LIPID OXIDATION PATHWAYS IN THE BROWN FAT CELL. *J. Biol. Chem.* **276,** 1486–1493 (2001).
68. Hondares, E. *et al.* Peroxisome Proliferator-activated Receptor α (PPARα) Induces PPARγ Coactivator 1α (PGC-1α) Gene Expression and Contributes to Thermogenic Activation of Brown Fat INVOLVEMENT OF PRDM16. *J. Biol. Chem.* **286,** 43112–43122 (2011).
69. Rachid, T. L. *et al.* Fenofibrate (PPARalpha agonist) induces beige cell formation in subcutaneous white adipose tissue from diet-induced male obese mice. *Mol. Cell. Endocrinol.* **402,** 86–94 (2015).
70. Rachid, T. L. *et al.* PPAR-α agonist elicits metabolically active brown adipocytes and weight loss in diet-induced obese mice. *Cell Biochem. Funct.* **33,** 249–256 (2015).
71. Uldry, M. *et al.* Complementary action of the PGC-1 coactivators in mitochondrial biogenesis and brown fat differentiation. *Cell Metab.* **3,** 333–341 (2006).
72. Cao, W. *et al.* p38 Mitogen-Activated Protein Kinase Is the Central Regulator of Cyclic AMP-Dependent Transcription of the Brown Fat Uncoupling Protein 1 Gene. *Mol. Cell. Biol.* **24,** 3057–3067 (2004).
73. Kajimura, S., Spiegelman, B. M. & Seale, P. Brown and Beige Fat: Physiological Roles beyond Heat Generation. *Cell Metab.* **22,** 546–559 (2015).
74. Lee, P. *et al.* Temperature-Acclimated Brown Adipose Tissue Modulates Insulin Sensitivity in Humans. *Diabetes* **63,** 3686–3698 (2014).

75. van der Lans, A. A. J. J. *et al.* Cold acclimation recruits human brown fat and increases nonshivering thermogenesis. *J. Clin. Invest.* **123,** 3395–3403 (2013).
76. Villarroya, F. & Vidal-Puig, A. Beyond the Sympathetic Tone: The New Brown Fat Activators. *Cell Metab.* **17,** 638–643 (2013).
77. Saito, M. & Yoneshiro, T. Capsinoids and related food ingredients activating brown fat thermogenesis and reducing body fat in humans: *Curr. Opin. Lipidol.* **24,** 71–77 (2013).
78. Blüml, S. In VivoQuantitation of Cerebral Metabolite Concentrations Using Natural Abundance13C MRS at 1.5 T. *J. Magn. Reson.* **136,** 219–225 (1999).
79. Miyake, M., Kakimoto, Y. & Sorimachi, M. A Gas Chromatographic Method for the Determination of N-Acetyl-l-Aspartic Acid, N-Acetyl-α- Aspartylglutamic Acid and β-Citryl-l-Glutamic Acid and Their Distributions in the Brain and Other Organs of Various Species of Animals. *J. Neurochem.* **36,** 804–819 (1981).
80. Pan, J. W. & Takahashi, K. Interdependence of N-acetyl aspartate and high-energy phosphates in healthy human brain. *Ann. Neurol.* **57,** 92–97 (2005).
81. Moffett, J. R., Ross, B., Arun, P., Madhavarao, C. N. & Namboodiri, A. M. A. N-Acetylaspartate in the CNS: From neurodiagnostics to neurobiology. *Prog. Neurobiol.* **81,** 89–131 (2007).
82. Moffett, J. R., Arun, P., Ariyannur, P. S. & Namboodiri, A. M. N-Acetylaspartate reductions in brain injury: impact on post-injury neuroenergetics, lipid synthesis, and protein acetylation. *Front. Neuroenergetics* **5,** 11 (2013).
83. Goldstein, F. B. Biosynthesis of N-acetyl-L-aspartic acid. *Biochim. Biophys. Acta* **33,** 583–584 (1959).
84. Knizley, H. The Enzymatic Synthesis of N-Acetyl-l-aspartic Acid by a Water-insoluble Preparation of a Cat Brain Acetone Powder. *J. Biol. Chem.* **242,** 4619–4622 (1967).
85. Truckenmiller, M. E., Namboodiri, M. a. A., Brownstein, M. J. & Neale, J. H. N-Acetylation of L-Aspartate in the Nervous System: Differential Distribution of a Specific Enzyme. *J. Neurochem.* **45,** 1658–1662 (1985).
86. Wiame, E. *et al.* Molecular identification of aspartate N-acetyltransferase and its mutation in hypoacetylaspartia. *Biochem. J.* **425,** 127–136 (2010).
87. Ariyannur, P. S. *et al.* Methamphetamine-induced neuronal protein NAT8L is the NAA biosynthetic enzyme: Implications for specialized acetyl coenzyme A metabolism in the CNS. *Brain Res.* **1335,** 1–13 (2010).
88. Tahay, G., Wiame, E., Tyteca, D., Courtoy, P. J. & Schaftingen, E. V. Determinants of the enzymatic activity and the subcellular localization of aspartate N-acetyltransferase. *Biochem. J.* **441,** 105–112 (2012).
89. Wang, Q., Zhao, M., Parungao, G. G. & Viola, R. E. Purification and characterization of aspartate N-acetyltransferase: A critical enzyme in brain metabolism. *Protein Expr. Purif.* **119,** 11–18 (2016).
90. Goldstein, F. B. The Enzymatic Synthesis of N-Acetyl-l-aspartic Acid by Subcellular Preparations of Rat Brain. *J. Biol. Chem.* **244,** 4257–4260 (1969).
91. Madhavarao, C. N., Chinopoulos, C., Chandrasekaran, K. & Namboodiri, M. a. A. Characterization of the N-acetylaspartate biosynthetic enzyme from rat brain. *J. Neurochem.* **86,** 824–835 (2003).
92. Lu, Z.-H., Chakraborty, G., Ledeen, R. W., Yahya, D. & Wu, G. N-Acetylaspartate synthase is bimodally expressed in microsomes and mitochondria of brain. *Mol. Brain Res.* **122,** 71–78 (2004).
93. Jalil, M. A. *et al.* Reduced N-Acetylaspartate Levels in Mice Lacking Aralar, a Brain- and Muscle-type Mitochondrial Aspartate-glutamate Carrier. *J. Biol. Chem.* **280,** 31333–31339 (2005).
94. Toriumi, K. *et al.* Deletion of SHATI/NAT8L increases dopamine D1 receptor on the cell surface in the nucleus accumbens, accelerating methamphetamine dependence. *Int. J. Neuropsychopharmacol.* **17,** 443–453 (2014).
95. Nordengen, K., Heuser, C., Rinholm, J. E., Matalon, R. & Gundersen, V. Localisation of N-acetylaspartate in oligodendrocytes/myelin. *Brain Struct. Funct.* **220,** 899–917 (2015).

96. Fujita, T. *et al.* Transport characteristics of N-acetyl-l-aspartate in rat astrocytes: involvement of sodium-coupled high-affinity carboxylate transporter NaC3/NaDC3-mediated transport system. *J. Neurochem.* **93,** 706–714 (2005).
97. Long, P. M. *et al.* N-Acetylaspartate (NAA) and N-Acetylaspartylglutamate (NAAG) Promote Growth and Inhibit Differentiation of Glioma Stem-like Cells. *J. Biol. Chem.* **288,** 26188–26200 (2013).
98. Hershfield, J. R. *et al.* Aspartoacylase is a regulated nuclear-cytoplasmic enzyme. *FASEB J.* **20,** 2139–2141 (2006).
99. Birnbaum, S. M., Levintow, L., Kingsley, R. B. & Greenstein, J. P. Specificity of Amino Acid Acylases. *J. Biol. Chem.* **194,** 455–470 (1952).
100. Wang, J. *et al.* Bimodal occurrence of aspartoacylase in myelin and cytosol of brain. *J. Neurochem.* **101,** 448–457 (2007).
101. Bitto, E., Bingman, C. A., Wesenberg, G. E., McCoy, J. G. & Phillips, G. N. Structure of aspartoacylase, the brain enzyme impaired in Canavan disease. *Proc. Natl. Acad. Sci. U. S. A.* **104,** 456–461 (2007).
102. Mehta, V. & Namboodiri, M. A. A. N-Acetylaspartate as an acetyl source in the nervous system. *Mol. Brain Res.* **31,** 151–157 (1995).
103. Nikolau, B. J., Oliver, D. J., Schnable, P. S. & Wurtele, E. S. Molecular biology of acetyl-CoA metabolism. *Biochem. Soc. Trans.* **28,** 591–593 (2000).
104. Pietrocola, F., Galluzzi, L., Bravo-San Pedro, J. M., Madeo, F. & Kroemer, G. Acetyl Coenzyme A: A Central Metabolite and Second Messenger. *Cell Metab.* **21,** 805–821 (2015).
105. Hoshino, H. & Kubota, M. Canavan disease: Clinical features and recent advances in research. *Pediatr. Int.* **56,** 477–483 (2014).
106. Matalon, R. *et al.* Aspartoacylase deficiency and N-acetylaspartic aciduria in patients with canavan disease. *Am. J. Med. Genet.* **29,** 463–471 (1988).
107. Matalon, R. *et al.* Knock-out mouse for Canavan disease: a model for gene transfer to the central nervous system. *J. Gene Med.* **2,** 165–175 (2000).
108. Serikawa, T., Ohno, Y., Sasa, M., Yamada, J. & Takaori, S. A new model of petit mal epilepsy: spontaneous spike and wave discharges in tremor rats. *Lab. Anim.* **21,** 68–71 (1987).
109. Maier, H., Wang-Eckhardt, L., Hartmann, D., Gieselmann, V. & Eckhardt, M. N-Acetylaspartate Synthase Deficiency Corrects the Myelin Phenotype in a Canavan Disease Mouse Model But Does Not Affect Survival Time. *J. Neurosci. Off. J. Soc. Neurosci.* **35,** 14501–14516 (2015).
110. Boltshauser, E. *et al.* Follow-Up of a Child with Hypoacetylaspartia. *Neuropediatrics* **35,** 255–258 (2004).
111. Burlina, A. P. *et al.* in *N-Acetylaspartate* (eds. Moffett, J. R., Tieman, S. B., Weinberger, D. R., Coyle, J. T. & Namboodiri, A. M. A.) 283–287 (Springer US, 2006).
112. Furukawa-Hibi, Y. *et al.* Absence of SHATI/Nat8l reduces social interaction in mice. *Neurosci. Lett.* **526,** 79–84 (2012).
113. Guo, F. *et al.* Ablating N-acetylaspartate prevents leukodystrophy in a Canavan disease model. *Ann. Neurol.* **77,** 884–888 (2015).
114. Benuck, M. & D'Adamo Jr., A. F. Acetyl transport mechanisms Metabolism of N-acetyl-l-aspartic acid in the non-nervous tissues of the rat. *Biochim. Biophys. Acta BBA - Lipids Lipid Metab.* **152,** 611–618 (1968).
115. D'Adamo, A. F. & Yatsu, F. M. ACETATE METABOLISM IN THE NERVOUS SYSTEM. N-ACETYL-l-ASPARTIC ACID AND THE BIOSYNTHESIS OF BRAIN LIPIDS*. *J. Neurochem.* **13,** 961–965 (1966).
116. Pessentheiner, A. R. *et al.* NAT8L (N-Acetyltransferase 8-Like) Accelerates Lipid Turnover and Increases Energy Expenditure in Brown Adipocytes. *J. Biol. Chem.* **288,** 36040–36051 (2013).
117. Prokesch, A. *et al.* N-acetylaspartate catabolism determines cytosolic acetyl-CoA levels and histone acetylation in brown adipocytes. *Sci. Rep.* **accepted,** (2016).

118. Pinent, M. *et al.* Differential transcriptional modulation of biological processes in adipocyte triglyceride lipase and hormone-sensitive lipase-deficient mice. *Genomics* **92,** 26–32 (2008).
119. Schweiger, M. *et al.* Adipose Triglyceride Lipase and Hormone-sensitive Lipase Are the Major Enzymes in Adipose Tissue Triacylglycerol Catabolism. *J. Biol. Chem.* **281,** 40236–40241 (2006).
120. Haemmerle, G. *et al.* Defective Lipolysis and Altered Energy Metabolism in Mice Lacking Adipose Triglyceride Lipase. *Science* **312,** 734–737 (2006).
121. Osuga, J. *et al.* Targeted disruption of hormone-sensitive lipase results in male sterility and adipocyte hypertrophy, but not in obesity. *Proc. Natl. Acad. Sci.* **97,** 787–792 (2000).
122. Huang, S. *et al.* A new microRNA signal pathway regulated by long noncoding RNA TGFB2-OT1 in autophagy and inflammation of vascular endothelial cells. *Autophagy* **11,** 2172–2183 (2015).
123. Lou, T.-F. *et al.* Cancer-Specific Production of N-Acetylaspartate via NAT8L Overexpression in Non-Small Cell Lung Cancer and Its Potential as a Circulating Biomarker. *Cancer Prev. Res. Phila. Pa* **9,** 43–52 (2016).
124. Zand, B. *et al.* Role of Increased n-acetylaspartate Levels in Cancer. *J. Natl. Cancer Inst.* **108,** (2016).
125. Marklund, N., Salci, K., Ronquist, G. & Hillered, L. Energy metabolic changes in the early post-injury period following traumatic brain injury in rats. *Neurochem. Res.* **31,** 1085–1093 (2006).
126. Signoretti, S. *et al.* N-Acetylaspartate Reduction as a Measure of Injury Severity and Mitochondrial Dysfunction Following Diffuse Traumatic Brain Injury. *J. Neurotrauma* **18,** 977–991 (2001).
127. Vagnozzi, R. *et al.* Hypothesis of the postconcussive vulnerable brain: experimental evidence of its metabolic occurrence. *Neurosurgery* **57,** 164–171; discussion 164–171 (2005).
128. Arun, P. *et al.* Acute Mitochondrial Dysfunction after Blast Exposure: Potential Role of Mitochondrial Glutamate Oxaloacetate Transaminase. *J. Neurotrauma* **30,** 1645–1651 (2013).
129. Sumi, K. *et al.* Induction of neuronal axon outgrowth by Shati/Nat8l by energy metabolism in mice cultured neurons. *Neuroreport* **26,** 740–746 (2015).
130. Bélanger, M., Allaman, I. & Magistretti, P. J. Brain Energy Metabolism: Focus on Astrocyte-Neuron Metabolic Cooperation. *Cell Metab.* **14,** 724–738 (2011).
131. Chakraborty, G., Mekala, P., Yahya, D., Wu, G. & Ledeen, R. W. Intraneuronal N-acetylaspartate supplies acetyl groups for myelin lipid synthesis: evidence for myelin-associated aspartoacylase. *J. Neurochem.* **78,** 736–745 (2001).
132. Wang, J. *et al.* Myelin Lipid Abnormalities in the Aspartoacylase-Deficient Tremor Rat. *Neurochem. Res.* **34,** 138–148 (2009).
133. Townsend, K. L. & Tseng, Y.-H. Brown Fat Fuel Utilization and Thermogenesis. *Trends Endocrinol. Metab. TEM* **25,** 168–177 (2014).
134. Strable, M. S. & Ntambi, J. M. Genetic control of de novo lipogenesis: role in diet-induced obesity. *Crit. Rev. Biochem. Mol. Biol.* **45,** 199–214 (2010).
135. Ahmadian, M., Duncan, R. E., Jaworski, K., Sarkadi-Nagy, E. & Sul, H. S. Triacylglycerol metabolism in adipose tissue. *Future Lipidol.* **2,** 229–237 (2007).
136. Wellen, K. E. *et al.* ATP-citrate lyase links cellular metabolism to histone acetylation. *Science* **324,** 1076–1080 (2009).
137. Ariyannur, P. S. *et al.* Nuclear-cytoplasmic localization of acetyl coenzyme A synthetase-1 in the rat brain. *J. Comp. Neurol.* **518,** 2952–2977 (2010).
138. Takahashi, H., McCaffery, J. M., Irizarry, R. A. & Boeke, J. D. Nucleocytosolic Acetyl-Coenzyme A Synthetase Is Required for Histone Acetylation and Global Transcription. *Mol. Cell* **23,** 207–217 (2006).
139. Menzies, K. J., Zhang, H., Katsyuba, E. & Auwerx, J. Protein acetylation in metabolism — metabolites and cofactors. *Nat. Rev. Endocrinol.* **12,** 43–60 (2016).
140. Qiang, L. *et al.* Brown Remodeling of White Adipose Tissue by SirT1-Dependent Deacetylation of Pparγ. *Cell* **150,** 620–632 (2012).

141. Rodgers, J. T. *et al.* Nutrient control of glucose homeostasis through a complex of PGC-1α and SIRT1. *Nature* **434,** 113–118 (2005).
142. Lagouge, M. *et al.* Resveratrol Improves Mitochondrial Function and Protects against Metabolic Disease by Activating SIRT1 and PGC-1α. *Cell* **127,** 1109–1122 (2006).
143. Hallows, W. C., Lee, S. & Denu, J. M. Sirtuins deacetylate and activate mammalian acetyl-CoA synthetases. *Proc. Natl. Acad. Sci. U. S. A.* **103,** 10230–10235 (2006).
144. Harms, M. J. *et al.* Prdm16 Is Required for the Maintenance of Brown Adipocyte Identity and Function in Adult Mice. *Cell Metab.* **19,** 593–604 (2014).
145. Mayer, N. *et al.* Development of small-molecule inhibitors targeting adipose triglyceride lipase. *Nat. Chem. Biol.* **9,** 785–787 (2013).
146. Cohen, P. *et al.* Ablation of PRDM16 and Beige Adipose Causes Metabolic Dysfunction and a Subcutaneous to Visceral Fat Switch. *Cell* **156,** 304–316 (2014).
147. Livak, K. J. & Schmittgen, T. D. Analysis of Relative Gene Expression Data Using Real-Time Quantitative PCR and the 2−ΔΔCT Method. *Methods* **25,** 402–408 (2001).
148. Ritter, J. B., Genzel, Y. & Reichl, U. Simultaneous extraction of several metabolites of energy metabolism and related substances in mammalian cells: Optimization using experimental design. *Anal. Biochem.* **373,** 349–369 (2008).
149. Mariño, G. *et al.* Regulation of Autophagy by Cytosolic Acetyl-Coenzyme A. *Mol. Cell* **53,** 710–725 (2014).
150. Buescher, J. M., Moco, S., Sauer, U. & Zamboni, N. Ultrahigh Performance Liquid Chromatography−Tandem Mass Spectrometry Method for Fast and Robust Quantification of Anionic and Aromatic Metabolites. *Anal. Chem.* **82,** 4403–4412 (2010).
151. Schweiger, M. *et al.* in *Methods in Enzymology* (ed. MacDougald, O. A.) **538,** 171–193 (Academic Press, 2014).
152. Zimmermann, R. *et al.* Decreased fatty acid esterification compensates for the reduced lipolytic activity in hormone-sensitive lipase-deficient white adipose tissue. *J. Lipid Res.* **44,** 2089–2099 (2003).
153. Mottillo, E. P., Bloch, A. E., Leff, T. & Granneman, J. G. Lipolytic Products Activate Peroxisome Proliferator-activated Receptor (PPAR) α and δ in Brown Adipocytes to Match Fatty Acid Oxidation with Supply. *J. Biol. Chem.* **287,** 25038–25048 (2012).
154. Burke, P. V. & Poyton, R. O. Structure/function of oxygen-regulated isoforms in cytochrome c oxidase. *J. Exp. Biol.* **201,** 1163–1175 (1998).
155. Jeong, J. Y., Jeoung, N. H., Park, K.-G. & Lee, I.-K. Transcriptional Regulation of Pyruvate Dehydrogenase Kinase. *Diabetes Metab. J.* **36,** 328 (2012).
156. Cantó, C. & Auwerx, J. PGC-1alpha, SIRT1 and AMPK, an energy sensing network that controls energy expenditure. *Curr. Opin. Lipidol.* **20,** 98–105 (2009).
157. Maeda, K. *et al.* Adipocyte/macrophage fatty acid binding proteins control integrated metabolic responses in obesity and diabetes. *Cell Metab.* **1,** 107–119 (2005).
158. Brandt, J. M., Djouadi, F. & Kelly, D. P. Fatty Acids Activate Transcription of the Muscle Carnitine Palmitoyltransferase I Gene in Cardiac Myocytes via the Peroxisome Proliferator-activated Receptor α. *J. Biol. Chem.* **273,** 23786–23792 (1998).
159. Kim, T. *et al.* Carnitine Palmitoyltransferase 1b Deficient Mice Develop Severe Insulin Resistance After Prolonged High Fat Diet Feeding. *J. Diabetes Metab.* **5,** (2014).
160. Pessentheiner, A. R. *et al.* NAT8L (N-Acetyltransferase 8-Like) Accelerates Lipid Turnover and Increases Energy Expenditure in Brown Adipocytes. *J. Biol. Chem.* **288,** 36040–36051 (2013).
161. Halvorson, D. L. & McCune, S. A. Inhibition of fatty acid synthesis in isolated adipocytes by 5-(tetradecyloxy)-2-furoic acid. *Lipids* **19,** 851–856 (1984).
162. He, L. *et al.* Carnitine Palmitoyltransferase-1b (CPT1b) Deficiency Aggravates Pressure-Overload-Induced Cardiac Hypertrophy due to Lipotoxicity. *Circulation* **126,** 1705–1716 (2012).
163. Cantó, C. *et al.* AMPK regulates energy expenditure by modulating NAD+ metabolism and SIRT1 activity. *Nature* **458,** 1056–1060 (2009).
164. Toriumi, K. *et al.* SHATI/NAT8L regulates neurite outgrowth via microtubule stabilization. *J. Neurosci. Res.* **91,** 1525–1532 (2013).

165. Miyamoto, Y. *et al.* Overexpression of Shati/Nat8l, an N-acetyltransferase, in the nucleus accumbens attenuates the response to methamphetamine via activation of group II mGluRs in mice. *Int. J. Neuropsychopharmacol.* **17,** 1283–1294 (2014).
166. Sumi, K. *et al.* Induction of neuronal axon outgrowth by Shati/Nat8l by energy metabolism in mice cultured neurons. *Neuroreport* **26,** 740–746 (2015).
167. Toriumi, K. *et al.* Deletion of SHATI/NAT8L decreases the N-acetylaspartate content in the brain and induces behavioral deficits, which can be ameliorated by administering N-acetylaspartate. *Eur. Neuropsychopharmacol.* doi:10.1016/j.euroneuro.2015.08.003
168. Miles, P. D. G., Barak, Y., He, W., Evans, R. M. & Olefsky, J. M. Improved insulin-sensitivity in mice heterozygous for PPAR-γ deficiency. *J. Clin. Invest.* **105,** 287–292 (2000).
169. Haskell-Luevano, C. *et al.* Voluntary exercise prevents the obese and diabetic metabolic syndrome of the melanocortin-4 receptor knockout mouse. *FASEB J.* **23,** 642–655 (2009).
170. Suzuki, M. *et al.* Tofogliflozin, a sodium/glucose cotransporter 2 inhibitor, attenuates body weight gain and fat accumulation in diabetic and obese animal models. *Nutr. Diabetes* **4,** e125 (2014).
171. Speakman, J. R. Measuring Energy Metabolism in the Mouse – Theoretical, Practical, and Analytical Considerations. *Front. Physiol.* **4,** (2013).
172. Stechman, M. J. *et al.* Establishing normal plasma and 24-hour urinary biochemistry ranges in C3H, BALB/c and C57BL/6J mice following acclimatization in metabolic cages. *Lab. Anim.* **44,** 218–225 (2010).
173. Kalliokoski, O. *et al.* Mice Do Not Habituate to Metabolism Cage Housing–A Three Week Study of Male BALB/c Mice. *PLoS ONE* **8,** (2013).
174. Kleiber, M. Body size and metabolism. *Hilgardia* **6,** 315–353 (1932).
175. Tschöp, M. H. *et al.* A guide to analysis of mouse energy metabolism. *Nat. Methods* **9,** 57–63 (2011).
176. Mottillo, E. P. & Granneman, J. G. Intracellular fatty acids suppress β-adrenergic induction of PKA-targeted gene expression in white adipocytes. *Am. J. Physiol. - Endocrinol. Metab.* **301,** E122–E131 (2011).
177. Ellis, J. M. *et al.* Adipose Acyl-CoA Synthetase-1 Directs Fatty Acids toward β-Oxidation and Is Required for Cold Thermogenesis. *Cell Metab.* **12,** 53–64 (2010).
178. Flowers, M. T. & Ntambi, J. M. Stearoyl-CoA Desaturase and its Relation to High-Carbohydrate Diets and Obesity. *Biochim. Biophys. Acta* **1791,** 85–91 (2009).
179. Jha, P. *et al.* Role of adipose tissue in methionine–choline-deficient model of non-alcoholic steatohepatitis (NASH). *Biochim. Biophys. Acta BBA - Mol. Basis Dis.* **1842,** 959–970 (2014).
180. Nedergaard, J. & Cannon, B. UCP1 mRNA does not produce heat. *Biochim. Biophys. Acta BBA - Mol. Cell Biol. Lipids* **1831,** 943–949 (2013).
181. Bae, D. D., Brown, P. L. & Kiyatkin, E. A. Procedure of rectal temperature measurement affects brain, muscle, skin and body temperatures and modulates the effects of intravenous cocaine. *Brain Res.* **1154,** 61–70 (2007).
182. Maurer, S. F., Fromme, T., Grossman, L. I., Hüttemann, M. & Klingenspor, M. The brown and brite adipocyte marker Cox7a1 is not required for non-shivering thermogenesis in mice. *Sci. Rep.* **5,** 17704 (2015).
183. Gerhart-Hines, Z. *et al.* The nuclear receptor Rev-erbα controls circadian thermogenic plasticity. *Nature* **503,** 410–413 (2013).
184. Li, P., Zhu, Z., Lu, Y. & Granneman, J. G. Metabolic and cellular plasticity in white adipose tissue II: role of peroxisome proliferator-activated receptor-α. *Am. J. Physiol. - Endocrinol. Metab.* **289,** E617–E626 (2005).
185. Fromme, T. & Klingenspor, M. Uncoupling protein 1 expression and high-fat diets. *Am. J. Physiol. - Regul. Integr. Comp. Physiol.* **300,** R1–R8 (2011).
186. Mottillo, E. P. *et al.* Coupling of lipolysis and de novo lipogenesis in brown, beige, and white adipose tissues during chronic β3-adrenergic receptor activation. *J. Lipid Res.* **55,** 2276–2286 (2014).
187. Ariyannur, P. S. *et al.* Do reductions in brain N-acetylaspartate levels contribute to the etiology of some neuropsychiatric disorders? *J. Neurosci. Res.* **91,** 934–942 (2013).

188. Festuccia, W. T., Blanchard, P.-G. & Deshaies, Y. Control of Brown Adipose Tissue Glucose and Lipid Metabolism by PPARγ. *Front. Endocrinol.* **2,** (2011).
189. Ahmadian, M. *et al.* Desnutrin/ATGL Is Regulated by AMPK and Is Required for a Brown Adipose Phenotype. *Cell Metab.* **13,** 739–748 (2011).
190. Fedorenko, A., Lishko, P. V. & Kirichok, Y. Mechanism of Fatty-Acid-Dependent UCP1 Uncoupling in Brown Fat Mitochondria. *Cell* **151,** 400–413 (2012).
191. Tang, T. *et al.* Desnutrin/ATGL Activates PPARδ to Promote Mitochondrial Function for Insulin Secretion in Islet β Cells. *Cell Metab.* **18,** 883–895 (2013).
192. Vance, J. E. & Vance, D. E. *Biochemistry of Lipids, Lipoproteins and Membranes*. (Elsevier, 2008).
193. Mashek, D. G., Li, L. O. & Coleman, R. A. Long-chain acyl-CoA synthetases and fatty acid channeling. *Future Lipidol.* **2,** 465–476 (2007).
194. Choudhary, C., Weinert, B. T., Nishida, Y., Verdin, E. & Mann, M. The growing landscape of lysine acetylation links metabolism and cell signalling. *Nat. Rev. Mol. Cell Biol.* **15,** 536–550 (2014).
195. Ouellet, V. *et al.* Brown adipose tissue oxidative metabolism contributes to energy expenditure during acute cold exposure in humans. *J. Clin. Invest.* **122,** 545–552 (2012).
196. Kramar, R., Hüttinger, M., Gmeiner, B. & Goldenberg, H. β-oxidation in peroxisomes of brown adipose tissue. *Biochim. Biophys. Acta BBA - Lipids Lipid Metab.* **531,** 353–356 (1978).
197. Rutanen, J. *et al.* SIRT1 mRNA Expression May Be Associated With Energy Expenditure and Insulin Sensitivity. *Diabetes* **59,** 829–835 (2010).
198. Festuccia, W. T., Laplante, M., Berthiaume, M., Gélinas, Y. & Deshaies, Y. PPARγ agonism increases rat adipose tissue lipolysis, expression of glyceride lipases, and the response of lipolysis to hormonal control. *Diabetologia* **49,** 2427–2436 (2006).
199. Kershaw, E. E. *et al.* PPARgamma regulates adipose triglyceride lipase in adipocytes in vitro and in vivo. *Am. J. Physiol. Endocrinol. Metab.* **293,** E1736–1745 (2007).
200. Bitterman, K. J., Anderson, R. M., Cohen, H. Y., Latorre-Esteves, M. & Sinclair, D. A. Inhibition of Silencing and Accelerated Aging by Nicotinamide, a Putative Negative Regulator of Yeast Sir2 and Human SIRT1. *J. Biol. Chem.* **277,** 45099–45107 (2002).
201. Borra, M. T., Langer, M. R., Slama, J. T. & Denu, J. M. Substrate Specificity and Kinetic Mechanism of the Sir2 Family of NAD+-Dependent Histone/Protein Deacetylases. *Biochemistry (Mosc.)* **43,** 9877–9887 (2004).
202. Anderson, R. M., Bitterman, K. J., Wood, J. G., Medvedik, O. & Sinclair, D. A. Nicotinamide and PNC1 govern lifespan extension by calorie restriction in Saccharomyces cerevisiae. *Nature* **423,** 181–185 (2003).
203. Smith, M. R. *et al.* A potent and selective Sirtuin 1 inhibitor alleviates pathology in multiple animal and cell models of Huntington's disease. *Hum. Mol. Genet.* **23,** 2995–3007 (2014).
204. Hession, A. O., Esrey, E. G., Croes, R. A. & Maxwell, C. A. N-Acetylglutamate and N-Acetylaspartate in Soybeans (Glycine max L.), Maize (Zea maize L.), and Other Foodstuffs. *J. Agric. Food Chem.* **56,** 9121–9126 (2008).
205. Karaman, S., Jr., J. B., Sykes, G. P. & Delaney, B. Subchronic oral toxicity assessment of N-acetyl-l-aspartic acid in rats. *Food Chem. Toxicol.* **49,** 155–165 (2011).
206. Karaman, S., Barnett Jr, J., Sykes, G. P., Hong, B. & Delaney, B. Two-generation reproductive and developmental toxicity assessment of dietary N-acetyl-L-aspartic acid in rats. *Food Chem. Toxicol.* **49,** 3192–3205 (2011).
207. Berlinguet, L. & Laliberté, M. Metabolism of N-Acetyl-L-Aspartic Acid in Mice. *Can. J. Biochem.* **44,** 783–789 (1966).
208. Kirmani, B. F., Jacobowitz, D. M. & Namboodiri, M. A. A. Developmental increase of aspartoacylase in oligodendrocytes parallels CNS myelination. *Dev. Brain Res.* **140,** 105–115 (2003).
209. Symonds, M. E., Pope, M. & Budge, H. The Ontogeny of Brown Adipose Tissue. *Annu. Rev. Nutr.* **35,** 295–320 (2015).
210. Vinter, J., Hull, D. & Elphick, M. C. Onset of thermogenesis in response to cold in newborn mice. *Biol. Neonate* **42,** 145–151 (1982).

211. Lee, Y.-H., Mottillo, E. P. & Granneman, J. G. Adipose tissue plasticity from WAT to BAT and in between. *Biochim. Biophys. Acta BBA - Mol. Basis Dis.* **1842,** 358–369 (2014).
212. Meier, H., Hoag, W. G. & McBurney, J. J. Chemical Characterization of Inbred-strain Mouse Milk I. Gross Composition and Amino Acid Analysis. *J. Nutr.* **85,** 305–308 (1965).
213. Won, E.-Y. *et al.* Gender-Specific Metabolomic Profiling of Obesity in Leptin-Deficient ob/ob Mice by 1H NMR Spectroscopy. *PLoS ONE* **8,** e75998 (2013).
214. Hardy, O. T. *et al.* BMI-independent inflammation in omental adipose tissue associated with insulin resistance in morbid obesity. *Surg. Obes. Relat. Dis. Off. J. Am. Soc. Bariatr. Surg.* **7,** 60–67 (2011).
215. Salek, R. M. *et al.* A metabolomic comparison of urinary changes in type 2 diabetes in mouse, rat, and human. *Physiol. Genomics* **29,** 99–108 (2007).
216. Ayala, J. E. *et al.* Standard operating procedures for describing and performing metabolic tests of glucose homeostasis in mice. *Dis. Model. Mech.* **3,** 525–534 (2010).
217. Cannon, B. & Nedergaard, J. Nonshivering thermogenesis and its adequate measurement in metabolic studies. *J. Exp. Biol.* **214,** 242–253 (2011).
218. Yoshida, T., Sakane, N., Wakabayashi, Y., Umekawa, T. & Kondo, M. Anti-obesity and anti-diabetic effects of CL 316,243, a highly specific beta 3-adrenoceptor agonist, in yellow KK mice. *Life Sci.* **54,** 491–498 (1994).
219. Grujic, D. *et al.* β3-Adrenergic Receptors on White and Brown Adipocytes Mediate β3-Selective Agonist-induced Effects on Energy Expenditure, Insulin Secretion, and Food Intake A STUDY USING TRANSGENIC AND GENE KNOCKOUT MICE. *J. Biol. Chem.* **272,** 17686–17693 (1997).
220. Olsen, J. M. *et al.* Glucose uptake in brown fat cells is dependent on mTOR complex 2–promoted GLUT1 translocation. *J. Cell Biol.* **207,** 365–374 (2014).
221. Sun, Z. Cardiovascular responses to cold exposure. *Front. Biosci. Elite Ed.* **2,** 495–503 (2010).
222. Shimizu, I. *et al.* Excessive cardiac insulin signaling exacerbates systolic dysfunction induced by pressure overload in rodents. *J. Clin. Invest.* **120,** 1506–1514 (2010).
223. Furukawa-Hibi, Y. *et al.* Absence of SHATI/Nat8l reduces social interaction in mice. *Neurosci. Lett.* **526,** 79–84 (2012).
224. Kahn, S. E., Hull, R. L. & Utzschneider, K. M. Mechanisms linking obesity to insulin resistance and type 2 diabetes. *Nature* **444,** 840–846 (2006).
225. Thorens, B. & Mueckler, M. Glucose transporters in the 21st Century. *Am. J. Physiol. - Endocrinol. Metab.* **298,** E141–E145 (2010).
226. Deng, D. *et al.* Crystal structure of the human glucose transporter GLUT1. *Nature* **510,** 121–125 (2014).
227. Katz, E. B., Stenbit, A. E., Hatton, K., DePinhot, R. & Charron, M. J. Cardiac and adipose tissue abnormalities but not diabetes in mice deficient in GLUT4. *Nature* **377,** 151–155 (1995).
228. Minokoshi, Y., Kahn, C. R. & Kahn, B. B. Tissue-specific Ablation of the GLUT4 Glucose Transporter or the Insulin Receptor Challenges Assumptions about Insulin Action and Glucose Homeostasis. *J. Biol. Chem.* **278,** 33609–33612 (2003).
229. Stenbit, A. E. *et al.* GLUT4 heterozygous knockout mice develop muscle insulin resistance and diabetes. *Nat. Med.* **3,** 1096–1101 (1997).
230. Kaiyala, K. J. *et al.* Identification of Body Fat Mass as a Major Determinant of Metabolic Rate in Mice. *Diabetes* **59,** 1657–1666 (2010).
231. Mystkowski, P. *et al.* Validation of whole-body magnetic resonance spectroscopy as a tool to assess murine body composition. *Int. J. Obes. Relat. Metab. Disord. J. Int. Assoc. Study Obes.* **24,** 719–724 (2000).
232. Randle, P. J., Garland, P. B., Hales, C. N. & Newsholme, E. A. THE GLUCOSE FATTY-ACID CYCLE ITS ROLE IN INSULIN SENSITIVITY AND THE METABOLIC DISTURBANCES OF DIABETES MELLITUS. *The Lancet* **281,** 785–789 (1963).
233. Zhang, L., Keung, W., Samokhvalov, V., Wang, W. & Lopaschuk, G. D. Role of fatty acid uptake and fatty acid β-oxidation in mediating insulin resistance in heart and skeletal muscle. *Biochim. Biophys. Acta BBA - Mol. Cell Biol. Lipids* **1801,** 1–22 (2010).

8 - Abbreviations

8. Abbreviations

AAT	aspartate aminotransferase (synonym: GOT, glutamate-oxalacetate transaminase)
acetyl-CoA	acetyl-coenzyme A
ACLY	ATP citrate lyase
α-KG	α-ketoglutarate
ANCOVA	analysis of covariance
ANOVA	analysis of variance
ASPA	aspartoacylase
Asp-NAT	L-aspartate N-acetyltransferase
ATGL	adipose triglyceride lipase (synonym: Desnutrin)
ATP	adenosine triphosphate
BAT	brown adipose tissue
BSA	bovine serum albumin
BMI	body mass index
β-OHB	β-hydroxybutyrate
BP	blood pressure
BW	body weight
(k)cal	(kilo-) calories
cAMP	cyclic adenosine monophosphate
CD	chow diet
cDNA	complementary DNA
C/EBP (α, β, δ)	CCAAT/enhancer binding protein (α, β, δ)
CIDEA	cell death-inducing DNA fragmentation factor α-like effector A
CNS	central nervous system
CPT1b	carnitine palmitoyltransferase 1b
Dex	dexamethasone
DG	diglyceride(s)
DMEM	Dulbecco's modified eagle medium
DMSO	dimethylsulfoxide
DNL	*de novo* lipogenesis
EDTA	ethylenediaminetetraacetic acid
EE	energy expenditure
ER	endoplasmic reticulum
eWAT	epididymal white adipose tissue
^{18}F-FDG-PET	^{18}Fluoro-2-deoxy-d-glucose positron emission tomography
FA	fatty acid(s)
FABP	fatty acid binding protein
FASN	fatty acid synthase
FBS	fetal bovine serum
FFA	free fatty acid
G3P	glycerol-3-phosphate
GLUT 1 / 4	glucose transporter 1 / 4
GYK	glycerol kinase
HAT	histone acetyltransferase
HFD	high fat diet
HPLC/HRMS	high pressure liquid chromatography / high resolution mass spectrometry

HRP	horseradish peroxidase
HSL	hormone sensitive lipase
iBACs	immortalized brown adipogenic cells
IBMX	3-Isobutyl-1-methylxanthine
ipGTT	intraperitoneal glucose tolerance test
ipITT	intraperitoneal insulin tolerance test
Iso	isoproterenol
kDa	kilo Dalton
ko	knock-out
LA	locomotor activity
L-glut	L-glutamine
LD	lipid droplet
MG	monoglyceride(s)
MGL	monoglyceride lipase
MM	maintenance medium for iBACs
mRNA	messenger ribonucleic acid
MS	mass spectrometry
NA	nicotinamide
NAA	N-acetylaspartate
NAAG	N-acetylaspartylglutamate
NAT8L	N-acetyltransferase 8-like (synonym: SHATI)
NE	norepinephrine
ntc	non-targeting control
ob	obese gene
OCR	oxygen consumption rate
o/e	overexpression, overexpressed
o/n	over night
PBS	phosphate buffered saline
PCR	polymerase chain reaction
PDK4	pyruvate dehydrogenase kinase 4
PGC-1α	PPARγ coactivator-1α
PIC	protease inhibitor cocktail
pMSCV	murine stem cell virus plasmid
PPAR (α/γ/δ)	peroxisome proliferator-activated receptor (α/γ/δ)
PPRE	peroxisome proliferator-activated receptor response element
P/S	penicillin/streptomycin
qRT-PCR	quantitative real-time polymerase chain reaction
RER	respiratory exchange ratio
RT	room temperature
RXRα	retinoid X receptor alpha
shRNA	small hairpin RNA
siRNA	small interfering RNA
SIRT1	sirtuin 1
SDS	sodium dodecyl sulfate
SNS	sympathetic nervous system
sWAT	subcutaneous (inguinal) white adipose tissue
T2D	type II diabetes
T3	3,5,3'-triiodothyronine
TBI	traumatic brain injury

TCA	Trichloroacetic acid
TG	triglyceride(s)
TZD	thiazolidinedione
UCP1	uncoupling protein 1
VCO_2	carbon dioxide production
VO_2	oxygen consumption
vol	volume
WAT	white adipose tissue
wt	wild type

8.1. Nomenclature

Genes are written in lowercase italics. Proteins are expressed in uppercase letters.

9 - Appendix

9. Appendix

9.1. Publication list

N-acetylaspartate catabolism determines cytosolic acetyl-CoA levels and histone acetylation in brown adipocytes. (equally contributing first author)
Prokesch A, **Pelzmann HJ**, Pessentheiner AR, Huber K, Madreiter-Sokolowski CT, Drougard A, Schittmayer M, Kolb D, Magnes C, Trausinger G, Graier WF, Birner-Gruenberger R, Pospisilik JA, Bogner-Strauss JG. 2016. ***Scientific Reports*** (accepted March 14th, 2016).

α/β-Hydrolase Domain Containing Protein 15 (ABHD15) – an Adipogenic Protein Protecting from Apoptosis.
Walenta E, Pessentheiner AR, **Pelzmann HJ**, Deutsch A, Goeritzer M, Kratky D, Hackl H, Oh da Y, Prokesch A, Bogner-Strauss JG. 2013. ***PLoS One***.

Metabolite and transcriptome analysis during fasting suggest a role for the p53-Ddit4 axis in major metabolic tissues.
Schupp M, Chen F, Briggs ER, Rao S, **Pelzmann HJ**, Pessentheiner AR, Bogner-Strauss JG, Lazar MA, Baldwin D, Prokesch A. 2013. ***BMC Genomics***.

NAT8L (N-Acetyltransferase 8-Like) Accelerates Lipid Turnover and Increases Energy Expenditure in Brown Adipocytes. (equally contributing first author)
Pessentheiner AR, **Pelzmann HJ**, Walenta E, Schweiger M, Groschner LN, Graier WF, Kolb D, Uno K, Miyazaki T, Nitta A, Rieder D, Prokesch A, Bogner-Strauss JG. 2013. ***Journal of Biological Chemistry***.